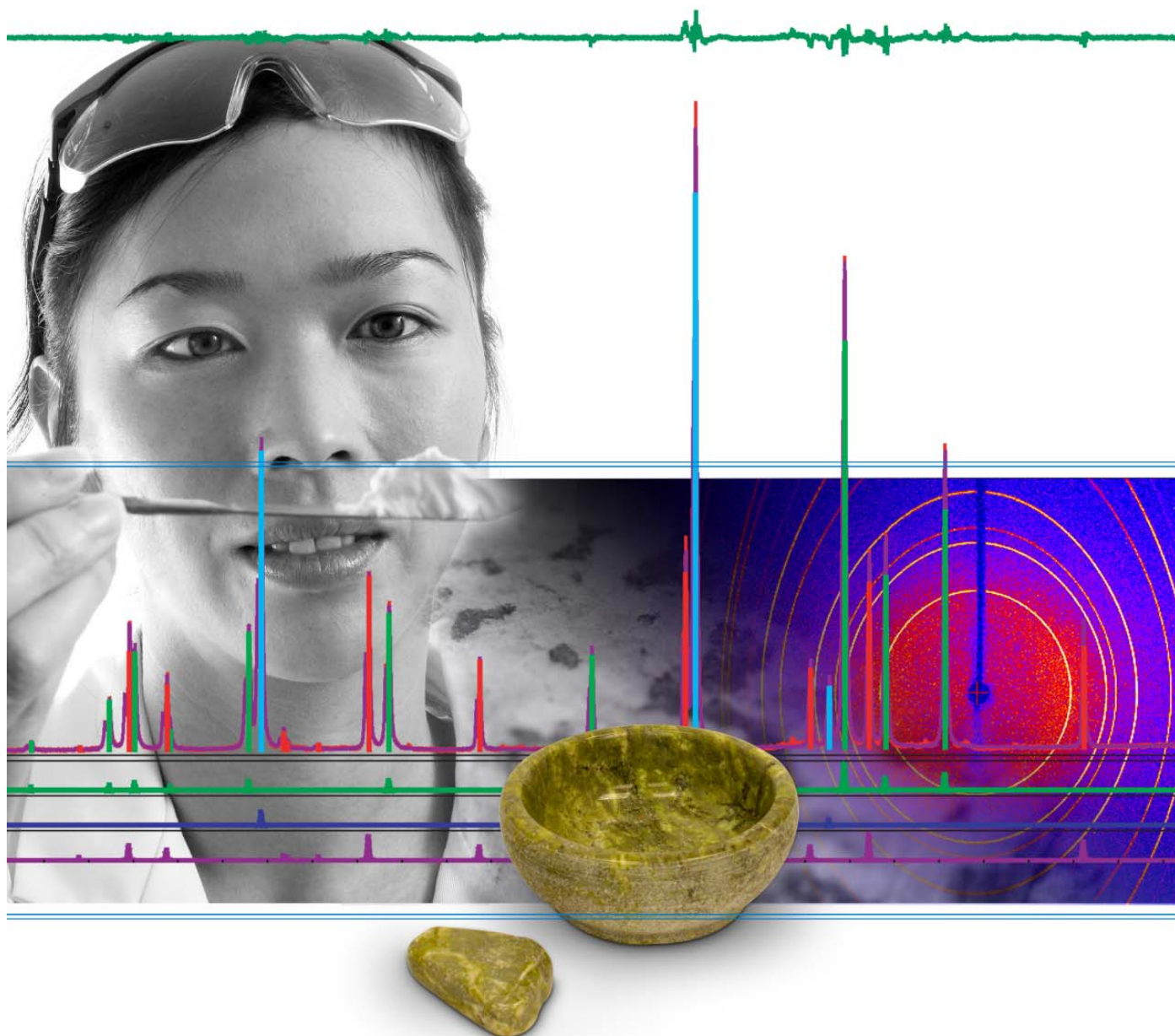**Rigaku**

# Introduction to
# Powder X-ray Diffraction

# Introduction to

# Powder X-ray Diffraction

# Introduction to

# Powder X-ray Diffraction

Jinpei Harada

Rigaku Corporation Press

Tokyo

# Contents

# Introduction: X-rays and Diffraction

Research on X-ray diffractometry and efforts to elucidate crystal structures using X-ray diffractometry have a long history. Discovered in 1895 by German physicist W. C. Roentgen (1845–1923), X-rays attracted significant interest for their capacity to penetrate opaque objects and for potential medical applications. However, despite extensive research, the nature of X-rays was not understood for many years.

X-rays are electromagnetic waves just like visible rays, but of extremely short wavelengths, about the size of an atom, a finding reported in 1912 by M. T. F. von Laue (1879–1960). At the time, crystals were assumed to involve configurations of periodically arranged atoms. An experiment based on the notion that short-wavelength X-rays would permit the observation of diffraction phenomena led to a notable discovery: the Laue image. This research result led to two key conclusions: 1) X-ray wavelengths are the size of an atom or shorter; and 2) Crystals are composed of atoms of approximately 0.1 nm in size, arranged in an orderly manner.

Shortly thereafter, W. H. Bragg (1862–1942) and his son, W. L. Bragg (1890–1971), announced the discovery of Bragg reflection, establishing the foundation for X-ray crystallographic analysis. Following this announcement, many scientists began using X-rays to analyze crystal and molecular structures. X-rays also proved to be useful in the evaluation of industrial materials, and are now used for many different applications.

First used to analyze crystals with simple structures, X-rays were later applied to the analysis of more complex molecular structures. X-rays are now used to analyze the structures of ribosomes (proteins) with a molecular mass of 2,500,000. These advanced applications have been made possible by the establishment of a solid theory on the scattering of X-rays caused by crystals and by the improvement of equipment achieved in line with technological progress. The latest devices feature automatic control

functions that enable the gathering of vast data volumes and rapid processing of the data, refinements to which computers and computing methods have contributed significantly. The state of the art in such devices has reached the point where they can be used effectively even by relatively inexperienced researchers.

X-ray diffractometry has two primary purposes. One is to analyze unknown crystal structures to elucidate their molecular structures. For this application, X-ray diffractometry is used for structural analysis. The other is to evaluate the characteristics of industrial materials at the atomic level and to use the data to grasp differences at infinitesimal scales that make materials superior or inferior.

The MiniFlex II is used for the latter purpose. This machine analyzes common polycrystalline materials, such as glass. An operator skilled in using the equipment can analyze a wide range of materials. Countless crystal structures have been analyzed to date and the results compiled and organized into databases. Comparing the data obtained with the MiniFlex II against such databases allows us to identify the structure of an unknown material.

Versatile and compact, the computer-controlled MiniFlex II is also easy to use. Due to these characteristics, the MiniFlex II is used in laboratories to teach structural analysis methods. Rather than providing an in-depth discussion of diffraction crystallography, this booklet seeks to show users how to perform structural analysis with the MiniFlex II. It begins by discussing Bragg's law of reflection. Once you understand Bragg's law, you will understand the operating principles of the MiniFlex II and understand how to use the equipment. Using the MiniFlex II in combination with existing databases will then allow you to analyze and evaluate the structure of unknown materials.

# Chapter 1: About X-Rays

## 1.1 X-rays

Like visible light, X-rays are electromagnetic waves, but at wavelengths quite different from those of visible light. The wavelengths of visible rays are several thousand angstroms[1]. X-ray wavelengths are far shorter: between 0.01 and 20 Å. **Fig. 1.1** compares electromagnetic waves at various wavelength regions. As electromagnetic waves, X-rays demonstrate wave behavior, including reflection and diffraction phenomena, while also exhibiting the behavior of energy particles.
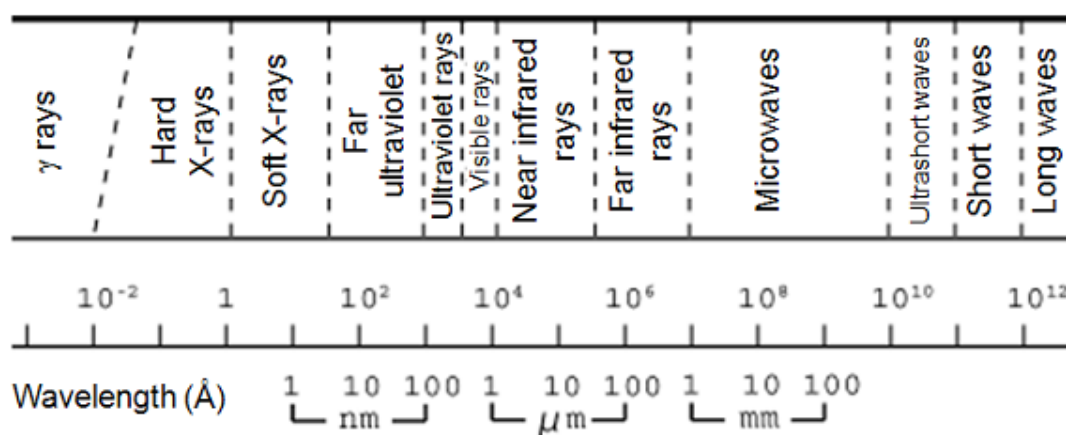


**Fig. 1.1:** Various electromagnetic waves

When you use a detector to detect X-rays, you are observing their particle characteristics. This is also true for visible rays. Detecting light means to sense the energy of a photon at a given location, confirming exposure to light. Strong light delivers many photons to a given location. If you decrease the intensity of the X-ray source, place a fluorescent plate at the location where a diffracted image appears, and observe it, you will see that the surface on which the diffracted image is formed is never

---

[1]  An angstrom, or Å, is a standard international unit of measure for X-ray diffraction crystallography; 1 Å equals 0.1 nanometer (1 ×10$^{-10}$ m, 1 × 10$^{-8}$ cm)

illuminated in its entirety at any given time. Only one spot on the diffracted image forming surface is illuminated at a given time; a different spot on the surface is illuminated the next moment. By recording the illuminated points and observing the image later, you will see a diffracted image identical to the image you would observe using a higher-intensity X-ray source. This behavior reflects the dual wave and particle nature of photons.

With $h$ as Planck's constant and $\nu$ as the frequency of X-ray electromagnetic waves, the energy of X-ray photons, $E$, is given by the following equation:

$$E = h\nu = hc/\lambda$$

If wavelength $\lambda$ is expressed in units of Å and energy $E$ in *keV*, we obtain a useful relational equation. Consider committing this equation to memory.

$$E\ [keV] = 12.4 / \lambda\ [Å] \qquad (1.1)$$

For example, the energy of an X-ray with a wavelength of 1 Å is 12.4 keV.

X-rays have powerful penetrating force that can be harnessed by medical X-ray equipment. They have relatively high energy levels: 30 keV or higher. Since the size of an atom is about 1 Å, X-rays with wavelengths equaling the atomic distance or longer (in a range up to 2 Å) can be used for X-ray diffractometry. Such X-rays range in energy from 7 to 20 keV.

## 1.2 Generating X-rays

X-rays are generated from an X-ray tube. The modern X-ray tube is based on the operating principle of the Coolidge tube invented by W. D. Coolidge in 1913, and the operating principle has not changed over time. **Fig. 1.2** shows a photo of the X-ray tube presently used, together with a cross-sectional diagram.
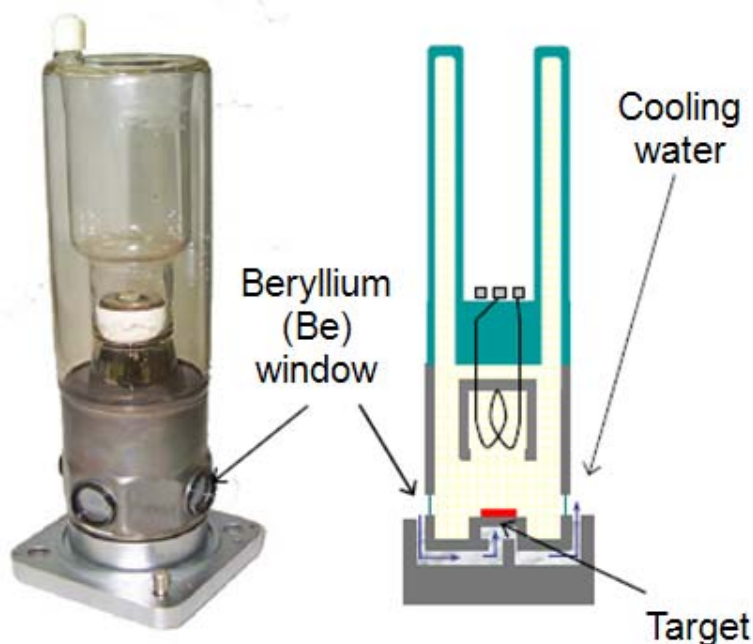
**Fig. 1.2: X-ray tube**. When the tungsten (W) filament heats up and a high voltage is applied between the target and filament in a high vacuum environment, the electron beam collides with the target at high speed, generating X-rays. To allow X-rays to pass beyond the cylinder, windows made of an approximately 0.25 mm thick beryllium plate are installed. Utmost caution should be exercised, since beryllium becomes highly poisonous when oxidized.

When an electric current is applied to a filament in a vacuum, the filament heats up and generates thermoelectrons. A high voltage is applied to the metal target to accelerate the electrons and direct them to the target, generating X-rays. This type of tube is called a sealed X-ray tube. Since the electron beam emitted from the filament scatters toward the target, an ordinary Wehnelt cylinder is positioned appropriately, and the proper inverse voltage is applied to the cylinder. This serves as an electrostatic lens, preventing scattering and resulting in an area of appropriate focus on the target. Upon impact with the target, X-rays radiate in all directions. Windows made of thin beryllium plates are mounted on the cylinder wall to allow X-rays to pass beyond the cylinder.

In this process, most of the kinetic energy of the electrons striking the target is converted into heat. Only a very small fraction of the energy ($\varepsilon$, the X-ray generation

efficiency) is converted into X-rays. This indicates that when accelerated electrons collide with atoms, the probability of their deceleration, which produces X-rays, is extremely low. ε is proportional to the atomic number of the target and the accelerating voltage. The following equation approximates X-ray generation efficiency.

$$\varepsilon = 1.1 \times 10^{-6} Z \cdot V(kV) \qquad (1.2)$$

If the target is made of Cu (atomic number 29) and a voltage of 55 kV is applied, ε can be calculated by substituting $Z = 29$ and $V = 55$ into **Equation 1.2**, yielding a value of $1.6 \times 10^{-3}$. This indicates that only 0.16% of the supplied energy is converted into X-rays. Since most of the energy is converted into heat, increasing the current will cause the irradiated section of the target to melt, weakening the vacuum and resulting in electrical discharge, factors that inhibit the stable generation of X-rays. Thus, cooling water is supplied to the target to keep the X-ray tube in a temperature range in which the target will not melt. The power limit (kV/mA) of the X-ray tube is defined by the cooling capacity.

Called the focus size, the size of the section used to generate X-rays is often significant. **Fig. 1.3** shows the geometrical relationship between the X-ray tube filament and target. Filaments are generally tungsten coils. Electrons discharged from the filament are controlled by an electrostatic lens consisting of a Wehnelt cylinder and the target, forming a band-like electron beam. The target is configured to be orthogonal to the beam. Thus, the actual shape of the X-ray source resulting on the target is nearly rectangular. The size is indicated as follows: W × L mm$^2$ (W and L indicate width and length, respectively). For example, a size is given as **10 × 1 mm$^2$** or **1 × 0.1 mm$^2$** (for an X-ray tube with a very small focus size).
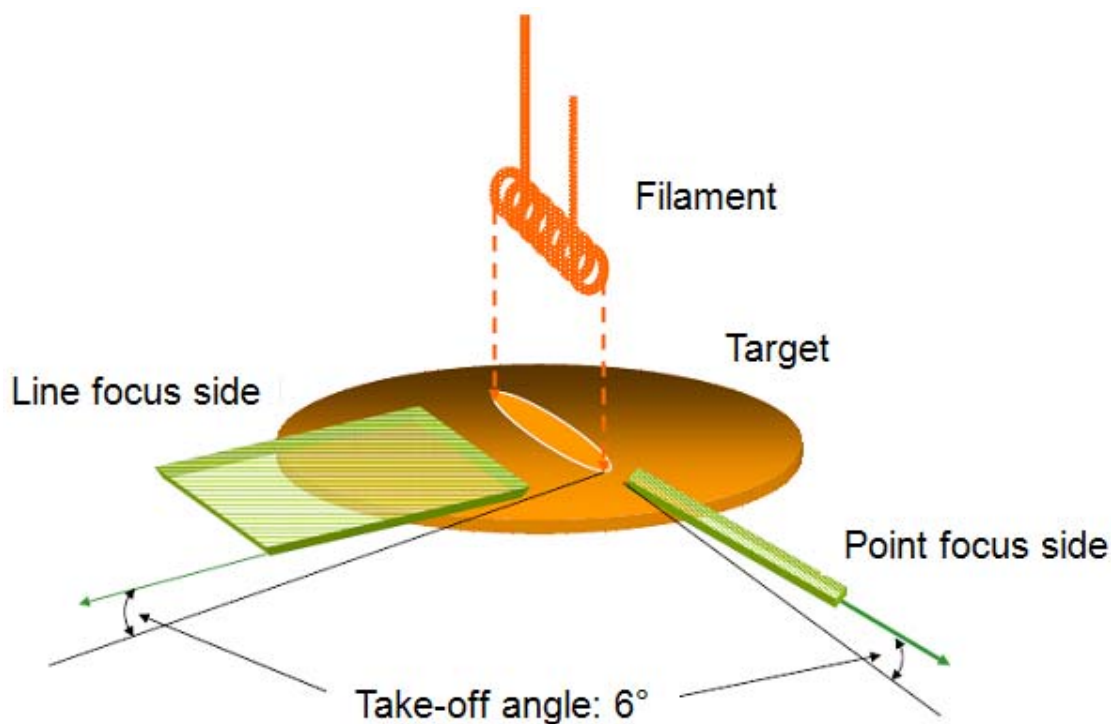
**Fig. 1.3**

Depending on the direction from which the X-ray target is viewed, the apparent size of the X-ray source varies. Beryllium windows are arranged so that X-rays can be emitted at an angle of 6° from the target surface. The intensity of the X-rays obtained at this angle is closest to maximum, and the apparent size of the X-ray source is 1/10 of W or L (because sin 6° = 1/10). In the case of a normal focus size of $10 \times 1$ mm², X-rays emitted along the filament's longitudinal axis appear to be $1 \times 1$ mm² in size. The window located in this direction is called the window on the point focus side. X-rays emitted from the side of the filament perpendicular to the above-mentioned direction appear to be $10 \times 0.1$ mm² in size. The window located in this direction is called the window on the line focus side.

## 1.3 X-ray spectrum

It is important to know the distribution pattern of the wavelength of X-rays generated

by the X-ray tube and the distribution of intensity versus energy (called the spectrum). How we obtain this information will be discussed later. **Fig. 1.4** shows the results obtained. In (a), the voltage was set to 33.5 kV and the spectrums were obtained using three types of target: Cr, Mo, and W. In (b), only the W (tungsten) target was used and the spectrums were obtained while setting the applied voltage to 20, 25, 30, 35, 40 and 50 kV.



(a)  (b)
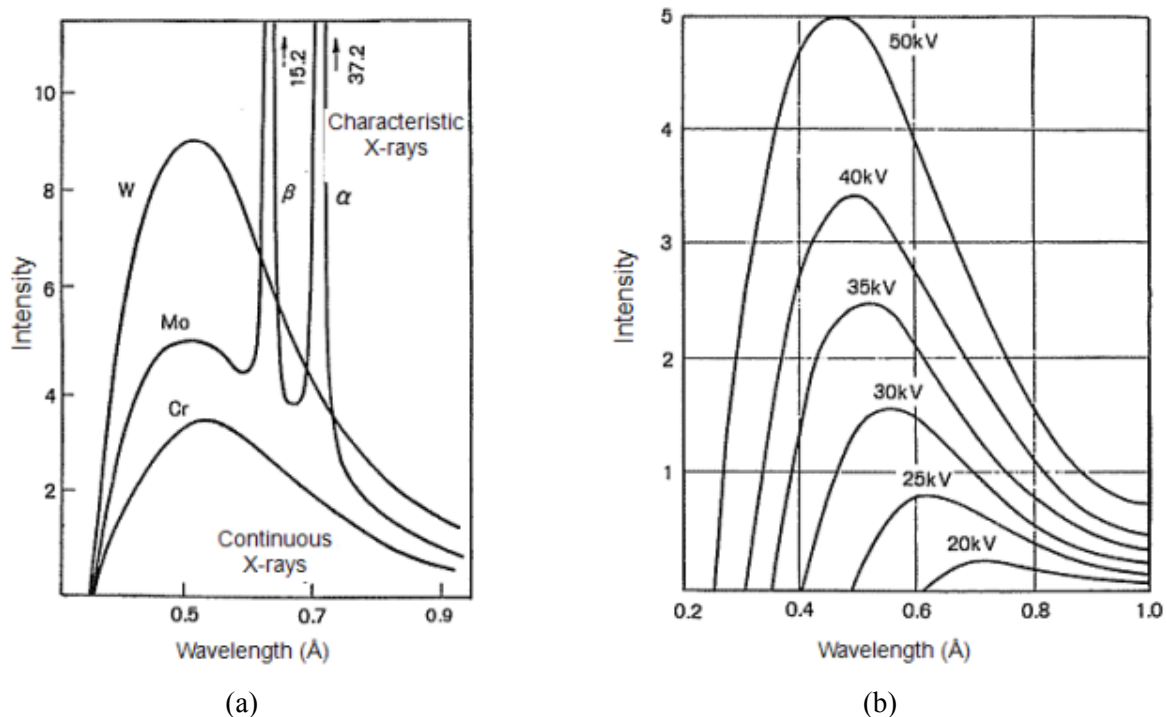
**Fig. 1.4:** Energy spectra. (a) X-ray spectrum; (b) Voltage versus X-ray spectrum (Target: Tungsten)

The spectrum obtained with the Mo target shown in 1.4(a) is a typical spectrum. The wavelength changes continuously and gradually in some sections, while sharp peaks appear at specific wavelengths in other sections. The former are called **continuous X-rays** or **white X-rays.** X-rays with a sharp peak are called characteristic X-rays. Briefly described below is the process for generating these two types of X-rays.

### 1.3.1 Continuous X-rays

When accelerated electrons strike the target material, their direction of travel is altered

by the effects of the electrical field created by the nuclei of the atoms in the target. The electrons emit electromagnetic waves and lose kinetic energy. This is called braking radiation (or **bremsstrahlung**). Since the X-ray energy theoretically cannot exceed the kinetic energy of the accelerated electrons, the minimum wavelength appears at shorter wavelengths in the spectrum of continuous X-rays.

The minimum wavelength, $\lambda_{min}$ (Å) = 12.4/V(kV), as seen from **Equation 1.1**. As **Fig. 1.4(a)** shows, $\lambda_{min}$ does not depend on the type of target but becomes longer as the applied voltage decreases. The lower applied voltage also decreases the intensity of X-rays. The intensity of X-rays is proportional to the total energy supplied to the target, which is proportional to the supplied electric power, W (= iV, where i is current and V the applied voltage), and is also proportional to X-ray conversion efficiency $\varepsilon$ ($\propto$ ZV). Thus, it is also proportional to iV·2Z.

On the other hand, if the supplied electric power is constant, intensity increases in proportion to the atomic number Z of the target material. The spectrum of continuous X-rays in **Fig. 1.4(b)** shows that X-ray intensity decreases as the wavelength becomes longer. This is because the longer the wavelength, the more readily X-rays are absorbed. X-rays of longer wavelengths generated at locations deep in the target are absorbed relatively easily.

### 1.3.2 Characteristic X-rays

Accelerated electrons striking the target stimulate K-shell or L-shell electrons associated with the inner shells of metal atoms inside the target, prompting transitions and generating atoms that lack electrons (electron holes) in their inner shells. These atoms are ionized. When this happens, electrons in other shells within the same atom fall into the holes, emitting electromagnetic waves (photons) with energies in the X-ray region. These are called characteristic X-rays. **Fig. 1.5** illustrates this phenomenon. **Characteristic X-rays** are described based on the energy structure created by the

electrons in the atoms, as shown in **Fig. 1.5(b)**. X-rays generated during the transition that occurs when the inner shells with holes are K shells are called K-series characteristic X-rays.
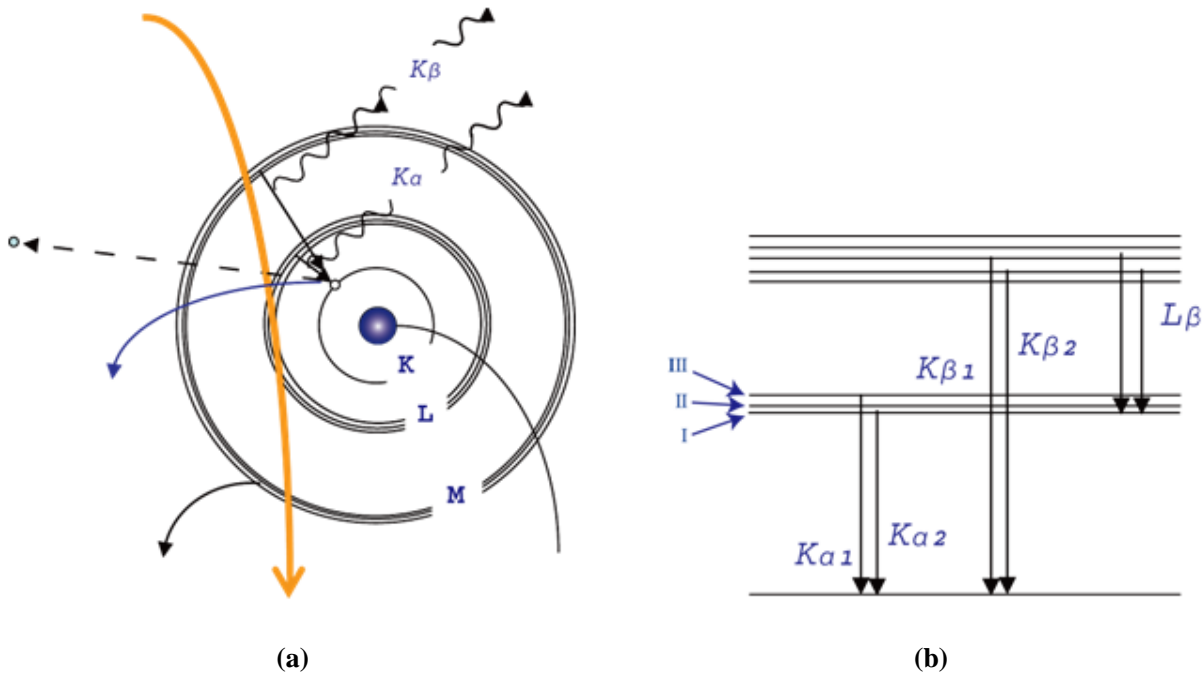


**Fig. 1.5** Characteristic X-ray generating mechanism. (a) Illustration of atomic model (b) Energy level of electrons in atom

When the inner shells with holes are L shells, the X-rays resulting from the transition are called L-series characteristic X-rays. Thus, characteristics X-rays are classified into several series: K, L, M, and so forth. To indicate X-rays of a certain series, a suffix (α, β, γ, etc.) is appended, from longest to shortest wavelength. Specifically, X-rays generated by electrons falling from the L shell or M shell to the K shell are indicated as Kα rays and Kβ rays, respectively. Furthermore, since the energy levels of the L shell and M shell are multilinear, the wavelengths of X-rays resulting from electron transfers from these levels differ slightly, and their intensities differ as well. Thus, a numeric suffix is added to differentiate them, such as $K\alpha_1$ and $K\alpha_2$. However, this suffix is not assigned in the order of the wavelength, but in the order from the

highest intensity. Kα₁ is higher in intensity than Kα₂, but the wavelength of Kα₁ is shorter than that of Kα₂. However, Kβ₁ is higher in intensity than Kβ₂, but its wavelength is longer than that of Kβ₂. The numeric suffix always indicates the order of intensity, but does not express the order of the wavelength.

Wavelengths of Kα₁ and Kα₂ vary depending on the type of target. For reference, **Table 1.1** shows the wavelengths of Kα₁ and Kα₂ resulting from targets commonly used for the applications discussed here.

| | Al | Cr | Fe | Co | Cu | Mo | Ag |
|---|---|---|---|---|---|---|---|
| $K\alpha_1$(Å) | 8.3417 | 2.2936 | 1.93998 | 1.79285 | 1.544398 | 0.71359 | 0.563798 |
| $K\alpha_2$(Å) | 8.3393 | 2.2897 | 1.93604 | 1.78896 | 1.540562 | 0.70930 | 0.559407 |
| $K\beta$(Å) | 7.9605 | 2.0849 | 1.75661 | 1.62079 | 1.392218 | 0.63229 | 0.49707 |

**Table 1.1** Wavelengths of $K\alpha_1$ and $K\alpha_2$ rays

Among characteristic X-rays, $K\alpha$ is of particularly high intensity, and is selected for use in X-ray diffraction. $K\alpha$ rays are in fact doublets of $K\alpha_1$ and $K\alpha_2$. It is important to remember this when using X-ray equipment in an experiment.

The maximum X-ray dose obtained from an X-ray tube depends on the melting point of the target element and specific thermal conductivity, issues related to X-ray tube design.

H. G. Moseley systematically studied the K series using elements from Al to Sn and discovered that the frequency (inverse of wavelength), ν, of a characteristic X-ray is proportional to the square of the value obtained by subtracting a certain value, σ, from the atomic number Z. This is called **Moseley's law** (1913). With K as a proportional constant, the frequency of a characteristic X-ray observed is expressed as follows: $\sqrt{v} = K(Z - \sigma)$. This law was discovered a year after Laue discovered X-ray diffraction phenomena in crystals. Given the primitive nature of the equipment used at the time, the pace of these discoveries is startling. Moseley's discovery is often said to have deepened our understanding of atomic numbers.

## 1.4 X-ray absorption

X-ray absorption is important for understanding quantitative analysis and calculating the depth of analysis. X-ray machines require materials with high X-ray absorption to shield X-rays. An established equation is used to calculate the required thickness of the shield to ensure safety, and familiarity with this equation is a good idea. In general, X-rays of shorter wavelengths have greater penetrating power and require greater care. On the other hand, X-rays of longer wavelengths tend to be absorbed by air and scatter readily. In this case, maintaining a certain distance from the X-ray source can ensure safety. However, because X-rays of longer wavelengths tend to be absorbed by air, they require high vacuum environments inside equipment.

### 1.4.1 Linear absorption coefficient $\mu$ and mass absorption coefficient $\mu/\rho$

The extent of the decrease in the intensity of X-rays resulting from passage through a material for the distance $dx$ is expressed as $-dI$. This value is proportional to incident X-ray dose, $I$, giving the following equation:

$$-dI = \mu\, I\, dx \qquad (1.3)$$

Using $\mu$ as the proportionality coefficient, this equation can be modified as follows:

$$dI/I = -\mu\, dx$$

If the intensity of the X-rays immediately before entering the material is $I_0$ and the intensity after traveling distance x in the material is $I$, we obtain the following equation:

$$I = I_0\, exp(-\mu x) \qquad (1.4)$$

Here, $\mu$ is called the **linear absorption coefficient**. When x is measured in cm, $\mu$ is expressed in units of $cm^{-1}$. The value $\mu/\rho$, obtained by dividing the above value by the density $\rho$, is called the **mass absorption coefficient**. This value is specific to the material

and is expressed in units of cm$^2$/g. Handbooks and other literature often provide a list of mass absorption coefficients, which can be used to calculate linear absorption coefficients.

For chemical compounds and composite materials, we can calculate the value $\mu/\rho$ by the following equation if we known the weight fractions, Wj, of the individual elements.

$$\mu/\rho = \sum_j W_j \cdot \left(\frac{\mu}{\rho}\right)_j \qquad (1.5)$$

In the case of powders, the true absorption coefficient depends on packing density. The value for a powder sample is estimated to be half the value of the corresponding solid material; therefore, the absorption coefficient is multiplied by ½ in most cases.

### 1.4.2 Absorption edge

For a given substance, the mass absorption coefficient ($\mu/\rho$) varies with wavelength. The mass absorption coefficient generally increases with longer wavelengths, as shown in **Fig. 1.6**. This graph, which plots X-ray energy (keV) on the horizontal axis, shows X-rays of lower energy have less penetrating power, while X-rays of higher energy have more penetrating power. Comparing C, Al, and Fe with Cu shows absorption coefficients are higher for heavy metals, assuming constant energy levels.

The graph indicates the presence of an energy level (or wavelength) at which the absorption coefficient changes discontinuously. For example, in the case of Cu, discontinuity occurs at 8.998 keV, which is equivalent to 1.378 Å, slightly shorter than the wavelengths of K$\alpha_1$ (1.541 Å) and K$\beta_1$ (1.389 Å). This is called the energy of the K absorption edge, or the wavelength of the K absorption edge.

When you look at the range of absorption coefficients for energy levels going from lower to higher, you will notice that the absorption rate decreases in proportion to the energy $\varepsilon^{-3}$ in the low energy region and that the absorption rate increases sharply by

nearly an order of magnitude due to the energy of the K absorption edge and then decreases again after that point in proportion to $\varepsilon^{-3}$. In terms of wavelength, the increase is in proportion to $\lambda^3$.
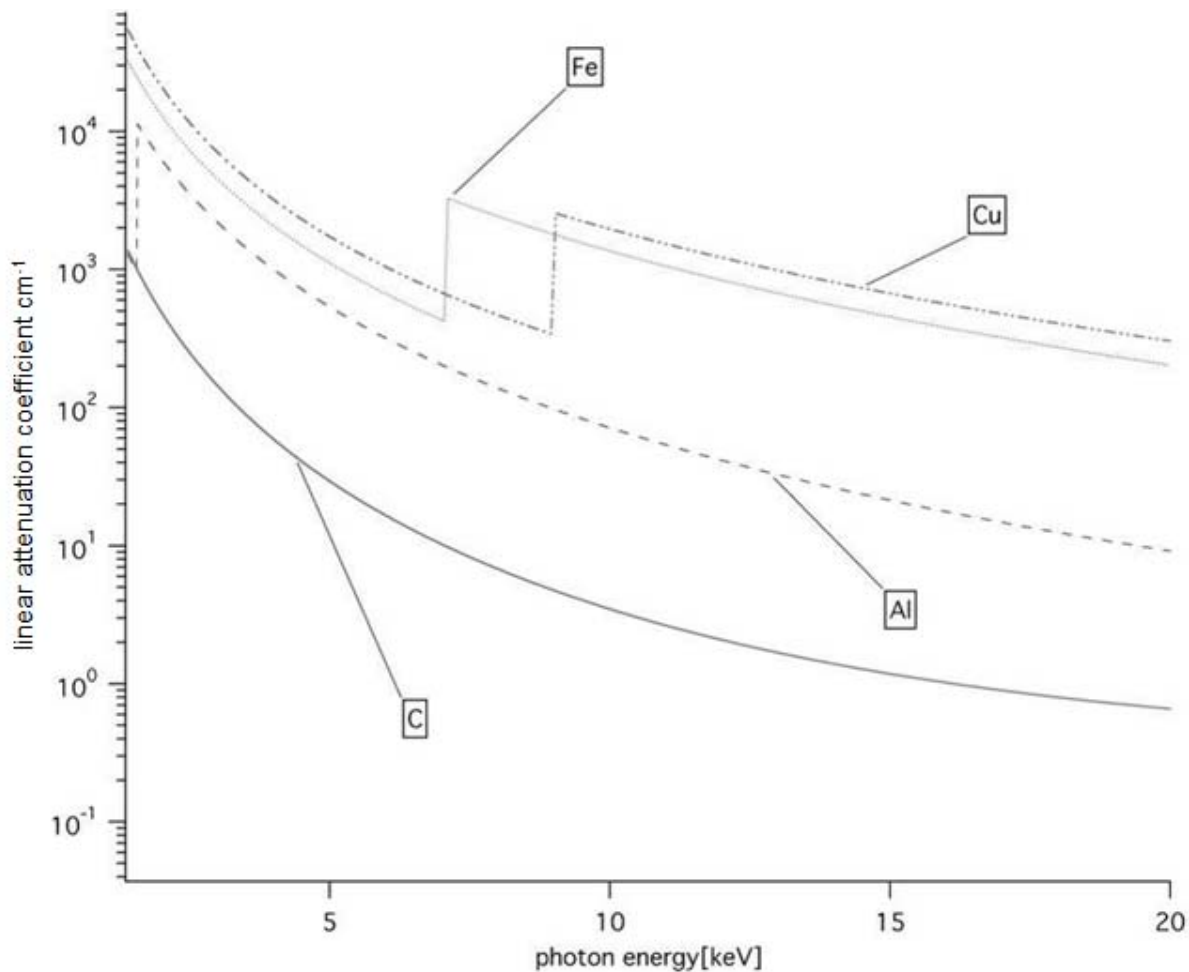


**Fig. 1.6** Wavelength dependence of mass absorption coefficients of Cu and other elements

A high absorption rate results at an energy level higher than the energy of the K absorption edge because X-rays are used for the excitation of fluorescent X-rays. Since X-rays at a lower energy level cannot be used for the excitation of fluorescent X-rays, their penetrating power is high. As the atomic number increases, the wavelength of the K absorption edge shifts toward the higher energy (shorter wavelength) side.

## 1.5 Applying X-rays

The schematic in **Fig. 1.7** illustrates an experiment in which X-ray film is placed behind a crystal sample that is irradiated with X-rays. In this experiment, we observe four phenomena, with each used for a specific purpose.
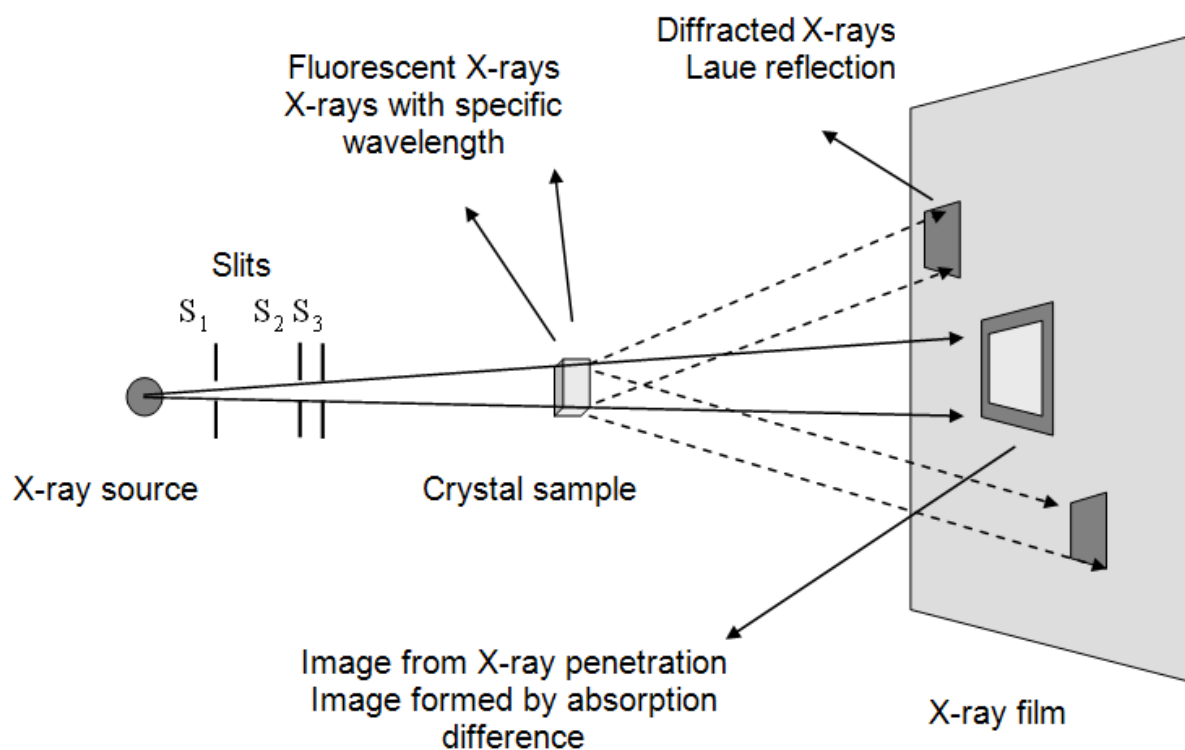


**Fig. 1.7** Schematic diagram of X-ray experiment

1) Most of the X-rays penetrate the sample and cast a shadow on the X-ray film. There is a contrast between the section where X-rays are absorbed at high rates and the section where X-rays are not well absorbed. This presents the inner structure of the crystal nondestructively. This is especially effective for confirming deposits inside the crystal sample that do not allow visible rays to pass. Since the 1895 discovery of X-rays by W. K. Roentgen (1845–1923), this has been a standard method for nondestructive observations of interiors

of all types of materials, not just of crystals.

2) Some of the absorbed X-rays excite electrons in atoms inside the crystal. When high energy electrons drop to a resulting empty energy level of the inner shell, secondary X-rays are emitted. These X-rays, called fluorescent X-rays, have a wavelength specific to the atom, allowing its identification. This method, called X-ray fluorescence analysis, is used to analyze chemical composition.

3) Some of the X-rays entering the crystal collide with the atoms comprising the crystal and scatter and diffract. The diffracted image, a collection of spots, reflects the symmetry properties of the crystal structure. Analysis of the scattering angle and the intensity of the spots reveals the size of the crystal lattice, the atoms in the crystal, and molecular configurations, providing detailed structural information. This is the principle underlying the X-ray diffraction method.

4) By increasing the size of the diffracted spots resulting from the Bragg reflection in X-ray diffraction and observing them in detail, we can identify sections in the crystal that satisfy the Bragg reflection condition and sections that do not. This method can be used to determine distortions in the crystal lattice on the order of arcseconds, making it possible to evaluate crystal quality. This method, called X-ray topography, can be used to assess the quality of artificially grown quartz and silicon monocrystals.

## 1.6 Effects of X-rays on the human body

Exposure to X-rays, either primary or secondary, can cause various ailments in the human body, with symptoms depending on the area of the body exposed and the exposure dose (intensity per unit area). Various units for measuring exposure dose have

been established, some of which are relatively unknown. We will define some terms before discussing safety precautions.

### 1.6.1 Primary and secondary X-rays

X-rays emitted from an X-ray tube form the direct X-ray beam. These are **primary X-rays**. When primary X-rays strike a material, whether a vapor, liquid, or solid, the X-rays scatter. These scattered X-rays are called **secondary X-rays**. The intensity of secondary X-rays is several orders of magnitude lower than that of primary X-rays. Thus, safety should emphasize shielding against primary X-rays.

In an X-ray analysis instrument, heavy metal plates with high absorption rates are typically used to cover the passage of primary X-rays and to contain the X-rays generated. This method is used by all X-ray analysis machines. However, secondary X-rays are always present near the passage of primary X-rays. This means measures must be taken to prevent the leakage of secondary X-rays. X-rays can leak through gaps smaller than 0.1 mm following repeated reflection.

### 1.6.2 X-ray intensity

A counter is used to measure **X-ray intensity**. The counter measures the number of X-ray photons passing through the counter tube window during a given time period. The measurement is called the **counting rate** and is expressed in cps (counts per second). Note that this does not measure the X-ray energy (hv), which is directly related to the penetrating power of X-rays. However, in certain cases, intensity is determined by the energy passing through a certain area during a given time. Do not confuse this with the above definition. In this case, the value is calculated by multiplying the above cps value by the energy of the X-ray photons. The unit of measurement is $erg/cm^2/sec$ or $keV/cm^2/sec$.

The SI unit for **exposure** or **irradiative dose** is C/kg. This is defined as the X-ray

dosage that generates positive and negative ions with an electrical charge of 1 C (coulomb) in 1 kg of air. Since the use of this unit leads to unwieldy values, a conventional unit called a Roentgen (R) is preferred in certain cases. A Roentgen is defined as the X-ray dosage that generates positive and negative ions with an electrical charge of 1 esu (= $3.3375 \times 10^{-10}$ C) in 0.001293 g of air. Expressed in SI units, 1R = $2.58 \times 10^{-4}$ C / kg.

**Exposure rate** (irradiation dose per unit time) is expressed in mR/h. In the case of X-rays with a wavelength of 1.54 Å (characteristic X-rays of CuKα), for example, 1 mR/h is the amount resulting from approximately 200 photons reaching an area of 1 $cm^2$ in one second. If we use a counter with 100% counting efficiency (no counting errors) with a window of 2.5 $cm^2$, the measurement is approximately 500 cps. Shown below are examples of exposure rates of primary X-rays in an ordinary X-ray diffractometer with a Cu target.

| Distance from focal spot (mm) | Tube voltage (kV) | Tube current (mA) | Exposure rate (C/kg/h) |
|:---:|:---:|:---:|:---:|
| 185 | 20 | 2 | $1.8 \times 10^{0}$ |
| 185 | 40 | 30 | $9.8 \times 10^{1}$ |
| 1000 | 40 | 30 | $3.4 \times 10^{-1}$ |

With the above primary X-rays, secondary X-rays will be approximately $10^{-8}$ to $10^{-6}$ C/kg/h, depending on location and conditions.

**Absorbed dose**, expressed in a unit called a gray (Gy), is the amount of energy absorbed by the material onto which X-rays are irradiated. An energy of 1 J (joule) absorbed by 1 kg of the irradiated material, regardless of radiation type or material, is defined as 1 Gy. The effects of the same absorbed dose on the human body may vary significantly, depending on the type of radiation. Thus, we use an equivalent value calculated by applying a correction factor called the relative biological effectiveness

(RBE). The unit of this measurement is the sievert (Sv). Because RBE is approximately 1 in the wavelength region used for X-ray diffraction analysis, 1 Gy roughly equals 1 Sv.

The exposure dose sustained during each medical use of X-rays is approximately 0.5 mSv in the case of chest diagnosis, or approximately 3 mSV in the case of stomach diagnosis. There are no restrictions on exposure doses for medical examinations or treatment. Full-body exposure to natural radioactivity is approximately 0.5 mSv to 1.2 mSv, varying somewhat from region to region.

### 1.6.3 Preventing exposure

The Ordinance on Preventing Ionizing Radiation Hazards has been established to prevent exposure to X-rays. It stipulates the following:

- Certified X-ray personnel are to be assigned to each control zone in which X-ray equipment is used.

- A control zone (area subject to exposure dose of 0.3 mSv/week) shall be established in a facility in which X-ray equipment is used. This zone shall be clearly identified. Individuals other than personnel certified on X-rays are not given access to this area.

- Certified X-ray personnel must carry a portable dose meter.

- Certified X-ray personnel must receive special medical examinations once every six months and examinations of the eyes and skin once every three months. Records of medical examinations are stored for a period of five years.

- The allowable exposure dose for certified X-ray personnel is 50 mSv per year and 30 mSv per three months. These values assume worst-case full-body exposure.

In view of the exposure rates mentioned above, exposure to secondary X-rays over the course of a year (based on 50 weeks per year and 40 hours per week) would appear

to exceed the allowable annual exposure dose. However, in reality, no tasks would result in exposure to secondary X-rays for 2000 hours in a single year.

The Rigaku MiniFlex II does not present exposure hazards as long as it is used correctly. However, there is a risk of certain health hazards caused by a short-term exposure to primary X-rays. For instance, placing a fingertip in primary X-rays of 1.8 C/kg/h for one minute will result in a dose of approximately 1 Sv. Since this is a localized exposure, it will cause only minor skin inflammation that eventually heals. In the case of localized skin exposure, the following symptoms may emerge after one to three weeks.

**1 to 3 Sv:** Skin inflammation (first-degree burn) (hair loss)

**5 to 12 Sv:** Skin inflammation (second-degree burn) (hyperemia, tumefaction, actinic erythema, hair loss)

**10 to 18 Sv:** Skin inflammation (third-degree burn) (actinic erythema, blisters, severe inflammation)

These conditions will heal. X-ray analysis equipment will never result in full-body exposure. You are directed to consult the specialized literature for information on potential exposures involving transmission method (X-ray radiography: radiographic imaging of welds) and isotope-related equipment.

### 1.6.4 Relationship between dose rate and counting rate

As mentioned earlier, $2.58 \times 10^{-7}$ C/kg/h equals approximately 500 cps. This value varies depending on the X-ray wavelength, counting efficiency, and/or the effective window area. Furthermore, the following factors can significantly change the above conversion rate and may increase the hazard level by several orders of magnitude. Using the appropriate counter is critical.

- Using a detector with a wide effective area to measure a thin beam may

underestimate the dose rate due to differences in area ratio.

- If a detector is subject to powerful X-rays, malfunctions may result in inaccurately low measurements.

- Since X-rays are not monochromatic, detection efficiency depends on wavelength.

- The position of the detector relative to the axis of the X-ray beam affects the counting rate.

# Chapter 2: Geometry of Crystal Lattices

Most industrial materials used today are crystalline substances. X-ray diffraction is used to identify and evaluate the structure of these materials. Knowledge of crystals will help you better understand X-ray diffraction data. This chapter presents a basic discussion of crystal lattices.

## 2.1 Space lattice and unit cell

Crystals are formed by the orderly and periodic arrangements of atoms, ions, or large or small molecules, called **space lattices**. A periodic structure is a structure consisting of repeated basic units. These structures are said to demonstrate *translational symmetry*. The basic unit is called the **unit cell**. For a one-dimensional periodic structure, the unit can be determined unambiguously. For two-dimensional or three-dimensional periodic structures, there are several ways to define the unit cell. Some guidelines apply: The unit cell should be as simple as possible. A simple unit cell means that the number of parameters used to describe the lattice is small. Once the arrangement of atoms or molecules in the unit cell is determined, the structure of that crystal is known to a certain extent. Current research now looks beyond molecular and atomic configurations to examine the distribution of bonded atoms and anisotropic thermal oscillation of atoms; the study of crystal structures often involves acquisition of such information.

If you consider three-dimensional periodicity, you will note that the unit cell must be a parallellepiped. The standard unit cell is shown in **Fig. 2.1**. To describe it mathematically, a total of six parameters must be specified: the lengths of the sides of three edge-sharing rhomboids, $a$, $b$, $c$, and the angles formed by the rhomboids, $\alpha$, $\beta$, $\gamma$. The three basic vectors, $\boldsymbol{a}$, $\boldsymbol{b}$, $\boldsymbol{c}$, may also be used to express the unit cell. If the basic vectors are used, any point on the crystal lattice can be expressed as shown below. This

expression may be more convenient.

$$r_{mnp} = n_1a + n_2b + n_3c \quad (2.\ 1)$$

Here, $n_1$, $n_2$, $n_3$ are integers, but since crystals are finite, it is reasonable to assume that these integers are also finite.
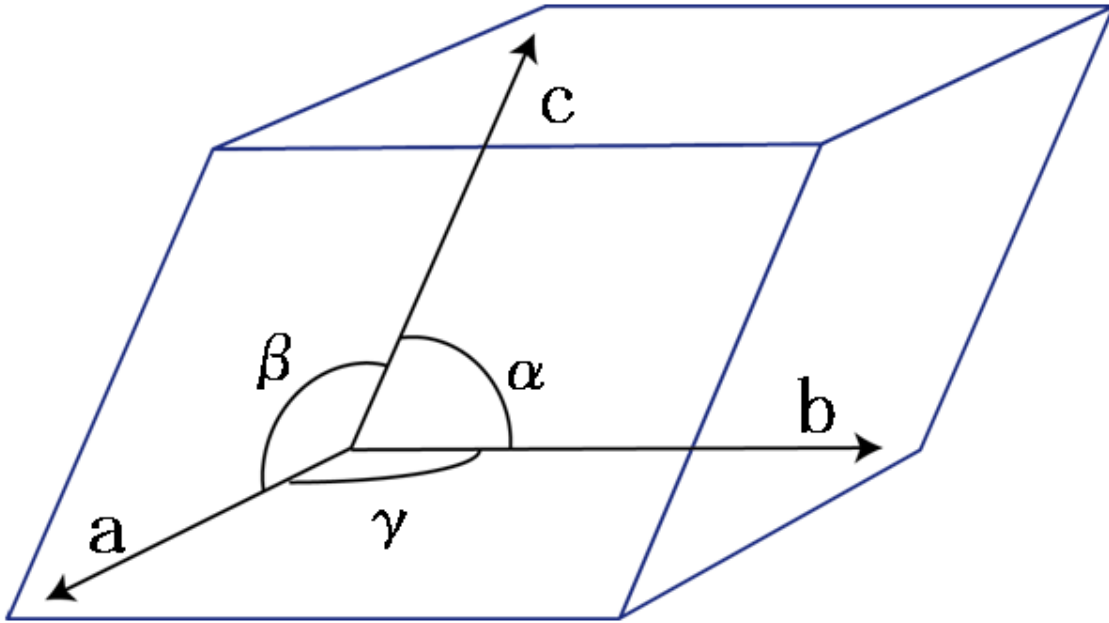


**Fig. 2.1:** The standard unit cell

## 2.2 Crystal system

Consider the symmetry properties of the lattice points of the three-dimensional lattice formed by the repeated arrangement of the unit cell in **Fig. 2.1**. In doing so, assume that the lattice is infinite, not finite, and consider the symmetry elements of the selected lattice points.

If we connect any two lattice points and examine symmetry properties in relation to the line connecting the two points, we identify the following symmetry elements:

1) One-fold rotational axis: Indicated by **1**. When rotated 360° around this axis, the

lattice returns to its original position. If we select two lattice points and examine the symmetry properties in relation to the connecting line, we find that a 360° rotation returns the lattice to its original position. Thus, this symmetry property exists around any axis.

2) Two-fold rotational axis: Indicated by **2**. When rotated 180° around the axis, the three-dimensional lattice overlaps with another lattice, making it indistinguishable from the original lattice.

3) Three-fold rotational axis: Indicated by **3**. When rotated 120° around the axis, the three-dimensional lattice overlaps with another lattice, making it indistinguishable from the original lattice.

4) Four-fold rotational axis: Indicated by **4**. When rotated 90° around the axis, the three-dimensional lattice overlaps with another lattice, making it indistinguishable from the original lattice.

5) Six-fold rotational axis: Indicated by **6**. When rotated 30° around the axis, the three-dimensional lattice overlaps with another lattice, making it indistinguishable from the original lattice.

6) Reflection plane: Indicated by **m**. Assumes a lattice plane that serves as a mirror. That lattice plane reflects the image of another lattice above the plane, and the reflected lattice overlaps with the lattice below that lattice plane, making it indistinguishable.

7) Inversion: Indicated by $\bar{1}$ (inversion center) Select a lattice point. When the vector from the lattice point to a selected origin is r, the lattice point is located at the −r position. This lattice is described as a lattice with an inversion center.

8) Rotation inversion or rotation reflection: Indicated by $\bar{1}$, $\bar{2}$ (=m), $\bar{3}(= 3 + \bar{1})$, $\bar{4}$, $\bar{6}(= 3 + m)$. Combination of rotation and inversion operations returns the lattice to the original position.

Symmetry operations of combinations of those described above are also symmetry

elements. Thus, mathematically, there are 32 **point groups** in total. Space lattices with these 32 symmetry elements can be divided into seven types, based on the shape of unit cell. These are called the **seven crystal systems**.

| Crystal system | Parameters | Number of parameters (Symmetry elements of space lattice) |
|---|---|---|
| Triclinic | $a \neq b \neq c$ <br> $\alpha \neq \beta \neq \gamma$ | $6\,(\bar{1})$ |
| Monoclinic | $a \neq b \neq c$ <br> $\alpha = \gamma = 90° \neq \beta$ | $4\,(2/m)$ <br> (b axis as the main axis) |
| Orthorhombic | $a \neq b \neq c$ <br> $\alpha = \beta = \gamma = 90°$ | $3\,(\,mmm\,)$ |
| Trigonal | $a = b = c$ <br> $\alpha = \beta = \gamma < 120° \neq 90°$ | $2\;(\bar{3}\;\text{and}\;\bar{3}\,m\,)$ |
| Tetragonal | $a = b \neq c$ <br> $\alpha = \beta = \gamma = 90°$ | $2\;(\,4/m\;\text{and}\;4/mmm\,)$ |
| Hexagonal | $a = b \neq c$ <br> $\alpha = \beta = 90°\quad \gamma = 120°$ | $2\;(\,6/m\;\text{and}\;6/mmm\,)$ |
| Cubic | $a = b = c$ <br> $\alpha = \beta = \gamma = 90°$ | $1\;(\text{m3 and m3m}\,)$ |

**Table 2.1:** Seven crystal systems

The following describes the method for indicating symmetry elements and explains their meaning. First, let's take a look at the main axis in a given unit cell, which is not necessarily the *a* axis. Write the symmetry element of the axis at the beginning. Thereafter, write the symbols of the symmetry elements for the second axis intersecting the main axis. To indicate that the axes cross at right angles, "/" is indicated immediately after the corresponding symmetry element. Thus, **2/m** means that there is a two-fold rotational axis around the main axis and a reflection plane at a right angle to that axis. The meaning of **4/mmm** is that there is a four-fold rotational axis, a reflection plane at a right angle to the four-fold rotation angle ("**/m**"), and two other reflection planes indicated by **mm**. You are advised to check these symmetry elements in the unit cell in **Fig. 2.2**.
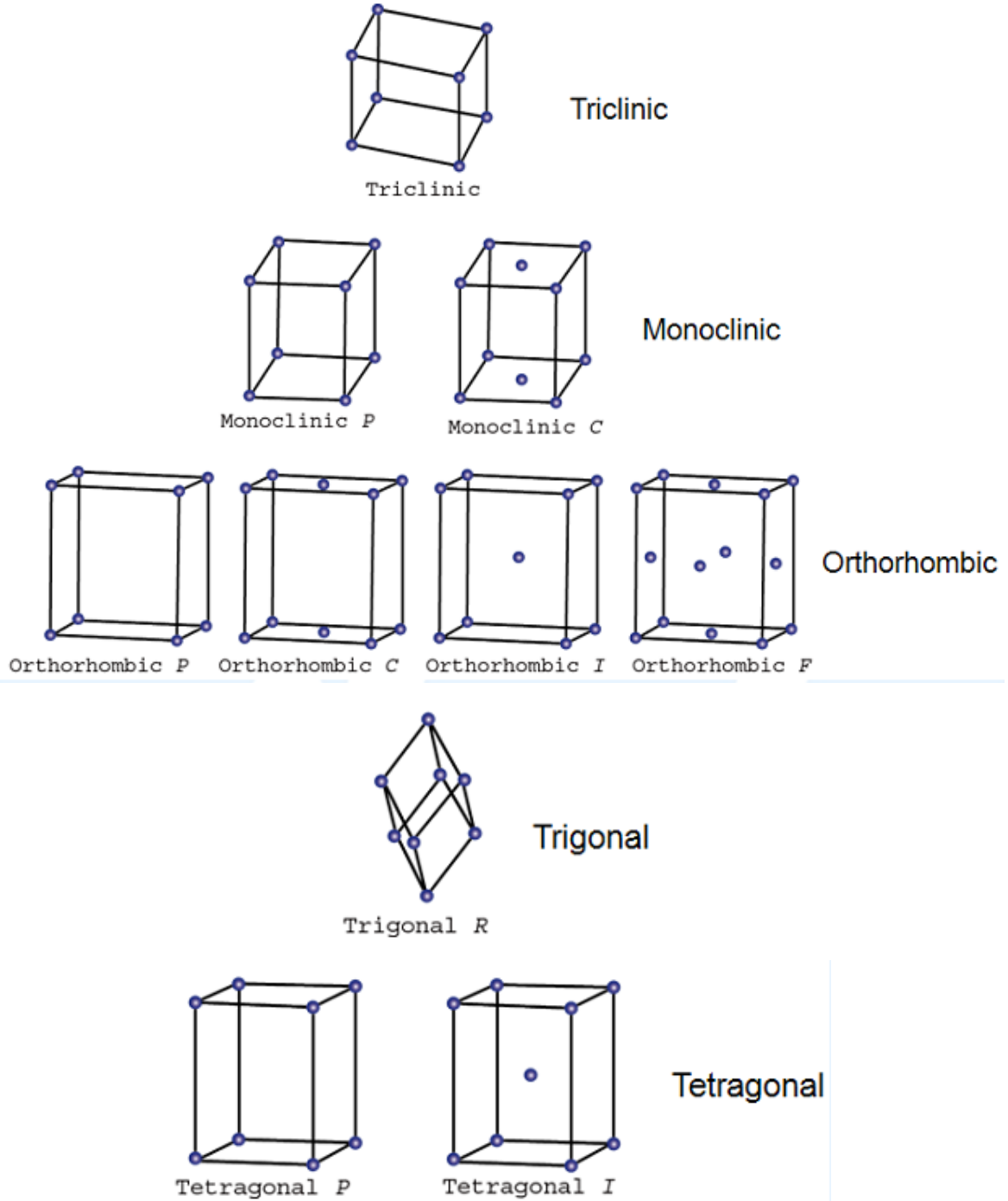
When translational symmetry is added to the symmetry elements of space lattice

and the **symmetry of the atomic configuration** in the unit cell is taken into consideration, the number of possible combinations of symmetry elements totals 230. This means that all three-dimensional atomic configurations can be classified into 230 types; therefore, actual crystals correspond to one of 230 **space groups**. However, examination of the three-dimensional symmetry of diffracted spots obtained by irradiating X-rays onto crystals shows only a group of lattice points with a center of symmetry. The number of such elements is only 11. They are called **Laue groups**. Although the three-dimensional lattices formed by diffracted spots must not be confused with crystal lattices, both are three-dimensional space lattices. Crystal lattices can also be expressed with 11 types of symmetry elements, as illustrated in **Fig. 2.2.**

## 2.3 Bravais lattice

Each of the seven lattices listed in **Table 2.1** includes only one lattice point in the unit cell. These lattices are called primitive lattices. Take one such lattice and create another lattice that is exactly the same. Place that lattice at a location slightly displaced from the original lattice position to create a compound lattice. This is called a **complex lattice**. To give the same symmetry as the original lattice to this complex lattice, it is necessary to combine more lattices of the same type. However, the number of combined lattices is limited. There are seven original lattices and seven additional lattices. Thus, a total of 14 complex lattices are created. This type of lattice was discovered first by Auguste Bravais (1811–1863) and is called the **Bravais lattice**. By convention, space lattices with sublattices at special positions to be added to primitive lattices are body-centered lattices, face-centered lattices, or base-centered lattices. As shown in **Fig. 2.2, t**here are 14 types: simple cubic, body-centered cubic, face-centered cubic, simple tetragonal, body-centered tetragonal, simple hexagonal, simple rhombohedral, simple orthorhombic, body-centered orthorhombic, face-centered orthorhombic, base-centered

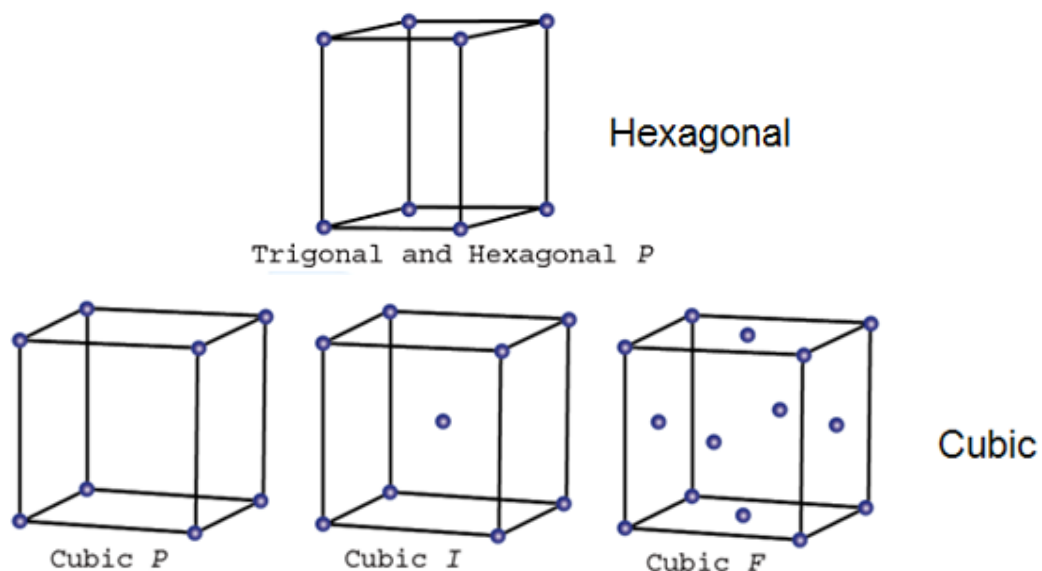orthorhombic, simple monoclinic, base-centered monoclinic, and simple triclinic.



Triclinic

Triclinic

Monoclinic

Monoclinic P    Monoclinic C

Orthorhombic

Orthorhombic P    Orthorhombic C    Orthorhombic I    Orthorhombic F

Trigonal

Trigonal R

Tetragonal

Tetragonal P    Tetragonal I

Hexagonal

Trigonal and Hexagonal P

Cubic

Cubic P          Cubic I          Cubic F

**Fig. 2.2** Bravais lattices

By changing the lattice vectors of one of the complex lattices shown in **Fig. 2.2**, a primitive lattice can be created. In such a case, the crystallographic axis changes from that shown in **Fig. 2.2**, and the lattice then belongs to a different crystal system. In addition, the atomic coordinates become difficult to intuitively grasp.
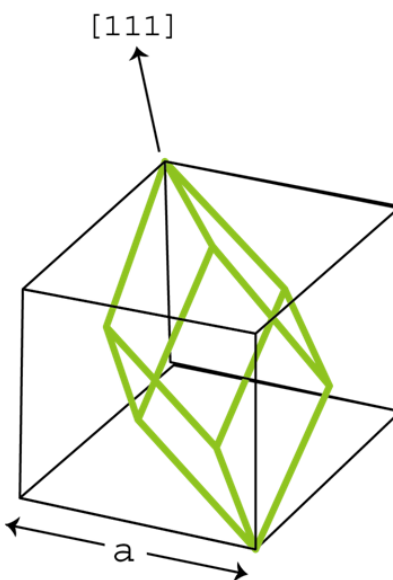


[111]

a

**Fig. 2.3** Face-center cubic lattice and its primitive lattice

As an example, **Fig. 2.3** shows a primitive face-centered cubic lattice. This is not a

cubic crystal but a triclinic system. What is important here is that selection of a crystal system is not unambiguous. Selecting an axis haphazardly would result in confusion. Ideally, select an axis with a high degree of symmetry as the main axis. If you discover an unknown crystal, consult specialized references to determine the appropriate crystal system.

## 2.4 Lattice plane and Miller indices

In a three-dimensional lattice, selecting and connecting three non-linear lattice points forms a plane. Such a plane is called a lattice plane (or the net plane of a lattice) or crystallographic plane. An infinite number of parallel planes with constant **interplanar spacing** (spacing between lattice planes) constitutes a three-dimensional lattice. There are an infinite number of such lattice planes in a space lattice. Since X-ray diffraction is closely associated with lattice planes, confusion can result if names are not given to lattice planes. We use three numbers, or indices, to identify a specific plane in a lattice.
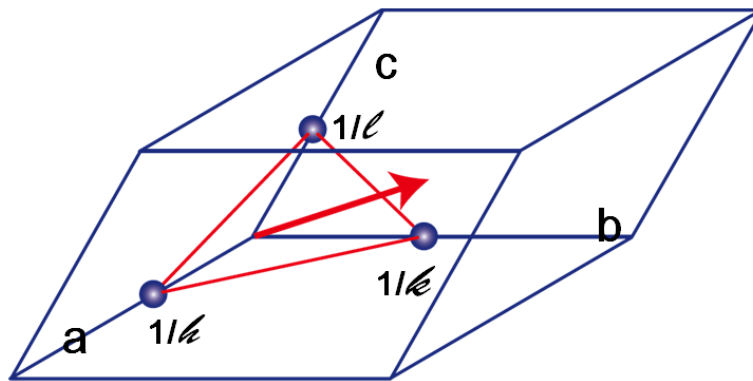


**Fig. 2.4:** Definition of Miller indices

As shown in **Fig. 2.4**, select three integers $h$, $k$, $l$ and envision a plane intersecting unit vector $a$ at $1/h$, unit vector $b$ at $1/k$, and unit vector $c$ at $1/l$. When this plane is extended, it always crosses the lattice points of the $a$-axis, $b$-axis, and $c$-axis. You can confirm this by drawing a diagram. The group of planes parallel to this lattice plane

consists of the *h* lattice plane, *k* lattice plane, and *l* lattice plane, based on the three integers *h*, *k*, *l*. Derived from Miller's discovery, these are called **Miller indices** (or plane indices).

While explanations may differ from book to book, they all mean the same thing, as you can confirm by drawing a diagram. Here is yet another way to explain this concept.

In a space lattice, select three points that are integral multiples of unit vectors *a*, *b*, *c*, with *h'*, *k'*, *l'* being the three integers. Let's name these points A, B, and C. Envision a lattice plane intersecting these points. Their inverse numbers are *1/h'*, *1/k'*, and *1/l'*. Then, find the integers *h*, *k*, *l* that maintain the same ratio as these three numbers. In other words, *h*, *k*, *l* are integers that are coprime and satisfy the following conditions: *h = m/h'*, *k = m/k'*, *l = m/l'*. The integers *h, k, l* are the same **Miller indices** derived earlier.

Here is another definition to consider when using Miller indices. If the **a**, **b**, and **c** axes of a unit lattice are equally divided by integers, *h*, *k*, *l*, and those points are connected, a plane will be formed. Since this plane always passes through the lattice points, it is a lattice plane. Next, examine the inverse numbers of the equally divided points *1/h*, *1/k*, and *1/l*. Needless to say, these inverse numbers are *h*, *k*, and *l*, which are Miller indices.

When considering the interplanar spacing of a plane group having indices, *h*, *k*, *l*, the distance from the origin to the plane shown in **Fig. 2.4** becomes the interplanar spacing of that lattice plane. Thus, the former expression is convenient. That single lattice plane or a plane group parallel to that plane is written as plane *hkl* or (*hkl*). The parentheses are a symbol used to indicate a lattice plane, and the directions of their normal lines are indicated in brackets [*hkl*] according to the rule established by the International Union of Crystallography (IUCr). A space lattice also contains a large number of equivalent lattice planes, all of which are expressed as {*hkl*}, and the orientation of all equivalent planes is indicated as <*hkl*>.

Let's examine some concrete planes. When a lattice plane lies parallel to a

crystallographic axis, its point of intersection with the other two axes is said to occur at infinity. For a lattice plane intersecting the **a** axis at lattice point *a* and the **b** and **c** axes at infinity, the inverse numbers are 1/1, 1/∞, 1/∞ respectively, and the integer ratios are 1, 0, 0. This is plane (100).

Next, consider a lattice plane intersecting the **a** axis at lattice point −*a* and the **b** and *c* axes at infinity. This plane is (−100), indicated ($\bar{1}$00). This plane can be envisioned as a plane viewed from the back side of the (100) plane. In certain cases, when we examine an actual crystal structure, the atomic configuration observed from the front side of the crystallographic plane may differ from the atomic configuration viewed from the back side. For example, we might observe a plane of atom A and a plane of atom B, then see planes of atom A and atom B again. The above expression is useful for indicating on which side of the crystallographic plane the observations occur.
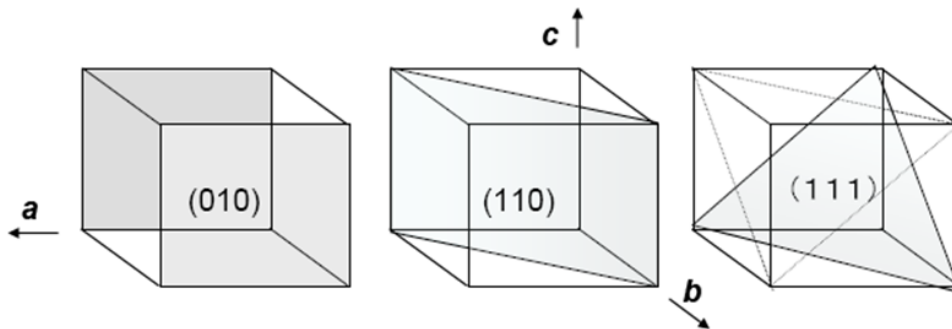


**Fig. 2.5**: Typical crystallographic planes

When a plane is further extended so that it intersects the **a** axis at a midway, ½, of the lattice point, and intersects the **b**- and *c*-axes at infinity, we obtain the plane (200). This plane is parallel to plane (100) and indicates a group of planes whose interplanar spacing is half that of the (100) plane. In general, the plane with interplanar spacing of *1/h* is (h00). Think of Miller indices as indices containing information on interplanar spacing and the orientation of the lattice plane. **Fig. 2.5** shows typical lattice planes in a cubic crystal system. You should familiarize yourself with these planes.

**Problem:** Describe the plane (111) in a face-centered cubic lattice. How are the atoms arranged on that plane? Draw a diagram of the atomic configuration on the plane above and on the plane below.

**Problem:** Confirm that the various methods of defining Miller indices described above are actually the same by drawing two-dimensional lattices.

## 2.5 Interplanar spacing

An important parameter when discussing space lattices is the interplanar spacing. The previous section stated that a space lattice consists of numerous lattice planes. A lattice plane is characterized by the direction of the normal to the plane and by interplanar spacing. Here, we examine the orientation and interplanar spacing of the lattice plane defined by the indices hkl, and see how these quantities are determined.

First, consider the unit vector n along the direction of the normal to a lattice plane. The value of the scalar product of n and a/h, b/k, or c/l determines interplanar spacing. The following equation expresses this relationship:

$$( \mathbf{a} \cdot \mathbf{n} \, / \, h ) \quad = \quad ( \mathbf{b} \cdot \mathbf{n} / k ) \quad = \quad ( \mathbf{c} \cdot \mathbf{n} / l ) \quad = / \, d_{hkl} \, / \qquad (2.2)$$

For cubic/orthorhombic crystal systems in which the a, b, and c axes intersect at right angles, and for hexagonal crystal systems, the relationship between $d_{hkl}$ and the lattice constant indicated in **Table 2.2** can be deduced by straightforward geometry. However, determining this relationship for monoclinic, triclinic, and trigonal crystal systems is more difficult. For such cases, we introduce the concept of the **reciprocal lattice** (see **Appendix B: Diffraction by crystals**). This concept makes the determination of the relationships relatively easy. **Table 2.2** summarizes the results of an examination based on this idea.

We can obtain various values for interplanar spacing $d_{obs}$ characteristic of a crystal sample through X-ray diffraction experiments (described in detail below). Organizing the obtained values makes it possible to determine the indices for the $d_{obs}$ based on an

established method. In short, we can determine the indices of the lattice planes. We can then determine the lattice constants using the above equations.

| Crystal system | Interplanar spacing *hkl* | Equation no. |
|---|---|---|
| Cubic | $(1/d_{hkl})^2 = (1/a)^2(h^2 + k^2 + l^2)$ | (2. 3) |
| Tetragonal | $(1/d_{hkl})^2 = (h^2 + k^2)/a^2 + l^2/c^2$ | (2. 4) |
| Orthorhombic | $(1/d_{hkl})^2 = (h^2/a^2) + (k^2/b^2) + (l^2/c^2)$ | (2. 5) |
| Hexagonal | $(1/d_{hkl})^2 = (4/3a^2)(h^2 + hk + k^2) + (l^2/c^2)$ | (2. 6) |
| Trigonal | $(1/d_{hkl})^2 = \{ (1/a^2)(h^2+k^2+l^2)\sin^2\alpha + 2(hk+kl+lh)(\cos^2\alpha - \cos\alpha) \} \times (1+2\cos^3\alpha - 3\cos^2\alpha)^{-1}$ | (2. 7) |
| (a) Monoclinic (b) | (a) $(1/d_{hkl})^2 = \{(h^2/a^2)+(k^2/b^2)-(2hk\cos\gamma/ab)\}/\sin^2\gamma + (l^2/c^2)$ <br> (b) $(1/d_{hkl})^2 = \{(h^2/a^2)+(l^2/c^2)-(2hl\cos\beta/ac)\}/\sin^2\beta + (k^2/b^2)$ | (2. 8) |
| Triclinic | $(1/d_{hkl})^2 = \{(h^2/a^2)\sin^2\alpha + (k^2/b^2)\sin^2\beta + (l^2/c^2)\sin^2\gamma + (2hk/ab)(\cos\alpha\cos\beta - \cos\gamma) + (2kl/bc)(\cos\beta\cos\gamma - \cos\alpha) + (2lh/ca)(\cos\gamma\cos\alpha - \cos\beta) \} \times (1 - \cos^2\alpha - \cos^2\beta - \cos^2\gamma + 2\cos\alpha\cos\beta\cos\gamma)^{-1}$ | (2. 9) |

**Table 2.2:** Crystal systems versus interplanar spacing *hkl*

The method of least squares is now often used to determine the lattice constants by computer. As mentioned in the previous section, determining the crystal system for completely unknown crystals is a major undertaking. However, a crystal is formed by bonded of atoms and molecules; thus, the crystal structure can be classified based on the types of bonds. Such knowledge is useful for identifying crystals of an unknown sample. Chapter 4 focuses on this aspect.

# Chapter 3: Bragg reflections and X-ray diffractometers

The concept of the reciprocal lattice is one element in explaining the theory of X-ray diffraction phenomena associated with crystals. Understanding this concept will aid in understanding all types of scattering phenomena. This chapter is designed to allow the reader to understand the Bragg reflections associated with powder X-ray diffractometry and certain crystal structures using a diffractometer, without the need for an in-depth knowledge of the concept of a reciprocal lattice—based instead on an understanding of light reflection, refraction, and interference phenomena. This chapter also summarizes the information obtained from sample substances based on the Debye-Scherrer diffraction profiles resulting from irradiating powder samples with X-rays.

## 3.1 Bragg reflections

**Fig. 3.1** shows a schematic diagram of the cross section of a group of parallel lattice planes in the space lattice of a crystal. The circles represent the atoms that comprise the crystal. The value $d$ indicates the interplanar spacing. We can examine the scattering phenomenon resulting from the irradiation of X-rays with wavelength $\lambda$ onto the lattice plane at angle $\theta$.

As a first step in this examination, consider the scattering of X-rays caused by the first-layer atomic plane A-A′. The X-ray beam entering at incident angle[2] $\theta$ relative to the surface is scattered by the atoms in the surface layer. It is reasonable to assume that the phenomenon observed is the same as if the plane A-A′ behaved like a flat mirror.

---

[2] In the case of visible light, this angle is called the glancing angle, and the incident angle is its complementary angle. In the case of X-ray diffraction, the angle is called an incident angle.

Regardless of incident angle $\theta$, scattered waves reinforce one another along the direction of the emergent angle equal to the incident angle. This mirror reflection occurs at any incident angle.
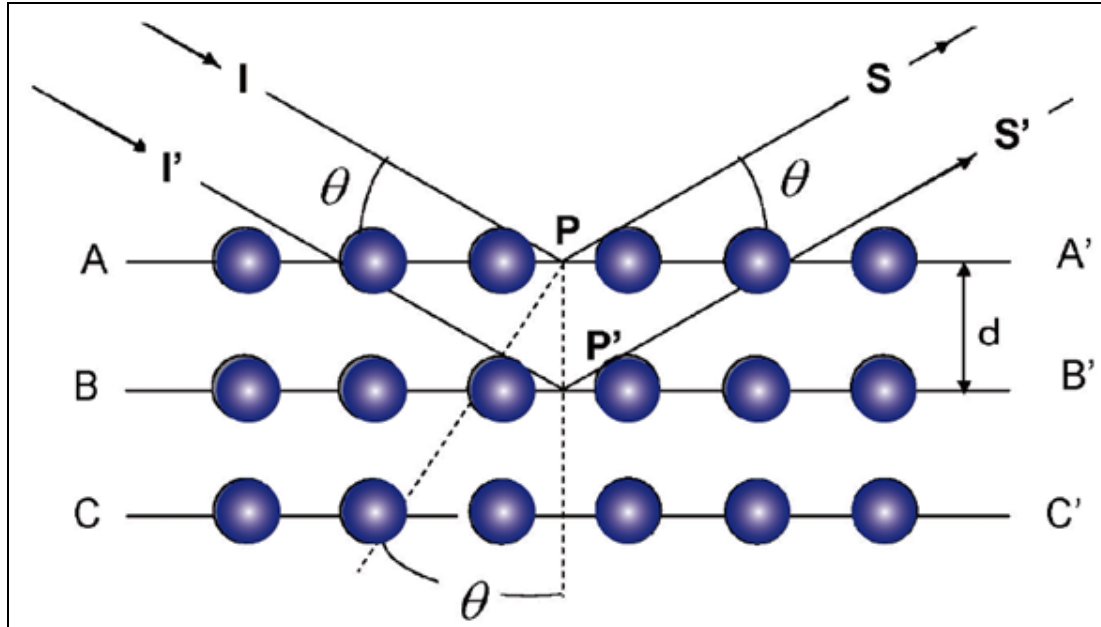


**Fig. 3.1:** Diffraction of X-rays by planes of atoms.

Next, consider X-rays scattered by the atomic plane B-B′ at distance $d$ from the aforementioned atomic plane. If the atomic plane A-A′ did not exist, atomic plane B-B′ would produce the same mirror reflection. However, when the two atomic planes cause scattering, the mirror-reflected waves from the top atomic plane and the mirror-reflected waves from the atomic plane below interfere, reinforcing each other when their phases overlap. As shown in **Fig. 3.1**, the path difference equals the difference between IPS and I′P′S′, which can be expressed as *2d sin θ*. When this path difference is an integral multiple of the wavelength, the reflected waves from the two atomic planes are mutually reinforcing. The reinforcing direction $\theta$ can be obtained as a positive integer with the following equation:

$$2d\sin\theta = n\lambda \quad (3.1)$$

This equation is based on a condition that results in the overlapping of the X-ray waves reflected from the surface atomic plane and one below it. The condition does not change even if the number of atomic planes increases. **Equation 3.1** is based on a condition in which all reflected waves from each lattice plane have the same phase and reinforce one another. This is called the diffraction condition. The equation was proposed in 1912 by W. L. Bragg (1890–1971) and his father, W. H. Bragg (1862–1942), in England. Therefore, X-rays reflected in direction $\theta$ are called **Bragg reflections, Equation 3.1** is called the **Bragg condition**, and $\theta$ is called the **Bragg angle**. This condition differs from the mirror reflection in that no reflection occurs if X-rays enter at an angle not meeting the above condition.

What is the difference between the phenomenon arising from two or three atomic planes and that arising from many atomic planes? The difference is the angle width at which the Bragg condition is satisfied. The higher the number of atomic planes, the narrower angle width $\Delta 2\theta$ becomes, making the condition more restrictive, as shown in **Fig. 3.2**. The bottom of the figure shows the intensity of the Bragg reflection observed at reflection angle $2\theta$. (The graph exaggerates somewhat the difference in full width at half maximum.) The Bragg reflection width $\Delta 2\theta$ is in inverse proportion to $N$ (the number of atomic planes). We can use this relationship to estimate the size of the crystal grain ($L = Nd$) using X-ray diffraction. (This is described in further detail below.) This is an important principle to keep in mind.

A more rigorous explanation of the full width at half maximum of the Bragg angle can be obtained by focusing on the phenomenon where an atomic plane causes mirror reflection. The **Laue condition**, derived from the theory of scattering from finite crystals discovered by M. T. F. von Laue (1879–1960), leads to a clear explanation of full width at half maximum. The latter involves the concepts of a **reciprocal lattice** and the **Ewald sphere**. By presenting the diffraction phenomenon using crystals, Laue demonstrated that X-rays are electromagnetic waves of short wavelengths in the same year that the
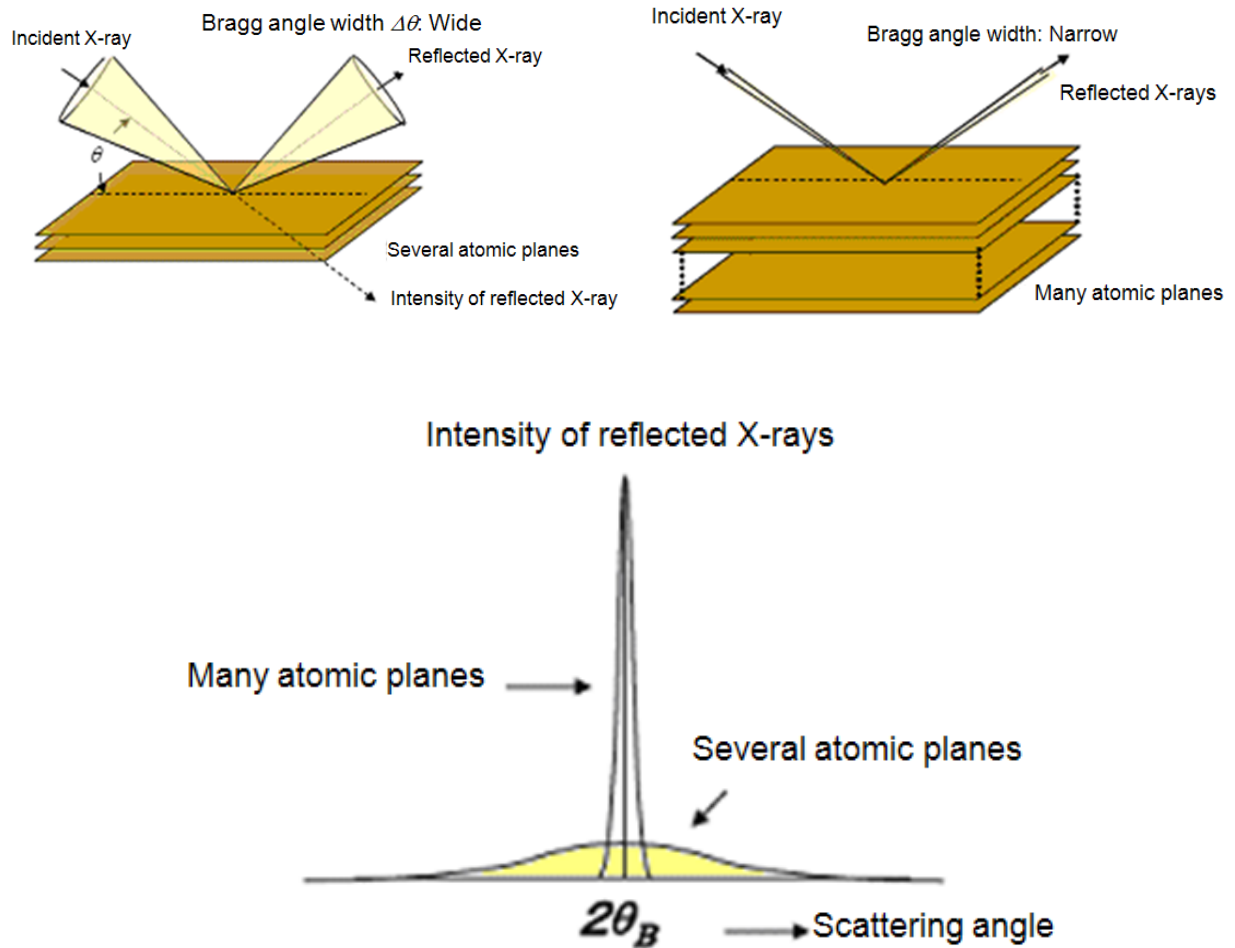
Braggs derived their famous equation.





**Fig. 3.2** Number of lattice planes and change in full width at half maximum. Greater numbers of atomic planes do not change the Bragg angle but reduce the full width at half maximum of the Bragg reflection.

We can try to calculate the value of Bragg angle. To simplify the calculation, we use 1 Å as the X-ray wavelength and assume that the interplanar spacing of the crystal is also 1 Å. If we substitute these values into the equation $\theta = \sin^{-1}(\lambda/2d)$, we obtain $\sin^{-1}(1/2)$. Thus, the Bragg angle is 30°. The scattering angle $2\theta$ is twice this value: 60°. As shown above, when the wavelength of X-rays used equals the size of interplanar spacing, the Bragg reflection appears at an easily observed angle.

Since crystals have a lattice structure, there are numerous lattice planes and their orientations exhibit three-dimensional regularity. This can be expressed by the three

indices *hkl*. If we know the unit cell parameters, we can easily calculate the interplanar spacing using equations (2.3) through (2.9). The Bragg angle for the lattice planes is also easily calculated by substituting equations (2.3) through (2.9) into equation (3.1). Since the Bragg angle $\theta$ depends on the indices *hkl*, its value, indicated as $\theta_{hkl}$, is given by the following equation: $\theta_{hkl} = sin^{-1}(\lambda/2d_{hkl})$. This equation indicates an inverse relationship between $\theta$ and *d:* a large interplanar spacing results in a smaller Bragg angle. The scattering angle $2\theta$ is directly observed and the X-ray wavelength is a known quantity, so the experimental data are sorted on *(sin θ)/λ*, which corresponds to *½d(hkl)*, the inverse of the interplanar spacing. These values can be used as physical quantities specific to each material, and are independent of the wavelength $\lambda$ of the X-rays used in a particular experiment.

## 3.2 Extinction rule for Bragg reflection

**Fig. 3.3** is a modified version of the crystal structure from **Fig. 3.1** that has atomic planes a-a′, b-b′, and so forth, inserted midway between interplanar spacing *d.* The inserted atomic planes are composed of the same atoms as the other planes, but these new atoms are not necessarily positioned immediately below or above the atoms in the adjacent planes. However, the mirror reflections from the atomic planes are identical to the reflections from the plane A-A′.

We consider the X-rays reflected in direction $\theta$ as before. These X-rays should be a combination of the X-rays reflected by the surfaces of the dark circles and X-rays reflected in the same direction by the light circles in the intermediate atomic plane a-a′. Since the interplanar spacing is half, the path difference of the X-rays reflected by the two planes can be calculated as follows: $2(d/2) \sin \theta = d \sin \theta$. **Equation 3.1** gives a phase difference of *n(λ /2).* This indicates that the X-ray waves reflected by the two planes overlap with the scale of mutual displacement equaling half the wavelength. Since the

X-rays scattered by dark-colored atoms and light-colored atoms are mutually displaced by a distance equal to half the wavelength along direction $\theta$, the reflected waves are cancelled and eliminated. This is called **extinction of Bragg reflections** or extinction of diffracted X-rays.
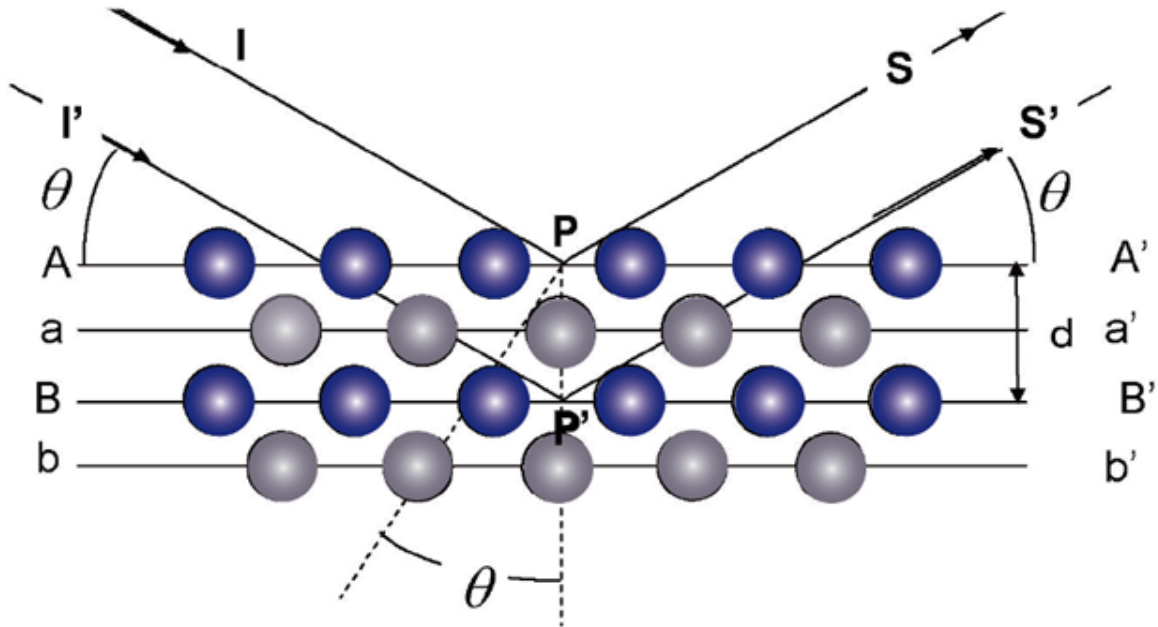
Fig. 3.3: The extinction of Bragg reflections

When the dark-colored atoms differ from the light-colored atoms, the different scattering amplitudes do not cancel out completely, resulting in combined reflected X-rays with lower intensity. As mentioned earlier, given the numerous lattice planes in a crystal, it is natural to assume all lattice planes result in Bragg reflections. However, for the reason described above, Bragg reflections may not occur from certain planes with certain interplanar spacing, or the intensity may be lower. This phenomenon constitutes an **extinction rule**.

## 3.3 Debye-Scherrer ring

Powder crystals and polycrystalline substances can be considered aggregates of

crystallites facing in different directions. Assume that we irradiate a beam of parallel X-rays having the same wavelength onto such a sample. We will observe X-rays scattered by the sample on an X-ray film (or two-dimensional detector) placed along the direction perpendicular to the incident X-ray beam. The observed image will be a concentric diffracted image similar to the one shown in **Fig. 3.4**. This is called the Debye-Scherrer ring.
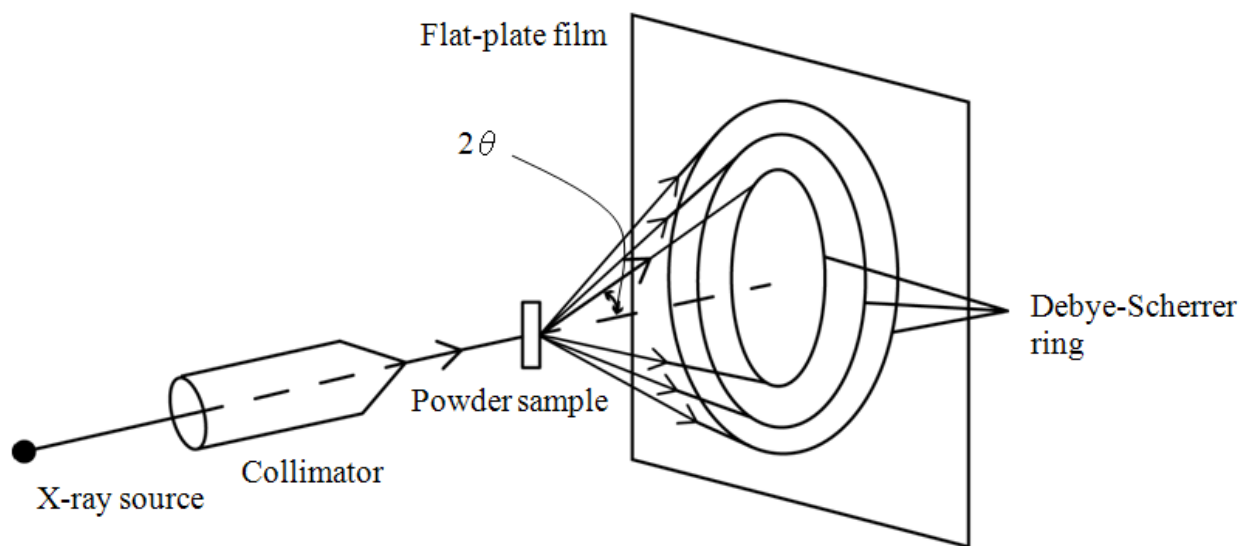


**Fig. 3.4:** Debye-Scherrer ring observed by irradiating monochromatic X-rays onto a powder sample

This concentric diffracted image is observed because crystallites with lattice planes (*hkl*) facing in the direction satisfying the Bragg condition are always found around the X-ray beam axis in a powder crystal sample, and the crystallites diffract X-rays in a cone shape at an angle of $2\theta_{hkl}$. On film, this appears as a circle with the incident beam at the center. Similarly, diffracted X-rays from lattice planes (*h′k′l′*) with different interplanar spacing travel along the axis line of the cone with different diffraction angle $2\theta'_B$. This results in numerous concentric circles on the film.

If we place a cylindrical film similar to the one shown in **Fig. 3.5** in place of the flat-plate X-ray film, we can observe all observable Bragg reflections from the sample in

the region in which the diffraction angle $2\theta$ is between 0 and $\pm\pi$. A diffraction machine capable of mounting strip-shaped film is called a Debye-Scherrer camera. Unfortunately, neither X-ray films nor Debye-Scherrer cameras are manufactured today, in part due to issues related to the disposal of waste development solution.
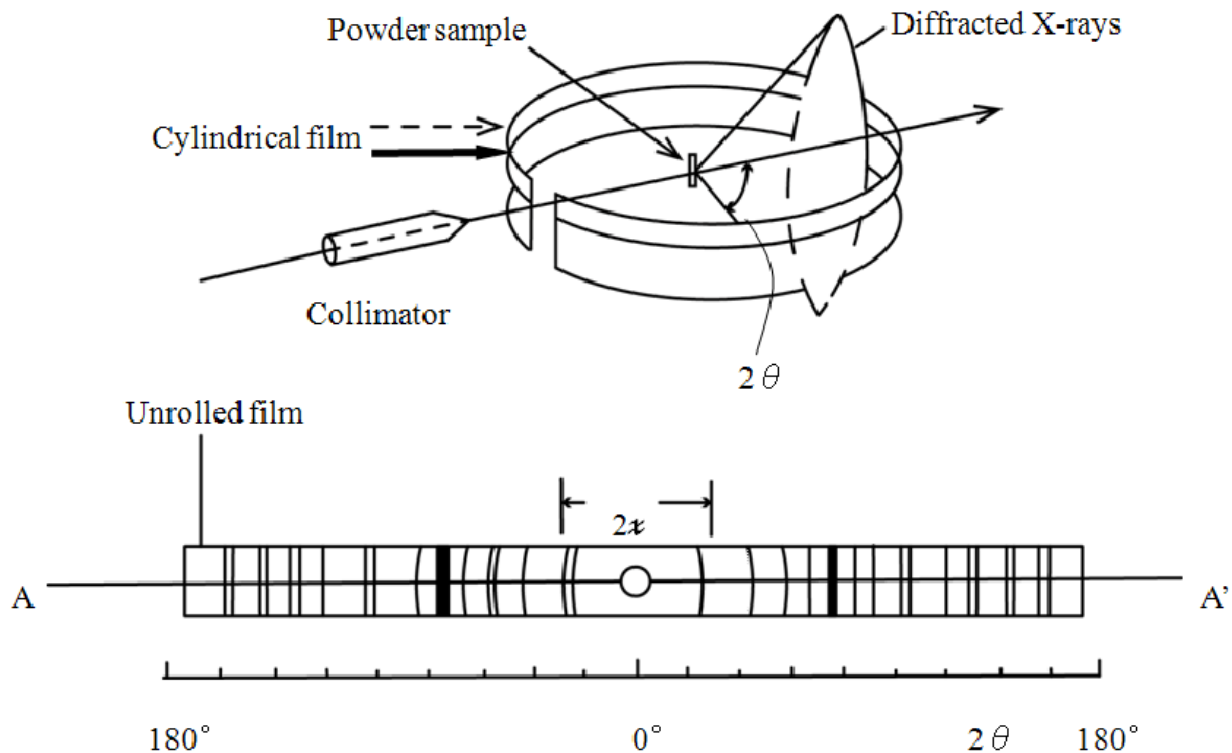


**Fig. 3.5:** Debye-Scherrer camera and observation data

X-ray film offers extremely high spatial resolution (the smallest feature that can be resolved) of 1 to 2 μm. However, due to its low sensitivity, this film requires long exposure times. Diffraction equipment using an imaging plate (IP) in place of the X-ray film to capture diffracted images is still available. **Fig. 3.6** shows a Debye-Scherrer pattern obtained from quartz powder using a cylindrical IP instead of narrow strip-shaped film. Since the film is cylindrical, the Debye-Scherrer rings appear distorted vertically and are elliptical in shape.

Instead of using X-ray film, scanning a counter with high counting efficiency and high intensity measurement accuracy along the surface of a strip-shaped film allows

quick observations of a similar Debye-Scherrer pattern. This type of measurement equipment is called an X-ray diffractometer. The Rigaku MiniFlex II is an X-ray diffractometer. A more detailed discussion is given below.
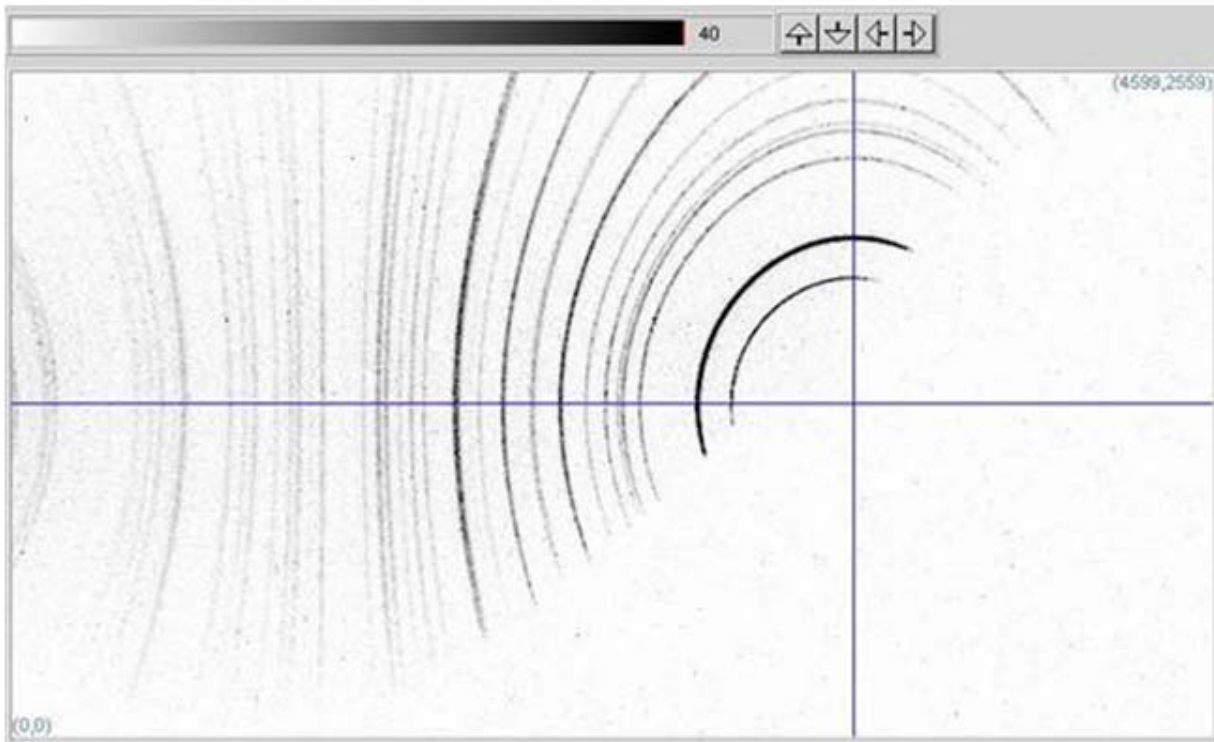


**Fig. 3.6:** Debye-Scherrer pattern of powdered quartz obtained with a cylindrical IP film

In Chapter 2, we learned that a crystal contains numerous lattice planes that can be designated using *hkl*. Unfortunately, it is not possible to measure Bragg reflections from all lattice planes. The Bragg reflections that can be observed with Debye-Scherrer cameras or X-ray diffractometers are reflections whose scattering angle $2\theta_{hkl}$ is in the range of 0 to $\pi$. By substituting the limit scattering angle, $2\theta_{h'k'l'} = \pi$, in **Equation 3.1**, we can obtain the limiting interplanar spacing $d_{min}$, which has a value of $\lambda/2$. This indicates that Bragg reflections from lattice planes whose interplanar spacing is half the wavelength of the X-rays used or less cannot be observed. Theoretically, this means that X-rays of shorter wavelengths would enable the observation of more Bragg reflections. However, the greater the angle of the Debye-Scherrer ring intervals, the higher their

density. Thus, we must reduce the diameter of the X-ray beam and take appropriate measures to prevent reflections from overlapping each other. Hence, the wavelength of X-rays to be used must be selected after considering the resolution capabilities of the equipment. Additionally, according to X-ray scattering theory, diffraction intensity is proportional to $\lambda^3$. Thus, the shorter the wavelength, the longer the measuring time.

# 3.4 X-ray diffractometer

### 3.4.1 Parallel beam method

The following discussion is somewhat more theoretical. We can form a thin, parallel X-ray beam by placing divergent slits (DS) in the vertical and horizontal directions of the X-rays emitted from a point-shaped (or point focus) X-ray source. When this thin bar-shaped beam is irradiated onto a sample and the counter is moved in a circular path around the sample, we observe a Debye-Scherrer ring, as explained in the previous section. Since a counter is used in this case, the valid efficiency becomes the difference in the sensitivity of the film to X-rays. X-ray diffractometers using the **parallel beam method** take advantage of this principle.
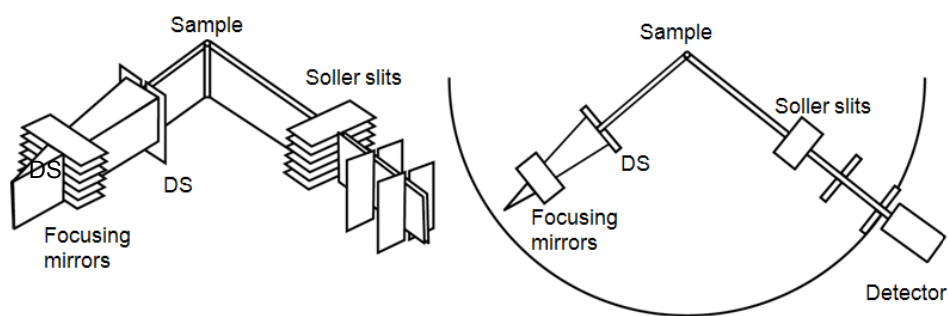


**Fig. 3.7:**   Principle of the parallel beam method

**Fig. 3.7** illustrates the operating principle. A line-shaped, elongated **X-ray line focus source** is used in place of the point focus source. In such cases, **vertical Soller slits (VSS,** or parallel slits), which consist of thin equally spaced absorbers, are mounted in place of

the vertical slits to prevent vertical dispersion of the X-rays. If a sample is bar-shaped, we use the transmission method for measurements. If the sample is in plate form, we use the reflection method. In this system, a receiving optical system comprised of receiving slits (RS), VSS, and scattering slits (SS) is placed in front of the counter.

### 3.4.2 Convergent beam method (B-B method)

With the convergent beam method shown in **Fig. 3.8**, we use wider horizontal divergent slits (DS) so that the X-ray beam from the X-ray source can irradiate more of a plate-shape sample. The X-rays symmetrically reflected by the sample are converged by thin receiving slits (RS) positioned equidistant from the sample, and the diffracted X-rays are counted by the counter. Since this method also incorporates a line focus X-ray source, vertical Soller slits are set on the incident and receiving sides, in the same way as in the system shown in **Fig. 3.7**.

Compared to the parallel beam method, the convergent beam method uses scattering X-rays more efficiently. This type of diffractometer is highly efficient, showing high intensity diffracted X-rays proportional to the divergence angle ratio. Developed by Bragg and Brentano, this method of powder X-ray diffractometry is called the **Bragg-Brentano (B-B) method**. Since diffracted X-rays are converged in front of the counter, it is also called the **convergent beam method**.
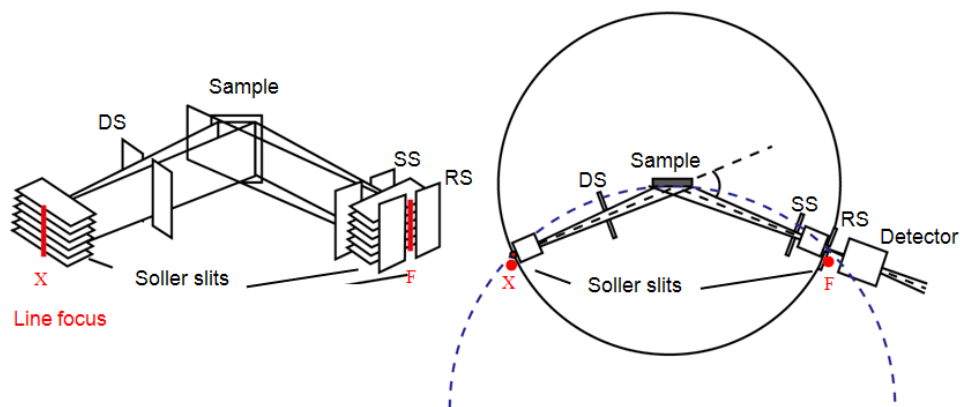


**Fig. 3.8**    Principle of the convergent beam (or Bragg-Brentano) method

In the case of the B-B method, to obtain symmetric reflections on the sample surface we must make the distance from the X-ray source to the rotation center of the sample surface equal to the distance from the rotation center to the receiving slits. We must also maintain the condition of symmetric reflection even when the diffraction angle $2\theta$ changes. This is achieved by maintaining the incident angle $\theta$ of the X-rays on the sample at half the diffraction angle $2\theta$ (or $\theta$). For this reason, the diffractometer is constructed to rotate the sample surface at $\theta$ relative to the counter rotation angle of $2\theta$. In short, this is a $\theta$ -$2\theta$ diffractometer incorporating a $2\theta$ -$\theta$ rotation mechanism. The **MiniFlex II** diffractometer employs a convergent optical system based on the B-B method. Although diffractometers based on the parallel beam method offer lower diffracted X-ray intensity than equipment using the B-B method, they are still in use, due to unavoidable aberration issues associated with the B-B method. This drawback is described further below.

### 3.4.3 Parallelization of X-rays

The easiest way to obtain an X-ray beam is to place a slit $S_1$ with a finite size $\sigma$ at distance $L_1$ after the X-ray source. What would this X-ray beam look like? We can visualize it by observing the image at distance $L_2$ from the slit. The image will be formed with a true image and a penumbra. The X-rays scattered by the edges of the slit project a background image, and the sizes of the true image and penumbra are determined geometrically by slit width, distance between the X-ray source and the slit, and the distance from the slit to the image. We can eliminate the penumbra by placing a second slit at a location removed by a distance L from the first slit. By selecting slit widths $S_1$ and $S_2$, and L, we can obtain a desired X-ray beam. However, $S_1$ and $S_2$ are generally the same in the basic setup, as shown in **Fig. 3.9**. The allowable divergence angle is given by $\Delta\theta = arc\ tan(s\ /2D)$, where $s$ is slit width and $D$ is the interval.
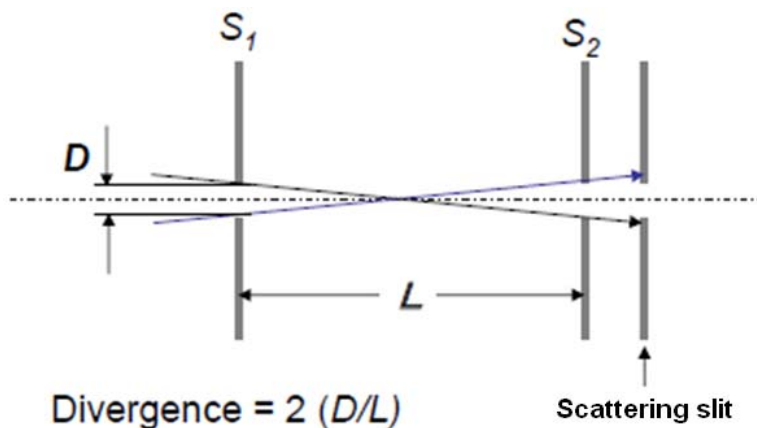
**Fig. 3.9:** Collimator

This slit system will always generate a penumbra for the second slit and X-rays are scattered by the second slit. To eliminate these artifacts, the second slit must be placed as close to the sample position as possible, or else a third slit with the same width must be mounted immediately after the second slit to prevent scattering. This slit is called a scattering slit.

The device used to achieve parallel X-ray beams is called a collimator. To improve data quality, a collimator can be used not just on the X-ray incident side, but on the receiving side as well.

### 3.4.4 Monochromatization of X-rays using crystals

A collimator only improves the parallelism of an X-ray beam. The energy spectrum (wavelength distribution) of the incident X-rays does not change. Except for special applications, for X-ray diffraction it is more convenient to use X-rays of only a specific wavelength. Obtaining X-rays of a certain wavelength is called monochromatization.

To monochromatize X-rays, we place a crystal or synthetic **multilayer** film (called a **monochromator**) immediately after the X-ray source to generate Bragg reflections of characteristic X-rays and collimate them for use as incident X-rays. Another monochromatization method involves placing the crystal between the sample and the detector to select diffracted X-rays of a specific wavelength. Regardless of which

method is used, monochromatization significantly reduces intensity, with the extent of the reduction depending on the quality of the crystal used as a monochromator.

Monochromator crystals include pyrolytic graphite, LiF, quartz, Si, and Ge. Si and Ge, which offer excellent crystalline properties, are often used to obtain X-ray beams with excellent parallelism. In certain cases, X-rays are Bragg-reflected two or three times for improved parallelism. However, since this attenuates intensity significantly, it is not suitable for use in laboratory applications.

**Fig. 3.10** shows a powder X-ray diffractometer that detects only monochromatic X-rays, using a spectrometer placed in front of the detector. The MiniFlex II is based on this configuration. Diffracted X-rays scattered by the sample and collected at focusing point F are dispersed by crystal M, and diffracted X-rays consisting only of $K\alpha$ rays are measured with counter SC. In this system, the crystal M is called a counter monochromator. In certain cases, Crystal M may be placed on the incident side.
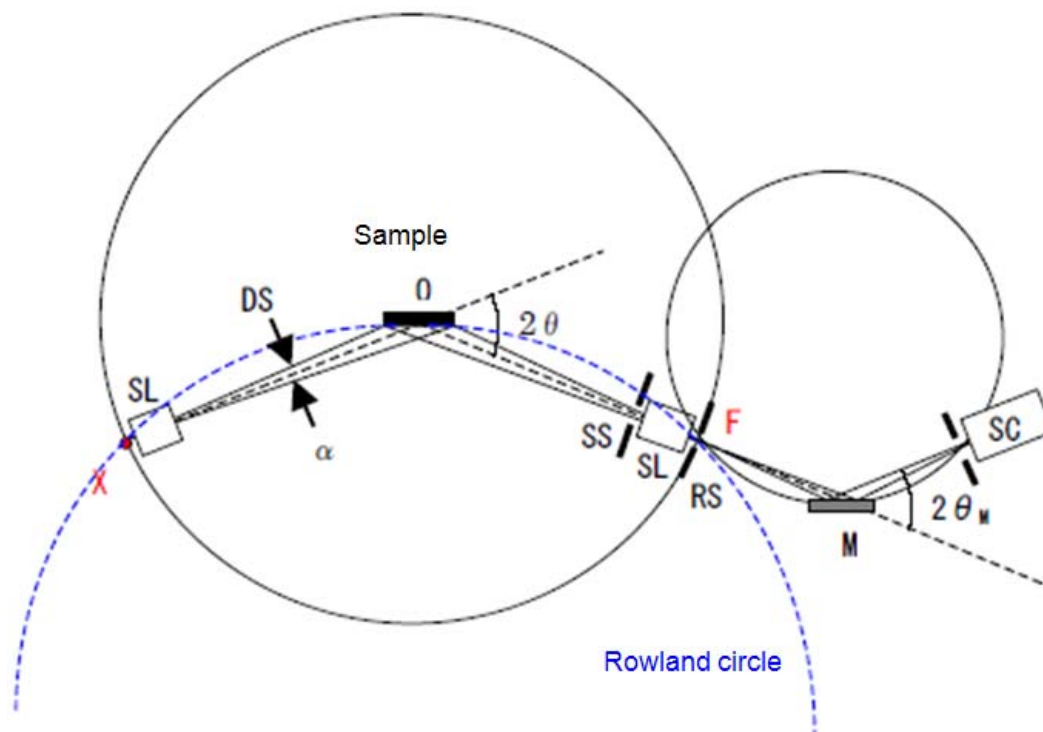


**Fig. 3.10:** Optical system featuring monochromator

### 3.4.6 Filter method

The simplest way to monochromatize X-rays is the $K\beta$ filter method. With this method, a material that absorbs X-rays near the $K\beta$ wavelength and allows X-rays with wavelengths close to $K\alpha$ characteristic X-rays to pass through is placed between the collimators or in front of the detector so that it will detect only diffracted $K\alpha$ rays. This method is called the **filter method** or **filter technique**. For example, to obtain $CuK\alpha$ from a Cu target, we use a $Ni$ filter; for $MoK\alpha$ rays, we use a $Zr$ filter. A high-quality optical system is key to obtaining high-quality data.

The inversion phenomenon, which occurs in a narrow region on the absorption end where the absorption of shorter-wavelength X-rays is greater, is often used to filter X-rays. Radiation emitted by an X-ray tube consist of white X-rays and characteristic X-rays. Specifically, X-rays generated using a copper target are comprised of white X-rays and CuKα (1.541 Å) and CuKβ (1.392 Å) characteristic X-rays. CuKα is more useful in actual applications.
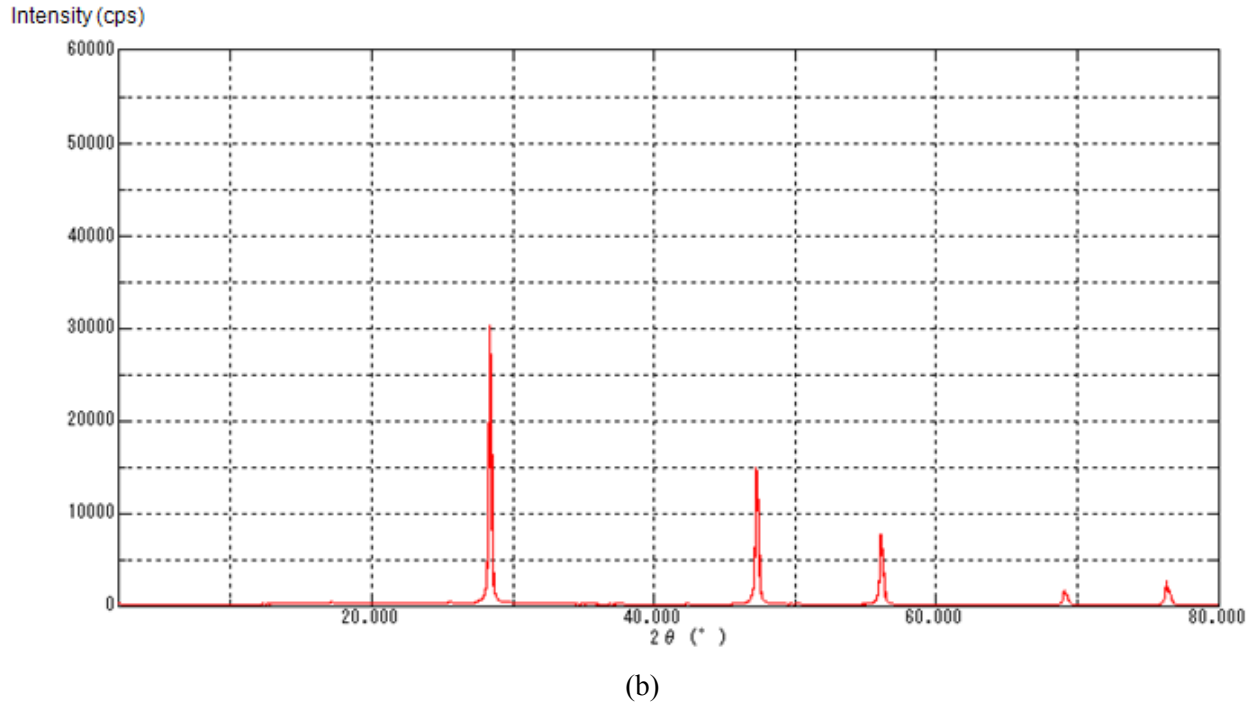


(a)

Intensity (cps)



(b)
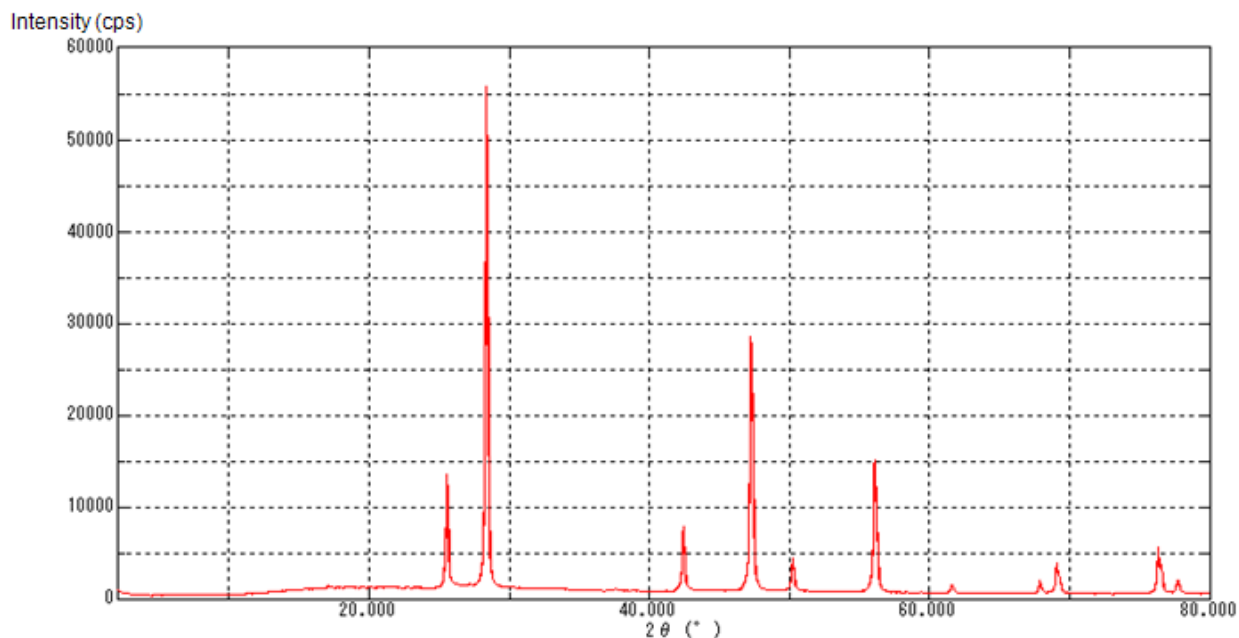
**Fig. 3.11:**   Function of $K\beta$ filter. For the data obtained without a filter (a), we observe diffraction peaks arising from $K\beta$ rays. With a filter in place (b), there are no peaks from diffracted $K\beta$ rays. The decrease in intensity is due to filtering effects.

This can be done with an X-ray spectrometer, but there is an easier way to suppress the diffraction of CuKβ. We can use Ni, which has an absorption end between CuKβ and CuKα. This approach takes advantage of the significantly greater absorption efficiency of CuKβ. By inserting an Ni film measuring about 0.015 mm thick into the diffractometer optical path, we can attenuate $K\beta$ rays to about 1/100 the strength of $K\alpha$ rays. This film is called a $K\beta$ filter. **Fig. 3.11** shows data for an experiment performed to evaluate the effects of a $K\beta$ filter.

**Problem:** Confirm that the reflection *hkl* mixed with even numbers and odd numbers (for example, reflections of 100 and 110) does not appear in FCC crystals, in accordance with the extinction rule.

**Problem:** We can calculate the lattice constant using the data and **Equation 1.8** given the interplanar spacing. Obtain the value of the lattice constant and compare it to the data in the literature. The measurement data shows values only for scattering angles of up to 90°. Indicate the maximum interplanar spacing at which X-ray scattering can be

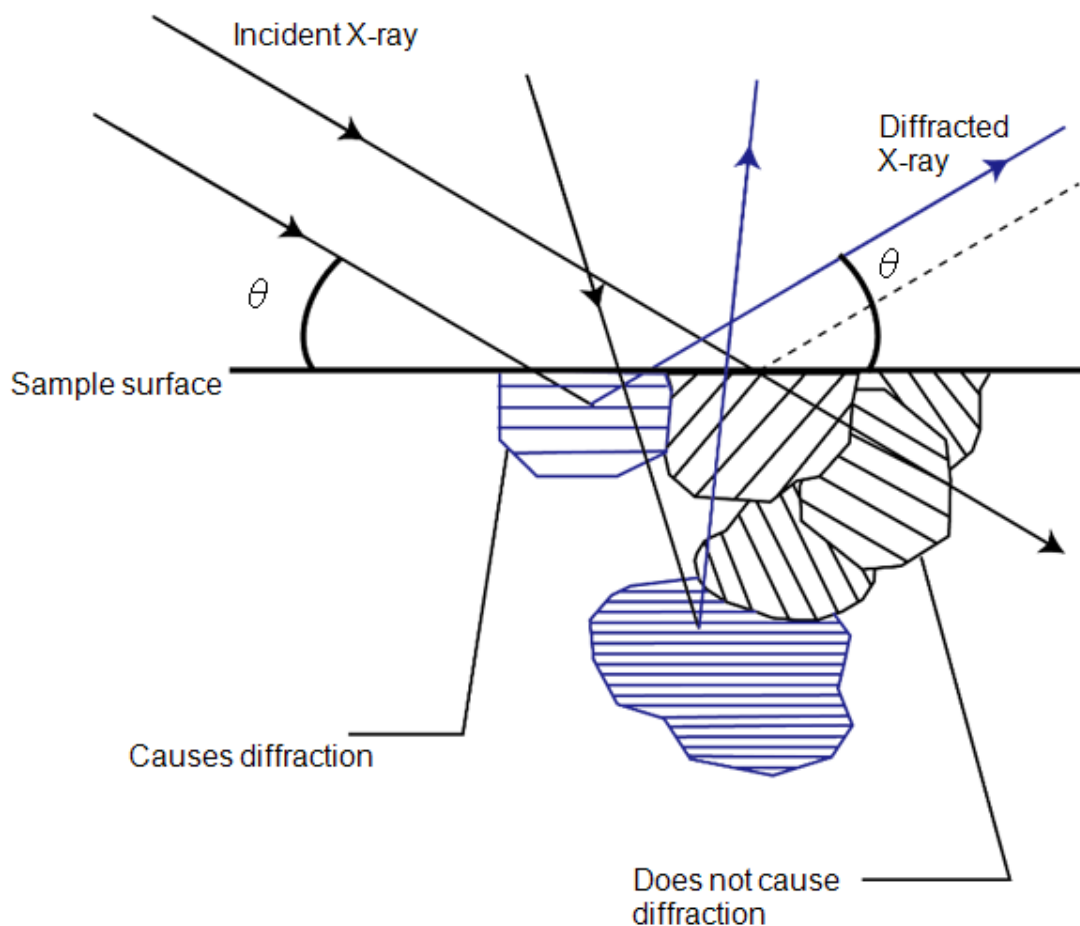observed when $2\theta$ is 180° by calculating the Miller indices.



**Fig. 3.5**: Orientation of crystal grains that satisfy the diffraction condition In a sample of flat plate shape, only crystal grains for which all lattice planes are parallel to the sample surface satisfy the diffraction condition. (BV: WHERE DOES THIS BELONG?)

### 3.4.6 Aberration problem of B-B method

The parallel beam method and the B-B method based on a convergent optical system both have their own drawbacks and advantages. Due to its high efficiency, the B-B method produces diffraction one or more orders of magnitude greater in intensity than data obtained with the parallel beam method. However, we need to be aware of several problems to measure the diffraction angle precisely or to examine the pattern (profile) of the diffracted X-rays.

As shown in **Fig. 3.8**, a circle (indicated by the dotted line) is formed by the

following three points: X-ray source position **X**; center **O** of the sample surface (also the rotation center of the goniometer); and counter receiving slit position **F**. This circle is called the **focusing circle** or the **Rowland circle**. If the surface of the sample plate forms a circular arc around the focusing circle, the diffracted X-rays diverging from one point on the focusing circle converge on the single point **F** on the receiving slit. The point of symmetry is the center **O** of the sample. However, the radius of the focusing circle changes when diffraction angle $2\theta$ changes. This necessitates a corresponding change in the radius of the circular arc of the sample surface. Due to the attendant difficulties, we use a plate-shaped sample instead of an arc-shaped sample. As a result, the X-rays from one point on the focusing circle disperse and do not converge at the point **F** on the receiving slit.

Additionally, because the X-ray source is not an ideal point source, the diffracted X-rays cover a diffuse area rather than converging to a point. This **aberration** is due to geometrical factors associated with the equipment configuration and cannot be eliminated. Consequently, the profile of the diffracted X-rays becomes asymmetrical or increases in width. With the B-B method, a change in the position of the sample surface causes unavoidable changes in the diffraction angle. Since precise measurements of interplanar spacing are essential for obtaining data on distortion in a sample, the parallel beam method is recommended for such applications. Keep this aberration issue in mind when using the B-B method.

If we use a diffractometer that employs a line focus X-ray source similar to the one shown in **Fig. 3.7** and **Fig. 3.8**, we must pay heed to another problem. As illustrated in these figures, vertical Soller slits (VSS) are used to eliminate the effects of X-rays dispersed vertically. When the intervals of the Soller slits are sufficiently reduced, the optical system should provide a parallel beam consisting of many individual parallel rays arranged vertically. However, if we increase the intervals to increase intensity, the vertical divergence angle of the beam will be less restricted, causing the **umbrella effect**,

which results in an asymmetrical profile for the diffracted X-rays. If the diffraction angle $2\theta$ is on the base-angle side past $\pi/2$, the diffracted X-rays exhibit a slope on the base-angle side. If the diffraction angle $2\theta$ is on the high-angle side past $\pi/2$, the diffracted X-rays exhibit a slope on the high-angle side. Examples are shown below.
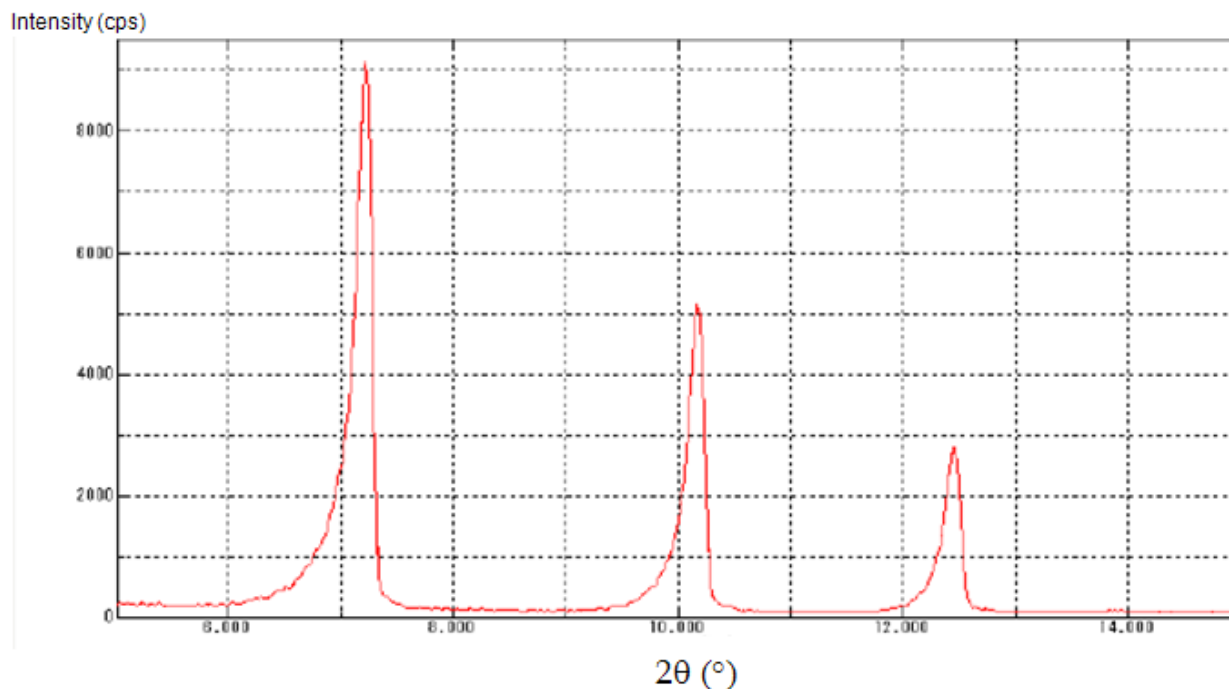


**Fig. 3.12:** X-ray diffraction pattern. The diffraction profile for zeolite-LTA obtained by the B-B method is asymmetrical, with the Bragg reflection exhibiting a slope on the base-angle side. On the high-angle side, however, the asymmetrical pattern shows a gentle slope on the high-angle side.

**Fig. 3.12** shows the results the umbrella effect resulting from CuK$\alpha$ rays diffracted from a zeolite-LTA sample. This material was selected for this example because it features a large lattice constant, and because diffracted X-rays on the base-angle side clearly manifest the umbrella effect. In commonly used optical systems, the vertical Soller slits (VSS) allow 2.5° divergence, while the DS and RS are 0.5° and 0.15 mm, respectively. For the vertical direction, fine Soller slits (VSS) are inserted to suppress the divergence to 0.5°. With the parallel beam method, each Bragg reflection becomes symmetrical, improving resolution. Although this exaggerates the umbrella effect,

intensity is increased roughly seven-fold. Where its drawbacks are not an issue, the B-B method is highly effective.

K$\alpha_1$ and K$\alpha_2$ overlap in the diffracted X-rays 100, but as the order increases to 310, then to 600, two peaks with the intensity ratio of 2:1 become visible.

### 3.4.7 Splitting of Debye-Scherrer ring due to K$\alpha_1$ and K$\alpha_2$ X-rays

If we enlarge the profiles of diffracted X-rays obtained with CsCl, Fe, or Al, we notice that the peak widths of reflections with large indices can be quite wide. **Fig. 3.13** shows the enlarged profiles for three selected diffracted X-rays obtained from CsCl. Although each appears as a single low order peak, they bifurcate as the order increases. We can surmise that these become two independent diffracted X-rays of very high order. Laboratories tend to use *K*$\alpha$ characteristic X-rays with the highest intensity obtainable from any X-ray target, since *K*$\alpha$ characteristic X-rays actually consist of two types of X-rays (called a doublet), distinguished as K$\alpha_1$ and K$\alpha_2$. Their intensity ratio is *I(K*$\alpha_1$*)* : *I(K*$\alpha_2$*)* = 1:2. In passing, the wavelengths of CuK$\alpha_1$ and CuK$\alpha_2$ are 1.54433 Å and 1.54050 Å; the difference between the two wavelengths is *$\Delta\lambda \propto 0.00383$* Å. Thus, the wavelength ratio is *$2.46 \times 10^{-3}$*. The difference between Bragg angles resulting from the wavelength difference is given by *$\Delta\theta = tan\theta\,(\Delta\lambda/\lambda)$*. When *$\theta$* is 70°, *tan70 = 2.75*. Thus, *$\Delta 2\theta$* reaches 0.78°. We must keep this in mind when using high order diffracted X-rays.
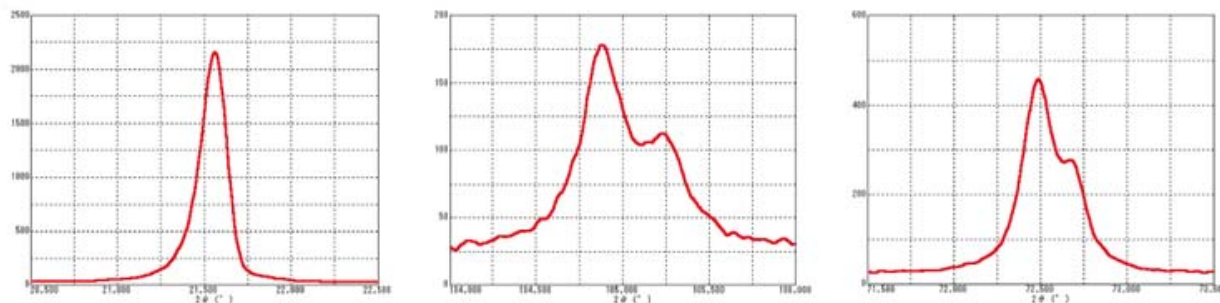


**Fig. 3.13:** Change in profile of diffracted X-rays from CsCl sample

# Chapter 4: Analysis of X-ray Diffraction Profile

This chapter gives actual data obtained with the MiniFlex II. To help provide a general grasp of structural analysis using X-ray diffraction, the following discussion shows how to analyze the data and what information about crystal structures can be obtained from the analysis results.

## 4.1 Examples of measurements with MiniFlex II

**Fig. 4.1** show three examples of data obtained using the MiniFlex II. The samples in these examples are cesium chloride, alpha iron ($\alpha$-Fe), and aluminum (Al). Since an X-ray source with a copper target was used with a tube voltage of 30 kV and a current of 15 mA, the CuK$\alpha$ ray wavelength 1.54 Å) was selected. The DS and RS slits (see **Fig. 3.3**c) are 1° and 0.3 mm, respectively. A pyrolytic graphite crystal (highly orientated graphite crystal: HOPG) was placed in front of the scintillation counter to detect only CuK$\alpha$ rays.
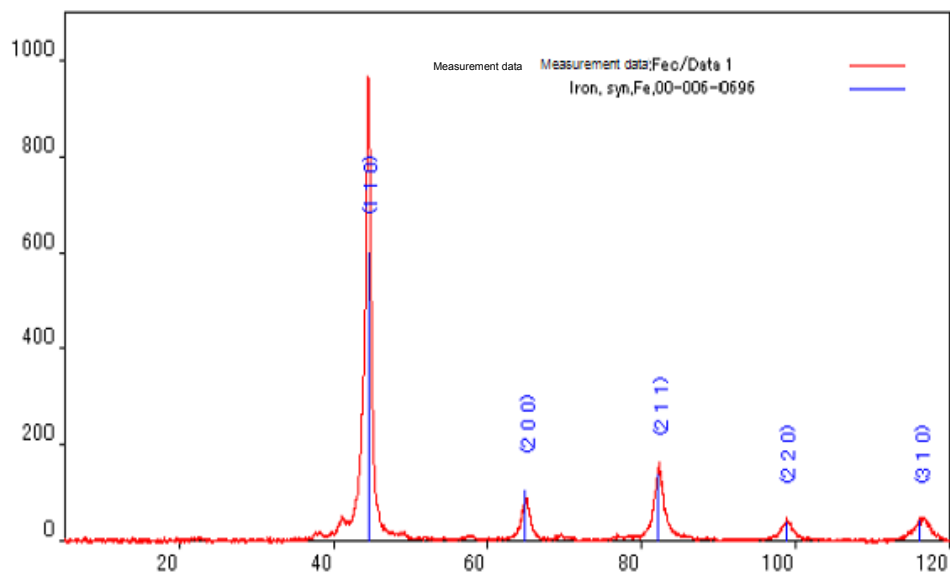


a) $\alpha$ -Fe
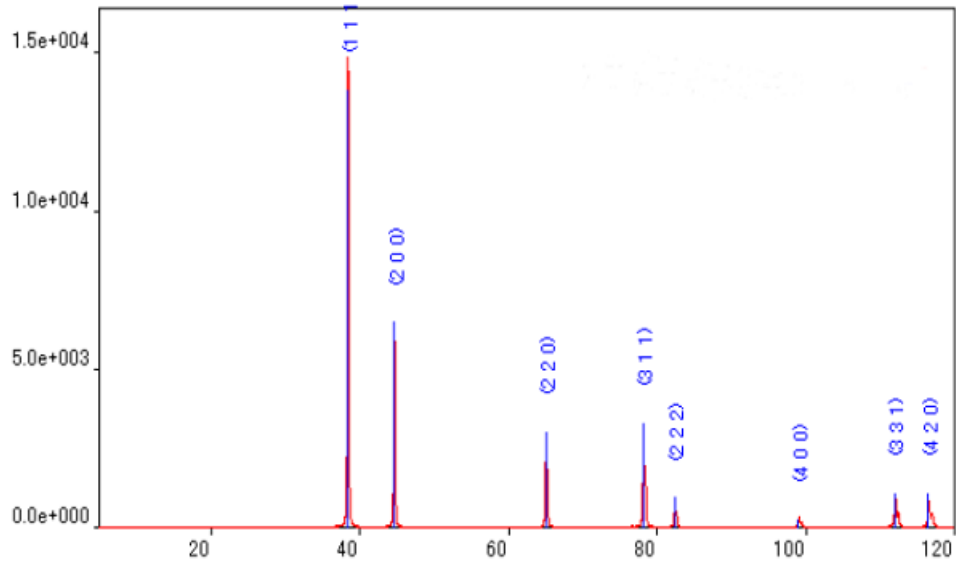
b) Al
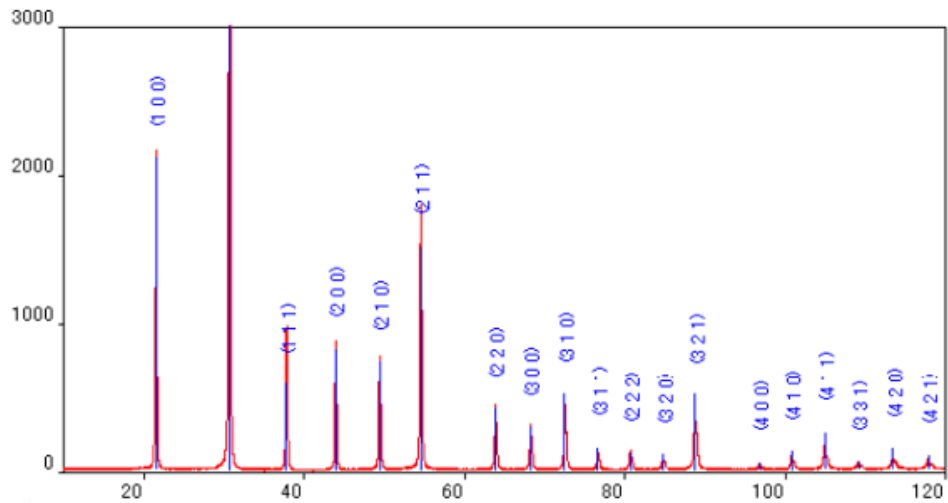


c) CsCl

**Fig. 4.1** Powder X-ray diffraction profiles observed with $\alpha$-Fe, aluminum, and cesium chloride using CuK$\alpha$ rays

Generally, the measured diffraction intensity is indicated in counts/sec (cps) or simply "counts" in a given time period. This value is plotted relative to the scattering angle $2\theta$ (degrees). For the vertical scale that expresses the intensity, a log scale is sometimes used. In the measurements shown here, $2\theta$ is measured at 0.02° intervals, with a measuring time at each point of 1.2 sec.

In **Fig. 4.1**, the diffracted X-rays are already given indices. If we compare these three

patterns, we will notice the following: 1) the Bragg angles $\theta_{hkl}$ of the diffracted X-rays $hkl$ are different in the three graphs, and 2) the patterns of change in the intensity of diffracted X-rays are different in the three graphs. The reason for the former is easy to understand. Although all three crystals are cubic, their lattice constants differ (4.120 Å, 2.866 Å and 4.049 Å for CsCl, $\alpha$-Fe and Al, respectively) resulting in the differences in Bragg angle $\theta_{hkl}$. The reason for the latter observation is that their extinction rules differ due to differences in the crystal structures. While Bragg reflections from all lattice planes are observed in the case of CsCl, only reflections from lattice planes of $h + k + l = 2n$ (i.e., even) are observed in the case of $\alpha$-Fe because it is a body-centered cubic lattice (BCC). On the other hand, Al is a face-centered cubic lattice (FCC); thus, only reflections from lattice planes that are either all odd numbers or all even numbers appear. Mixed reflections from odd-numbered and even-numbered lattice planes are not observed. If we understand the angles that cause diffracted X-rays to appear and the applicable extinction rules, we can associate them with the crystal structure.

We note another distinctive feature. When scattering angle $2\theta$ increases, the overall intensity of all diffracted X-rays decreases, since X-ray scattering is caused by atoms. This topic will be discussed later, along with the extinction rule.

We must keep in mind yet another aspect when using samples shaped like flat plates. Even with polycrystal samples, if the angle of the incident X-rays $\theta$ is the same as the angle $\theta$ of diffracted X-rays in the measurement, as with the B-B method, the lattice planes of the crystal gains being observed are always parallel to the sample surface, as shown in **Fig. 3.7**. This diffraction condition is called the condition of symmetrical reflection.

## 4.2 Indexing diffracted X-rays and determining lattice constant

Indices of diffracted X-rays are indicated in the diffraction profiles of CsCl, Fe, and Al

shown in **Fig. 4.1** since their crystal structures are well known. Assume that we have obtained a diffraction profile from an unknown material using the MiniFlex II. The first step is to index the diffracted X-rays and determine the unit cell. This is a difficult and time-consuming task, but is nevertheless an important first step in structural analysis. In general, we start with highly symmetrical crystal systems with fewer parameters. Specifically, this means we start with cubic or hexagonal crystal systems before proceeding to other crystal systems of more parameters. Although this is a trial-and-error approach, analysis should be performed systematically. Various articles discuss the topic, some dating back to 1949. They are listed below for our reference.

Another indexing method currently used is based on data already compiled. Structures of a great many substances, both organic and inorganic, have been analyzed already, and the data is registered and stored by several organizations, including the IUCr and ICCD. By extracting the structures of substances related to the sample, we can use the data to assign indices. Software available for such purposes can be used to refine the lattice constant of a unit cell. You can also use the application included as part of the PDXL software bundle.

Here, we will take a close look at iron ($\alpha$-Fe), a BCC metal, shown in **Fig. 4.1a**. **Table 4.1** shows possible lattice planes *hkl* in order from largest to smallest with respect to interplanar spacing, assuming a cubic crystal system. The table shows observed diffracted X-rays and the corresponding $2\theta(obs)$ in the next row. The results of calculating $1/(2d_{hkl}) = \sin\theta/\lambda$ using this value and the value of interplanar spacing $d_{hkl}$ are indicated for each, followed by the lattice constant calculated based on each reflection. For reference, the existing lattice constants are given in the last row. Comparing these constants with $a(obs)$ can be helpful for evaluation of errors.

As we can see by examining the table, correct indexing of observed diffracted X-rays is difficult. This is due to unobservable diffracted X-rays, described by the extinction rule discussed in **Chapter 3**. Since incorrect indexing prevents the

determination of certain lattice constants and causes other discrepancies, errors are recognized immediately. If incorrect indexing occurs, we simply repeat the procedure. In the case of BCC above, only diffracted X-rays with indices of $h + k + l = 2n$, such as 110, 200, 211, and 220, are observed. Diffracted X-rays with indices of $h + k + l = 2n+1$ (i.e., odd) do not appear. Proper indexing is possible only when we take the extinction rule into consideration.

| hkl | 100 | 110 | 111 | 200 | 210 | 211 | 220 | 221 | 310 |
|---|---|---|---|---|---|---|---|---|---|
| $2\theta(obs)$ | — | 44.517 | — | 64.998 | — | 82.198 | 98.580 | — | 116.285 |
| $\frac{1}{2}d_{hkl}$ | — | 0.246 | — | 0.349 | — | 0.427 | 0.492 | — | 0.551 |
| $d_{hkl}(obs)$ | — | 2.034 | — | 1.434 | — | 1.172 | 1.016 | — | 0.907 |
| $a(obs)$ | — | 2.876 | | 2.867 | — | 2.870 | 2.874 | — | 2.868 |
| $a\ (calc)$ | — | 2.866 | — | 2.866 | — | 2.866 | 2.866 | — | 2.866 |

**Table 4.1** Interplanar spacing $d_{hkl}$ and $sin\theta/\lambda$ value of $\alpha$-Fe crystal lattice

Indexing diffracted X-rays from a completely unknown sample is considerably more difficult. Without understanding the extinction rule, indexing is a difficult task. However, understanding the extinction rule means that we already have an overview of the sample crystal. This is why we rely on the trial-and-error method.

**References**

- T. Ito: *Nature*, **164** (1949) 755-756

- J. W. Visser: *J. Appl. Cryst.* **2** (1969) 89-XXX

- D. Louer and N. Louer: *J. Appl. Cryst.* **5** (1972) 271-XXX

- Yoshihito Takagi, Tomohiko Taniguchi, Hiroshi Yamaguchi, Hideaki Nakata: *Journal of the Ceramic Society of Japan* 98 (1988) 13

**Problem:** After reading the following chapter, confirm the extinction rule for Al in an experiment using an Al sample and the MiniFlex II.

**Problem:** Examine which reflections in **Table 4.1** disappear and which are not observed. To do so, draw a model of BBC crystal.

## 4.3 Change in the intensity of diffracted X-rays

Looking at the obtained Debye-Scherrer diffraction profiles (observed intensity $I(2\theta)$ relative to $2\theta$) once again, in addition to that of the CsCl sample, we see that the diffraction peaks of a certain width appear against a smooth background. It is hard to identify the cause of the scattering that results in this background, but we can suspect one of the following two factors:

1) the sample contains scatterers (structures) that give a smooth background;

2) the optical system of the equipment does not remove scattered X-rays from a specific direction, due to a malfunction.

In the latter case, we need to determine the cause. In the former, however, the data presents valuable information on scatterers within the sample. Nonetheless, since diffraction peaks are caused by many crystals comprising the sample, we must focus on the crystallite structures that result in diffracted X-rays in our analysis. For the time being, we will not investigate the scatterers that result in this background, focusing instead on our analysis on crystallite structures.

The example of a diffraction profile without a background shown in **Fig. 4.1** can be seen in X-rays diffracted from a CsCl sample. Diffracted X-rays are observed as a peak with a certain width. To determine the reason for this width, we need to examine whether it is attributable to the inferior resolution of the diffraction equipment. All diffractometers have a resolution limitation; this problem cannot be avoided. The resolution capability of the equipment used must be identified in advance. Typically, diffracted X-rays from a material with a large grain size, such as Si and LaB$_8$, are measured and used as a reference. Another factor that gives rise to peak width is closely related to the account given in **Section 3.1**, which explained that the condition for Bragg reflections becomes less strict if the crystallites causing Bragg reflections are small and

the number of lattice planes is also small. This allows the width of the diffracted X-ray beam to be expanded. If the number of lattice planes increases, the condition becomes more restrictive, reducing the width of the diffracted X-ray beam. The width $\Delta2\theta$ of the diffracted X-ray beam is inversely proportional to $L = Nd_{hkl}$ of crystallites in the sample. This represents important information on the crystallites contained in the sample.

Next, we will discuss the height of the peak of the diffracted X-ray beam and diffraction intensity. The height of the peak of the diffracted X-ray beam and the diffraction intensity change significantly, depending on the indices of reflection. This phenomenon is related to the extinction rule discussed in **Section 3.1** and varies in degree, depending on the atomic arrangement in the unit cell. Details are discussed in a later section on the crystal structure factor and extinction rule. Under conditions in which diffraction occurs, X-rays have a peak because scattering by the $N$ number of lattice planes becomes coherent. The scattering amplitude at the peak position should be $N$ times greater than the scattering power of X-rays scattered by the lattice planes. Since the diffraction intensity at a peak position is the square of this value, it is proportional to $N^2$.

Based on the above two factors, the Bragg reflection from a crystallite has a profile in which the intensity $I_p(hkl)$ at the peak position $\frac{1}{2}d_{hkl}$ is proportional to the square of the number of lattice planes in the crystallite, $N^2$, and peak width $\Delta2\theta$ is proportional to $1/N$. The integral value is proportional to the square of the scattering power of the lattice planes in the crystallite and proportional to the number $N$ $(= N^2/N)$ of lattice planes that cause scattering. Confirming the peak position of Debye-Scherrer diffraction in an experiment is difficult, since the peak position often deviates. However, if we observe the profile and obtain the integral value $J_{hkl}$, we can confirm our values with relatively high accuracy. Integral values are often used when discussing the intensity of Debye-Scherer diffraction. The integrated intensity $J_{hkl}$ is given by the following equation:

$$J_{hkl} = \int I_{hkl}(2\theta)\, d2\theta \ \infty\ (I_p \times \Delta 2\theta_B)\,/\,2 \quad (4.1)$$

We must proceed carefully when implementing this integration for Debye-Scherrer diffraction to obtain information on the crystal structure by comparison to the intensity actually measured. Based on the necessary considerations, we can summarize the result in the following equation:

$$J_{h,k,l} \ \infty\ Lp * m_{h,k,l} * A(\mu) * N|F_{h,k,l}|^2 * \Delta\,(sin\ \theta_{hkl} = \tfrac{1}{2}d_{hkl}) \qquad (4.2)$$

In the above equation, $Lp$ is the Lorentz-polarization factor, $m_{h,k,l}$ is the multiplicity, and $A(\mu)$ is the absorption factor. $N$ indicates the number of unit cells that cause diffraction, and $F_{h,k,l}$ is the crystal structure factor expressing the amplitude of the X-rays scattered by the unit cell along direction $hkl$. Conditional equation $\Delta(sin\ \theta_{hkl}\text{-}\tfrac{1}{2}d_{hkl} = 0)$ uses a $\Delta$-function to indicate the scattering angle $2\theta$ that enables the lattice plane $h,k,l$ to satisfy the Bragg condition.

Among the factors, $\Delta(sin\ \theta_{hkl}\text{-}\tfrac{1}{2}d_{hkl} = 0)$ indicates the Bragg condition and gives information pertaining to the crystal lattice. This factor is discussed in **Section 4.1**. A factor describing the extinction rule (dependence of diffraction intensity on the Miller indices hkl) is called the crystal structure factor. Deciphering this factor is the key task in analyzing crystal structures. Analysis shows which atom is located where in the unit cell. If we can clarify the two factors above, we can say that we understand the structure of the crystallite. The other factors in **Equation 4.2** can be regarded as correction factors used in the process to obtain the crystal structure factor from integrated reflection intensity (relative intensity suffices). The physical implications are described below.

## 4.4 Essential correction factors

### 4.4.1 Lorentz-polarization factor

Since X-rays are electromagnetic waves, the component of the electrical field vector

changes each time X-rays scatter. Since the square of the scalar of the electrical field vector is proportional to intensity, a significant change in intensity occurs, depending on the direction of diffraction. The item that reflects this effect is called the polarization factor. In cases of directly measured Debye-Scherrer diffracted X-rays from a powder sample using a detector, the factor is expressed by *(1 + cos²2θ)/2*. When X-rays are monochromatized by a crystal before the detection, the factor is expressed by *(1 + cos²2θ cos²2θ_M)/2*. This applies no matter where the monochromator is located. In this equation, *2θ_M* indicates the angle of X-rays monochromatized by the monochromator. **Appendix A** discusses and illustrates its significance.

When X-rays are irradiated onto a powder sample, X-rays are diffracted in a cone shape, with a diffraction angle of *2θ*. Using a detector, we observe only the X-rays diffracted onto the equatorial plane. In this case, we must calculate the percentage of the quantity of crystallites that contribute to the Bragg reflection with the indices of *hkl* in question. This calculation shows that the change 1 / *(sinθsin2θ)* occurs, depending on diffraction angle *2θ*. This is called the Lorentz factor. The integrated reflection intensity contains two factors that depend on scattering angles, collectively called the Lorentz-polarization factor (LP factor) and expressed by the following equation:

$$LP = (1+cos^2 2\theta)/(sin\theta sin2\theta) \qquad (4.3)$$

Note: Solving this equation requires the concept of a reciprocal lattice. The Appendix explains the concept of a reciprocal lattice and how to derive the LP factor.

### 4.4.2 Multiplicity

For the sake of discussion, assume that the sample crystal has a cubic crystal system. Suppose that the lattice plane *h00* causes diffraction. For this Bragg reflection, lattice planes *0h0* and *00h* should contain crystallites in an orientation causing Bragg reflections. The corresponding probability is the same as with crystallites in the lattice

plane *h00*. We can say the same for lattice planes $\bar{h}00$, $0\bar{h}0$, and $00\bar{h}$. In short, the Bragg reflection *h00* contains a total of six lattice planes. This means that the reflection *h00* has six equivalent planes. Next, consider the lattice plane *hk0*. The lattice planes $\overline{hk}0$, $h\bar{k}0$, $\bar{h}k0$ as well as the lattice planes *kh0*, $\bar{k}h0$, $k\bar{h}0$、$\overline{kh}0$ contribute to Bragg reflection with equal probability. This also applies to the lattice planes *0hk* and $0\bar{h}k$. In a cubic crystal system, there are 24 equivalent lattice planes for the Bragg reflection of the above indices. We infer that larger numbers of equivalent lattice planes mean more planes contributing to Bragg reflection. This must be taken into consideration. The number of equivalent lattice planes is referred to as **multiplicity**, and this factor is included in integrated reflection intensity. Here, the coefficient is indicated by $m_{hkl}$. In a cubic crystal system, $m_{hkl}=48$ for any *h,k,l*. This is more easily understood if we perform the following calculations in the proper sequence. First, calculate the number of possible equivalent planes in the first quadrant. In the plane *h,k,l*, if we exchange *k* with *l* while *h* is fixed, we have *h,l,k*. Next, in the plane *k,h,l* in which *k* and *h* have been exchanged, there exists a plane *k,l,h* in which *h* and *l* are exchanged, with *k* fixed. Similarly, there is a possibility of the plane *l,h,k* in the plane *l,k,h* in which *l* and *h* have been exchanged. We see that there are six equivalent planes in the first quadrant. A cubic crystal system contains eight equivalent quadrants, with 48 planes in total (*6 × 8 = 48*). This is the maximum value.

We should also perform calculations for other crystal systems. There are 16 planes in a tetragonal crystal system and eight planes in an orthorhombic crystal system. We can easily make a mistake in counting the number of equivalent lattice planes in ordinary crystal systems if we fail to consider the symmetrical property. We must proceed carefully.

### 4.4.3 Absorption correction

With the B-B method, the measurement condition requires the incident angle of the incident X-rays on a sample with a flat plate shape to be the same as the emergent angle

of the diffracted beams. This is called the condition of symmetrical reflection. In the following, we will look at common asymmetry and see what happens when its special condition is for symmetrical reflection. We can examine the absorption of X-rays when the incident X-rays with incident angle $\theta_1$ are diffracted by a flat-plate sample at angle $\theta_2$. The absorption coefficient $A(\mu)$ can be analytically obtained as shown in **Appendix C-3** and is given by the following equation:

$$A(\mu) = sin\theta_2 / (sin\theta_1 + sin\theta_2) \cdot \mu \qquad (4.4)$$

In the B-B diffractometer, the sample plate and detector are driven by the $\theta-2\theta$ scan system to maintain the condition of symmetric reflection for a plate-shaped sample at all times. When $\theta_1 = \theta_2$, **Equation 4.4** is significantly simplified as follows:

$$A(\mu) = \frac{1}{2}\mu \qquad (4.5)$$

The value remains constant, unaffected by incident angle $\theta$. However, the value of $\mu$ can change depending on the method of sample preparation, and careful attention is required. When the value of $\mu$ is large, X-rays do not penetrate deeply, leaving only the sample surface as the valid plane. The value of $A(\mu)$ is regarded as constant and incorporated into the proportionality constant. It does not affect integrated intensity in the slightest. If the value of $\mu$ is small, however, the value of $A(\mu)$ changes depending on sample thickness. Thus, the calculations must be performed correctly. If the sample surface is noticeably irregular, absorption varies between areas that result in smaller scattering angles and areas that result in large scattering angles. This is yet another factor to keep in mind.

## 4.5 Factors deriving from crystal structure

### 4.5.1 Crystal structure factors and the extinction rule

As stated earlier, the crystal structure factor $F(h,k,l)$ is the amplitude of X-rays scattered

by the unit cell along direction *hkl*. Now, assume a crystallite with a simple unit cell in which one atom is located at the origin (0, 0, 0) and a different atom is located at the coordinates $r_1(x_1, y_1, z_1)$ (see **Fig. 4.2a**). Consider the corresponding X-ray scattering and diffraction phenomena. X-rays are irradiated onto the unit cell from direction $s_i$ and scattered along direction $s_f$. The amplitude of the X-ray waves is given by $F(s_i, s_f)$. The value of $F(s_i, s_f)$ can be expressed by the following equation:

$$F(s_i, s_f) = f_0 + f_1 \exp\{(2\pi i / \lambda)(s_i - s_f)r_1\} \qquad (4.6)$$

In the **Equation 4.6**, $f_0$ and $f_1$ indicate the atom scattering amplitudes at positions (0, 0, 0) and $(x_1, y_1, z_1)$. The first term of the equation indicates the wave scattered along direction $s_f$ and with amplitude $f_0$ from the incident X-rays entering along direction $s_i$. The second term indicates the addition of the scattering amplitude $(f_1)$ for an atom positioned at $(x_1, y_1, z_1)$. However, since the position of that atom is shifted by $r_1$, the atom is displaced from the scattering wave indicated by the first term. Hence, we must incorporate the phase difference. This is the reason for adding the phase term $\exp\{(2\pi i / \lambda)(s_i - s_f)r_1\}$ to the equation. In **Equation 4.6**, $s_i$-$s_f$ is the vector representing the direction of propagation of the X-rays.
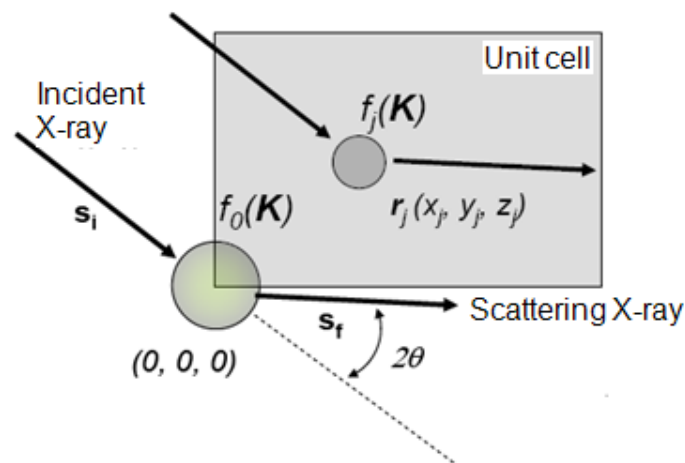


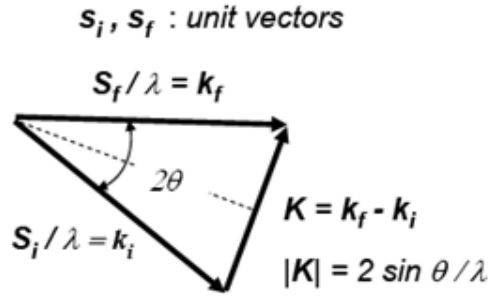**Fig. 4.2(a)** X-ray scattering caused by unit cell

**Fig. 4.2 (b)** Change of X-ray direction of propagation and scattering vectors

The change of wave number vector is indicated by $(s_i\text{-}s_f)/\lambda$, which is obtained by dividing the above value by the wavelength, as shown in **Fig. 4.2b**. This is called the scattering vector and indicated by $K$. Given this, the phase item can be expressed easily as $exp(2\pi iKr_1)$. Here, $Kr_1$ indicates the scalar product. Consequently, the scattering amplitude of a unit cell containing many atoms (crystal structure factors) can generally be expressed by the following equation:

$$F(K) = \Sigma_j f_j(K) \, exp(2\pi i \, Kr_j) \qquad (4.7)$$

As shown in **Fig. 4.2b**, the scalar component of the scattering vector $K$ is $2 \sin \theta/\lambda$, where $2\theta$ is the scattering angle. Since the scattering caused by atoms depends on scattering angle $2\theta$ (described further below), $f_j(K)$ is used as the fraction of $K$ to express it. The scalar product $Kr_j$ in **Equation 4.7** becomes $|K| = 2 \sin \theta/\lambda = 1/d_{hkl}$ at the location where $K$ satisfies the condition of Bragg reflection. Using the expression $d_{hkl}$ shown in **Equation 2.3** in Chapter 2, we can simply rewrite the equation as follows: $Kr_j = hx_j + ky_j + lz_j$. Given Bragg reflection indices $h,k,l$ and the coordinates $(x_j, y_j, z_j)$ of the atom, we can easily calculate the crystal structure factor using the following equation:

$$F(h,k,l) = \Sigma_j f_j(\sin \theta / \lambda) \, exp\{2\pi i \, (hx_j + ky_j + lz_j)\} \quad (4.8)$$

**Equation 4.8** yields the **scattering factor** of a unit cell, or the **scattering amplitude**. This is called the **crystal structure factor**. This factor is a physical quantity that directly reflects the crystal structure.

Bragg reflection is a diffracted wave resulting from the scattering and interference of X-rays scattered by crystal lattices formed by periodically arranged unit cells. When the number of unit cells contributing to interference is given by $N$, the amplitude of Bragg reflection is a product obtained by multiplying $F(h,k,l)$ by $N$. Thus, the diffraction intensity is proportional to the square of this value and is given by $N^2|F(h,k,l)|^2$.

### 4.5.2 Atomic scattering factor

In the following, we discuss the scattering amplitude $f_j(K)$ of X-rays scattered by atom $j$. The explanation aims to deepen our understanding that the amplitude changes according to the scalar component ($|K| = sin\ \theta/\lambda$) of the scattering vector $K$.

Elastic scattering (scattering without energy transfer in the process) by charged X-ray particles is known as **Thomson scattering**, and the scattering amplitude is known to be $e^2/mc^2$, where $e$ indicates the electrical charge of the charged particles, $m$ expresses mass, and $c$ is the speed of light. Since X-rays are electromagnetic waves, they deflect along the direction of the electrical field vector. The change in the deflection direction must be taken into consideration. When this effect is treated separately, Thomson scattering becomes isotropic scattering. Isotropic scattering means scattering occurs in all directions with equal probability, and the scattering amplitude is a constant value, $e^2/mc^2$.

Since an atom is made up of a positively charged nucleus and the negatively charged electrons that surround the nucleus, scattering of X-rays by an atom is regarded as Thomson scattering from a structure configured with such charged particles. However, since the mass $m$ of the nucleus is substantially greater than that of the electrons, the Thomson scattering factor of the scattering caused by the nucleus is so small that it can be ignored. As a result, only Thomson scattering due to the distribution $\rho(r)$ of the electrons around the nucleus is considered and regarded as the **atomic scattering factor**. Hence, it can be calculated by multiplying $\rho(r)$ by the phase item

*exp{2πiKr}* and by integrating the product.

$$f_j(\mathbf{K}) = \int \rho_j(\mathbf{r})\, exp\{2\pi i\mathbf{K}\mathbf{r}\}d\mathbf{r} \qquad (4.9)$$

This equation without Thomson scattering factor $e^2/mc^2$ indicates the scattering amplitude attributable to the atomic structure, or the **atomic structure factor**. In the 1930s, various charge distribution patterns were hypothesized and reliable calculated values reported. Recommended values are listed in the *International Tables for Crystallography* Vol. III p. 201 (1960) and *International Tables for Crystallography C* (1990) published by the International Union of Crystallography. Please refer to these reference materials.
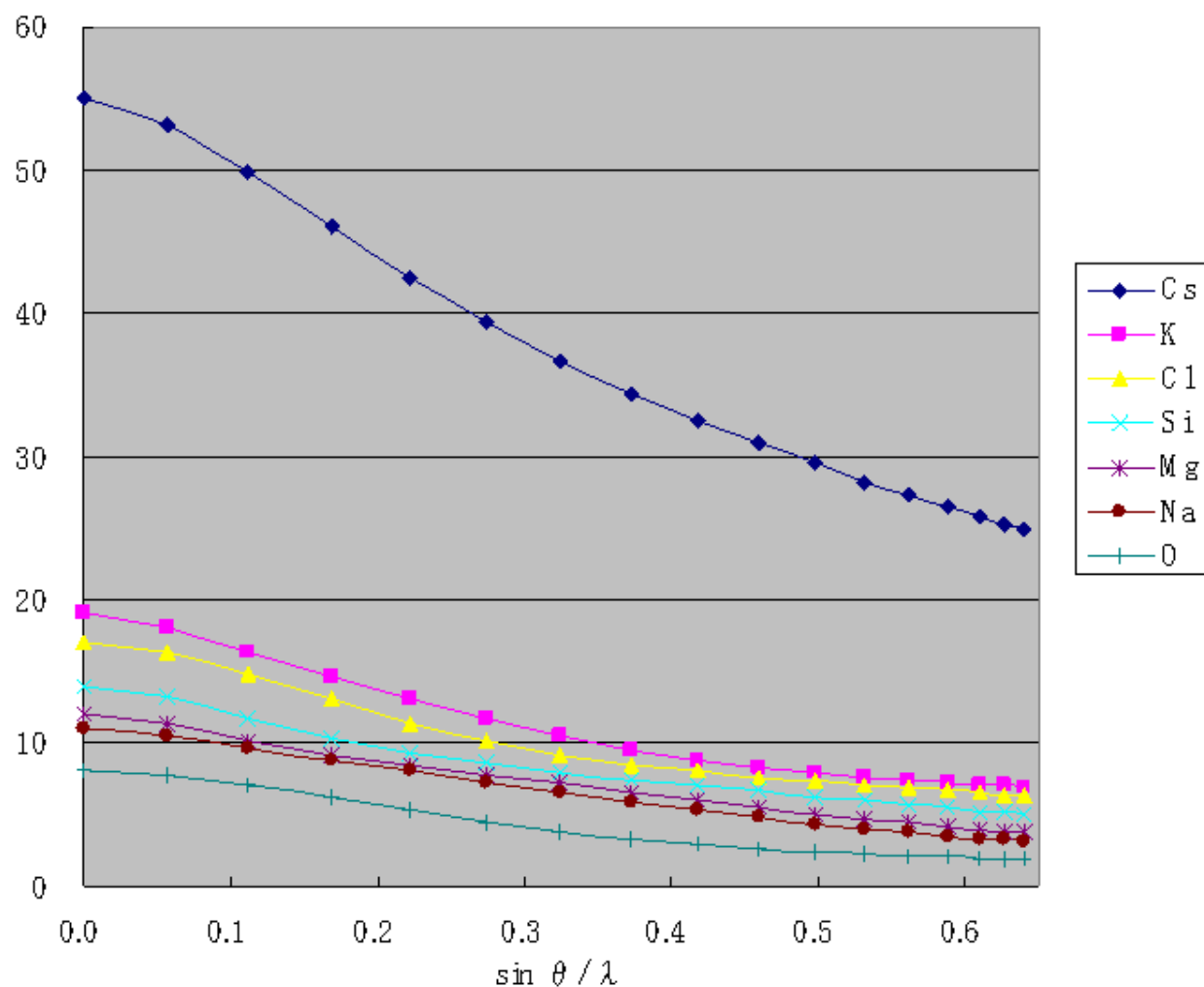


**Fig. 4.3** Atomic scattering factors

In **Fig. 4.3**, atomic scattering factors for several elements including Cs and Cl are plotted relative to *sin θ/λ*. As we can see, *sin θ/λ* is expressed by a curve that shows the gradual attenuation of the scattering amplitude when the scattering angle increases from 0. This means this scattering is "strong in the forward direction and weak in the backward direction" (characteristic of forward scattering). In the previous chapter, diffracted images resulting from a number of different materials were shown. In those examples, the intensity of diffracted X-rays became significantly weaker when the scattering angle increased. Now we can understand that this phenomenon stemmed from the above fact.

The table of atomic scattering factors is immense, and using the table to calculate crystal structure factors is inconvenient. An equation that uses several Gaussian functions to approximate the above curve has been proposed[3].* The following is a commonly used equation that uses four Gaussian functions for approximation.

$$f(\sin\theta/\lambda) = \sum_{j=1}^{4} A_j \exp\left\{-a_j(\sin\theta/\lambda)^2\right\} \quad (4.10)$$

The constant $A_j\, a_j\ (j = 1, ...4)$ varies for each element and can be obtained from the table. **Table 4.2** shows some examples.

**Problem:** By referring to Table 4.2, plot $f(\sin\theta/\lambda)$ in a graph.

| Atom | a1 | b1 | a2 | b2 | a3 | b3 | a4 | b4 |
|------|------|------|------|------|------|------|------|------|
| O | 3.0485 | 13.2771 | 2.2868 | 5.7011 | 1.5463 | 0.3239 | 0.8670 | 32.9089 |
| Na | 4.7626 | 3.2850 | 3.1736 | 8.8422 | 1.2674 | 0.3136 | 1.1128 | 129.4240 |
| Mg | 5.4204 | 2.8275 | 2.1735 | 79.2611 | 1.2269 | 0.3808 | 2.3073 | 7.1937 |
| Si | 6.2915 | 2.4386 | 3.0353 | 32.3337 | 1.9891 | 0.6785 | 1.5410 | 81.6937 |
| Cl | 11.4604 | 0.0104 | 7.1964 | 1.1662 | 6.2556 | 18.5194 | 1.6455 | 47.7784 |
| K | 8.2186 | 12.7949 | 7.4398 | 0.7748 | 1.0519 | 213.1870 | 0.8659 | 41.6841 |
| Cs | 20.3892 | 3.5690 | 19.1062 | 0.3107 | 10.6620 | 24.3879 | 1.4953 | 213.9040 |

**Table 4.2** Table of constants of atomic scattering factors approximated using two Gaussian functions

[3] References: V. Vand, P. F. Eiland & R Pepinsky: *Acta Cryst.* **10** (1957) 303; J. B. Forsyth & M. Wells: *Acta Cryst.* **12** (1959) 412

A few items are worth noting regarding atomic scattering factors. One is that when the value $sin(\theta/\lambda)$ becomes 0, the value of the scattering factor equals the atomic number Z due to being in a fully charged state, as we see when we substitute K = 0 into **Equation 4.9**. When atoms are ionized, the total number of electrons Z increases by only *m*, as shown by Z ± m, and this effect takes place on the base-angle side of the scattering factor. This calculated value is obtained from the computation based on the assumption that the electron distributions in all atoms are spherical. If atoms are bonded with covalent bonds, the electron distribution is distorted. In the case of light elements in particular, the percentage of bonded electrons is high in all electrons. The effect of the distortion is significant, but this effect is not reflected in the table. Anisotropic atomic scattering factor is sometimes involved. Refer to the following reference materials for further discussion of this topic.

[Include a list of reference materials]

### 4.5.3 Temperature factor

The temperature factor, $T_j(sin\theta/\lambda)$, is called the Debye-Waller factor. For a discussion of how this value is obtained, refer to **Appendix B7**. The following discussion focuses on the necessity of the temperature factor and presents some equations.

In **Equation 4.7**, used to calculate the crystal structure factor, and **Equation 4.8**, the position of the atom is assumed to be $r_j$ *(xi, yj, zi)*. In actual crystals, however, thermal oscillations of the lattices cause entire crystal lattices to oscillate, resulting in changes over time. The square of the amplitude of oscillation increases in proportion to absolute temperature *T* in a harmonic approximation range. The degree of oscillation varies according to the measurement temperature. Thus, the position of an atom in a unit cell is written $r_j(t) = <r_j> + u_j(t)$, reflecting the change occurring over time *t*. When this is substituted into the equation for the structure factor, we obtain the function *F( hkl, t)*, which indicates that the structure factor also changes with time. How large is this

change? Based on lattice oscillations, the change is on the order of picoseconds. In comparison, even the shortest time for the observation of scattered X-rays is on the order of milliseconds. The observation result is an average of values that varies over a very long period of time. The structure of crystals observed using X-ray diffraction is, therefore, a space average and a time average. Time average and space average are the same, and the average structure factor can be expressed by the following equation:

$$<F(K)> = \Sigma_j f_j(K) T_j(K) \, exp(2\pi i \, K <r_j>) \quad (4.11)$$

In **Equation 4.11**, $< >$ indicates that a statistical average is used, while $<r_j>$ indicates the equilibrium position of the j-atom. $T_j(K)$ is a correction item for the thermal oscillation relating to the atomic scattering factor $f_j(K)$. This is called the temperature factor. Using isotropic approximation that assumes that the amplitude of thermal oscillation of an atom is the same in any direction, we can obtain $T_j(sin\ \theta/\lambda)$ with the following equation:

$$T_j(sin\,\theta/\lambda) = exp\{- 8\pi^2 <u_j^2>(sin\,\theta/\lambda)^2\} \quad (4.12)$$

$$8\pi^2 <u_j^2> = B_j \quad (4.13)$$

Here, $u_j$ indicates the amount of displacement from the average atom position, $<r_j>$, in the unit cell occupied by the j-atom due to thermal oscillation. $<u_j^2>$ is a thermal average of the square of the "displacement." There are several ways to calculate the thermal average of $<u_j>$ associated with the thermal oscillation of the lattices. However, in the range in which we can use an approximation of harmonic potential, this can be treated as the thermal oscillation of an atom of mass $m$ in the potential expressed by the quadratic curve shown in **Fig. 4.3a**. This value changes depending on the measured temperature, but is generally proportional to absolute temperature T in a region where statistical mechanics allows for high-temperature approximation. The value $B_j$ obtained by multiplying the above average value by $8\pi^2$ is called the **temperature parameter**.

This parameter must be determined together with the atomic coordinates in crystal structure analysis. If we take a closer look at **Equation 4.12**, we observe a Gaussian function. An increase in the value of $\sin\theta/\lambda$ further reduces the atomic scattering factor, since the above factor is multiplied by the atomic scattering factor. The degree of this decrease becomes greater when $<u_j^2>$ is large. As shown in **Fig. 4.4**, in actual space, atoms with the electron distribution $\rho(r)$ are placed in a potential expressed by the quadratic function, and thermal oscillations take place near the equilibrium position $<r_j>$. Thus, the electron distribution is apparently in a spread condition, as represented by $\rho'(r)$.
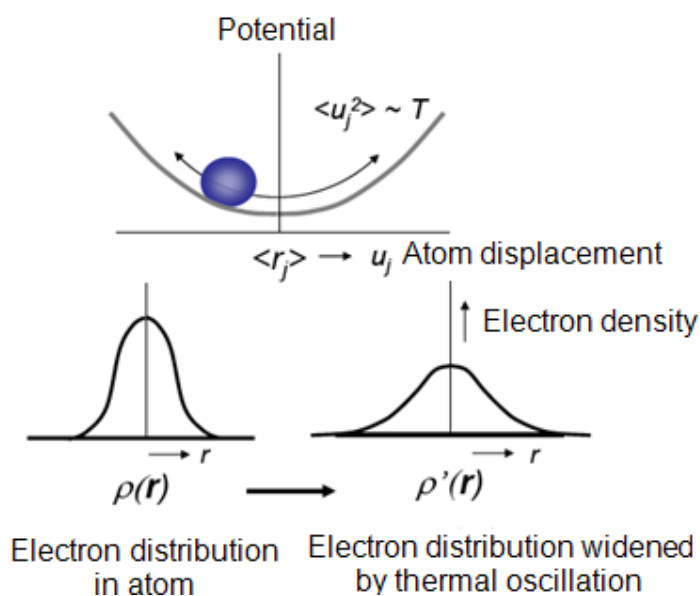


**Fig. 4.4** Spreading of an atomic charge distribution due to thermal oscillation of lattices

Ordinarily, the value of $B_j$ is large for crystals with a low melting point and small for crystals with high melting points. If the value of $B_j$ obtained in a structural analysis is abnormally large or small, an underlying factor may be responsible. For example, the absorption coefficient may have changed due to the scattering angle; or the irradiated region may have changed due to the scattering angle. Careful attention is in order.

The Gaussian function in **Equation 4.12** is isotropic. This is because the equation was developed based on the assumption that the thermal oscillation of atoms is

isotropic. However, atoms in a crystal are not necessarily in an isotropic environment. In such cases, we must derive an anisotropic temperature factor. This booklet does not delve further into this topic. For a discussion of the thermal oscillation of atoms in an anisotropic potential, refer to the article: Makoto Sakata, Jinpei Harada, *Journal of the Crystallographic Society of Japan* **22** (1980) 387-403.

## 4.6 Simulation of diffraction intensity

Measurement of the diffraction $2\theta$ at which Debye-Scherrer diffracted X-rays are observed provides information on the crystal system. We can focus on the change in intensity of the diffracted X-rays to obtain information on the crystal structure. Discussed below are specific procedures for analysis using the value observed from CsCl.

The second column of **Table 4.3** gives the values of the diffraction angle $2\theta(obs)$ at which diffracted X-rays are observed. The interplanar spacing $d$ as calculated from the diffraction angle is also indicated. The sample is the familiar CsCl, which is cubic. The crystal lattices are indexed based on this assumption. The indices are given in the fifth column of the table. The seventh column shows the lattice constants $\alpha(obs)$ calculated from the diffraction angle $2\theta(obs)$ based on these indices. All obtained values should be identical to the lattice constant. To see their deviations, we plot $\alpha(obs)$ in relation to the observation angle $2\theta$ (**Fig. 4.5a**). Clearly, the value measured with diffracted rays on the base-angle side differs significantly from the value obtained from the observation on the high-angle side. Based on the equation for Bragg reflection, we see that using diffracted X-rays on the base-angle side produces large errors. For precision measurements of the lattice constant, we need to use the diffracted rays on the high-angle side.

The extinction rule seen with Bragg reflection becomes clearer if we calculate the crystal structure factor. In the discussion about extinction rule in Section 3.2, we have

noted that if we know the crystal structure, we can calculate the crystal structure factor and determine what extinction rule applies. Using CsCl as an example, we will demonstrate that the above is true and try to deepen our understanding of the integrated reflection intensity **Equation 4.2**.

As is well known, CsCl is a cubic crystal with a molecule in each unit cell and Cs and Cl atoms located at the following coordinates:

$$Cs: (0, 0, 0) \quad Cl: (½, ½, ½)$$

We can substitute these into **Equation 4.8**. Given atomic scattering factors $f_{Cs}$ and $f_{Cl}$, we thereby obtain the following equation:

$$F(h,k,l) = f_{Cs} + f_{Cl}\, exp\{\pi i\, (h + k + l)\} \quad (4.12)$$

This gives the crystal structure factor for CsCl. If we plug $h + k + l = 2n$ into this equation, $exp\{\pi i\, (h + k + l)$ becomes 1. If we plug $h + k + l = 2n+1$ into this equation, $exp\{\pi i\, (h + k + l)$ becomes $-1$. Thus, we obtain the following extinction rule:

$$When\ h + k + l = 2n:\ F(h,k,l) = f_{Cs} + f_{Cl} \quad (4.13\ a)$$

$$When\ h + k + l = 2n+1:\ F(h,k,l) = f_{Cs} - f_{Cl} \quad (4.13\ b)$$

For indices $h,k,l$, the phase of the diffracted X-rays for which $h + k + l$ is an even number will be the same for X-rays scattered by Cs and Cl atoms; the diffracted X-rays are mutually reinforcing. The scattering amplitude or structure factor becomes $f_{Cs} + f_{Cl}$. On the other hand, the phase of diffracted X-rays for which $h + k + l$ is an odd number will be opposite, and the diffracted X-rays are mutually attenuating. The structure factor becomes $f_{Cs} - f_{Cl}$. Since intensity is proportional to the square of this value, this tendency demonstrates that the extinction rule shown above is valid.

| No. | 2θ (deg) | Imas | d | hkl | $h^2+k^2+l^2$ | a | fcs | fcl | F | m | (LP) | Ical =m F²(LP) | Imas/Ical |
|---|---|---|---|---|---|---|---|---|---|---|---|---|---|
| 1 | 21.534 | 265.6 | 4.123 | 100 | 1 | 4.1233 | 49.3 | 14.9 | 34.4 | 6 | 47.2 | 342.4 | 0.78 |
| 2 | 30.676 | 1000.0 | 2.912 | 110 | 2 | 4.1184 | 45.8 | 12.9 | 58.8 | 12 | 23.6 | 1000.0 | 1.00 |
| 3 | 37.772 | 145.9 | 2.380 | 111 | 3 | 4.1219 | 43.2 | 11.7 | 31.6 | 8 | 15.9 | 128.9 | 1.13 |
| 4 | 43.903 | 123.8 | 2.061 | 200 | 4 | 4.1212 | 41.1 | 10.8 | 51.9 | 6 | 12.0 | 197.4 | 0.63 |
| 5 | 49.398 | 129.4 | 1.843 | 210 | 5 | 4.1221 | 39.5 | 10.1 | 29.4 | 24 | 9.6 | 203.4 | 0.64 |
| 6 | 54.507 | 336.4 | 1.682 | 211 | 6 | 4.1204 | 38.0 | 9.6 | 47.6 | 24 | 8.1 | 448.3 | 0.75 |
| 7 | 63.857 | 82.0 | 1.457 | 220 | 8 | 4.1197 | 35.7 | 8.8 | 44.6 | 12 | 6.2 | 149.7 | 0.55 |
| 8 | 68.230 | 60.4 | 1.373 | 300 | 9 | 4.1203 | 34.8 | 8.6 | 26.2 | 6 | 5.5 | 116.4 | 0.52 |
|  | 68.230 |  | 1.373 | 221 | 9 | 4.1203 | 34.8 | 8.6 | 26.2 | 24 | 5.5 |  |  |
| 9 | 72.478 | 89.2 | 1.303 | 310 | 10 | 4.1206 | 33.9 | 8.3 | 42.3 | 24 | 5.0 | 219.8 | 0.41 |
| 10 | 76.619 | 26.8 | 1.243 | 311 | 11 | 4.1212 | 33.1 | 8.1 | 25.0 | 24 | 4.6 | 70.8 | 0.38 |
| 11 | 80.685 | 30.7 | 1.190 | 222 | 12 | 4.1220 | 32.4 | 8.0 | 40.4 | 8 | 4.3 | 57.2 | 0.54 |
| 12 | 84.718 | 20.7 | 1.143 | 320 | 13 | 4.1221 | 31.7 | 7.8 | 23.9 | 24 | 4.0 | 56.4 | 0.37 |
| 13 | 88.724 | 112.1 | 1.102 | 321 | 14 | 4.1222 | 31.1 | 7.7 | 38.8 | 48 | 3.8 | 279.5 | 0.40 |
| 14 | 96.747 | 10.4 | 1.031 | 400 | 16 | 4.1221 | 29.9 | 7.4 | 37.3 | 6 | 3.5 | 29.5 | 0.35 |
| 15 | 100.787 | 27.2 | 1.000 | 410 | 17 | 4.1224 | 29.4 | 7.3 | 22.1 | 24 | 3.3 | 79.5 | 0.34 |
|  | 100.787 |  | 1.000 | 322 | 17 | 4.1224 | 29.4 | 7.3 | 22.1 | 24 | 3.3 |  |  |
| 16 | 104.889 | 46.9 | 0.972 | 411 | 18 | 4.1224 | 28.9 | 7.2 | 36.1 | 24 | 3.2 | 154.5 | 0.30 |
|  | 104.889 |  | 0.972 | 330 | 18 | 4.1224 | 28.9 | 7.2 | 36.1 | 12 | 3.2 |  |  |
| 17 | 109.061 | 13.6 | 0.946 | 331 | 19 | 4.1227 | 28.4 | 7.1 | 21.3 | 24 | 3.2 | 35.0 | 0.39 |
| 18 | 113.364 | 31.4 | 0.922 | 420 | 20 | 4.1225 | 27.9 | 7.0 | 34.9 | 24 | 3.1 | 92.9 | 0.34 |
| 19 | 117.802 | 20.6 | 0.900 | 421 | 21 | 4.1225 | 27.5 | 6.9 | 20.6 | 48 | 3.1 | 64.0 | 0.32 |

**Table 4.3** Extinction rule for CsCl and comparison of calculated integrated intensity values and actual measurements

We can make our calculations more concrete. The tenth row of **Table 4.3** shows the results of calculations to obtain the crystal structure factor for CsCl for the indices *hkl*, $F_{hkl}$ *(calc)*, by substituting a numeric figure for the atomic scattering factor. **Fig. 4.5b** is a graph produced by plotting $F_{hkl}$ *(calc)* in relation to the diffraction angle *2θ*. By looking at these results, we can confirm the extinction rule of **Equation 4.13a** and **Equation 4.13a**. The 13th row of **Table 4.3** gives the integrated intensity $J_{hkl}$ *(calc)* obtained by multiplying $F_{hkl}$ by itself and then multiplying the result by the correction items, calculated multiplicity $m_{hkl}$ and the $L_P$ factor. Since this value can be compared to actual measured values, its ratio to $J_{hkl}(obs)/J_{hkl}$ *(calc)* is shown in the 14th row of the table.

**Fig. 4.5c** is a graph produced by plotting $J_{hkl}(obs)/J_{hkl}$ *(calc)* for *2θ* of each diffracted beam. If the calculated integrated intensity is consistent with actual measurements, it should be constant, regardless of the relationship to *2θ*. While diffracted X-rays demonstrate some fluctuations, they tend to decrease with *2θ*, as indicated by the guide line in the figure. This means that any overestimates of the calculated value are likely to

increase when the value of *2θ* increases. In the calculations above, while the results do not correspond systematically to actual measurements, this discrepancy is easily attributable to the omission of the temperature factor in the above discussion. Introducing the temperature factor will improve accuracy.

The atoms and molecules in a crystal are always oscillating due to crystal lattice oscillations, resulting in continuous fluctuations. Within a harmonic approximation range, the degree of fluctuation increases in proportion to temperature. The effects of thermal oscillation cannot be ignored even at room temperature and attenuate the intensity of diffracted rays of high-order indices.

In an expanded simulation example, if the locations of Cs and Cl atoms are also occupied by Fe atoms, the structure becomes a body-centered cubic lattice. In this case, diffracted X-rays for which $h + k + l$ is an even number appear and the value becomes $2f_{Fe}$. However, diffracted X-rays for which $h + k + l$ is an odd number become 0 and disappear completely. This is consistent with the extinction rule for the BCC crystal structure. Check **Fig. 4.1** to verify that the diffraction profile indicates the phenomena mentioned above.
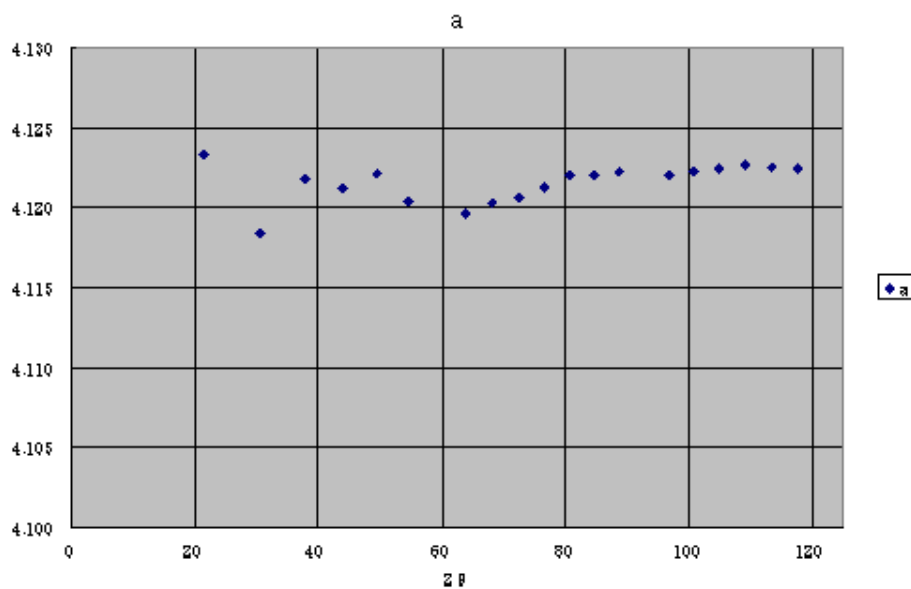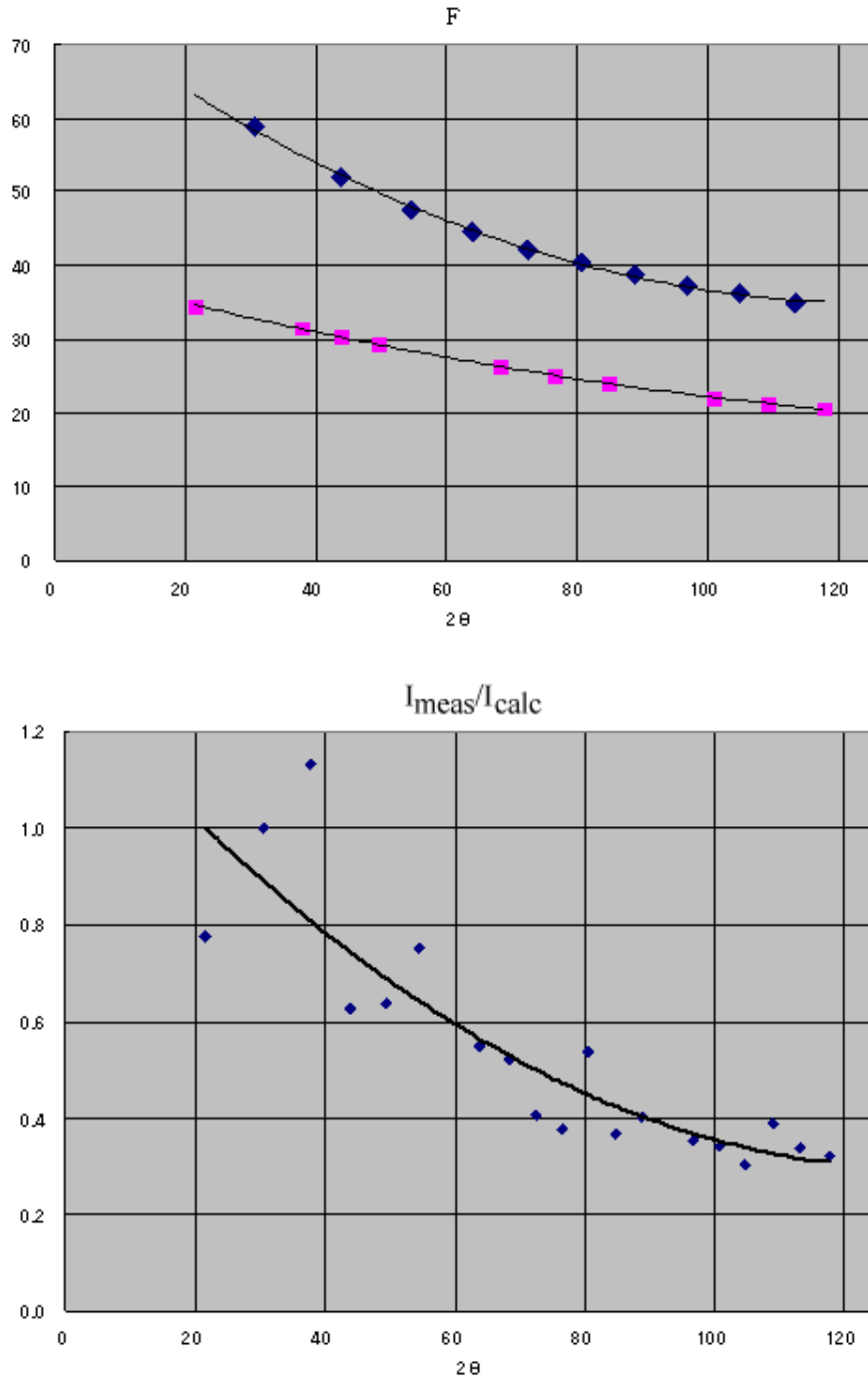
**Fig. 4.5** *2θ* versus *J(Obs)/J(Calc)*. As the value of *2θ* increases, the systematic discrepancy of *J(Obs)/J(Calc)* becomes more pronounced.

# Chapter 5: Identification and Characterization of Polycrystalline Materials by X-Ray Diffraction

X-ray diffractometers are used for crystal structure analysis; that is, to examine unknown materials at the atomic level and determine their crystal structures. Extensive past research has examined and identified the crystal structures of many materials. The resultant data has been compiled and stored by several organizations, giving us access to extensive databases. Comparing this data to the diffracted X-rays obtained from an unknown material lets us determine what crystallites a sample contains and makes it possible to subject a sample to structural analysis as part of a process we call *identification*. The following chapter discusses the procedures involved in this process and how they can be used to characterize the state of a material.

## 5.1 Identification (qualitative analysis)

In qualitative analysis by X-ray diffraction, we compare the diffraction patterns obtained from an unknown material against the diffraction patterns of known materials. If the measured data contains diffraction patterns previously recorded for known materials, the sample is determined to contain these materials. Due to the technique used, qualitative analysis based on the powder X-ray diffraction method is called *identification*. This term has a unique meaning in the field of X-ray diffraction. The accuracy of the analysis we perform depends significantly on the reliability of the diffraction profiles for known materials used for comparison. The database most often used is called the ICDD (International Center for Diffraction Data) database. The International Center for Diffraction Data began issuing ICDD cards in the 1980s based on compiled data. As of May 2010, the ICDD provides PDF-2 (Powder Diffraction File -

2) and PDF-4 on CD-ROM. These files are generally used by research scientists and similar individuals. However, for analyses of limited scope, we can prepare structural data for known substances through our own calculations. We can then compare the measured data to our calculations to perform identification.

PDF-2 2009 is a database primarily of inorganic materials, containing information on interplanar spacing (d-values), relative intensity, Miller indices, chemical formulas, compound names, mineral names, structural formulas, crystal systems, melting points, density, and so forth. However, the CD-ROM supplied by the ICDD lacks a search function. Users can elect to purchase DDview, an application offered by the ICDD, or obtain other equivalent software. PDF-4 consists of three parts: a) PDF-4 Inorganic 2009 (including minerals, totaling 291,440 data items); b) PDF-Organics 2010 (406,733 data items); and c) PDF/Mineral 2009 (34,212 data items). PDF-4 includes DDview and removes the need for a separate search program.

**Note that the MiniFlex II comes with a search program developed by Rigaku, called PDXL.**

### 5.1.1 Information provided on the ICDD cards

**Fig. 5.1** shows the ICDD card for a mineral called anatase, a form of titanium oxide ($TiO_2$). The number at the upper left corner of the card, 21-1272, is the card number for $TiO_2$. The leftmost figure in the first row indicates the d-value of the reflection of maximum intensity. Since this reflection intensity is used as a reference value, relative intensity $I/I_1$ has a value of 100. The d-values for three strong reflections and their intensity ratios ($I/I_1$), respectively, follow these figures. To chemical formula ($TiO_2$) and mineral name (Anatase) are indicated. The symbol in the upper right corner ($\star$, i, C, or O) indicates the quality of the data. The symbol $\star$ indicates that the data is reliable. The letter "i" indicates that the intensity of diffracted X-rays has been reviewed and found to be less accurate than data with $\star$. The letter "C" indicates the data is calculated. The

symbol "O" indicates the data is unreliable. If no symbol or letter appears at this location, the data has not been evaluated. Beneath this information, the card gives measurement conditions, crystal data, optical data, and data sources to the left, and observed d-values, intensity ratios, and Miller indices *hkl* to the right.

## Card No.

21-1272

| d | 3.52 | 1.89 | 2.38 | 3.52 | (TiO$_2$)12U | Chemical formula, mineral name | | | | | |
|---|------|------|------|------|--------------|--------------------------------|---|---|---|---|---|
| I/I$_1$ | 100 | 35 | 20 | 100 | Titanium Oxide | | | | | | (Anatase) |

Rad. CuK$\alpha_1$ $\lambda$ 1.54056    Filter Mono **Measurement**
Cut off              I/I$_1$ Diffractometer **conditions**
Ref. National Bureau of Standards,
       (1969)

Sys. Tetragonal              S.G. I4$_1$/amd (141)
a$_0$  3.7852 b$_0$            c$_0$ 9.513
$\alpha$           $\beta$           $\gamma$        **Crystal data** 134 93.
Ref. Ibid.

$\epsilon\alpha$           n$\omega\beta$
2V        D            mp       **Optical data**
Ref. Ibid.

Pattern at 25°C.  Internal standard: K.
Sample obtained from National Lead Co., South Amboy, New Jersey, USA.
Anatase and another polymorph brooki **Data source,** are converted to rutile (tetragonal) 700°C.                                  **etc.**
Merck Index, 8th Ed., p. 1054.

| d A | I/I$_1$ | hkl | d A | I/I$_1$ | hkl |
|-----|---------|-----|-----|---------|-----|
| 3.52 | 100 | 101 | 1.0436 | 4 | 321 |
| 2.431 | 10 | 103 | 1.0182 | 2 | 109 |
| 2.378 | 20 | 004 | 1.0070 | 2 | 208 |
| 2.332 | 10 | 112 | 0.9967 | 2 | 323 |
| 1.892 | 35 | 200 | .9555 | 4 | 316 |
| 1.6999 | 20 | 105 | .9464 | 4 | 400 |
| 1.6665 | 20 | 211 | .9246 | <2 | 307 |
| 1.4930 | 4 | 213 | .9192 | 2 | 325 |
| 1.4808 | 14 | --- | ---- | - | 411 |
| 1.3641 | 6 | **d-value, intensity, hkl** | | | |
| 1.3378 | 6 | | | | |
| 1.2795 | <2 | 107 | .8819 | ~2 | 413 |
| 1.2649 | 10 | 215 | .8793 | 2 | 404 |
| 1.2509 | 4 | 301 | .8464 | 2 | 420 |
| 1.1894 | <2 | 008 | .8308 | <2 | 327 |
| 1.1725 | 2 | 303 | .8268 | 4 | 415 |
| 1.1664 | 6 | 224 | .8102 | 2 | 309 |
| 1.1608 | 4 | 312 | .7974 | 4 | 424 |
| 1.0600 | 2 | 217 | .7928 | 2 | 0012 |
| 1.0517 | 4 | 305 | | | |

**Fig. 5.1** ICDD card. Example of card 21-1272 TiO$_2$ (Anatase) obtained from a data search

### 5.1.2 Search based on ICDD cards

The first step in identification is to find the d-value of the strongest reflection. Materials are divided into 45 groups, arranged from the group with the largest d-value to the group with the smallest d-value. Within the selected group, we compare the d-values for three reflections and their intensity ratios to narrow our search. After selecting a number of candidates, we compare the d-value and intensity ratio of the observed reflections in detail to those of the candidates to identify the sample material.

The number of effective digits is three or four. An angle accuracy of 0.050 to 0.1° is sufficient. The intensity value may be the intensity at the peak position (peak intensity), since the full width at half maximum can be regarded as proportional to the integrated

intensity, if all reflections are equal. Described below are specific search procedures using this card 21-1272 from **Fig 5.1**.

(1) Pre-processing (peak search)

For qualitative analysis, we need to calculate the interplanar spacing (d-value) and relative intensity of the peak. Before performing a peak search, we have to eliminate the background and smooth the data. This is done by entering processing conditions. In doing this, we must set an accurate position for the background and avoid excessive smoothing. To locate and identify trace components, we must also avoid dropping small peaks and exaggerating other peaks.

(2) Primary search

We perform a primary search to list candidate compounds from the ICDD file on the hard disk. Since this search examines tens of thousands of ICDD cards, specifying the appropriate search conditions is critical. This means specifying the ICDD card file (including sub-files), contained elements, and so forth. The search will return compounds meeting the search conditions entered here. The search file and error windows are discussed in detail below.

a. Search file: Select the inorganic materials file if the sample is an inorganic compound and the organic materials file if the sample is an organic compound. Subfiles include minerals, metals and alloys, common phase, corrosive phase, forensic pathology phase, educational packages, cement phase, explosive phase, polymer materials, zeolite patterns, NBS patterns, superconducting materials, and pigment/paint files.

b. Error window: Depending on the state of the sample (e.g., eccentricity, solid/solution), the interplanar spacing shown may not perfectly match the standard data. The observed peak position is given a margin to allow judgment of a match with standard data. The extent of this margin is called the error window.

(3) Secondary search

The standard data for the compounds in the primary search results is superimposed on patterns obtained from the sample on the PC screen. (Compare the d-value and relative intensity in the entire diffraction profile obtained against the standard data to check for correspondence.) If the standard data overlaps the measured profile almost exactly, the sample can be identified. Compare the diffraction profiles while referring to the coefficient of reliability. If you come across unidentified diffracted X-rays, identify them in the same way. Repeat this identification process until no diffracted X-rays remain to be examined.
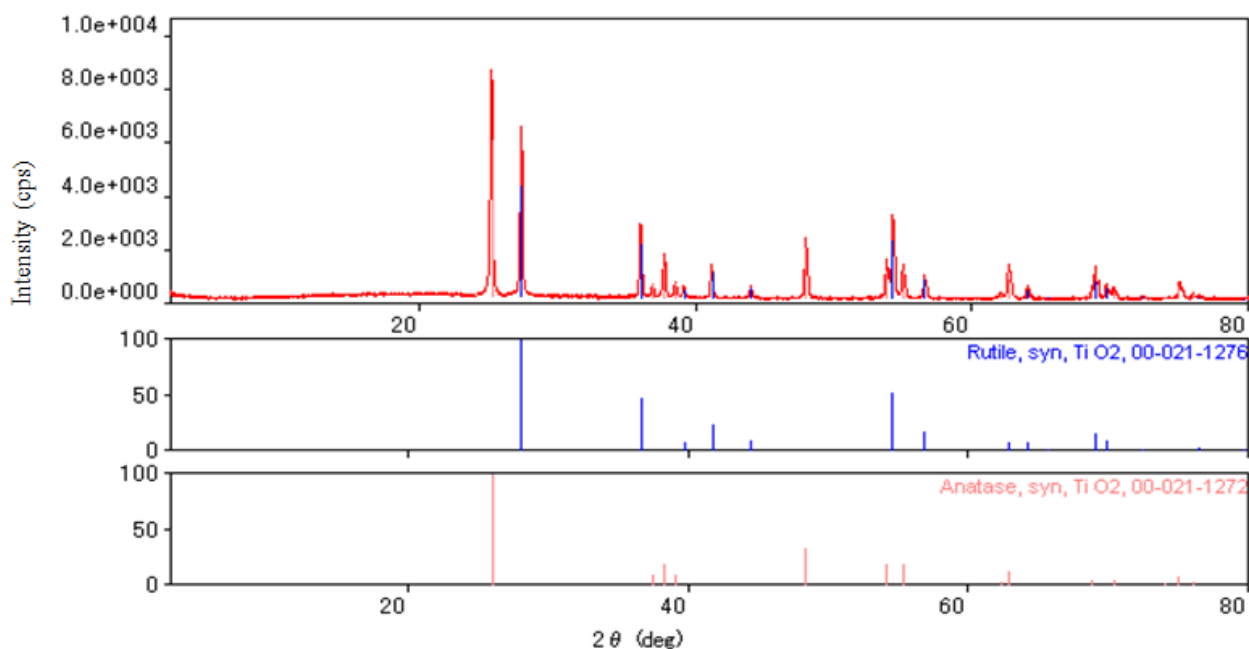


**Fig. 5.2** Example of identification. The result of identification using the X-ray diffraction data (red profile) obtained from a compound of two types of TiO$_2$, anatase and rutile, and ICDD data; all observed reflections can be explained as involving either anatase or rutile.

As an example, **Fig. 5.2** shows the observed data (red profile) of a sample, a compound of anatase and rutile, obtained with the MiniFlex II. An ICDD search produced anatase and rutile as results. The data for these materials explains all observed reflections. We can obtain the coefficient of reliability using the d-value, relative intensity, and the number of matching peaks. The larger the coefficient, the more reliable the analysis. Keep in mind that this value is a benchmark. The final

judgment must be made by humans. Let's see how closely the angle and intensity in the obtained data match the data registered in the ICDD file. **Fig. 5.3** shows the results of a comparison to anatase. The degree of correspondence here is acceptable.
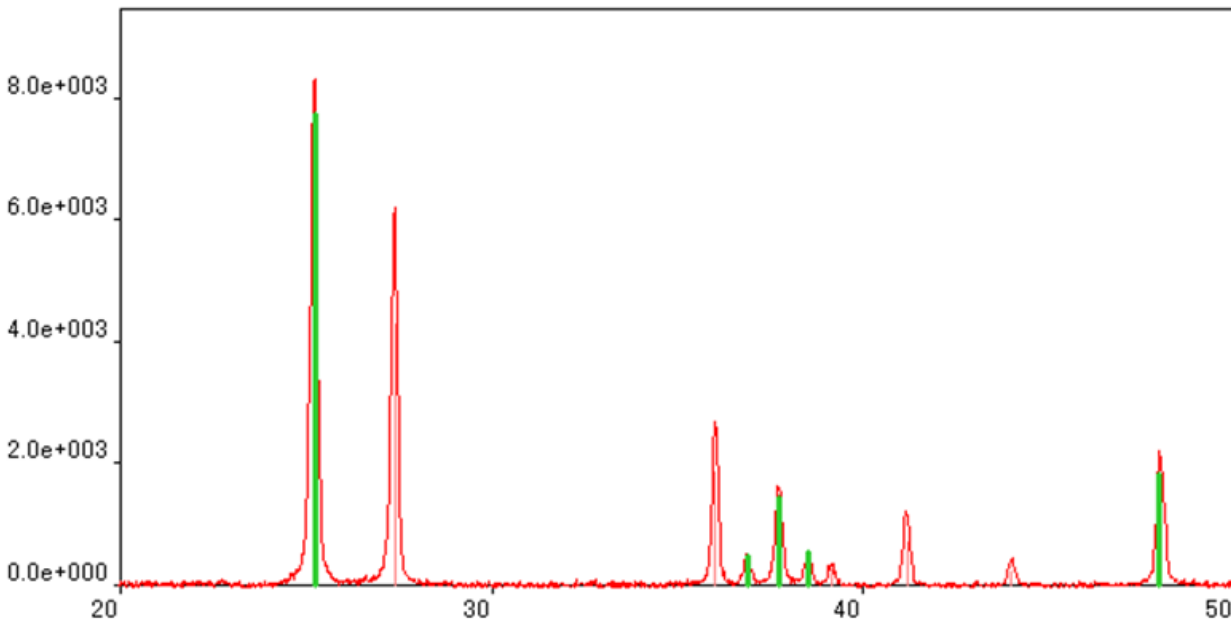
**Fig. 5.3** Comparison of anatase data (thick green line) registered in ICDD and actual measurement (red)

### 5.1.3 Cautionary note for the identification process

During the identification process, the d-value and $I/I_1$ of the diffracted X-ray from the sample may differ slightly from the ICDD data. The factors leading to this discrepancy fall into three categories: a) causes originating from improper adjustment of equipment and sample; b) causes stemming from characteristics specific to the sample; and c) causes attributable to poor reliability of the ICDD data.

a) Adjustment of the equipment and sample

(1) Needless to say, the MiniFlex II must be serviced and maintained. If the goniometer's zero point deviates by angle $\Delta 2\theta$, for example, all diffracted X-rays will shift by $\Delta 2\theta$. Such errors are due to mechanical misalignments.

(2) In the results of measurements based on the B-B method, the peak profile becomes asymmetrical. With $2\theta = 90°$ at the center, reflections appearing on the

low-angle side are sloped on the base-angle side, while reflections appearing on the high-angle side are sloped on the high-angle side. If this umbrella effect is problematic, reduce the divergence angle of the incident optical system in the vertical direction to mitigate the effect.

(3) If a K$\beta$ filter is used in the measurement, high-intensity diffracted X-rays will be accompanied by diffracted K$\beta$ rays, so caution is in order. This problem can be avoided by placing an analyzing crystal (monochromator) in front of the detector.

(4) Most diffractometers, including the MiniFlex II, lack sufficient resolution to distinguish between the K$\alpha_1$ and K$\alpha_2$ contained in CuK$\alpha$ rays. If the average grain diameter of crystallites in the sample is large and the level of integrity is high, diffracted X-rays of K$\alpha_1$ and K$\alpha_2$ may separate on the high-angle side and appear as independent diffracted X-rays. Again, caution is in order.

(5) If the X-ray tube used is old and the surface of the target is contaminated, characteristic X-rays attributable to impurities in the contamination may mix. If the filament material, tungsten (W), adheres to the target, WL$\alpha$ (= 1.476 Å) rays will appear. Note that the detected wavelength will be between CuK$\alpha$ rays and CuK$\beta$ rays.

(6) Note that the observed data may also include scattering rays caused by the sample holder and equipment cover.

  b) Characteristics specific to the sample

When we perform X-ray diffraction with a powder crystal sample, the diffraction intensity ratio can change depending on the sample preparation method or characteristics specific to the sample, contributing to abnormalities in the profile of the diffracted X-rays and impeding proper identification of the sample. However, investigating these causes involves analyzing the state of the sample. Actual cases are listed below as reference examples.

(1) In a powder sample with large grain diameter (approx. 10 μm or larger), the

cone-shaped Debye-Scherrer diffracted X-rays (see **Fig. 3.4**) become narrower, causing intensity irregularities and degrading the reproducibility of the relative intensity. In certain cases, relative intensity $I/I_I$ can vary by several tens of percent. We can minimize this effect by grinding the sample so that the grain diameter is less than approximately 10 μm (until particles cannot be felt by a fingertip) or by rotating the sample around the axis perpendicular to the sample surface.

(2) If the grain diameter is 0.1 μm or smaller, on the other hand, the Debye-Scherrer diffracted X-rays become wider and tend to overlap on the high-angle side, making identification difficult.

(3) In a powder sample with needle-shaped crystal grains or flat-plate-shaped crystal grains, certain diffracted X-rays (for example, diffracted X-rays from the plane (001) in the case of crystal grains that are elongated along the c axis) will exhibit sharp edges along the axis of width, but diffracted X-rays in the perpendicular direction will expand in width.

(4) The crystal grains in the sample may be oriented preferably. Relative intensity can vary significantly, depending on the degree of preferred orientation. In extreme cases, we observe reflections of only specific indices. This can occur in crystal samples with a layered structure, such as clay minerals and graphite powder, and in foils and fibrous materials. This can also be a problem specific to a certain sample.

(5) In certain cases, a material of the same structure with a slightly different lattice constant may be mixed in. This occurs when the impurities remain in a sample that becomes a solid solution. For example, the lattice constant of $BaTiO_3$ is 3.97 Å. However, a solid solution of $SrTiO_3$ with a = 3.91 Å will result in locally irregular composition, causing the diffracted X-rays to separate. In certain cases, the shape of the unit cell may be slightly distorted, degrading symmetry. This can be seen in materials with a perovskite structure (such as $BaTiO_3$) and intermetallic compounds. In these cases, the profile of the diffracted rays becomes noticeably asymmetrical. For

samples with imperfect solid solutions of CaO in MnO, the profiles exhibit slopes on the high-angle side. These problems can also be specific to a certain sample.

(6) In samples with stacking faults (e.g., graphite, talc), the profile of the diffracted X-rays from an irregular surface will exhibit a slope on the high-angle side.

c) Problems attributable to unreliable ICDD data

(1) Much of the data obtained before 1950 is based on measurements obtained by the photographic method, which is sometimes associated with unreliable analysis results. Although old data has been replaced with new data as it becomes available, the ICDD data may still contain older, unreliable data.

(2) If we use X-rays of a wavelength different from the data indicated on the ICDD card to analyze an unknown sample, relative intensity may differ from the ICDD data. Try to use the appropriate X-rays.

### 5.1.4 Focus on characteristic diffracted X-rays

When performing qualitative analysis of crystals that generate characteristic diffracted X-rays, such as clay minerals[1,7] and rock minerals[8], we need to focus on characteristic diffracted X-rays to determine the materials included. Shown below is an example.

When X-rays of the CuK$\alpha$ wavelength are used to measure a sample of $\alpha$-quartz (SiO$_2$) powder, we observe strong diffracted X-rays at diffraction angles of 20.70 and 26.5° ($2\theta$). We observe a quintuplet at 68°. **Fig. 5.4** shows the quintuplet in the diffraction profile. This diffraction pattern is unique to $\alpha$-quartz and is not found with other materials. If we see this diffracted X-ray pattern, we can conclude that the sample contains $\alpha$-quartz. Here, we examine the diffraction profile of the sample being analyzed, identify characteristic features, and identify materials using these features as a guide. In the case of $\alpha$-quartz, however, the intensity of the quintuplet is weak, so we need to perform a careful inspection.
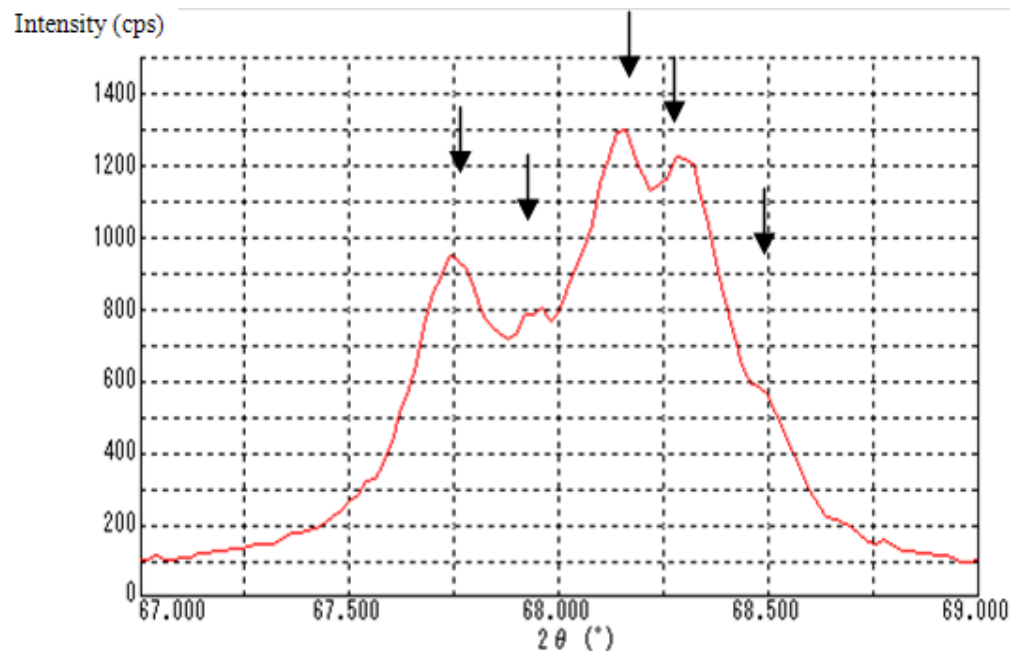
**Fig. 5.4** Characteristic diffraction profile of α-quartz, with quintuplet ($2\theta$ = approx. 68°). This is called a "five finger" pattern.

### 5.1.5 Identifying organic compounds

Despite the abundance of organic compounds, there are fewer registered ICDD cards for organic compounds than for inorganic compounds. This means the systematic identification technique used for inorganic compounds such as clay minerals, rock minerals, and metals is less suitable for the identification of organic compounds. Since organic compounds can be characterized by unique molecular shapes, their diffraction patterns are often complex. Nonetheless, if the diffracted X-rays of homologous compounds and allied compounds of the organic compound to be identified are available as reference information, we can perform qualitative analysis (identification) in the same way as for inorganic compounds.

## 5.2 Characterization of the state of polycrystalline materials

### 5.2.1 Crystallized state and amorphous state

Substances occur in three states: vapor, liquid, or solid. At the atomic level, the solid

state can be further divided into two states: amorphous and crystalline. The structural differences between these states are obvious when you inspect **Fig. 5.5**. These diagrams were created based on the famous two-dimensional diagrams of quartz and silica glass developed by W.H. Zachariasen in 1932. Both compounds have the same chemical symbol, $SiO_2$. Quartz is in a crystallized state; the Si-atoms, represented by small black circles, are covalently linked via oxygen atoms, indicated by red circles, in an orderly pattern. In contrast, in silica glass, the Si-atoms are covalently linked via oxygen atoms, but their arrangement lacks regularity. The amorphous state was initially recognized as a structure unique to glass, but has since been identified in pure silicon and in alloys of certain compositions. Methods for manufacturing these substances in the amorphous state have been established for various applications that require its superior uniformity.
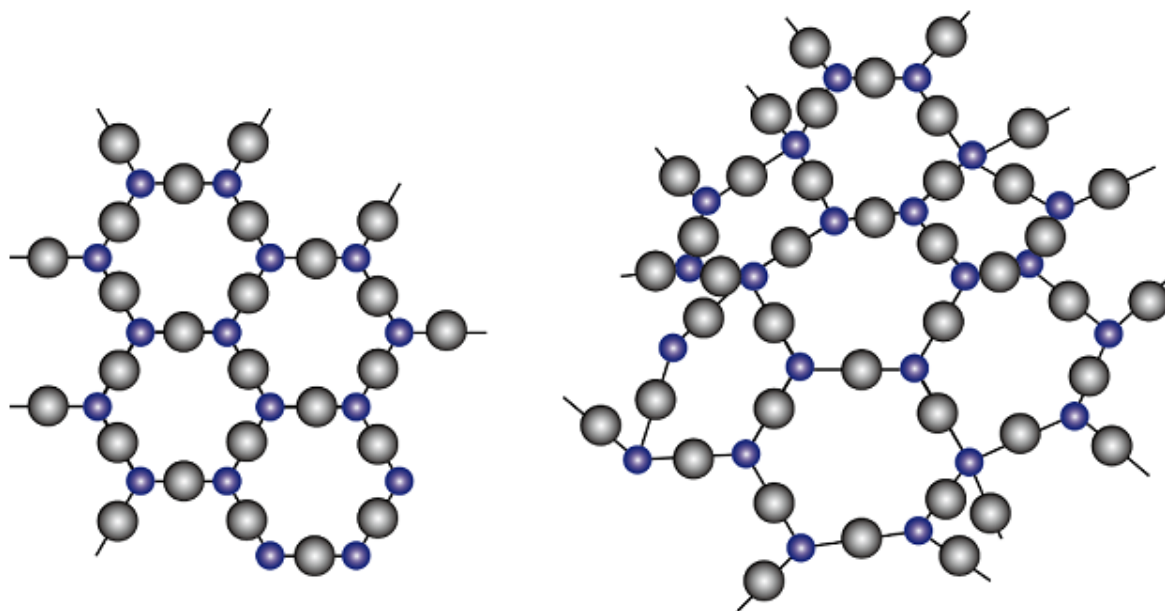


**Fig. 5.5** Crystallized (quartz) and amorphous (silica glass) states of $SiO_2$. Silicon atoms are represented by black circles and oxygen atoms by red.

The preceding addressed the morphology of solids. The results in **Fig. 5.5** were obtained by analyzing X-ray diffraction patterns, and the differences are obvious. **Fig. 5.6** shows the results of analysis using the MiniFlex II. In the crystallized state,

represented by the red pattern, sharp diffracted X-rays enable plane indexing. In comparison, we see no sharp peak in the diffraction pattern for silica glass (blue pattern), only a broad crest near a $2\theta$ value of 28°. This crest is attributable to the interference of scattered X-rays from Si atoms and nearby O atoms. The disorderly structure, lacking the long periodical continuity of Si-O bonds, results in the broad spread of the diffracted X-rays.
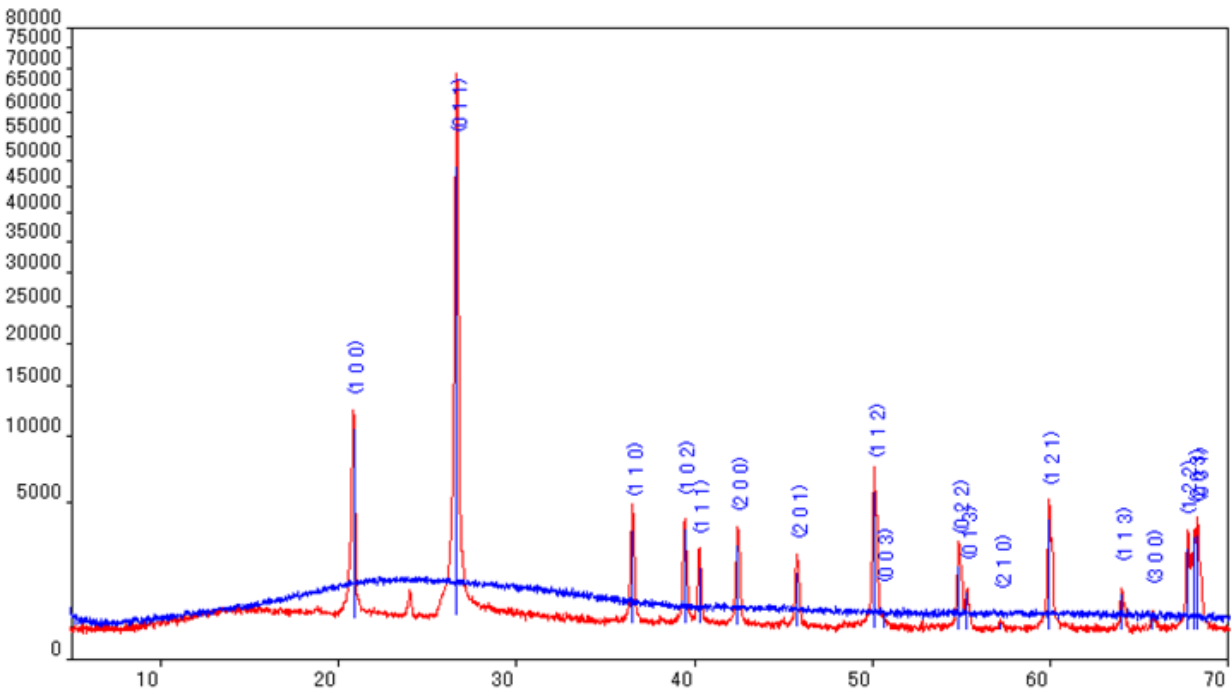


**Fig. 5.6** Diffraction profiles for quartz powder (red) and silica glass (blue)

We can increase the temperature to liquefy a sample of quartz or silica glass, and observe the diffraction profile obtained from the sample in liquefied condition. The resulting diffraction pattern is virtually identical to that of the sample in the amorphous state. We infer that samples in the liquid and amorphous states have the same microstructure, since they yield the same diffraction patterns. The difference between the two states is fluidity: In the liquid state, atoms and molecules are in a state of flux; in the amorphous state, their fluidity is extremely low. However, even with such extremely low fluidity, due to the fluidity of atoms and molecules in this configuration, elastic

deformation will occur if we apply a force to silica glass for an extended period. The key aspect here is that the crystallized and amorphous states occur at ordinary temperatures and pressure, although their microstructures can appear quite different at first glance. In the crystallized state, atoms and molecules are arranged in an orderly pattern. In the amorphous state, they are arranged randomly, aside from the constraint imposed by interatomic distances to the closest atom. According to solid state physics, the free energy is more or less equal for the two states.

This is better understood if we compare the latent heat of vaporization used to break up atoms and molecules with the latent heat of liquefaction. A material in a crystallized state heated under constant pressure will vaporize. Suppose that the latent heat used to increase the temperature to achieve liquefaction is $L_m$ and that the latent heat used to further increase the temperature to achieve vaporization is $L_v$. For most materials, the latent heat of fusion is significantly less than the latent heat of liquefaction. The ratio $L_m/L_v$ is about 0.03 to 0.04, whether the material is a metallic or ionic crystal. One would suppose, then, that the structural difference (the change from an orderly configuration to the disorderly state) between solid and liquid states is very small and that most of the latent heat of liquefaction is used to achieve a fluid configuration of atoms and molecules.

We used silica glass above to explain the amorphous state. In the structures of polymer resins called plastics, while crystallization may appear here and there, the overall configuration remains amorphous.

### 5.2.2 Various states of crystallization

Using $SiO_2$ as an example, we showed above that the solid state can be crystalline or amorphous. Using the X-ray diffraction method, we can classify the crystalline state into the six types shown in **Fig. 5.7**. First, we can classify the crystallized state as a single crystal state or polycrystalline state. The materials discussed in this booklet are in a

polycrystalline state. A single crystal, on the other hand, can be understood as a crystallite in a polycrystalline material. To see this, picture an overgrown crystallite. We can also picture natural gems like quartz, emerald, or diamond to visualize the single crystal state. Single crystals can be further divided into perfect single crystals and mosaic single crystals if we perform our investigations with the X-ray diffraction method. Although the main topic here is the method of characterizing materials in the polycrystalline state, we will take a brief detour to address the topic of materials in the single crystal state.
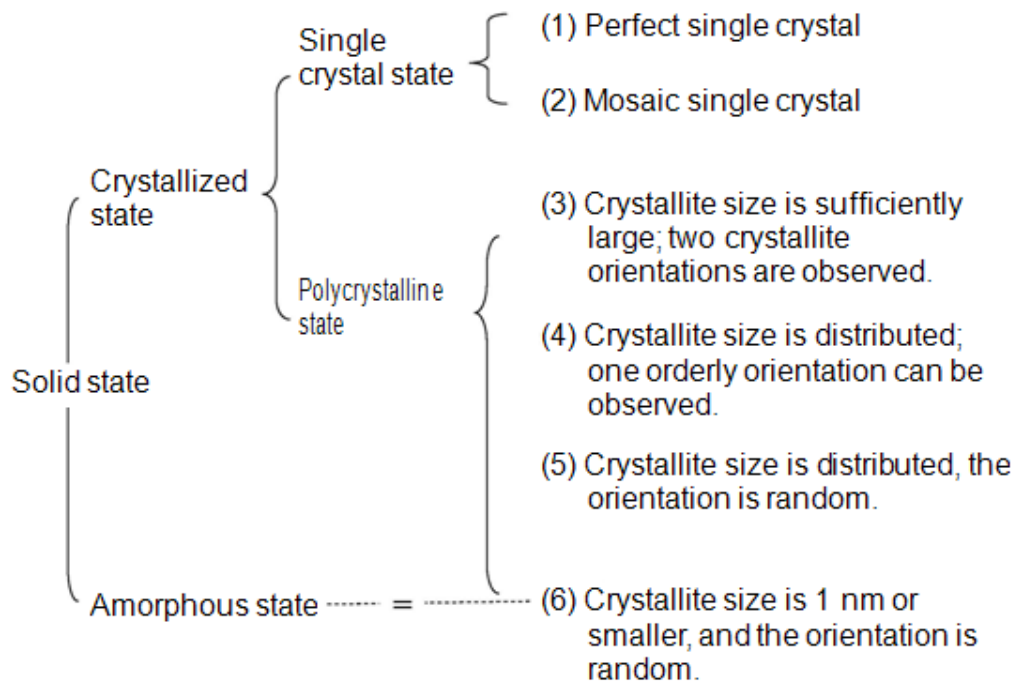


**Fig. 5.7** Possible solid states

For X-ray diffraction, a narrow, monochromatized, parallel X-ray beam is created and irradiated so that the crystal lattice plane satisfies the Bragg condition. The diffracted X-rays are then observed by a detector set in the direction of diffraction. In this condition, we observe the Bragg reflection while the crystal is rotated little by little. This observation method is called **rocking curve** measurement. If the sample has minimal lattice defects and the crystals feature an ideal periodic structure, the **full**

**width at half maximum (FWHM)** will be an angle of less than a dozen arcseconds. This crystal is called a perfect single crystal. We can calculate FWHM by applying **dynamic diffraction theory** to **perfect single crystals**. Crystals can be characterized by comparing measured values to calculated values. If the crystal structure contains numerous lattice defects, the FWHM becomes wide, varying from several arcminutes to several tens of arcminutes. This crystallized state is called a mosaic crystal ((2) in **Fig. 5.7**). The corresponding FWHM is used as a reference to express the integrity of a single crystal. In short, FWHM is an index of crystal growth techniques. Ideal crystals currently known include Si, quartz, and ice. The compound semiconductor crystals used in the semiconductor industry have been gradually improved over time.

On the other hand, samples that generate Debye-Scherrer diffraction patterns are said to be in a polycrystalline state. Crystals of common metal materials and ceramics are in this state. If we take a piece of iron or aluminum, polish the surface, remove the section deformed during processing with a corrosive liquid, then observe it under an optical microscope, we will see aggregates of grains of various shapes measuring several micrometers or less. If we observe those grains with an electron microscope like SEM or TEM, we will see that certain grains are composed of several small crystals (called crystallites), while others are single crystals. The condition shown in **Fig. 5.7** (5) is the polycrystalline state that results in a uniform Debye-Scherrer diffraction profile. As explained in Chapter 4, the integrated reflection intensity indicated by the diffraction profile can be described with calculations based on diffraction theory. This diffraction theory is equivalent to the Born approximation, a well-known scattering theory. This is called the kinematical diffraction theory to distinguish it from the dynamic diffraction theory.

We will now focus on the polycrystalline state (6). Imagine a condition (5) in which the average size of the crystal grains is 10 nm or less. In general, if the size of the crystal grains decreases, the number of atoms on the surface will increase sharply relative to

the number of all atoms comprising the crystal grain. For example, when the grain size reaches 1 nm, the value becomes 100%, meaning that all constituent atoms become part of the surface. Since the percentage of atoms on the surface increases, we can no longer define a lattice plane. The Debye-Scherrer diffracted X-rays forming the diffraction profile will have a wider ring and overlap the adjacent ring. This is the diffraction profile of an amorphous material. The condition shown in **Fig. 5.7** (6) indicates the amorphous state.

Consider the condition described in (4) using the condition indicated in **Fig. 5.7** (5) as a reference. In the polycrystalline state described in (5), we can define an average diameter for the crystal grains around which a certain range of various diameters is observed, and crystal grains are oriented in various random directions. This condition is called a disorderly state or randomly oriented state. In polycrystalline materials of a certain type, crystallites are oriented in the direction of a single crystal axis, although grain sizes may be distributed. This polycrystalline condition is called a textured orientation or a preferred orientation. Such materials exhibit random orientation in a direction perpendicular to the axis of orientation; this state is called uniaxially textured orientation.
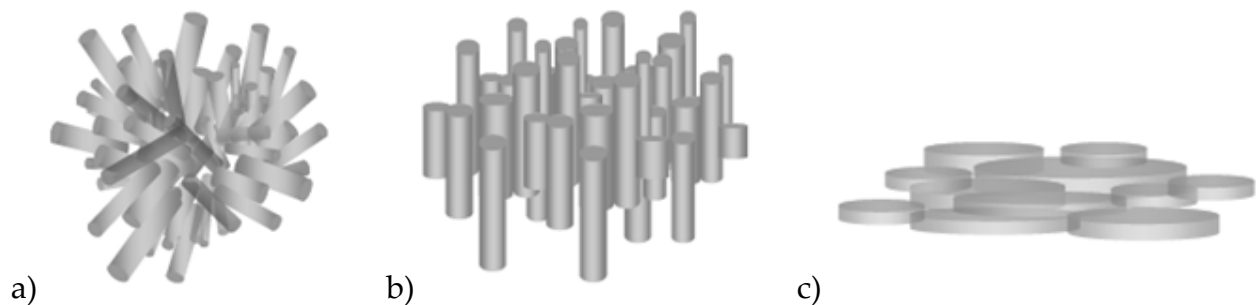


a)          b)          c)

**Fig. 5.8** Samples in a polycrystalline state. Sample (a) illustrates a state in which bar-shaped crystallites are randomly oriented, as described in **Fig. 5.7** (5). Sample (b) is in the preferred orientation described in (4). Sample (c) illustrates a state in which plate-shaped crystallites are in the preferred orientation.

This condition is equivalent to the condition indicated in **Fig. 5.7** (4) and is shown in

**Fig. 5.8** (a) and (b). This state is often observed in fibrous crystal materials and is commonly encountered in metals extended under certain temperatures. In materials in this state, crystallites have a flat plate shape (discussed in a later section). Since the diffraction profile shows noticeable anisotropy, we can use the X-ray diffraction method to characterize macro-structures. To describe the intensity of diffracted X-rays resulting from textured orientation, we must understand the state of orientation. Several correction equations incorporating a parameter indicating the approximate degree of orientation have been proposed; this booklet does not address the specifics of this topic.

In a polycrystalline sample, we also observe crystal grains oriented along two crystal axes. This biaxial orientation is the condition shown in **Fig. 5.7** (3). Fine common salt, for example, exhibits crystal grains that are uniformly cubical, much like dice. This is called a crystal habit. The orientation of all crystal axes shows two relatively well-aligned crystal axes, as if the cubical crystallites were aggregated, although this condition cannot be fully attributed to the crystal habit. This is called biaxial orientation. In this case, crystal grains have a certain average size, around which a certain range of different sizes is observed. In certain cases, we may encounter biaxial orientation with large crystal grains, due to defects in crystals in a single crystal in which crystal orientation partially varies. This is the mosaic crystal state shown in **Fig. 5.7** (2). High-resolution X-ray diffraction can evaluate and identify this state.

### 5.2.3 Average size of crystallites

The Debye-Scherrer diffracted X-rays expressed by the indices *hkl* face in a direction in which the orientation satisfies the Bragg condition for *hkl*. However, they constitute a group of diffracted X-rays from numerous crystallites of different sizes. We focus instead on a profile for one crystallite contributing to the diffracted X-rays. As explained in Chapter 4, the width of Debye-Scherrer diffracted X-rays is in inverse proportion to the number of lattice planes in that direction. The function that determines the profile of

the diffracted beam is called the Laue function $(sin^2Nx / sin^2x)$. The Laue function can be approximated by the Gaussian function below.

$$(sin^2Nx / sin^2x) = N^2 \exp\{-(Nx)^2/\pi\} \qquad (5.1)$$

In **Equation 5.1**, N indicates the number of lattice planes, while $x$ expresses the displacement from diffraction angle $2\theta$. Since this is a Gaussian function, when the value of N is large, the profile of the diffracted X-rays becomes sharp, and when N is small, the profile has a gradual shape.

Since the diffracted X-rays we actually observe consist of diffracted beams from many different crystallites, we can regard them as diffracted X-rays from crystallites of different sizes. When grain sizes are distributed, the profile becomes the sum of Gaussian functions. However, diffracted X-rays can be approximated by a single Gaussian function, and its full width at half maximum is the inverse of the average value of many crystallites. Using the measurement of full width at half maximum, we can estimate the average size of the crystallites. Applying this principle, we can use the width of Debye-Scherrer diffracted X-rays to determine the average size, or average grain diameter, of the crystallites that contribute to the diffracted X-rays. Since the average grain diameter is $L$ (in Å) and the full width at half maximum of diffracted X-rays is $B_{hkl}$ $(2\theta)$, we derive the following equation based on their inversely proportional relationship:

$$L(Å) = 0.94 \lambda(Å) / B_{hkl}(2\theta) \cos \theta \qquad (5.2)$$

Here, if we express $\lambda$, the wavelength of X-rays used in the experiment, in Å, and the full width at half maximum $B_{hkl}$ $(2\theta)$ in radians, the grain diameter $L(Å)$ is given in Å. This equation was developed by Scherrer and is called **Scherrer's formula**.

If we substitute 1.54 Å ($CuK\alpha$) for $\lambda$, 45° for $\theta$, and 90° for the diffraction angle $2\theta$ in **Equation 5.2**, the average grain diameter becomes 230 Å when the full width at half

maximum $B_{hkl}(2\theta)$ of the diffracted X-rays is 0.5° (= 0.00875 rad.). If we observe a sample with a grain diameter of 2000 Å at the same diffraction angle, the full width at half maximum becomes 0.06°, and the resolution of the equipment must be at least 1/3 of that value: The resolution must be about 2/100°.

(a)

(b)

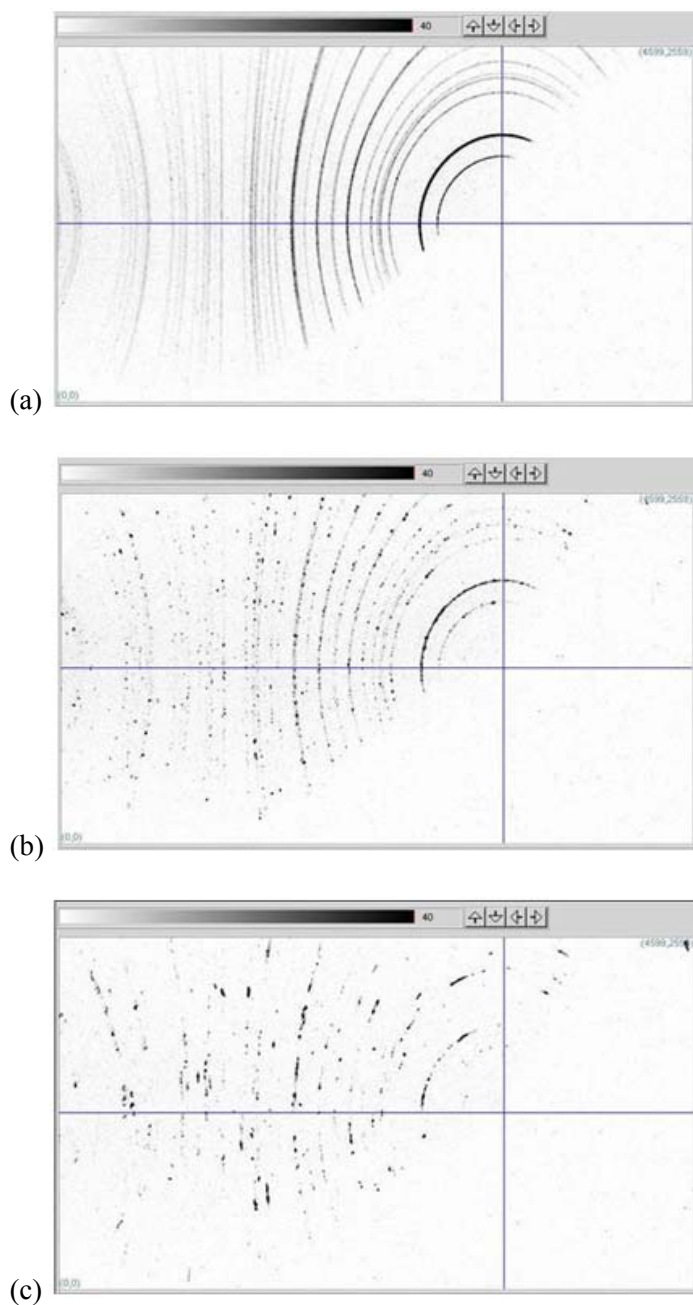(c)

**Fig. 5.9** Debye-Scherrer diffraction profiles obtained from quartz powder samples. Sample grain diameter: (a) small; (b) moderately coarse; and (c) very coarse. As grain diameter increases in the sequence (a) to (c), the diffracted X-rays lose uniformity.

If the average crystal grain exceeds 1 μm, the number of crystallites on the X-ray irradiated surface contributing to diffraction decreases. In addition to generating very sharp profiles for the diffracted X-rays, this results in nonuniform Debye-Scherrer rays. Such a profile is said to be *spotty*. **Fig. 5.9** show examples of results obtained with a cylindrical X-ray camera equipped with an imaging plate detector instead of the MiniFlex. The samples are quartz powders of varying average grain diameters. As these diagrams show, larger grain diameters result in increasingly spotty diffracted X-rays.

### 5.2.4 Condition in which crystallites have distortion distribution

In the discussion thus far, we have assumed that all crystallites in our samples are free of defects and that their lattice planes are aligned neatly. However, in actual samples, crystallites are not flawless perfect crystals. The interplanar spacing may be shorter or longer than average in areas where defects are found. These conditions increase the full width at half maximum of Debye-Scherrer diffracted X-rays. To understand this, we examine the equation for Bragg diffraction. Suppose interplanar spacing $d$ is distorted by $\Delta d$ in the Bragg equation, causing the diffraction angle $2\theta$ to shift by $-2\Delta\theta = 2\ \Delta d/d\ tan\theta$. Elongation and contraction result in the distribution of diffraction angles, with the average value located at the center. This explains the increased width of diffracted X-rays. If the average distortion is $<\Delta d/d> = \eta$, the spread $B'_{hkl}$ of the diffracted X-rays is given by the following equation:

$$B'_{hkl} = 2\eta\ tan\ \theta \qquad (5.3)$$

According to **Equation 5.3**, the full width at half maximum grows wider as the scattering angle $2\theta$ increases. Derived by Hall, this equation is called the Hall formula. The combination of **Equation 5.2** for full width at half maximum based on crystal grain size and **Equation 5.3** is called the Hall-Scherrer formula.

$$B^o_{hkl}\ (cos\ \theta\ /\ \lambda\ ) = 2\eta\ (\ sin\ \theta\ /\ \lambda) + 0.94\ \lambda\ /L(\text{Å})\ (5.4)$$

In **Equation 5.4**, the sum of the spread $B_{hkl}$ due to grain diameter and spread $B'_{hkl}$ due to internal distortion, $B^o_{hkl} = B_{hkl} + B'_{hkl}$, is assumed to be the measured value of full width at half maximum. If we plot the observed value $B^o_{hkl}$ ($\cos\theta / \lambda$) against ($\sin\theta/\lambda$), the resulting curve is linear. The slope of this line gives the distortion, while the intercept of ($\sin\theta/\lambda$) = 0 gives the grain diameter.

### 5.2.5 Preferred orientation

Now we address the condition of preferred orientation. The previous discussion gave a warning for identifying a given sample: If the crystal grains are needle-shaped or flat, the width of certain diffracted X-rays will be sharp, and the diffracted beam perpendicular to that direction will grow wide. As explained in §5.2.1, this phenomenon can be understood by examining the Scherrer **Equation 5.2** that indicates that the width of the diffracted X-rays is inversely proportional to the average size of the crystal grains. For example, in a sample made up of hexagonal crystals whose plane *(001)* in the direction *00l* is flat, the width of the diffracted X-rays in the direction *00l* is wider than the diffracted X-rays of the indices *hk0* in the perpendicular axis. In a sample made up of needle-shaped crystallites, the diffracted X-rays in the direction of the needle shape are sharper than the diffracted X-rays along the perpendicular axis.

If the crystallites have the same external shape, the width of the diffracted X-rays will vary, depending on the indices, and the Debye-Scherer diffraction profile will exhibit anisotropy. This is because when the orientation of crystals in the sample tends to align in one direction when the crystallites are bar-shaped (see **Fig. 5.8b**) or flat (see **Fig. 5.8c**). Needless to say, diffracted X-rays obtained from such a sample will be highly anisotropic. **Fig. 5.10** shows schematic diagrams for diffraction patterns expected to result when we use flat-plate X-ray film to observe these two cases. In **Fig. 5.10a**, the width of the diffracted X-rays is narrow vertically along the bar, and the Debye-Scherrer ring is made up only of diffracted spots at the top and bottom, since there is no tilted

bar. The intensity distribution along the ring is highly anisotropic. In **Fig. 5.10b**, the crystallites are in the shape of a flat plate, and overlapping preferred orientation results. This generates diffracted spots in the same way as in the case shown in **Fig. 5.10a**, and the diffraction is also anisotropic, but the spots are wider than in the case of **Fig. 5.10a**. In comparison, in **Fig. 5.8a**, the crystallites are bar-shaped but not oriented in a specific direction. This exemplifies a random orientation.
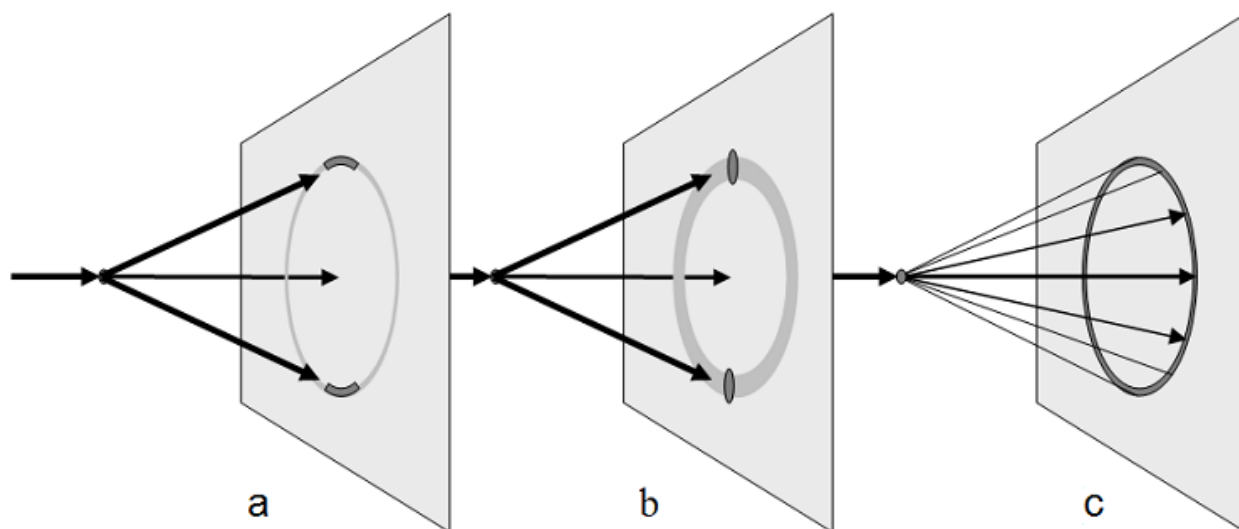


**Fig. 5.10** Anisotropic Debye-Scherrer ring resulting from special shape of crystallites

In actual observations, we see not just one Debye-Scherrer ring similar to the one shown in **Fig. 5.10**, but all possible diffraction rings. At first glance, the pattern obtained is complex. However, if we observe the diffracted X-rays over a wide range using flat-plate or cylindrical X-ray film, we notice a certain regularity. Further analysis will provide not just the average size of the crystallites, but information on their shapes. **Fig. 5.11** shows the diffraction profile obtained from a copper plate with preferred orientation due to rolling. The diffraction intensity is anisotropic and is not uniform along the Debye-Scherrer ring. However, the overall pattern is symmetrical. We obtained this observation result by using a two-dimensional detector. Diffractometers such as the MiniFlex measure the location along the equatorial line on the film;

therefore, in certain cases, diffracted X-rays of certain indices appear very strong, but diffracted X-rays of other indices do not appear at all. We will understand the occurrence of such phenomenon if we examine the figure closely. This diffraction profile is called the diffraction profile of preferred orientation. If we use an X-ray diffractometer, we see only the equatorial plane of the figure. However, we can also perform analyses by introducing the orientation functions (March-Dollase function and spherical function) that correct for diffraction intensity. This booklet lists reference documents but does not address these topics in detail.



**Fig. 5.11** Diffraction profile of rolled copper plate. Variation of intensity is seen along the Debye-Scherrer diffraction ring, but with certain recognizable regularity.

1) W. A. Dollase: *J. Appl. Crystallogr.* 19, (1986) 267
2) M. Ahtee, M. Nurmela, P. Suoritti and M. Jaervinen: *J. Appl. Crystallogr.* 22, (1989) 261

## 5.3 Quantitative analysis (Rietveld analysis)

Until now, we have discussed qualitative analysis and characterization of polycrystalline states using an X-ray diffractometer. Can X-ray diffraction be used for qualitative analysis? The answer is: Yes. To do so, we add a specified standard sample and use its intensity for comparison. A method developed in recent years allows us to

reproduce an entire powder diffraction profile, compare it to the observed data, and determine the parameters necessary. These analytical programs are easily obtained and the analysis is easily performed. Since these programs allow qualitative analyses, the method is now widely used. Introduced by H. M. Rietveld (1969), the method is called the **Rietveld refinement** or **Rietveld method**.

The MiniFlex II incorporates an analysis program called PDXL that contains a Rietveld refinement program. We encourage you to try this method, although the specifics lie beyond the scope of this booklet. At present, you should understand what calculations are needed to reproduce an entire powder X-ray diffraction pattern for comparison to a measured profile. The basic idea is the same as explained in the section describing structural analysis. The difference is that when the method of least squares is applied to fit parameters, parameters pertaining to the optical system used and parameters that affect sample orientation are used, as well as structural parameters (such as lattice constant, atom position, and temperature factor). Note these parameters when using the program. The R-factor, which gives the degree of correspondence between the observed value and a calculated value, is given as a percent value. The value is expressed by the following equation:

$$R = [S\{\ Ij(obs) - Ij(calc)\}/\ SIj(obs)] \times 100 \quad (5.5)$$

If the value of R is 10% or less, the structure can be identified with a fair degree of certainty. If the value is less than 10% but above 5% or so, parameters for atom position need to be examined further. If the value is less than 5%, the quality of the data must be reviewed. If we obtain a value of less than 3%, the analysis has proceeded near-perfectly. Errors in the parameters obtained are expressed as standard deviations.

# Chapter 6: Crystal Structure and Bonding Power

The knowledge of certain relationships between basic crystal structures and the bonding forces that act on atoms and molecules making up the crystal structures helps us analyze crystal materials. This is the focus of this chapter. The following five bonds give rise to crystals: metallic, ionic, covalent, hydrogen, and Van der Waals. Described below are typical crystals formed by each of these bonds. You will learn that crystals composed of differing bonds can have identical crystal structures. The relationship between crystal structure and bond is not one-to-one. When you take a closer look, you will understand that bonding force is not the only force that dominates crystal structures. This will become clear as we proceed.

## 6.1 Crystal structures of metallic materials

The agglomeration mechanism of metals is formed with ions, created by the nuclei and inner-shell electrons, shared within the potential generated through their periodic arrangement (although not necessarily periodic), and with no restrictions imposed on outer-shell electrons by specific ions. The crystal structure itself represents the periodic arrangement of ions.

The crystal structures of metals generally fall into one of three groups, each based on a simple structure: the body-centered cubic structure, or BCC (bcc), shown in **Fig. 6.1a**; the face-centered cubic structure, or FCC (fcc), shown in **Fig. 6.1b**; and the hexagonal closed packed structure, or HCP (hcp), shown in **Fig. 6.1c**.

Table 6.1 summarizes the number of atoms in the unit cell, the coordinates of the atoms, and the number of closest neighbor atoms.
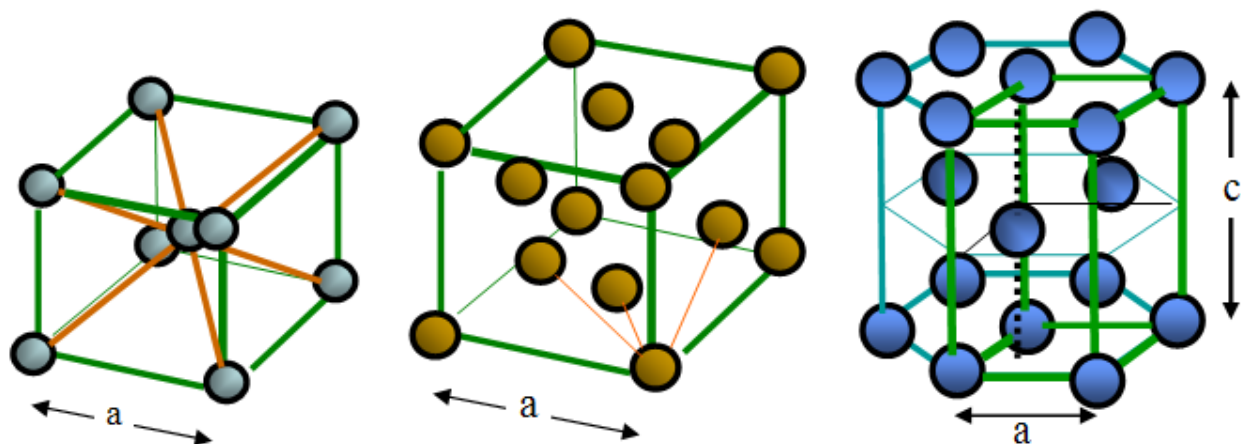
**Fig. 6.1** (a) body-centered cubic, or BCC, structure; (b) face-centered cubic structure, or FCC, structure; (c) hexagonal closed packed, or HCP, structure.

| Structure | Number of atoms in unit cell | Coordinates of the atoms | | Number of closest neighbor atoms |
|---|---|---|---|---|
| BCC | 2 | 0, 0, 0 | ½, ½, ½ | 8 |
| FCC | 4 | 0, 0, 0 | ½, ½, 0 | 12 |
| | | 0, ½, ½ | ½, 0, ½ | |
| HCP | 2 | 0, 0, 0 | 2/3, 1/3, ½ | 12 |

**Table 6.1** Crystal structures and atom coordinates

From **Figure 6.1**, we see that each atom in the BBC crystal structure has eight closest neighbors. For FCC and HCP, this number is 12. While the FCC and HCP structures may initially seem very different, they are actually quite similar. That is why both have 12 closest neighbor atoms. When viewed from the direction [111], the FCC lattice appears as a two-dimensional atomic plane comprised of hexagonal lattices formed by precisely arranged atomic spheres of the same size. When atoms are positioned on the recessed areas formed on the atomic plane, a new atomic plane is created. When atoms are placed again on that new atomic plane, a new atomic plane is created. This is called a stacking layer structure.

Examining the atomic plane (111) indicated in yellow in **Fig. 6.2**, we see that there are two types of recessed areas, each formed by three atoms. These are a barycentric position (blue circle) of the equilateral triangle formed by three yellow atoms and the

barycentric position (red circle) of the inverted triangle. Let's refer to these recessed areas as the B-site and the C-site. The positions occupied by the yellow atoms are not the blue atomic plane B-site or red atomic plane C-site, but they are other recessed areas on the red atomic plane. Let's call them the A-site. The FCC structure is made of three types of two-dimensional hexagonal lattice—A-site, B-site, and C-site—stacked repeatedly in sequence. This is called ABC stacking.



**Fig. 6.2** FCC structure viewed from direction [111];

If we examine the HCP structure in the same way, we observe that HCP also features a stacking layer structure, but one consisting of two sites arranged repeatedly in the order of A, B, A, B,… not three sites. This is called an AB stacking structure. The direction [111] of the FCC and the direction [001] (c-axis direction) of the HCP can be characterized by the crystal axes featuring these relationships.

So far, we have examined three types of crystal structure in metals. Let's examine the differences in the diffraction profiles obtained from them. Since we have studied the diffraction profiles of $\alpha$-Fe featuring a BCC crystal structure and Al featuring an FCC crystal structure in the previous sections, we will discuss the diffraction profile of Co, which features an HCP crystal structure. **Fig. 6.3** shows the diffraction profile for Co obtained with the MiniFlex II. We can see three diffracted beams, characteristic of the hexagonal crystal system, on the low diffraction angle side. This is one difference between HCP and BCC or FCC. Gaining a familiarity with diffraction profiles makes it

possible to distinguish these three crystal structures by just looking at the profiles. In the diffraction profile shown in **Fig. 6.3**, the reflections are not indexed. Try indexing them, referring to the examples given in the previous chapter. Also, calculate the crystal structure factor so that we can gain a better understanding of crystal structures and the extinction rule.
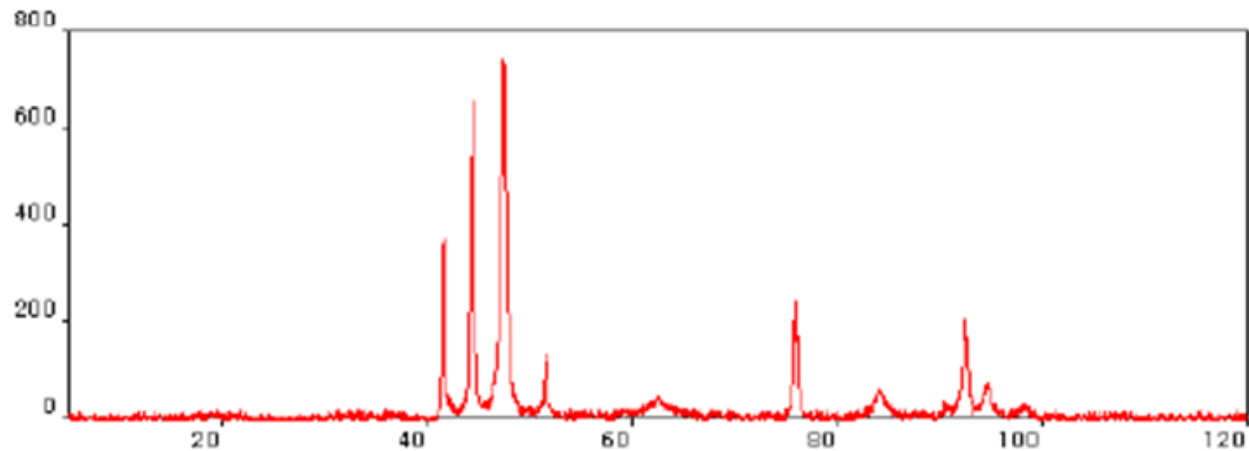


**Fig. 6.3** X-ray diffraction profile obtained from Co powder with CuKα rays using MiniFlex II

Assuming that the FCC and HCP are created by stacking two-dimensional atomic layers in an ideal spherical shape as described above, the axial ratio, c/a, of the HCP has no relation to the atomic size (atomic radius) and is a constant determined geometrically by the structure. In such cases, c/a should be $(8/3)^{1/2} = 1.633$. However, as we can see in **Table 6.2**, helium (He) is the only ideal crystal. The only other metals approaching this ideal are Mg, with 1.623, and Co, with 1.622. All others show values far from the ideal. Does this mean we should not assume that atoms are spherical? This is an interesting question, and a number of other basic questions will be raised in relation to this issue. Al, Cu, and other metals feature the FCC structure, but Mg and Zn have the HCP structure, although all are metals. In the periodic table, the elements belonging to the Ia, VIa, and VIIa groups feature the BCC structure, as if to suggest that the elemental structure is related to the number of outer-shell electrons.

| | | | | | | | | | | | | | | | | | |
|---|---|---|---|---|---|---|---|---|---|---|---|---|---|---|---|---|---|
| H hcp | | | | | | | | | | | | | | | | | He hcp |
| Li bcc | Be hcp | | | | | | | | | | | | | | | | Ne fcc |
| Na bcc | Mg hcp | | | | | | | | | | | Al fcc | | | | | Ar fcc |
| K bcc | Ca fcc | Sc hcp | Ti hcp | V bcc | Cr bcc | Mn | Fe bcc | Co hcp | Ni fcc | Cu fcc | Zn hcp | Ga | | | | | Kr fcc |
| Rb bcc | Sr fcc | Y hcp | Zr hcp | Nb bcc | Mo bcc | Tc hcp | Ru hcp | Rh fcc | Pd fcc | Ag fcc | Gd hcp | In | | | | | Ke fcc |
| Cs bcc | Ba bcc | La | Hf hcp | Ta bcc | W bcc | Re hcp | Os hcp | Ir fcc | Pt fcc | Au fcc | Hg | Tl hcp | Pb fcc | | | | Xe fcc |

**Table 6.2** Metal elements and crystal structures

We examined the typical crystal structures of the metal elements. One metal alone is rarely used as a raw material; typically, metals are used in combination with other metals. Most metals we encounter in our daily lives are alloys of multiple metals, although the proportion of such metals in certain alloys may be miniscule. The crystal structure of an alloy depends on the mixing ratio and the temperature at which the metal is formed, and these parameters also affect its mechanical and electrical characteristics. Conversely, to understand the characteristics of metals, we must examine changes in the crystal structure.

Consider the example of brass, a binary alloy consisting of copper and zinc, shown in **Figure 6.4**. In their pure forms, Cu and Zn are stable when they are in the FCC and HCP configuration, respectively. When Zn is mixed with Cu, it forms the FCC structure called the α-phase until its content reaches about 35 atomic%. According to the Hume-Rothery rules, if the diameters of two atoms are approximately equal, the range of solid solubility is wide, as in the case of CuZn. In the α-phase, the FCC structure of the mother phase of Cu is mixed with Zn in a disorderly manner. This is called a disordered structure.

However, if the content of Zn reaches 50 atomic%, it becomes impossible to distinguish the mother phase. The range of solid solubility remains within several

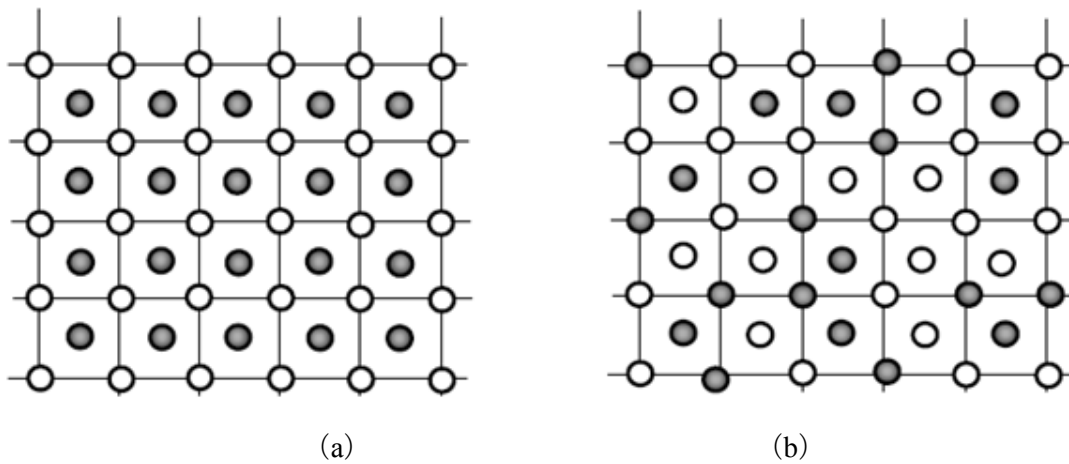percent, and the crystal structure becomes neither FCC nor HCP, but BCC. This is called the β-phase.



**Fig. 6.4** Schematic two-dimensional diagrams of ordered and disordered structures of CuZn. (a) Ordered structure: Stable at low temperatures, (b) Disordered structure: Stable at temperatures above 360°C

Even in the β-phase, both Cu and Zn are in the state of completely solid solutions in a disordered state at temperatures around 460°C and higher. But at lower temperatures, if the Cu is at the origin (0, 0, 0) of the unit cell, Zn is located at the body-centered cubic position (½, ½, ½), and the condition shifts to the ordered state. This structure is called the CsCl structure and is explained in the following section explaining ionic crystals.

If we gradually increase the temperature from relatively low levels, the crystal will show the orderly CsCl structure at room temperature, but change to BCC at temperatures above 360°C. If we observe the reflection that does not appear according to the extinction rule for the BCC (called a superlattice reflection) from the low-temperature phase, we will see that the reflection disappears at 360°C. This is because a phase transition occurs, and Cu and Zn shift from an orderly arranged structure to a disorderly structure, as shown in **Fig. 6.4**. This change does not occur suddenly at the transition temperature; rather, the change to the disordered state takes place gradually, starting at about 300°C. The structure formed during the course of the phase transition is called a short range order structure.

# 6.2 Structure of ionic crystals

Sodium chloride (NaCl), in which the positive ion, Na$^+$, and the negative ion, Cl$^-$, are alternately arranged and bound by Coulomb's force, is a typical ionic crystal. Generally speaking, the term *ionic crystal* refers to crystals formed by more than two types of ions with positive and negative charges bound by Coulomb's force. Metal atoms (e.g., Li, Na, K, Rb, and Cs) belonging to the Ia group in the periodic table and featuring the above-mentioned bonds can easily discharge one s-electron from the outer shell, forming positive ions with a closed-shell structure having spherical electron distributions. On the other hand, nonmetal atoms belonging to the VIIb group such as F, Cl, Br, and I have electrical characteristics that allow a relatively easy shift to a closed-shell structure of sp$^8$ by accepting a single electron. This results in negative ions. There is no anisotropy in crystals formed by Coulomb's force acting between ions, and their bonding energy exceeds that of metals, because the bonding power of Coulomb's force reaches far.

Of the several structural types determined by crystal structure, five are described here: the CsCl structure, NaCl structure, ZnS structure, wurtzite structure (a polytype of ZnS), and perovskite CaTiO$_3$.

### 6.2.1 CsCl and NaCl crystal structures

**Fig. 6.5** shows typical CsCl structures. First, let's examine the unit cell in **Fig. 6.5a**. The locations of ions contained in the unit cell are as follows. The Cs$^+$ ion is at the body-center position (½, ½, ½), while the Cl$^-$ ions are located at the corners (0, 0, 0) of the cubic lattice. Since one molecule is present in the unit cell, the unit cell is electrically neutral. At first glance, the electrical charge of the unit cell appears to be out of balance. However, the positive ion in the unit cell counts as "1," while the contribution of the negative ion at a corner is "1/8." Thus, the number of negative ions in the unit cell is 1 (8

× 1/8), and this is balanced by the positive ion at the body center. Next, let's consider the ion at the body center. This ion is surrounded by eight ions of a different type and bound by Coulomb's force. The second nearest neighbor ions are of a different type, and there are six ions in total. These must have a repulsive force. Thus, the number of neighbor ions increases alternately, but Coulomb's force acting between the ions declines in proportion to the square of the distance. Therefore, the structure retains the overall balance of forces.



(a)　　　　　　　　　　　　　　(b)
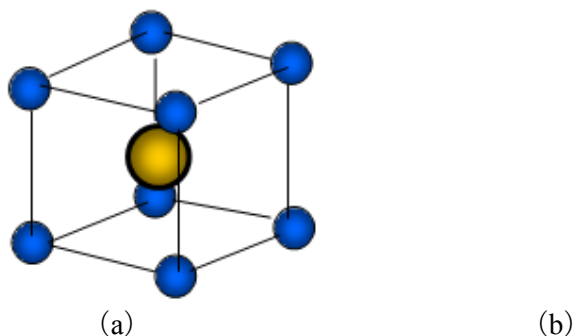
**Fig. 6.5** Unit cell of CsCl structure and (b) its extended structure

**Fig. 6.5b** shows an extended view of this crystal structure. The diagram shows this ion crystal consists of a simple cubic lattice created by $Cs^+$ ions and another simple cubic lattice created by $Cl^-$ ions; these two lattices are displaced by (½, ½, ½) in the body-center direction to form complex lattices. This feature of the CsCl structure is not unique, as ionic crystals typically form complex lattices as described above.

**Table 6.3** lists crystals that have the CsCl structure and their unit cell dimensions. These include not only ionic crystals, but binary alloys such as CuZn and combinations of $NH_4$ group and Cl ions, such as $NH_4Cl$.

| CsCl | TlBr | TlI | CuPd | CuZn | AlNi | BeCu | AgMg | LiHg | $NH_4Cl$ |
|---|---|---|---|---|---|---|---|---|---|
| a = 4.120 Å | 3.986 | 4.205 | 3.0014 | 2.954 | 2.881 | 2.702 | 3.280 | 3.287 | 3.88 |

**Table 6.3** Crystals that have the CsCl crystal structure

**Fig. 6.6** shows the unit cell of the NaCl structure. This belongs to the cubic crystal system, and we find four molecules in the unit cell. Positive ions (Na) are located at

face-centered cubic positions—(0, 0, 0), (½, 0, ½), (0, ½, ½), and (½, ½, 0)—while negative ions (Cl) are positioned at face-centered cubic lattice points—(0, 0, ½), (½, 0, 1), (0, ½, 1), and (½, ½, ½)—with the origin at (0, 0, ½), which is displaced by half the lattice constant of the unit cell in the direction [0, 0, 1]. This structure results in complex lattices with the positive face-centered cubic lattice and negative face-centered cubic lattice displaced by ½ in the direction [0, 0, 1].
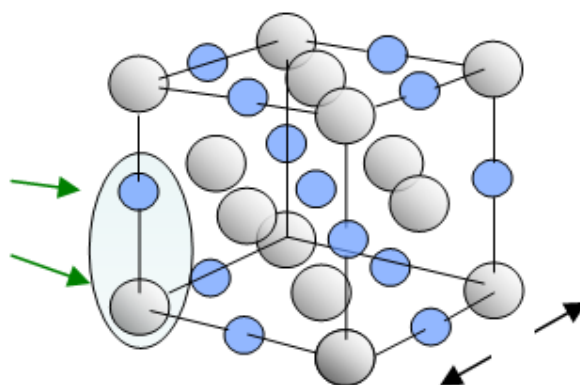


**Fig. 6.6** Structure of unit cell of NaCl crystal The large spheres and small spheres in the diagram represent Cl ions and Na ions, respectively.

The balance of ions in the unit cell is neutral, as in the case of CsCl. This is easily understood if we see that half of the ions at the face-center position contribute to the unit cell and ¼ of the ions located halfway to the crest contribute to the unit cell. In this structure, one ion of either type is always surrounded by six nearest neighbor ions, and the second nearest neighbor ions are 12 ions of the same type. Crystals that take this structure are indicated in **Table 6.4**, but the structure is not limited to ionic crystals.

| LiF | NaCl | KCl | KBr | AgBr | MgO | MnO | PbS |
|---|---|---|---|---|---|---|---|
| a= 4.027 Å | 5.6402 | 6.2952 | 5.770 | 6.775 | 4.216 | 4.443 | 5.931 |

**Table 6.4** Chemical compounds with the NaCl crystal structure. The numbers below indicate the size of the unit cell.

**6.2.2 Zincblende structure or copper chloride structure and wurtzite structure**

**Fig. 6.7a** shows a unit cell of **zincblende structure** (or cubic zinc sulfide structure) consisting of $Zn^{2+}$ ions which belong to the IIb group in the periodic table and $S^{2-}$ ions

which belong to the VIb group. Though it appears complex at first glance, the structure belongs to the cubic crystal system and the complex lattices are comprised of the FCC lattice created by $Zn^{2+}$ ions and the FCC lattice of $S^{2-}$ ions displaced by ¼ in the body-center direction. There are four ZnS molecules in the unit cell, and the positions of these ions are given below:

Coordinates of $Zn^{2+}$: (0, 0, 0),    (½, 0, ½),    (0, ½, ½),    (½, ½, 0)

Coordinates of $S^{2-}$:   (¼, ¼, ¼),    (¾, ¼, ¾),    (¼, ¾, ¾),    (¾, ¾, ¼)
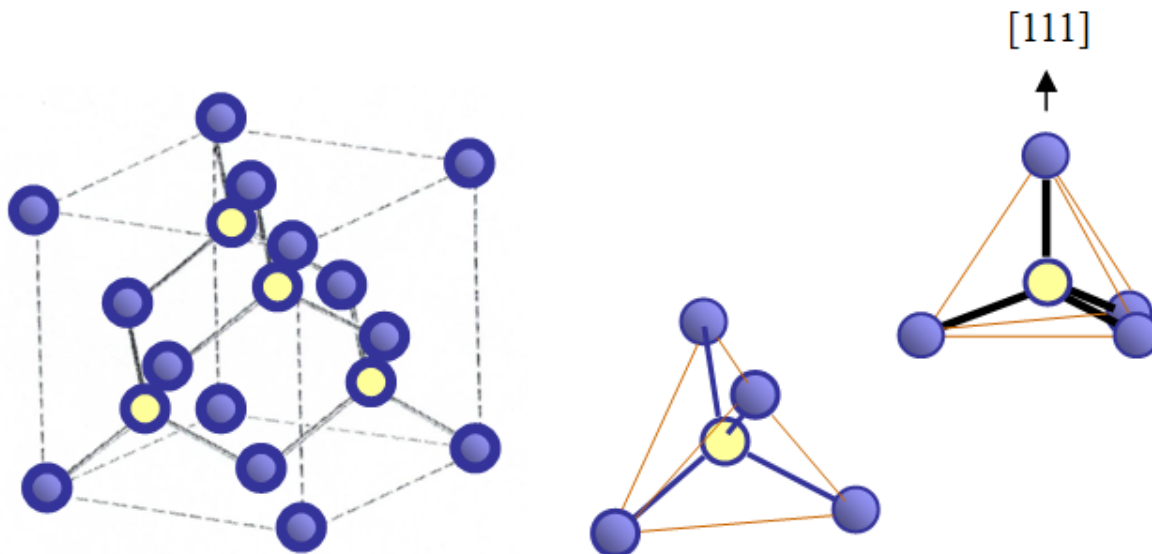


**Fig. 6.7** Ion crystal of zincblende structure. (a) Arrangement of ions in unit cell; (b) Ions are surrounded by the nearest neighbor ions of a different type arranged tetrahedrally. $Zn^{2+}S^{2-}_4$ can be regarded as the component element of this ion crystal.

If we focus on one ion and count the nearest neighbor ions, we will find four ions. The number is significantly smaller than that in the CsCl or NaCl structure. As shown in **Fig. 6.7b**, a tetrahedron surrounds these ions. The second nearest neighbor ions are of the same type, but the number is only eight. The structure with a small number of neighbor ions can be considered as a low-density crystal structure.

If we examine the tetrahedron unit by viewing the plane (110) with direction [111] as the z-axis, we see the ion configuration shown in **Fig. 6.8**. The sulfur ions represented by large circles in the diagram are stacked in the order ABCABC..., just like the FCC

structure of metals. This is because these ions adopt the FCC structure by nature. In Zn, an electrical double layer comprised of $Zn^{2+}$ and $S^{2-}$ is stacked in the order ABCABC.... If the electrical double layer stacking ABCABC... exists, there must also be an electrical double layer stacking of ABAB.... Such polytype structures belonging to the hexagonal crystal system are not limited to ZnS; they are also found with the substances shown in **Table 6.5**. This structure is called the wurtzite structure, or hexagonal zinc-sulfide structure. Interestingly enough, the axial ratio, c/a, is very close to the ideal value of 1.633, as indicated in **Table 6.5**.
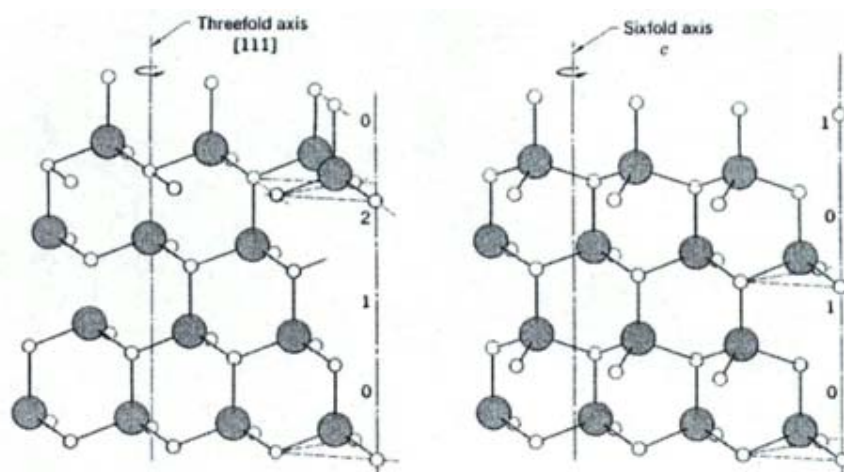


**Fig. 6.8** ZnS structure (cubic) and wurtzite (hexagonal) structure. In the structure shown in (**a**), the electrical double layer comprised of $Zn^{2+}$ and $S^{2-}$ is stacked in the order ABCABC.... In the wurtzite structure, the electrical double layer is ideally stacked in the order ABAB.... We observe a three-fold symmetry around the axis [111] in a cubic crystal, but when the wurtzite structure changes to a multiple-structure, that axis becomes the c axis of the hexagonal crystal, thus resulting in six-fold symmetry.

We use IIb-VIb-group ionic crystals as an example here, but the combination of ionic crystals is not limited to this group. As shown in **Table 6.5**, there are various combinations of Ib-VIIb-group ionic crystals and IIIb-Vb-group ionic crystals. If the valence value increases, it becomes difficult to determine whether the atoms have been ionized. Although some ion bonding remains, it is weak, and the covalent bond of electrons is stronger. As in the case of silicon carbide (SiC), Vb-Vb-group substances are classified as covalent crystals, not ionic crystals. For your reference, **Fig 6.9** shows the

differences in diffraction profile between the zincblende structure and wurtzite structure. The wurtzite structure is characterized by three strong diffracted beams, (100), (002), and (101), which appear first in the hexagonal crystal system.
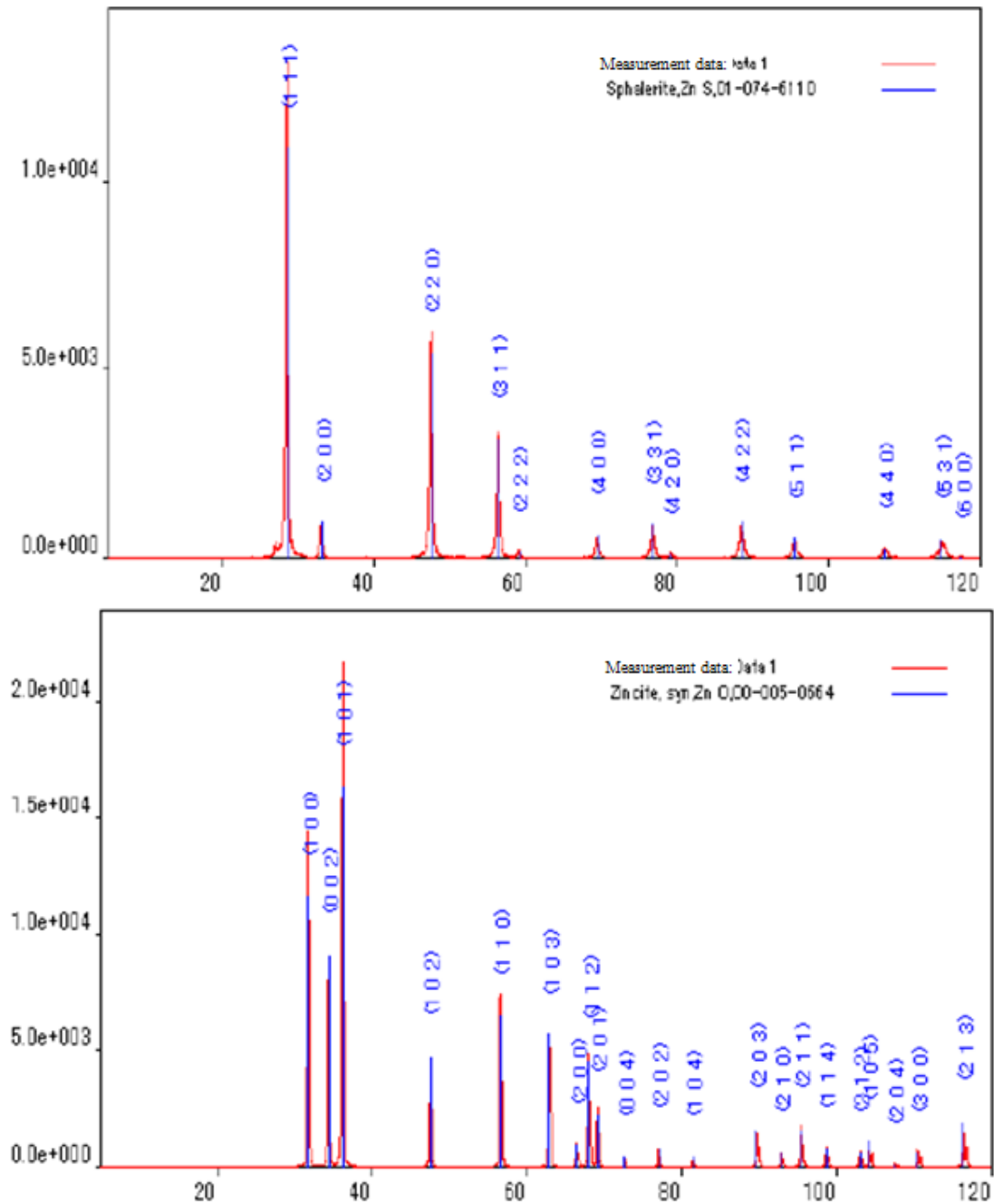


**Fig. 6.9** X-ray diffraction profiles of ZnS structure (top) and ZnO wurtzite structure (bottom)

| Name of crystal | Cubic crystal (zincblende structure) | Hexagonal crystal (wurtzite structure) | | Remarks (bonding) |
|---|---|---|---|---|
| SiC | a = 4.358Å | a= 3.079Å | c = 5.053Å | (Covalent) |
| AlF | 4.32 | - | | IIIb-VIIb |
| CuF | 4.264 | - | | Ib - VIIb |
| CuCl | 5.4202 | - | | Ib - VIIb |
| ZnO | - | 3.249 | 5.205 | IIb - VIb |
| ZnS | 5.4109 | 3.811 | 6.2334 | IIb - VIb |
| ZnSe | 5.670 | 3.974 | 6.506 | IIb - VIb |
| ZnTe | - | 4.273 | 6.989 | IIb - VIb |
| AgI | 6.466 | - | | Ib - VIIb |
| αAgI | 5.106 (Im-3m) | | | |
| CdS | 5.720 | 4.140 | 6.715 | IIb - VIb |
| CdSe | - | 4.299 | 7.010 | IIb - VIb |
| InAs | 6.055 | - | | IIIb - Vb |
| InSb | 6.478 | - | | IIIb - Vb |

**Table 6.5** Zincblende structure and wurtzite structure

**Problem:** Referring to the X-ray diffraction profiles shown in **Fig. 6.9**, confirm their intensity modulations by calculating their crystal structure factors.

### 6.2.3 Structure of CaF$_2$ crystal

Another ionic crystal worth mentioning here is the CaF$_2$ crystal structure. Thus far, we have examined binary ionic crystals. In these crystals, the ionic valence value is the same, but the crystal is formed by ions of different types, A$^+$ and B$^-$. There are crystals of another type, in which one type of ion has a valence value of 2, and another type of ion has a valence value of 1, but since two such ions exist, electrical neutrality is maintained.
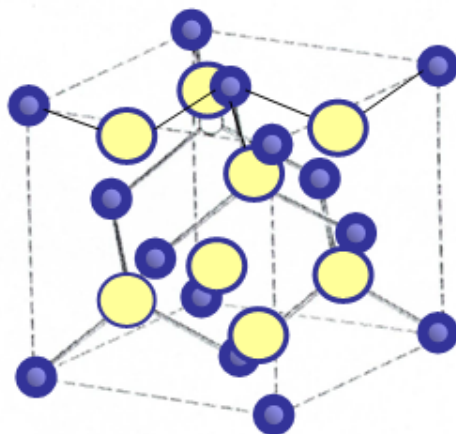


**Fig. 6.10** Unit cell of CaF$_2$ structure

**Fig. 6.10** shows the unit cell of $CaF_2$. A $Ca^{2+}$ ion with a valence value of 2 is located at the FCC position, while $F^-$ ions having a valence value of 1 are in the FCC configuration with (¼, ¼, ¼) and (¼, ¾, ¼) as the origins. This ionic crystal maintains electrical balance in its unit cell. **Table 6.6** shows the crystals of this type. As we see in the table, there are generally two halogen ions having a valence value of 1 for each alkali ion having a valence value of 2. But in many cases, as we see with $Cu_2S$, there are two metal positive ions $Cu^+$ having a valence value of 1 (which belongs to the Ib group in the periodic table) for each negative ion $S^{2-}$ having a valence value of 2 (which belongs to the VIb group). The stacking [111] indicates the two layers formed by ions having a valence value of 1 sandwich ions having a valence value of 2 to maintain electrical neutrality.

| Name of material | Lattice constant | Distance between nearest neighbor ions (Å) | Remarks |
|---|---|---|---|
| $CaF_2$ | 5.463 | 2.36 | IIa - VIIb |
| $SrF_2$ | 5.800 | 2.50 | |
| $SrCl_2$ | 6.977 | 3.02 | |
| $BaF_2$ | 6.200 | 2.68 | |
| $CdF_2$ | 5.389 | 2.34 | II b - VIIb |
| $PbF_2$ | 5.940 | 2.57 | IVb - VIIb |
| $CsO_2$ | 6.620 | 2.34 | Ia   - VIb |
| $PrO_2$ | 5.394 | 2.32 | IIIa - VIb |
| $ThO_2$ | 5.598 | 2.41 | |
| $ZrO_2$ | 5.090 | 2.20 | IVa - VIb |
| $Li_2O$ | 4.610 | 2.00 | Ia – VIb |
| $Li_2S$ | 5.719 | 2.47 | |
| $Na_2S$ | 6.539 | 2.83 | |
| $Cu_2S$ | 5.564 | 2.42 | Ib – VIb |
| $Cu_2Se$ | 5.854 | 2.49 | |

**Table 6.6** Ionic crystals with $CaF_2$ structure

The X-ray diffraction profile shown in **Fig. 6.11** was obtained from a $CaF_2$ powder sample using the MiniFlex II and CuKα rays. The observed curve is indicated in red, while the intensity modulation obtained from an ICDD search is shown in blue. The graph shows a close match between the two.
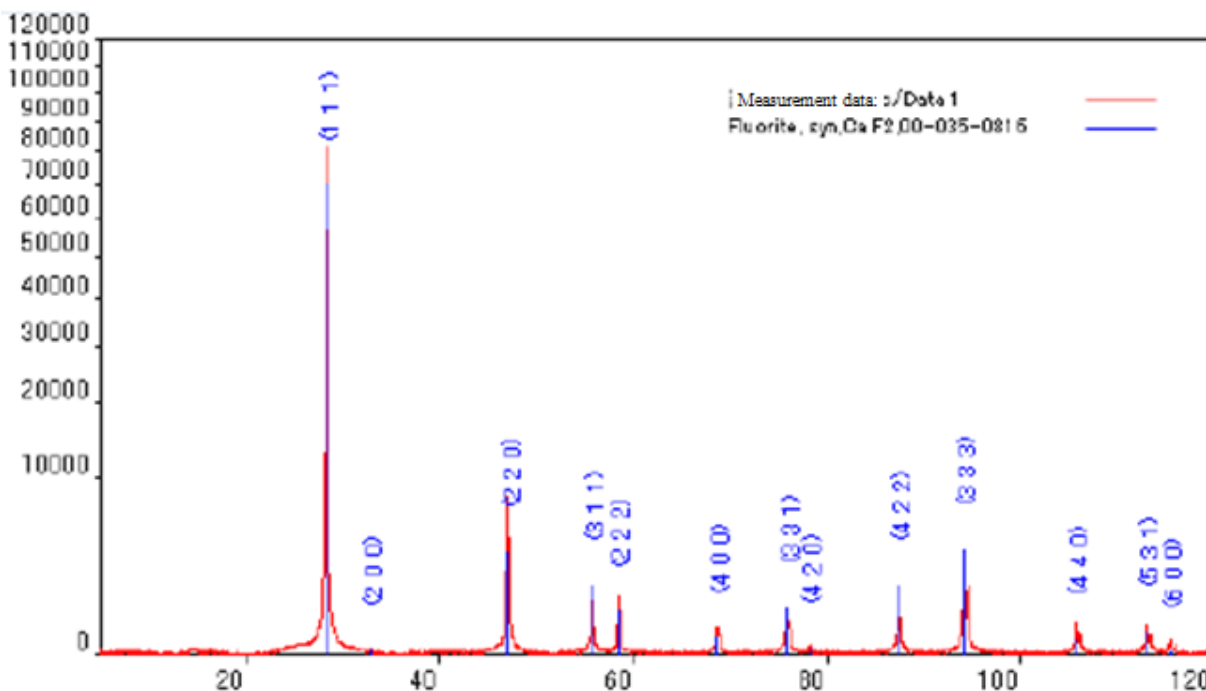
**Fig. 6.11** X-ray diffraction profile of CaF$_2$ obtained using MiniFlex II. The observed curve is indicated in red, while the intensity modulation obtained from an ICDD search is shown in blue.

### 6.2.4 Perovskite crystal structure

The **perovskite structure** is somewhat more complex than those discussed above. This is a cubic crystal, abbreviated as RMX$_3$, and the representative crystal is perovskite (CaTiO$_3$). **Fig. 6.12** shows the ion configuration in the unit cell. The positive ion R$^{2+}$ having a valence value of 2 is located at each corner of the unit cell, while the positive ion M$^{4+}$ having a valence value of 4 is located at the body center. To achieve electrical balance, negative ions X$^{2-}$ having a valence value of 2 are positioned at the face-centered cubic positions. From a different perspective, this structure can also be described as follows: The simple cubic lattice is formed by the positive ions R at the corners; six X$^{2-}$ negative ions at face-center positions form an octahedral cluster of MX$_6$, around the M$^{4+}$ located at the body-center position. The R$^{2+}$ positive ions at the corners occupy vacant spaces within the cluster. The structure is electrically balanced.

**Fig. 6.13** shows the X-ray diffraction profile observed using the MiniFlex II and

CuKα rays. Although this is a cubic crystal, complete extinction does not occur on any reflection plane and all reflections appear. But since oxygen (O) atoms are smaller than calcium (Ca) or titanium (Ti) atoms, the corresponding contribution to scattering can be regarded as very small. On the other hand, the atomic numbers of Ca and Ti are 20 and 22, respectively, and they may be mutually canceling or reinforcing. Since they have the positional relationships of a BCC lattice, we can expect intensity modulation, based on the extinction rule applicable to the BCC lattice. Keeping this in mind makes it possible to index reflections easily.
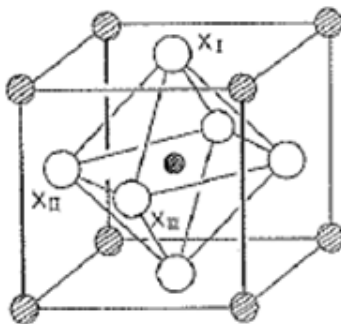


**Fig. 6.12** Perovskite crystal structure. Positive ions (striped circles) having a valence value of 2 are located at the corners of the cubic crystal, while negative ions (open circles) having a valence value of 2 form an octahedron. A positive ion, M (solid circle), having a valence value of 4, is located at the center. Thus, this structure maintains its electrical balance.

This structure has a center of symmetry and is an electrically neutral insulating body. However, the cluster group deforms readily due to the difference in radius between R and M ions. As deformation occurs, the structure changes to another crystal system of reduced symmetry, such as a tetragonal, orthorhombic, or triclinic structure. Polarity also appears (polarization), and the dielectric characteristic (electric-field-dependent phenomenon of electric displacement resulting from the application of an electrical field to crystals) changes significantly. Certain crystals become ferroelectric (polarization condition) while others become antiferroelectric (polarization condition differing from that in adjacent unit cell). Such crystals polarize when external pressure

is applied. If we apply an electrical current, the crystals deform (**piezoelectric effect**). Crystals with this characteristic are used in various applications.
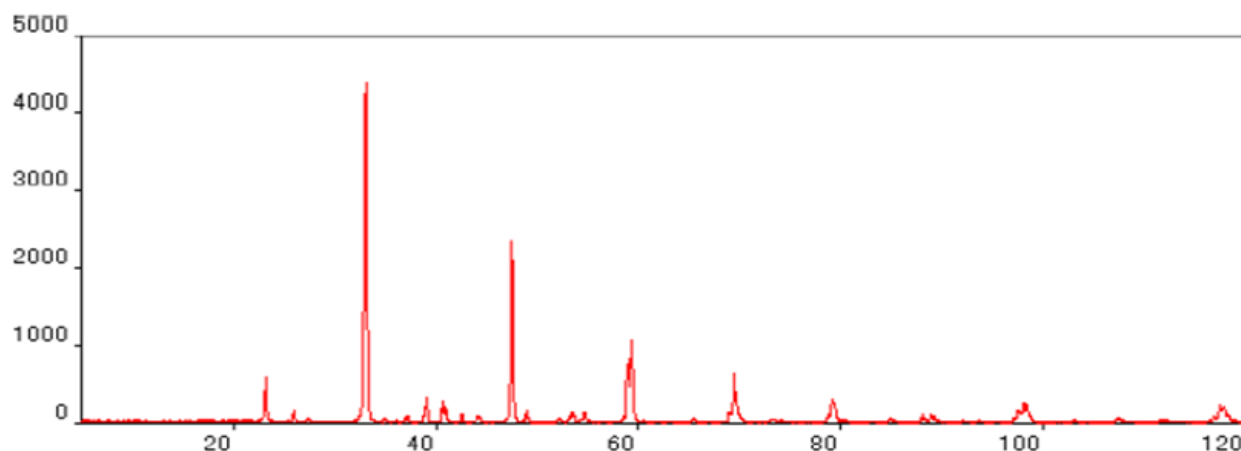


**Fig. 6.13** X-ray diffraction profile obtained from $CaTiO_3$ powder using $CuK\alpha$ rays

If we examine dielectric characteristics across a wide temperature range, we will see certain cases in which distinctive phase transitions occur. For instance, barium titanate ($BaTiO_3$) changes in the following sequence: paraelectric cubic crystal $\rightarrow$ ferroelectric tetragonal crystal $\rightarrow$ monoclinic crystal with different ferroelectric axis $\rightarrow$ triclinic crystal with further changed ferroelectric axis. In the case of lead zirconate ($PbZrO_3$), the following phase transition occurs: paraelectricity $\rightarrow$ superlattice structure with antiferroelectricity.

Phase transitions from a ferroelectric phase with polarity in a certain direction to a ferroelectric phase with polarity in another direction occur as well. We mentioned that the $MX_6$ octahedron in $SrTiO_3$ and $LaAlO_3$ is readily deformed. However, the octahedron in $TiO_6$ will not deform, as shown in **Fig. 6.14a**. Instead, it rotates around the crystallographic axis <001> and changes its direction while maintaining consistency with the octahedrons located above, below and on the right and left sides, thus achieving phase transition to a superlattice structure. This is called structural phase transition. **Fig. 6.14b** shows the superlattice structure viewed from the direction <001>.
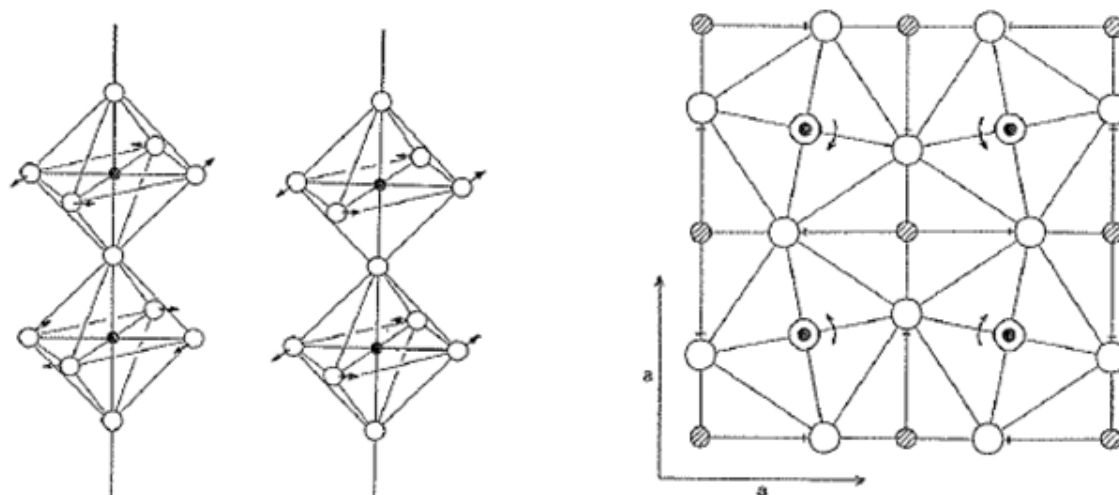
**Fig. 6.14** Superlattice structure seen in SrTiO$_3$ and other crystals. The TiO$_6$ cluster tends to generate rotational vibration around the crystallographic axis. It is believed that freezing of that vibration mode results in the transition to a superlattice structure. Two possible rotation vibrations are shown in (a), while a superlattice structure after freezing is indicated in (b).

**Table 6.7** lists the names of materials with this crystal structure, lattice constants, and possible phase transitions. Note that this is not a complete list.

| Name of crystal | Lattice constant | Phase transition temperature (°C) | Remarks |
|---|---|---|---|
| BaTiO$_3$ | 3.994 4.03 (P4mm) | 130, 5, -75 | Ferroelectric transition |
| KNbO$_3$ | 3.997 4.06 (P4mm) | 435, 225, -10 | Attributable to MX$_6$ deformation |
| PbTiO$_3$ | 3.904 4.150 (P4mm) | 490 | |
| KTiO$_3$ | None | < -273 | |
| NaNbO$_3$ | 3.927    3.934 | 643, 572, 520, 480, 365 | Antiferroelectric phase transition |
| PbZrO$_3$ | ? | 233 | MX$_6$ deformation |
| PbHfO$_3$ | 4.140? | 215 | |
| SrTiO$_3$ | 3.905 | -168 | Phase transition to superlattice structure |
| KMnF$_3$ | 4.190 | -87, -181 | Attributable to MX$_6$ rotation |
| LaAlO$_3$ | None | 535 | |
| CsPbCl$_3$ | 5.605 | 47, 42, 37 | |
| CsPbBr$_3$ | 5.870 | 131, 89 | |

**Table 6.7** Perovskite crystal and crystal phase transition

Shown here are the basic structures and their main phase transitions. We can also modulate these basic structures: for example, by mixing two or more crystals with a

number of characteristics to synthesize new crystals, such as $(R^a_{1-x}, R^b_x)(M^a_{1-y} M^b_y) X_3$. Mixing ratios are readily varied with powder ceramics, and various materials with unique characteristics are currently being developed.

## 6.3 Covalent crystals

Carbon, silicon, germanium, and tin, which belong to the IVb group in the periodic table, feature a diamond[4] structure composed of carbon atoms. In this structure, atoms are attracted by **covalent bonding** (or **homopolar binding**). They represent a structure typical of covalent crystals. **Fig. 6.15a** symbolically expresses this type of bond. Carbon, silicon, and germanium have four outer-shell electrons but require four electrons to achieve stable closed shells. They borrow four electrons from surrounding neighbor atoms to meet this need, providing their own four outer-shell electrons to neighbor atoms. In other words, covalent bonding achieves stability by sharing electrons with other atoms to create closed shells.

### 6.3.1 Diamond structure crystal

**Fig. 6.15b** is a diagram showing a unit cell of a diamond structure crystal. This structure is occupied by atoms of one type belonging to the IVb group in a zincblende structure, regardless of positive or negative ions. In this structure, we find two FCC lattices, displaced ¼, ¼, ¼ in the body-center direction. Inside the unit cell, eight atoms are positioned at the following locations:

   0, 0, 0;   ½, ½, 0;   ½, 0, ½;   0, ½, ½;   ¼, ¼, ¼;   ¾, ¾, ¼;   ¾, ¼, ¾;   ¼, ¾, ¾.

Just as with the zincblende structure, one atom—for example, the atom at coordinates ¼, ¼, ¼—is surrounded by four neighbor atoms, forming a tetrahedron

---

[4]  Certain substances display different crystal structures under identical temperature and pressure, which are called polymorphs. Due to the differences in crystal structure, the physical properties vary as well. A typical example is carbon: Graphite and diamond are polymorphs to each other. In recent years, polymorphs such as fullerenes and carbon nanotubes have been discovered and attracted attention.

when connected to these four atoms. In this case, each atom is located at the center of the tetrahedron and borrows four electrons from the four atoms at the apices of the tetrahedron to produce an apparent closed-shell structure and achieve stability.
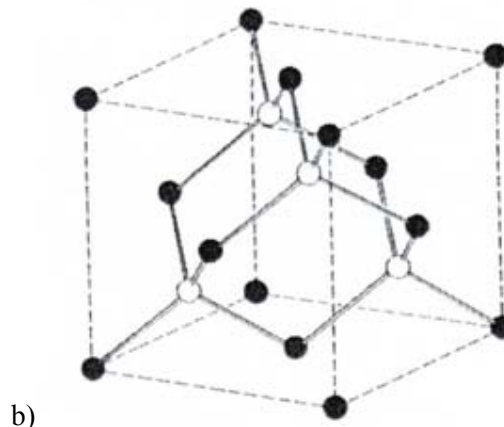


a) MISSING FIGURE                              b)

**Fig. 6.15** Covalent bonding (a) and diamond crystal structure (b). The diagram in (a) illustrates the covalent bonding symbolically. The diagram in (b) shows a diamond structure. This structure is the same as a zincblende crystal structure, but with atoms of the same type, not different ions. There are four neighbor atoms with which bonding electrons are shared.

Unlike in the zincblende structure, this structure features covalent bonding with shared electrons. With ionic bonds, electrons are distributed in a spherical configuration having each ion positioned at the center. In the case of covalent bonding, electrons are located between and shared by the atoms. Consider the example of diamond. The carbon atom has a total of four electrons in the s-orbital and p-orbital of the L shell, extending in the direction of neighbor carbon atoms to form an $sp^3$ hybrid orbital and sharing electrons with four neighbor carbon atoms. Thus, bonding electrons are found between the carbon atoms. The presence of these bonding electrons can be confirmed through X-ray crystal structure analysis.[5] The lattice constant is 3.56 Å for diamond and 5.43 Å and 5.65 Å for Si and Ge, respectively. Tin (Sn) also belongs to the IVb group and is known to have a diamond structure. However, it is stable at temperatures below 7°C; its lattice constant is 6.46 Å.

---

[5]  Kato et al. report announced circa 1964

Silicon (Si) has been used as the basic material for semiconductor elements since the 1960s, and there is growing demand for high-quality, large-diameter single crystals. This has led to the excellent powder samples currently available. Active research on this material has led to highly precise lattice constants. Si is often used as a standard sample in powder X-ray diffraction. **Fig. 6.16** shows the X-ray diffraction profile obtained with the MiniFlex II.
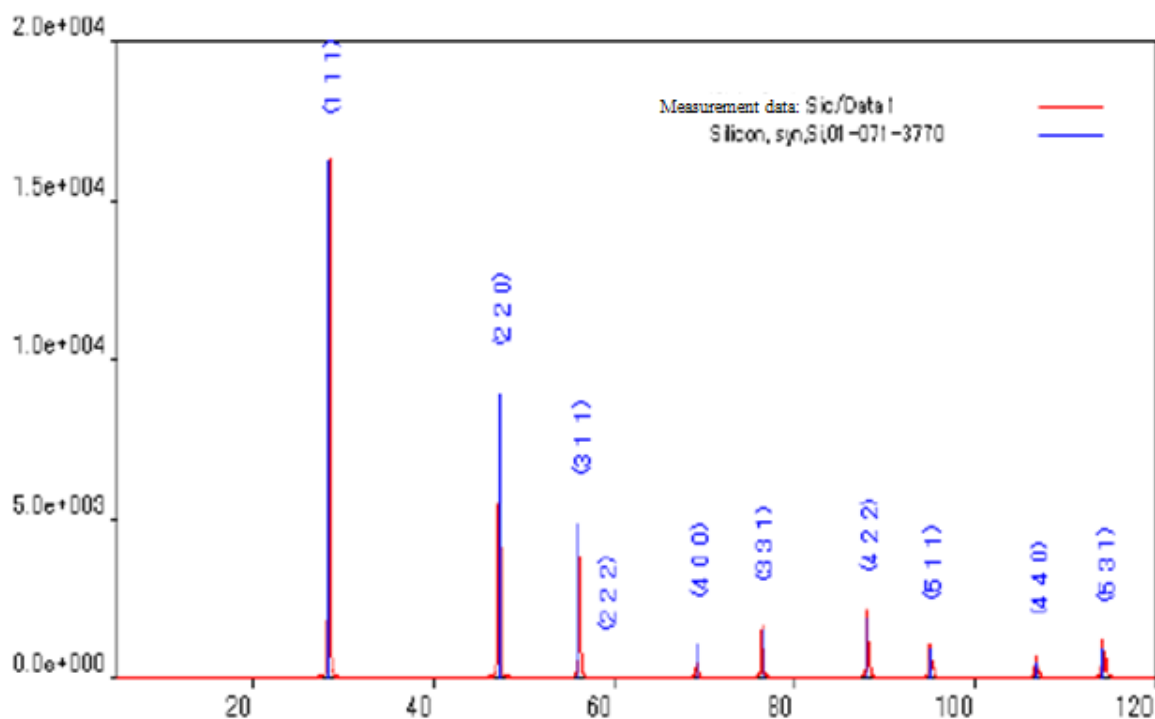


**Fig. 6.16** X-ray diffraction profile of silicon powder. The measurement was obtained with the MiniFlex II. The diffracted X-rays show very sharp peaks.

**Problem:** The diffracted image obtained from a diamond structure displays a unique extinction rule. Describe this extinction rule.

### 6.3.2 Structure of quartz

The scientific name for crystals[6] of pure $SiO_2$ is quartz. As shown in **Fig. 6.17**, two forms exist: right-handed and left-handed, distinguishable by their external appearance. In terms of physical properties, the two types of quartz feature opposite **optical rotatory**

---

[6] In Japan, the term "crystal" in general refers to a large beautiful crystal. Such usage is not observed in other countries.

**power** (rotating phenomenon caused by deflected surface of light passing through a crystal). The two types are also called right-angled quartz and left-angled quartz.
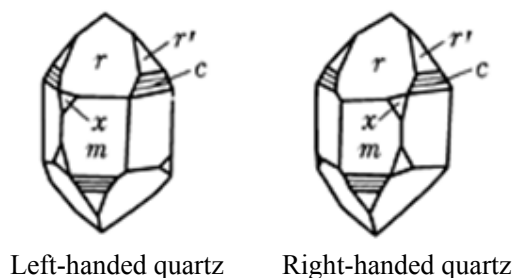


Left-handed quartz     Right-handed quartz

**Fig. 6.17** Two external quartz shapes

As its appearance indicates, quartz belongs to the trigonal crystal system and can be expressed with symmetry P3$_2$21. The lattice constants are a = b = 4.912(1) Å, c = 5.402(1) Å, $\alpha$ = $\beta$ = 90°, $\gamma$ = 120°, and the unit cell contains three molecules. Given the coordinates of the Si and O atoms in the unit cell, the unit cell can be illustrated as shown in **Fig. 6.18**. The position of the Si atom in the unit cell can be expressed as follows, based on the following parameters: x = 0.5302, y = 0, z = 1/3:

$$(x, y, z); \quad (-y, x-y, z+(1/3)); \quad (-x+y, 1x, z+(2/3))$$

In **Fig. 6.18a**, the Si atom (blue) is located at the center of the tetrahedron formed by O atoms (red). The Si atom and four O atoms are bound by covalent bonds. The structure consists of a three-dimensional network of tetrahedrons, shown in **Fig. 6.18b**. This crystal has **piezoelectricity**, a characteristic that is attributed to the deformation resulting from the electrical field or stress caused by the regular tetrahedron surrounding the Si atom. In passing, piezoelectricity is believed to have been first observed (in 1811) in quartz.

**Fig. 6.19** shows the X-ray diffraction profile. Based on this diffraction pattern, we can see the absence of disappearing reflections. All reflections can be observed, and they appear intricate.

Heated to temperatures around 575°C, quartz undergoes a phase transition, becoming hexagonal-crystal high-temperature quartz. We now know that the change is

not directly from the low-temperature structure to the high-temperature structure, but that the structure changes twice in sequence within a narrow temperature range.
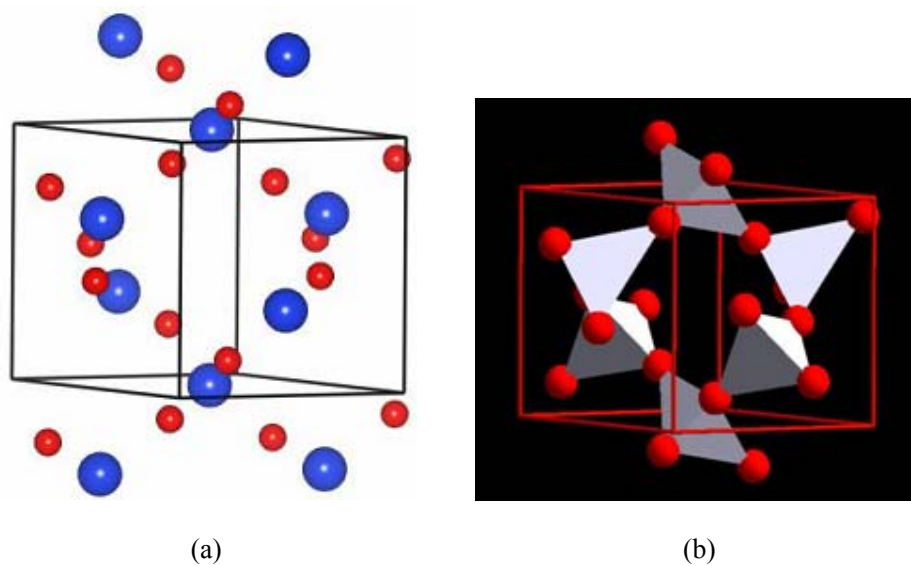


(a)                                                           (b)
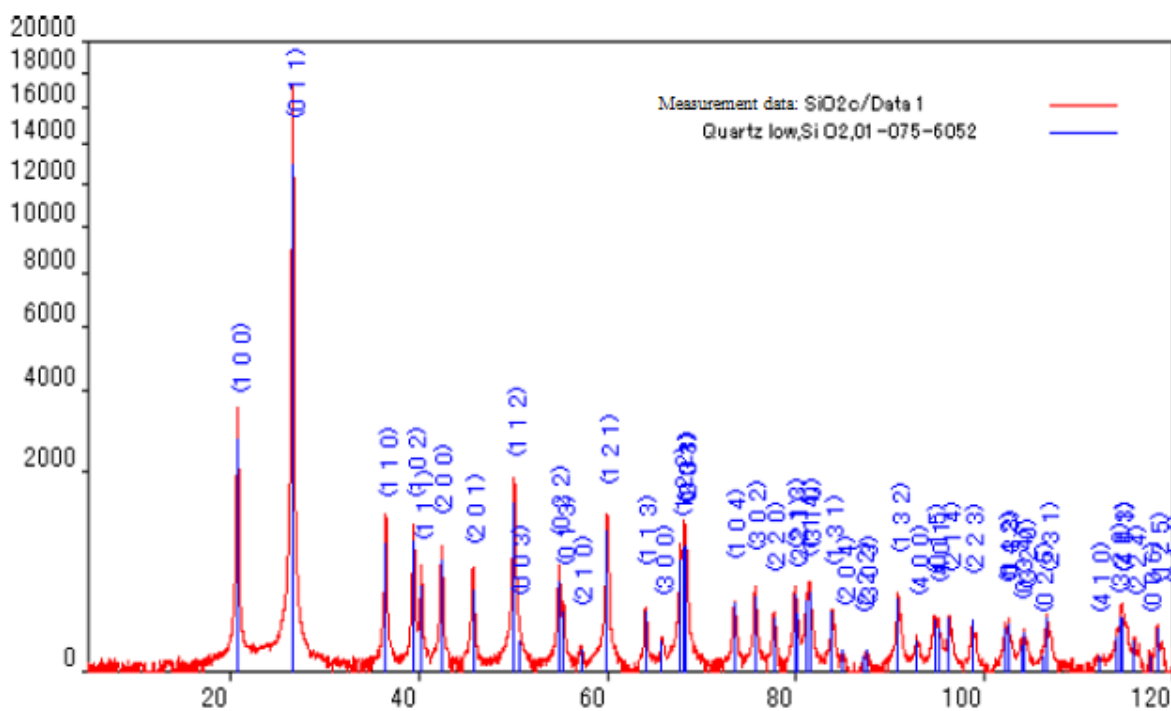
**Fig. 6.18** Crystal structure of quartz



**Fig. 6.19** X-ray diffraction profile of quartz obtained using CuKα rays

**Problem:** Referring to the diffraction profile shown in **Fig. 6.19**, extract the indices of a

strong reflection and examine the reflection-causing plane of the crystal lattice.

**Problem:** Earlier in this booklet, we mentioned that unique diffracted X-ray patterns called "five fingers" appear in the diffraction profile of quartz. Referring to **Fig. 6.19**, try to determine their indices.

## 6.4 Graphite crystal structure

**Fig. 6.20** shows the crystal structure of graphite. Carbon atoms are located at the connecting points of orderly arranged hexagonal lattices, forming an atomic plane. In graphite, atomic planes are displaced laterally and stacked to form layers. Graphite is also called black lead, but is more commonly called graphite today. The diagram shows the unit cell with a dotted line.
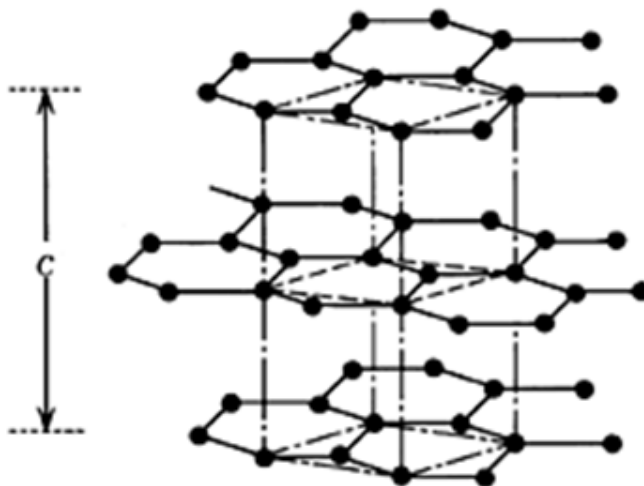


**Fig. 6.20** Crystal structure of graphite. The area indicated by the dotted line is the unit cell.

Graphite belongs to the hexagonal crystal system, and the lattice constants are a = 2.456 , c = 6.696 Å. The unit cell contains four carbon atoms, positioned at 0, 0, 0 and 1/3, 2/3, 0 on the plane of z = 0, and at 0, 0, ½ and ½, 2/3, ½ on the plane of z = ½. In the plane, the C atom is surrounded by three neighbor atoms. The interatomic distance is 1.42 Å. Although this distance is less than the C-C distance of 1.54 Å in the diamond structure, it is longer than the distance of 1.39 Å resulting from the formation of a

benzene ring by carbon atoms. This structure indicates a covalent bond between C and C. The distance between the planes is long, 3.35 Å, and the planes are bound by the weak Van der Waals force. This structure allows easy sliding of the atomic planes. This is why powder graphite feels smooth and graphite is easily bent. The existence of many polytypes is also believed to be attributable to this bond.

Graphite has a melting point of 3550°C, higher than any other element. Its heat conductivity, elasticity, magnetic susceptibility, and thermal expansion exhibit noticeable anisotropy. With respect to the state of the electrons of the carbon atoms, atoms in the plane are bound by σ-binding of $sp^3$, but one surplus electron in the outer shell is an unpaired π electron, and a C-ion plane with two-dimensional periodicity contributes to conduction, providing the same electric conductivity as a metal. However, conductivity in the c-axis direction is lower by four orders of magnitude, and we observe significant anisotropy. The excellent electric and thermal conductivity of graphite is attributable to the arrangement of the atoms in the plane.

When carbon hydride is placed on a high-temperature base and compressed for thermal decomposition, the graphite layer grows with good orientation. This is called pyrolytic graphite. The (002) plane of graphite has a long interplanar spacing, making graphite suitable for use as an analyzing crystal. However, single crystals of graphite are difficult to obtain. Pyrolytic graphite is suitable for this purpose, and this crystal is used frequently.

**Fig. 6.21** shows the diffraction profile obtained from a pyrolytic graphite sample using the MiniFlex II. It features a very strong 002. By comparison, all other reflections are weak. The full width at half maximum of each reflection is wider that those of other crystals. These characteristics derive from the small crystallite size and numerous flaws in the crystal. The lattice plane of a crystal used for monochromatization of X-rays is the plane 002. This is because the intensity from this plane is high, and the diffraction angle appears on the base angle side, making it easy to use.
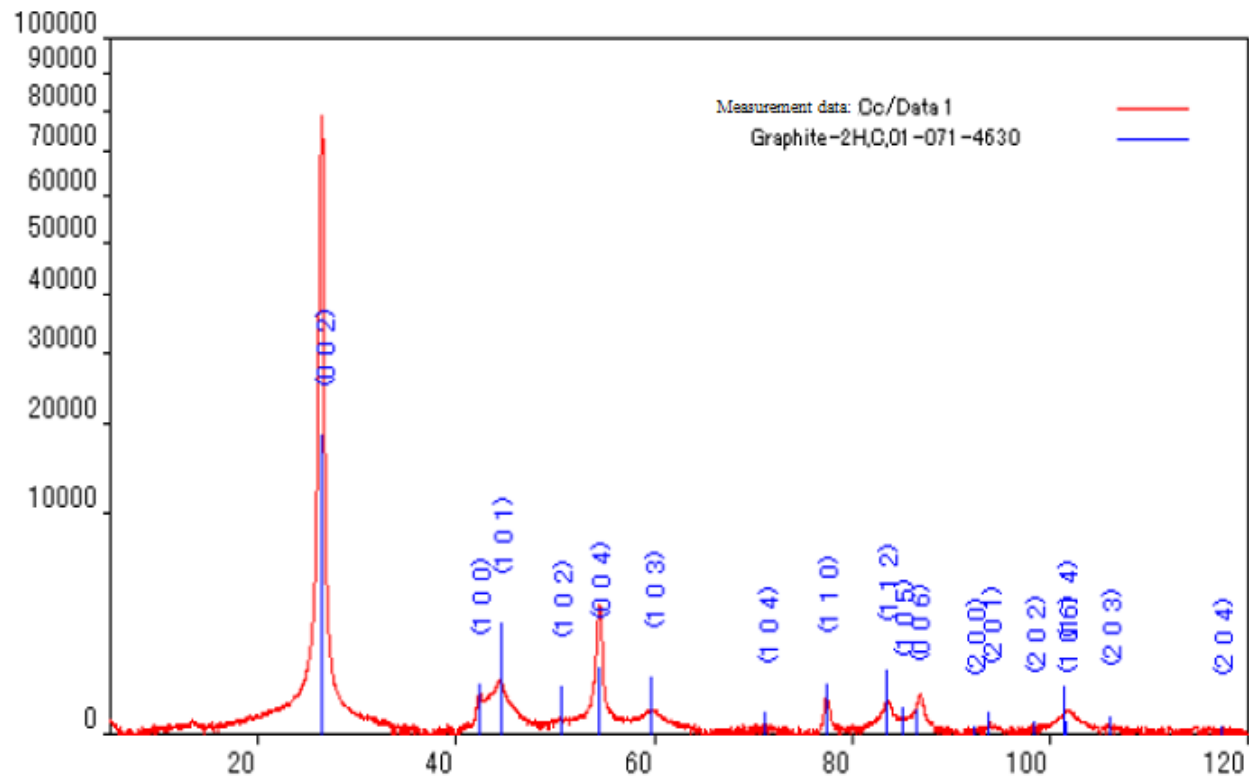
**Fig. 6.21** X-ray diffraction profile of graphite obtained using CuKα rays

If carbonaceous high polymers are carbonized at high temperatures, we obtain glassy carbon. In this black carbon material, graphitization has not progressed in terms of structure, and disorderly three-dimensional bonds are found between carbon atoms. The material is not in a crystal state and offers high resistance to heat and chemicals.

## 6.5 Molecular crystal

Some crystals are called molecular crystals. These differ from the crystals discussed thus far in their mechanism of agglomeration. Because agglomeration depends on the weak Van der Waals force acting between molecules, the corresponding melting point is significantly lower than that of crystals bound by other forces, and the latent heat of fusion is also small. In many substances, the molecular structure seen in the gas state remains virtually unchanged, even when crystallized. We say "virtually" here because

the interatomic distances in molecules in the vapor state differ slightly from those in a crystallized state. Putting that aside, to elucidate the crystal structure, we crystallize the substance in certain cases and apply X-ray diffraction for crystal structure analysis. Confirming the atom positions in the unit cell lets us grasp the molecular structure. This method is currently used to examine the structures of organic molecules. The widely performed structural analyses of proteins are a good example. Since crystal structure depends on the shape and size of the molecules, crystals with good symmetry are rather rare.

There are many other examples of such crystals, but we will take a very simple **molecular crystal** as an example and give a brief discussion. First, we introduce how the structures changes when inert gases like He, Ne, A, Kr, and Xe; diatomic molecules in the gas state under ordinary temperature and pressure like $H_2$, $N_2$, $O_2$, $CO_2$, $Cl_2$, and $Br_2$; and HF, HCl, HBr, $H_2O$, $H_2S$, $H_2Se$, $NH_3$, $PH_3$ and $CH_4$ liquefy under low temperatures, then solidify and crystallize. Of these, helium (He) assumes the HCP structure, while Ne, A, Kr, and Xe assume the FCC structure. Although we cannot explain here why only He assumes the HCP structure, given that the inert atoms are regarded to have spherical electron distributions, the structure appears reasonable.

Consider diatomic molecules, represented by $H_2$. These molecules also assume the HCP structure, except at extremely low temperatures. Since diatomic molecules are shaped like cocoons, although it is not easy to imagine, the molecules move as if freely rotating near their barycentric positions even when crystallized. Thus, we can regard them as spherical. At low temperatures, the rotational motion becomes inactive. It would be interesting to learn what structure it adopts in this state.

Hydrogenated molecules assume interesting structures, except for substances associated with hydrogen bonds, such as HF, $H_2O$, and $NH_3$. Just as with $H_2$, the rotational energy of molecules near the melting point is less than the thermal energy $k_BT$, and free rotation is possible. The molecule is considered to be a sphere and to

assume the FCC structure. As temperature decreases, however, the structure changes, becoming more complex. These substances are hard-to-handle gases, solidifying at low temperatures and making experiments difficult. For these reasons, research has not advanced beyond that done quite some time in the past. Certain reference materials are listed for your reference.

# 6.6 Crystal bound by hydrogen bonding

Atoms of the same type (X-X) or of different types (X-Y) are often bound by hydrogen (H), forming X-H-X or X-H-Y. In most cases, X and Y are light elements that change readily to negative ions, such as fluorine (F), oxygen (O), and nitrogen (N). These bonds are achieved as follows: The hydrogen atom between the two atoms releases an electron and becomes a proton ($p^+$). The released electron is received by X or Y, resulting in a negative ion. This attracts $p^+$ due to Coulomb's force. We can regard this as localized ion bonding. This type of interatomic binding mode is called hydrogen bonding. We observe hydrogen bonds within single molecules, but they also act between molecules and contribute to the agglomeration mechanism. This bond has directionality and is stronger than Van der Waals forces. Its effects can be observed in a crystallized material as deformation of the molecular structure of the gas state.

### 6.6.1 Crystal structure of ice

Ice crystals are representative crystals bound by hydrogen bonds. At atmospheric pressure, water freezes and changes to ice when temperatures fall. The resulting structure is a ZnS structure hexagonal crystal system, called the $I_h$ phase. In this crystal structure, all Zn and S positions are occupied by O atoms. Each oxygen atom is surrounded by four neighbor oxygen atoms in a tetrahedral arrangement, and one hydrogen atom is always found between the O atoms. Two hydrogen atoms always

exist spatially near each oxygen atom. At a given moment, each oxygen atom in this structure appears to configure an H₂O molecule. The hydrogen atom is in the O-H⋯O configuration at a given point in time, belonging to the oxygen atom on the left side, but in an O⋯H-O configuration, belonging to the oxygen atom on the right side, in the next. We see this bond when an electron from the H atom moves to an oxygen atom, leaving the hydrogen atom as a bare proton (p⁺) and the oxygen atom as a negative ion, O⁻, and generating localized ionic bonds of O⁻- p⋯O⁻. This structure exists only momentarily. The average structure is expressed O-p/2 ⋯ p/2-O. The proton occupies one of the two positions between the two oxygen atoms, with the probability of occupying either position being ½. In this structure, the bonds between oxygen atoms are partially strengthened in the manner described above. This is the difference from molecular crystals bound by the Van der Waals force.

| Ice | Crystal sstem | Density (g/cm³) | Ice | Crystal system | Density (g/cm³) |
|---|---|---|---|---|---|
| I$_h$ | Hexagonal | 0.92 | V | Monoclinic | 1.23 |
| I$_c$ | Cubic | 0.93 | VI | Tetragonal | 1.31 |
| II | Rhombohedral | 1.17 | VII | Cubic | ~1.50 |
| III | Tetragonal | 1.16 | VIII | Cubic | ~1.66 |

**Table 6.8** Eight phases of ice reported and accepted. The phase equivalent to that of ice has been found in D₂O. IV and IX have been reported, both in the metastable phase.

If temperature and pressure change, the crystal structure of ice changes to another stable structure within a certain range of pressures and temperatures. As shown in **Table 6.8**, a total of eight phases have been identified and accepted. Phase *II* and above are high-pressure phases appearing at pressures of $2 \times 10^8$ Pa and beyond. Phase *I$_c$* is the phase of ice observed when water vapor is sprayed on a substance cooled to low temperatures in a vacuum. In metals cooled in a faulty vacuum condition, condensation can occur on the metal surface. Such condensation contains ice with this structure. The

132

crystal structure is a ZnS structure of a cubic crystal system, which is closely associated with $I_h$. This is a diamond structure wherein Zn and S atoms are replaced by O atoms. Electron diffraction studies confirm that a hydrogen atom occupies either of two positions between oxygen atoms, just like in $I_h$.
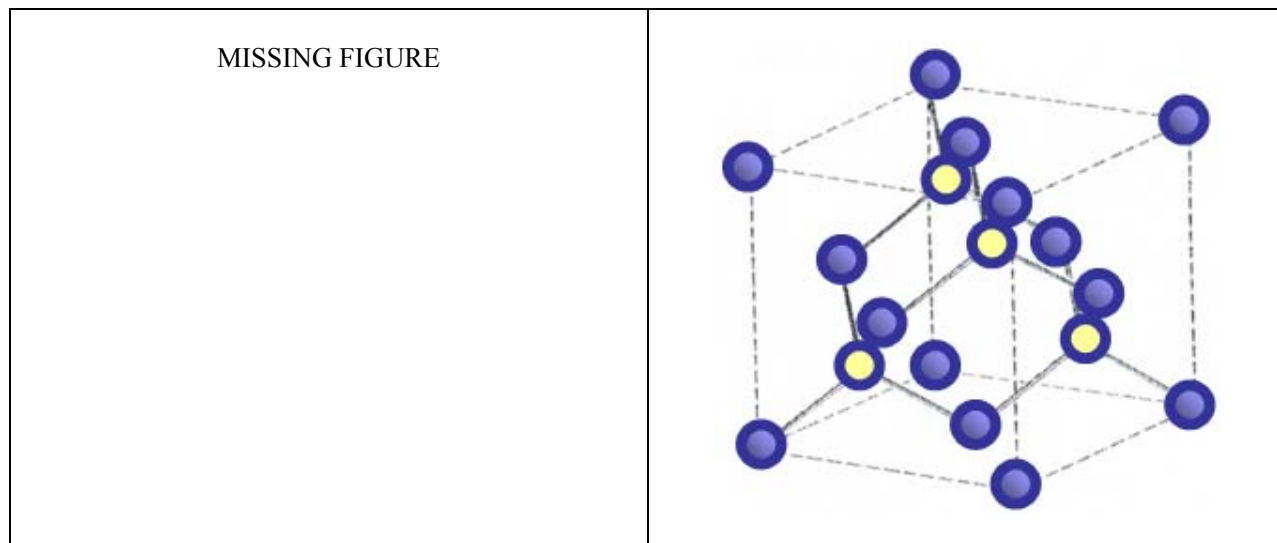


**Fig. 6.22** (a) Ice of hexagonal crystal structure; (b) Ice of cubic crystal structure

This booklet has been prepared to provide users with a knowledge of X-ray diffraction. To deepen your understanding of the crystal structure of ice, the positions of hydrogen atoms are discussed here. However, confirming the positions of hydrogen atoms is a difficult task to perform via X-ray diffraction. Crystal structure analysis using X-rays generally disregards hydrogen for two reasons. First, the oxygen atom has eight electrons, while the hydrogen atom has one. In terms of contributions to X-ray scattering amplitude, the ratio between oxygen and hydrogen is 8:1. The intensity contributing to scattering and diffraction is proportional to the square of the amplitude. This points to the difficulty of this kind of analysis, but does not rule it out as impossible. The second reason is the bonding state. If a hydrogen atom is bound to another atom, the electron of the hydrogen atom is bound to the other atom. Hence, the one electron does not locally exist around the proton or the nucleus of the atom. In the case of the $I_c$ or $I_h$ structure (**Figure 6.22**), since one electron is shared by two oxygen

atoms, this is even harder to confirm.

The problem posed by this half hydrogen model drew attention as a potential key to understanding hydrogen bonds. It was solved by neutron diffraction and electron diffraction. Using neutrons provides the following advantage in certain cases: The scattering amplitude is not dependent on the atomic number Z, since scattering by neutrons in atoms is equivalent to scattering by atomic nuclei. However, hydrogen causes inelastic scattering even when it has a single neutron, creating high background relative to the signal. Since replacing hydrogen with deuterium provides an advantage, neutron diffraction experiments formerly used ice made by freezing deuterated water. These efforts led to the confirmation of the half hydrogen model[7].

If we use electron diffraction, electrons block the Coulomb potential created by the nuclei of atoms, resulting in the scattering of Coulomb-type potential (blocked Coulomb potential). Attributed to electron distortion, this induces a multi-pole potential, and electrons scatter dramatically. This is one advantage over X-rays[8]. In the case of hydrogen bonds, even if electrons are attracted by oxygen atoms, the scattering of electrons caused by the Coulomb potential attributable to protons cannot be disregarded. This is the reason why this method was used to find that the hydrogen bonds of $I_c$ are half hydrogen bonds[9].

### 6.6.2 Hydrogen-bound crystals other than ice

Examples of hydrogen-bound crystals similar to ice include hydrogen fluoride (HF) and ammonia ($NH_3$). In addition, the results of electron diffraction experiment studies indicate hydrogen sulfide is hydrogen-bound in a low-temperature phase.

Other substances such as potassium dihydrogen phosphate ($KH_2PO_4$) display a unique ferroelectricity attributable to hydrogen bonds. We will use this compound as an

[7]  S. W. Peterson and H. Levy, *Acta. Cryst.* **10** (1957) 70
[8]  J. Harada and Y. Kashiwase, *J. Phys. Soc. Jpn.* **17** (1962) 829
[9]  K. Shimaoka, *J. Phys. Soc. Jpn.* **15** (1960) 106

example. Potassium dihydrogen phosphate is abbreviated KDP, which stands for *Kaliumdihydrogenphosphat* in German. Under ordinary temperatures, it belongs to the tetragonal crystal system; the unit cell is a = 7.4532 Å, c = 6.9742 Å, and it is paraelectric. At temperatures below $T_c$ = 123K, it assumes an orthorhombic structure and is ferroelectric. This phase transition is classified as an order-disorder ferroelectric phase transition. KDP has drawn the interest of many researchers.

**Fig. 6.23**  Schematic diagram of KDP's crystal structure of high-temperature phase

The structure of the high-temperature phase consists of a positive potassium ion, $K^+$, and a tetrahedral structure $(H_2PO_4)^-$ having a valance value of 1. The oxygen atoms at the four corners of this tetrahedron $(PO_4)$ form O-H---O type hydrogen bonds (nearly perpendicular to the c axis: located in plane ab) with the oxygen atoms of the four adjacent $(PO_4)$ via hydrogen atoms. The number of H atoms in one $(PO_4)$ is two, and these two H atoms are not regularly bound with any particular one of the two oxygen atoms, but randomly distributed. In the structure of the low-temperature phase, the spatial arrangement of O atoms is virtually identical to that in the high-temperature phase, but the $K^+$ and P atoms are moved slightly—by 0.04 Å and 0.08 Å, respectively—and result in deformation. Hydrogen atoms exist locally only for the O atom on one side, forming $(H_2PO_4)^-$. In $KD_2PO_4$ (called DKDP), in which deuterium atoms replace hydrogen atoms, and the transition temperature rises to $T_c$ = 213K. As a typical substance displaying an order-disorder ferroelectric phase transition, KDP is often compared to $BaTiO_3$ and its shift phase transition.

## 6.7 Other highlighted crystal structures

We have discussed the most basic and easy-to-understand crystal structures to be used as materials. The purpose of this booklet is to familiarize readers with X-ray

diffractometry and to allow them to identify or analyze materials. We have not dealt with complex structures or specialized materials, with the exception of KDP, mentioned near the end of this section. Nor have we mentioned the structures of recently highlighted materials: high-temperature superconducting materials, special cement minerals, asbestos-related materials, magnetic materials, pharmaceutical crystals, and special materials required for inorganic/organic chemistry. We leave it to the reader to select a material of interest and to pursue his or her own in-depth research.

# Chapter 7: X-Ray Diffractometer Operation Techniques

This chapter describes important and useful information regarding the functions of X-ray diffractometer components and sample preparation to be studied before using the MiniFlex II.

## 7.1 Detector

Humans cannot perceive X-rays directly. Instead, we use the interactions between X-rays and a particular substance to convert X-rays into detectable form. This generally involves the following methods:

(1) Photographic effect

- Photographic film, dry plate, etc.

(2) Ionization effect

- Ion chamber, Geiger counter (GMC), proportional counter (PC)
- Position-sensitive proportional counter (PSPC), one-dimensional and two-dimensional detector
- Solid-state detector, one-dimensional array (SSD, SDD)
- Solid-state two-dimensional pixel detector

(3) Scintillation effect

- Fluorescent plate, scintillation counter (SC), CCD
- Photostimulable phosphor film (IP)

In addition, researchers are also exploring an X-ray image orthicon tube (IO) that harnesses the photoconductive effect and X-ray television. A detailed account lies beyond the scope of this booklet.

Since photographic emulsions for visible light are also sensitive to X-rays, the photographic method was used for quite some time. A single, easily stored film can record information on detection position and X-ray intensity. However, sensitivity and accuracy are inferior to counters developed more recently, and the development of exposed film raises environmental concerns. Photographic film is no longer used;

photostimulable phosphor film (IP) has replaced photographic film. In place of a two-dimensional detector, the MiniFlex II employs a scintillation counter. The advantages of the scintillation counter are described below.

### 7.1.1 Scintillation counter (SC)

A scintillation counter (SC) is a counter tube that harnesses the light-emitting phenomenon (fluorescence) of a solid substance. **Fig. 7.1** illustrates its structure. The photomultiplier (or phototube) has a photocathode on which a light-emitting scintillator is mounted. When X-rays enter, the scintillator emits light. Upon exposure to this light, the photocathode discharges electrons toward the vacuum side. The electrons released are accelerated toward the electrode. The electrode is a secondary dynode, and, upon collision with it, more electrons are released, which then strike the next secondary dynode to multiply the number. Repeating this process more than ten times, we can increase electrons exponentially (approx. $10^6$ times) as they travel through the tube, ultimately generating an output of pulses of several mV. Generally, NaI single crystals containing very small amounts of thallium (Tl) are used as scintillators. These crystals are excited by incident X-rays and emit a bluish-purple light.
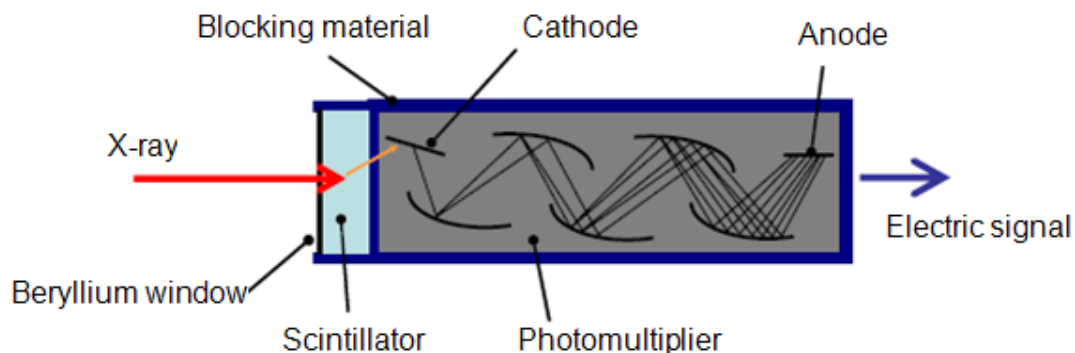
**Fig. 7.1** Structure of a scintillation counter

Since the amount of light emitted by the scintillator is proportional to the energy of the incident X-ray photons, the height of the resulting electric pulses is also proportional to energy levels. The energy of the X-rays can be analyzed, but the

system's energy resolution is inferior to that of proportional counters. Noise is relatively high. With X-rays of wavelengths 3 Å or longer, the pulse height of the signal is about the same as that of noise, making it difficult to distinguish the signal. We can disregard this problem, since the X-rays used for X-ray diffraction have shorter wavelengths than CrKα rays (2.289 Å).

We calculate the counting efficiency of a counter by dividing the converted pulse count (not pulse height) by the number of incident X-ray photons. In the wavelength region used for X-ray diffraction, efficiency is close to 100%. Almost all X-ray photons entering the scintillator crystals contribute to light emissions and are converted into electric signals. **Fig. 7.2** shows the counting efficiency. As wavelengths become longer, counting efficiency decreases, due to absorption by absorbers in the path and the window material.
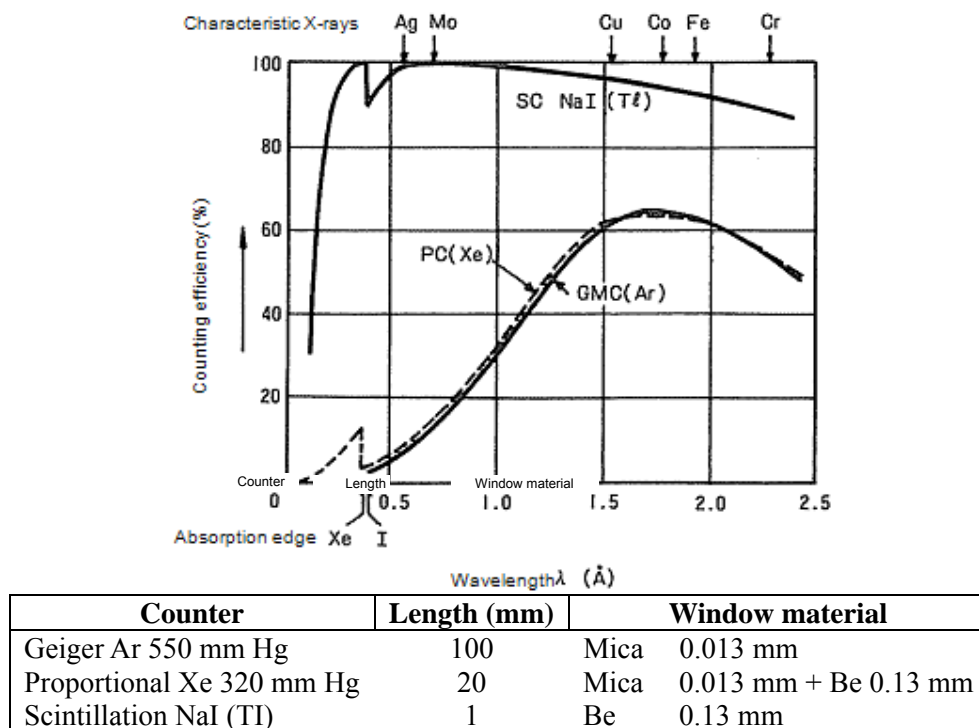


| Counter | Length (mm) | Window material | |
|---|---|---|---|
| Geiger Ar 550 mm Hg | 100 | Mica | 0.013 mm |
| Proportional Xe 320 mm Hg | 20 | Mica | 0.013 mm + Be 0.13 mm |
| Scintillation NaI (TI) | 1 | Be | 0.13 mm |

**Fig. 7.2** Counting efficiency of the counter (calculated value)

## 7.2 Electronic circuit panel

We explained above that the scintillation counter converts received X-ray photons into an electric pulse signal. Since the pulse height is proportional to the energy of the photons, only the electric pulses of a certain pulse height need to be counted. The electronic circuit panel (ECP) is an electronic device that performs counting (recording). **Fig. 7.3** shows a block diagram of the electronic circuit panel. In most cases, the **scintillation counter** (SC) and **preamplifier** are integrated into a single unit, shown as a single block in the diagram. Following impedance conversion by the preamplifier, the main amplifier amplifies the signal and feeds it to the **pulse height analyzer** (PHA), where pulses of unnecessary pulse heights are deleted. The signal then enters the scaler and is read by a computer. The scaler counts the pulses received as a signal within the time set for the timer (fixed time or preset time) and outputs the count as a digital signal to a computer.
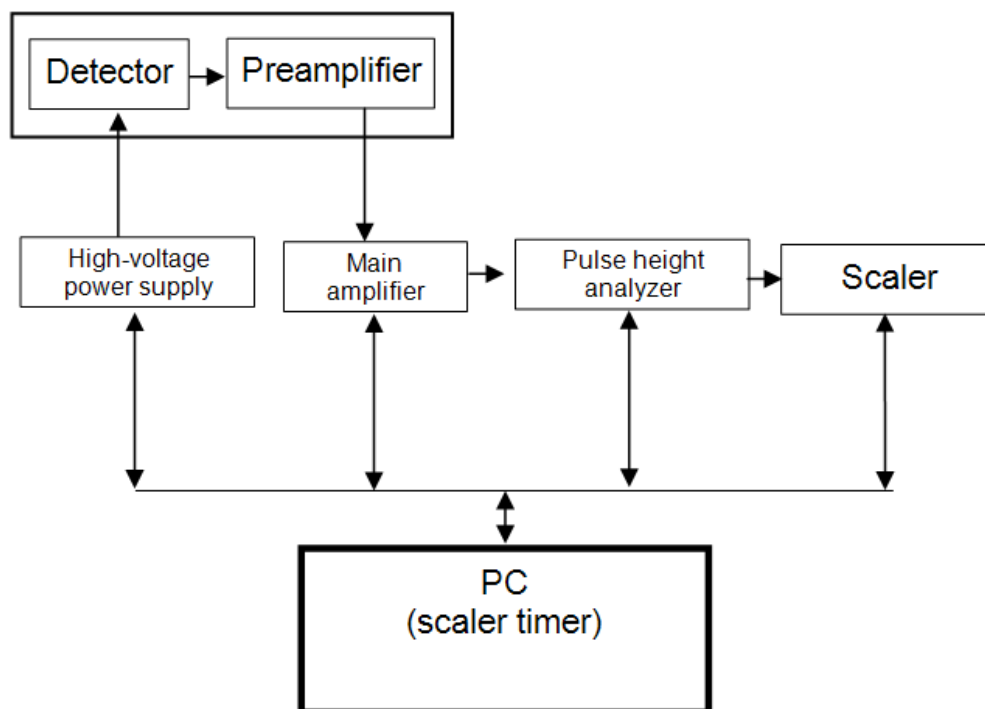
**Fig. 7.3** Block diagram of counting equipment

### 7.2.1 Pulse height analyzer functions

If we measure X-rays (monochromatic X-rays) of a certain energy level with a scintillation counter and analyze the height value of the obtained pulses with a pulse height analyzer (PHA), we obtain a distribution curve similar to the one shown in **Fig. 7.4**. The horizontal axis indicates the pulse height value, while the vertical axis shows the incident pulse count or number of incident X-ray photons. Called a pulse height distribution curve, this curve expresses the energy spectrum of the measured X-rays. This distribution curve can be contracted or expanded horizontally by adjusting the amplifier gain or voltage supplied to the detector. By appropriately adjusting these parameters, we obtain a curve with two peaks, similar to the one in the figure. The pulse height value on the horizontal axis produces a peak near the center, which reflects the energy distribution of incident X-rays. The other peak at the zero pulse height position corresponds to electrical noise. The PHA eliminates this noise and the broad slope section of the peak on the high-pulse-height side. This function is called discrimination. The width of the accepted pulse height values is called the window width. If the window width is set, only the pulse signal within that width is sent to the scaler. The PHA also provides this function.
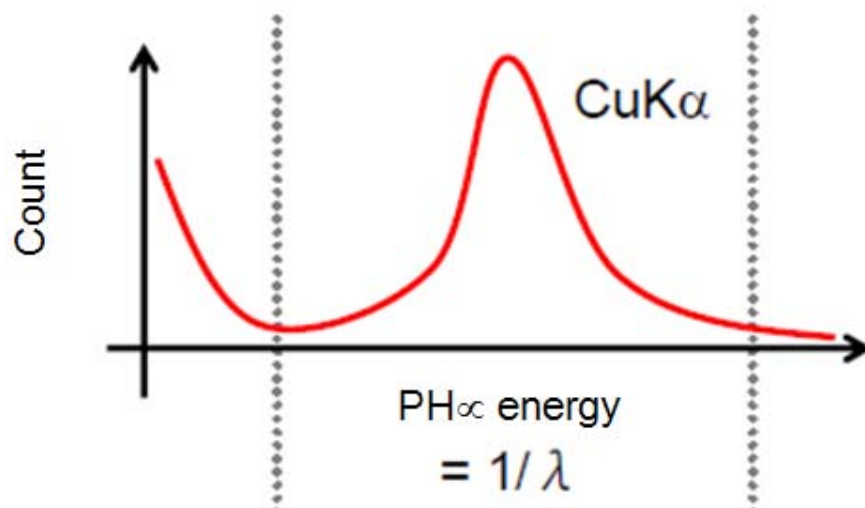


**Fig. 7.4** Pulse height distribution curve of scintillation detector

**Fig. 7.4** shows the distribution curve obtained from observations of CuKα X-rays using an SC. The distribution curve is wide, with a peak position at the center, due to the energy resolution of the SC. If E indicates the pulse height value of the peak and ε represents the full width at half maximum, the following equation gives energy resolution η of the counter. This is usually given as a percent value.

$$\eta = ( \, \varepsilon \, / \, E \, ) \times 100(\%) \quad (7.1)$$

Although the energy resolution is near-constant relative to X-rays of a certain energy, the value changes when we replace the counter. Thus, this is understood as a capacity specific to the counter. For example, if we use a proportional counter (PC) to measure monochromatic X-rays with a very narrow energy width, the measurement will always show a certain distribution pattern. This is because one of the factors that determine the energy resolution of a counter is the "fluctuation" that occurs during the process of converting X-ray photons into an electric signal inside the detector. In the case of an SC, the number *(N)* of primary electrons caused by the photocathode of the photomultiplier is N = 3/sec to 6/sec for CuKα X-rays. The statistical fluctuation is $(N)^{1/2} =$ 1.7 to 2.5. Calculating $\{(N)^{1/2} / N\} \times 100(\%)$ yields $1 / (N)^{1/2} \times 100(\%) = 40$ to 60%. Thus, the energy resolution is 40 to 60%.

### 7.2.2 MiniFlex II measuring instrument

The MiniFlex II is designed to allow direct control of the measuring instrument from the screen of a PC connected to the unit. Refer to the manual for detailed operating procedures and startup/shutdown procedures. The MiniFlex II incorporates the following notable safety features:

1) X-rays are not generated when the equipment is turned off.

2) Opening the door of the sample chamber closes the shutter and automatically shuts down X-ray generation.

3) The shielding function is calculated and designed to prevent X-ray leaks during measurements.

4) Note that removing components or parts without permission or intentionally disabling safety measures will compromise safety.

**Problem** 1.1 The X-ray tube was removed. Now, a drop of water is visible on the window. Describe the correct countermeasure.

**Problem** 1.2  If the water circulating pump stops or the door of the sample chamber is open, the Ready lamp does not turn on, and the equipment cannot be set to X-Ray ON. What other reason might prevent X-Ray ON?

## 7.3 Selecting the X-ray tube

**Fig. 7.5** shows a graph of measurements of diffracted X-rays from the plane (311) in $Fe_3O_4$ (powder) using five different types of X-ray tube. A K$\beta$ filter was used for all measurements.
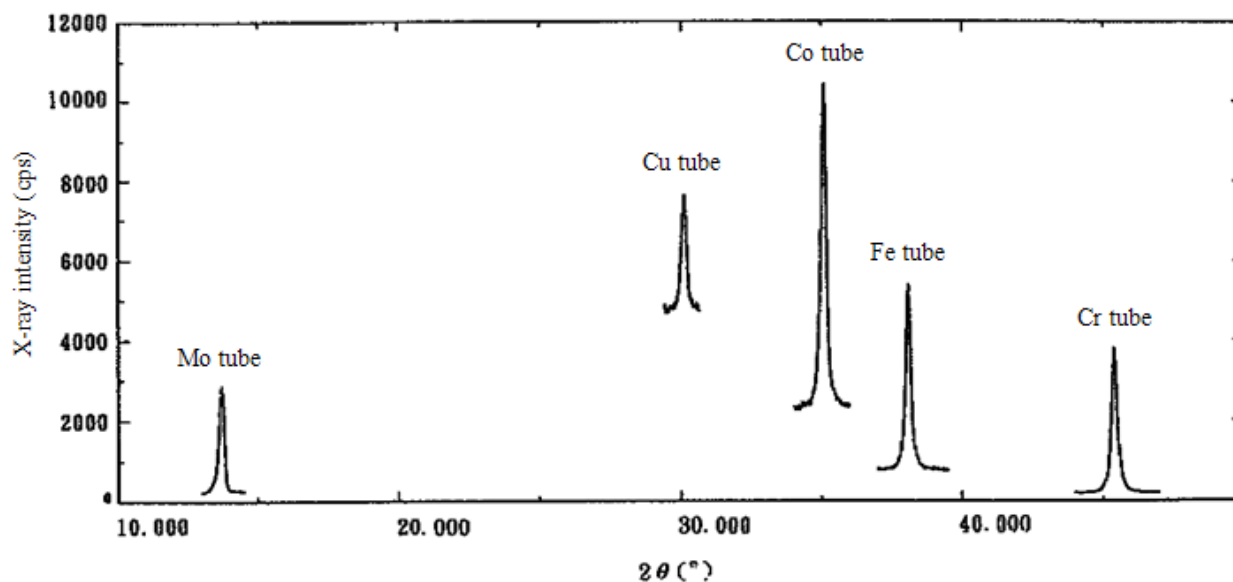


**Fig. 7.5** Differences in peak position and peak/background ratio of tubes

The wavelength of the K$\alpha$ rays generated by the Mo tube is shortest, followed by the Cu, Co, Fe, and Cr tubes, in that order. The angle of the diffracted beam shifts

toward the high-angle side in the same sequence. The Cu tube is typically used in powder X-ray diffraction because it offers high power and a wavelength in a relatively easy-to-use range. Short wavelengths result in dense clusters of reflections (peaks); long wavelengths limit the number of observable peaks. This graph shows that peak intensities and peak/background (P/B) ratios vary significantly depending on the type of tube used. The background value differs greatly from tube to tube, primarily due to the fluorescent X-rays from the sample.

A Cu tube is not suitable for samples containing Fe because the wavelength of X-rays generated by the tube is suitable for exciting fluorescent X-rays from Fe, causing high backgrounds. If you wish to analyze Fe-based samples by the Kβ filter method, we recommend using an Fe X-ray tube. Using the diffractometer with a spectrometer on the receiving side (also called a receiving monochromator) eliminates not just Kβ, but fluorescent X-rays. The background will remain low, even if you use a Cu tube to measure Fe samples. Using the Cu X-ray tube with a diffractometer equipped with a receiving monochromator is now becoming more common for all sample types. As shown in the diagrams, if the Fe-based samples are of the mainstream type, the intensity of diffracted X-rays will be several-fold stronger with a Co tube (with monochromator) than with the Cu tube, a nonnegligible advantage.

**Fig. 7.6** compares the data for an Fe material measured with an Mo tube and a Cu tube (with monochromator). In both graphs, we detect an α phase and a γ phase. However, a careful comparison shows more αFe in the data obtained with the Mo tube. Due to X-ray absorption, X-rays from the Mo tube penetrate deeper into the sample than X-rays from the Cu tube, and the ratio of the α and γ phases changes with depth[10]. This Fe sample has more α phase in the deeper layers than in the surface layer. However, reaching this conclusion requires measurements with X-rays of two different wavelengths.

---

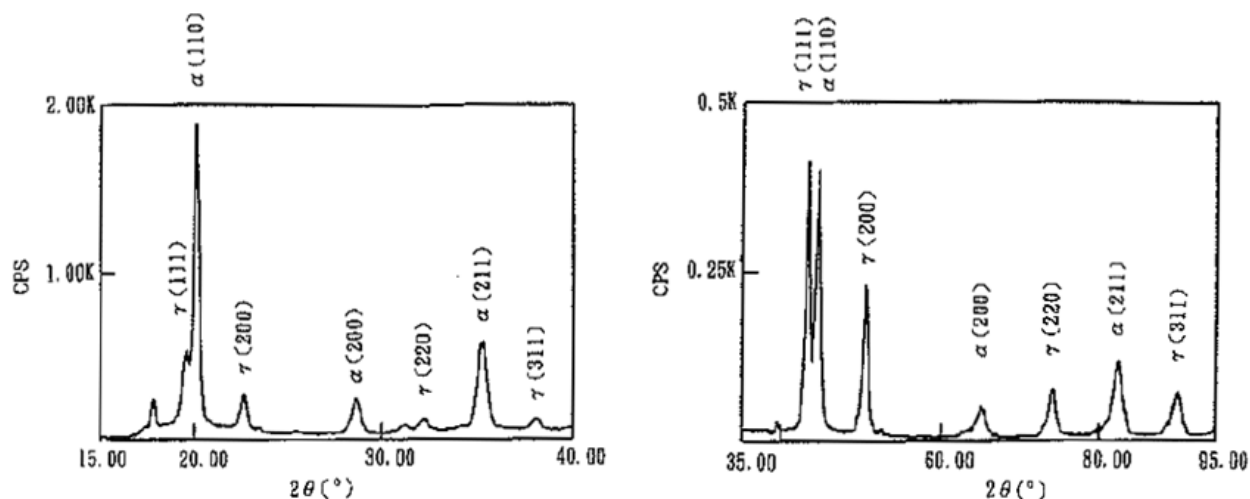[10]  We can calculate the difference in analysis depth using the equation in §3.6.

**Fig. 7.6** Differences in data obtained with Mo tube (left) and Cu tube (right)

## 7.4 Ideal tube voltage and tube current

If V and $V_c$ indicate tube voltage and excitation voltage respectively, the intensity of characteristic X-rays is proportional to tube current i and to the $n^{th}$ power of $(V − V_c)$. We can achieve stronger intensity by increasing the tube voltage in the region near the excitation voltage and by increasing the tube current once the tube voltage reaches a certain level. **Table 7.1** shows the most appropriate tube voltage for different tube types. For Mo tubes, which have high excitation voltage $V_c$, the tube voltage is set high. For Cr tubes, which have low excitation voltage, the tube voltage is set low.

Continuous X-rays are proportional to the square of the tube voltage and to tube current. However, they only increase the background in normal X-ray diffraction data. For characteristic X-rays, the tube voltage that results in maximum intensity is not the tube voltage that results in the highest peak/background (P/B) ratio. **Table 7.1** shows the results of various measurements. A receiving monochromator removes continuous X-rays, allowing us to select the condition that provides maximum intensity. If we use a Kβ filter, we must also select the condition that achieves the highest P/B ratio.

| Tube | Excitation voltage (kV) | Suitable tube voltage (kV) | |
|---|---|---|---|
| | | Maximum intensity | Maximum P/B ratio |
| Mo | 20.00 | 60 | 45-55 |
| Cu | 8.86 | 40-55 | 25-35 |
| Co | 7.71 | 35-50 | 25-35 |
| Fe | 7.10 | 35-45 | 25-35 |
| Cr | 5.98 | 30-40 | 20-30 |

**Table 7.1**     Suitable tube voltage

## 7.5 Relationship between divergence slit width and irradiated width

Irradiated width A on a sample is determined by the size of the divergence slits (DS) with divergence angle 2$\beta$, distance R (goniometer radius) between the X-ray focal point and the center of sample, and diffraction angle 2$\theta$. This can be calculated using the equation shown below. Since the irradiated width differs from the left side to the right side of the sample (side closer to X-ray source and side farther from the X-ray source), the sum of the two is called the irradiated width.

$$A = A1 + A2 = [1/sin\ (\theta\ +\ \beta)\ +\ 1/sin(\theta - \beta)]\ R\ sin\beta$$

**Fig. 7.7** shows the irradiated widths in the MiniFlex II with the goniometer radius R of 150 mm when we use standard slit DSs with divergence angles of 1.25° and 0.625°. The sample width on a standard sample plate is 20 mm. When DS = 1.25°, the irradiated width is smaller than the sample width in the angle range of 2$\theta \geq$ 20°. But caution is in order, since the irradiated width exceeds the sample width at lower angles. If DS = 0.625°, 2$\theta$ exceeds 10°, allowing us to obtain a diffraction profile with the correct intensity ratio.

Note: The goniometer radius varies from model to model and can be 285 mm, 185 mm, 150 mm, and so forth. If we use a DS with the same divergence angle in these

goniometers, the irradiated width will vary widely. If we regard the DS that results in an irradiated width of 20 mm at $2\theta \approx 20°$ as a standard DS, the equivalent DS for each goniometer radius is as follows:

R = 150 mm → DS = 1.25°
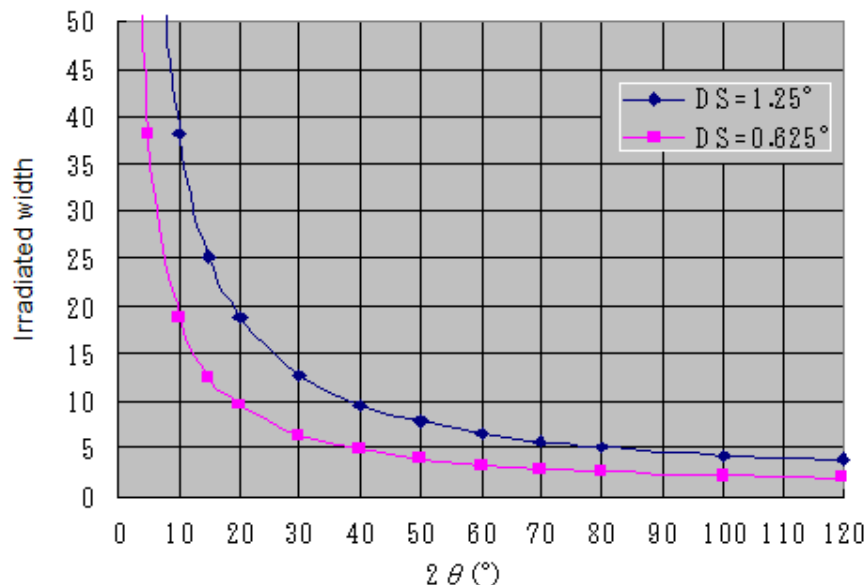R = 185 mm → DS = 1°
R = 285 mm → DS = 2/3°



**Fig. 7.7** Irradiated width of MiniFlex II (R = 150 mm)

## 7.6 Depth of sample to be analyzed

Since all samples absorb X-rays to a certain degree, we must know the depth to which the X-rays penetrate before analysis. If the sample has a crystal layer distributed along the axis of thickness, it is especially important to identify the X-ray penetration depth of the sample to be analyzed. In addition, we need to consider whether the thickness of the prepared sample is suitable. Suppose we analyze a sample prepared on a glass plate and the data obtained shows a diffraction profile corresponding to an amorphous substance (often called a halo profile). If the sample has a small $\mu/\rho$ value, based on the knowledge just gained, we will realize immediately that the profile is due to the halo

generated by the glass plate.

Consider the thickness of sample that would allow it to be considered semi-infinite. The ratio $G_t$ of the intensity of diffracted X-rays obtained from a sample of finite thickness to the intensity from a semi-infinite sample is defined by the following equation:

$$G_t = \frac{\int_0^2 dI}{\int_0^\infty dI} = 1 - \exp\left(\frac{-2\mu t}{\sin \theta}\right)$$

$$1 - G_t = \exp\left(-\frac{2\mu t}{\sin \theta}\right)$$

Here, we substitute $Kt$ for $- \ln (1 - Gt)$.

$$Kt = 2\mu t / \sin \theta \quad (7.\,2)$$

Consider the meaning of **Equation 7.2** under conditions where the incident angle ($\theta=90°$) results in maximum penetration. For example, estimate Kt when the penetrating distance reaches 90% of the semi-infinite case. The calculation of $-ln(1 - 0.90)$ yields $Kt = 2.3$. If $\mu t$ is half of that value, 1.15, it is acceptable. In the case of a semi-infinite sample, the calculation yields $\mu t = 3.45$ based on $Kt = 6.9$, if we assume $Gt = 99.9\%$. Based on this, when we use the reflection method, a thickness that satisfies $\mu t \approx 3$ is sufficient. If we use the transmission method, on the other hand, a sample thickness of about $\mu t = 1$ is suitable. This thickness reduces the intensity of transmitted X-ray to 1/e, but this corresponds to Gt = 90% according to **Equation 7.2**. The intensity of the diffracted X-rays decreases if the thickness exceeds or is less than the value above.

## 7.7 Irradiated height above the sample to be analyzed

Just like the irradiated width on the sample, the irradiated height above the sample needs to be estimated in advance. The irradiated height is determined by the basic

layout of the optical system and does not depend on the diffraction angle, making it relatively easy to manage. **Fig. 7.8** shows the basic layout of the incident-side optical system, viewed from the side. F indicates the focal point of X-rays. The vertical length represents the size of the focal point. The focal length and DS slit height are both set to 10 mm. Since Soller slits are located between F and DS, the beam height remains the same between them, as shown in the diagram. After the beam passes through the DS slits, it spreads in a divergence angle to the degree allowed by the Soller slits. This is shown in **Fig. 7.8**. The intensity is uniform at the 10-mm section at the center. The vertical spread is the divergence allowed by the Soller slits. The intensity is reduced by the penumbra effect.
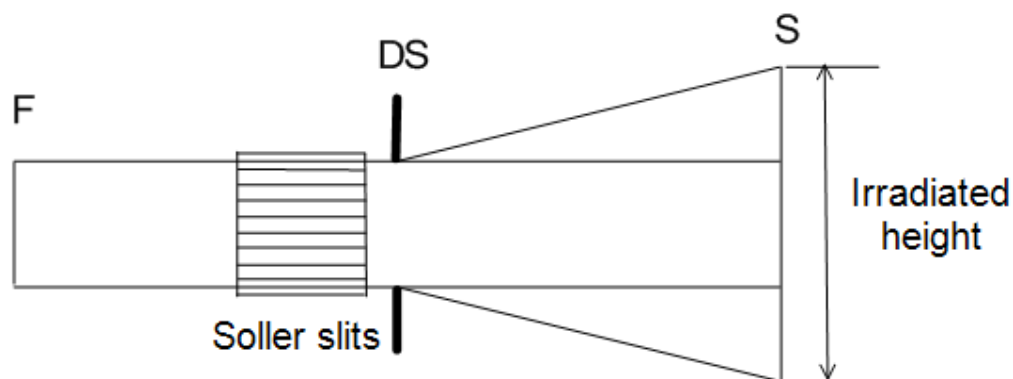


DS−S = 58 mm, Soller slit divergence angel = ±2.5°
Irradiated height = 10 mm + 2 * 58 * tan2.5° = 15.06 mm

**Fig. 7.8** Irradiated height (MiniFlex II)

## 7.8 Relationship between slit width and resolution

Equipment resolution is determined by the optical system used in the diffractometer. How well diffracted X-rays in proximity can be separated is sometimes assessed to determine equipment resolution. The "five fingers" that appear in the scattering angle range betwee 67° and 69° when we analyze quartz with CuKα rays are frequently used for this purpose. Three interplanar spacings show close values, and the diffracted

X-rays overlap. The diffracted rays of $K\alpha_1$ and $K\alpha_2$ begin to separate to create a total of six diffracted X-rays. However, since the diffracted $K\alpha_2$ rays from the second lattice plane and the diffracted $K\alpha_1$ rays from the third lattice plane overlap, we observe five peaks. **Fig. 7.9** shows data comparing the resolution of the five fingers measured with a goniometer with R = 185 mm while varying RS width[11] and DS width.
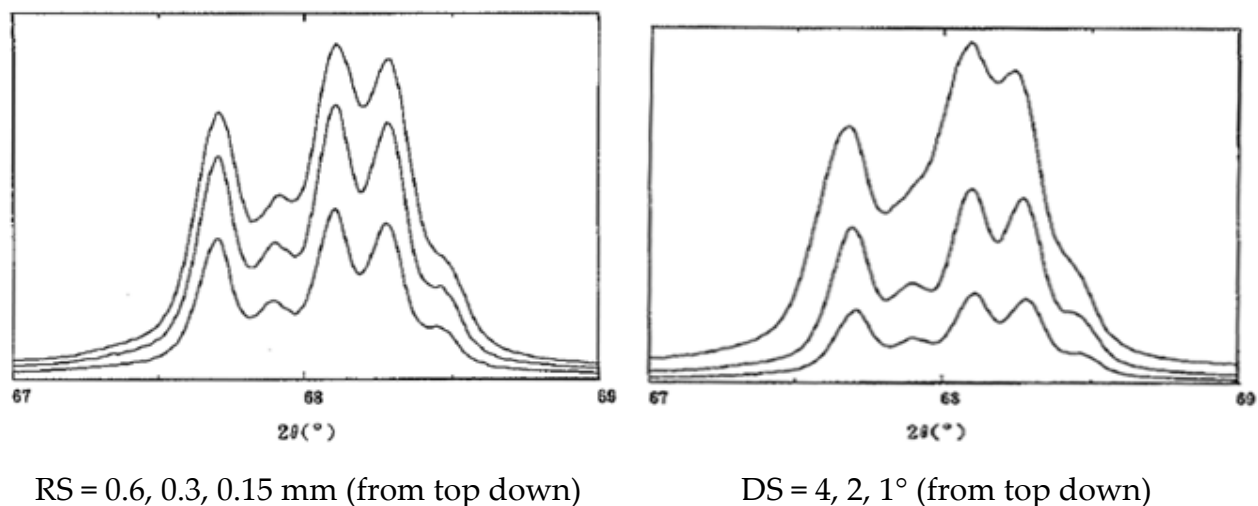


| RS = 0.6, 0.3, 0.15 mm (from top down) | DS = 4, 2, 1° (from top down) |

**Fig. 7.9** Slit width and resolution

If the RS width on the receiving side is increased two-fold, then four-fold, integrated intensity increases by approximately two-fold and four-fold—but resolution decreases. Since the sample itself has a peak width, the RS width should not be reduced unnecessarily at the cost of intensity. In many cases, we use a value of RS = 0.3 mm (R = 150 to 185 mm). The RS equivalent to RS = 0.3 mm for R = 185 mm is 0.45 mm for R = 285 mm.

The right-hand section of **Fig. 7.9** shows the effects of widened DS width on the incident side. Expanding the irradiated width increases intensity but reduces resolution.

---

[11] In the MiniFlex II, RS = 0.3 mm, fixed

## 7.9 Absorption coefficient $\mu/\rho$ and background

If the energy of incident X-rays exceeds the energy necessary to excite fluorescent X-rays from the element occurring in the sample, those X-rays are used to excite the fluorescent X-rays, reducing the percentage of diffracted X-rays. This weakens diffraction intensity and increases the background attributable to the fluorescent X-rays. Here, it is preferable to avoid using X-rays with a wavelength having large $\mu/\rho$ relative to the primary sample components. For instance, when analyzing the structure of a material containing Co, Fe, and Mn, we should avoid using CuKα or CuKβ, which are characteristic X-rays of Cu with a large $\mu/\rho$ for those elements.

## 7.10 Shift in diffraction angle due to longitudinal displacement of sample surface

If the sample surface is displaced longitudinally when we use the focusing method optical system for the B-B method, the diffraction angle of the observed diffracted beam will be displaced. This was previously explained in the section discussing the B-B method. If the sample surface is displaced longitudinally, the sample surface—the diffracting plane—will not be located on the rotating axis for the θ rotation of the sample, resulting in an incorrect diffraction angle with respect to the diffractometer. This diffraction angle deviation $\Delta 2\theta$ relative to the off-center distance $\Delta L$ is given by the following equation: $\Delta 2\theta = -tan^{-1}(2\Delta L \cos \theta / R)$.

**Fig. 7.10** shows how the $\Delta 2\theta$ calculated using this equation changes relative to the diffraction angle $2\theta$. Even a small displacement in the sample position of 0.1 mm or 0.05 mm will generate a significant error when the diffraction angle 2θ becomes small. In general, the higher the diffraction angle 2θ, the smaller the error. Ideally, we should use diffracted X-rays that appear at high angles when we require precise measurements

of lattice constants.
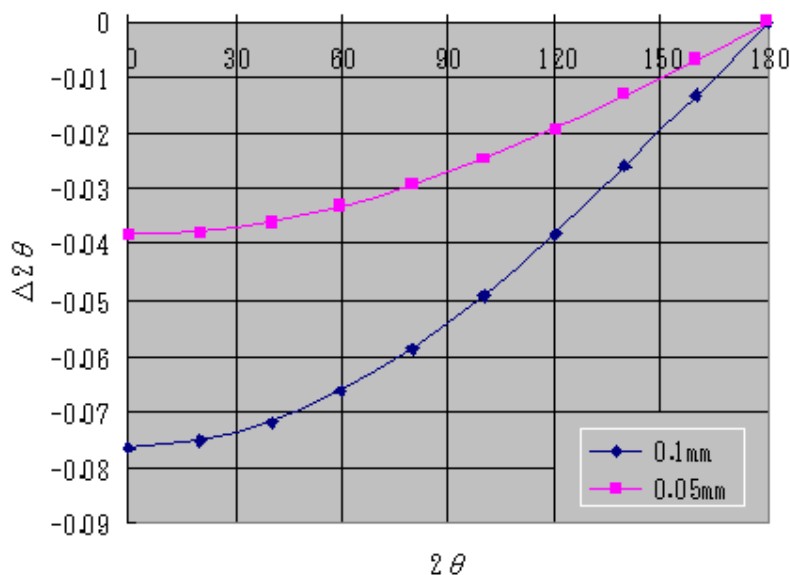


$$\Delta2\theta = -tan^{-1}(2\Delta L \cdot cos\ \theta\ /\ R)$$
$\Delta L$ = Distance of sample surface from reference surface, R = 150 mm

**Fig. 7.10** Longitudinal displacement of sample surface and shift in angle

The shallower glass sample plate provided for use with the MiniFlex II measures 0.2 mm in depth. If a sample is prepared in the ordinary manner, a sample surface displacement of 0.05 mm will not occur. However, if a sample surface deviation of 0.05 mm should occur, the angle deviation on the low-angle side would be 0.04° at most. If the purpose of the analysis is to identify the sample (qualitative analysis), this deviation falls within the permissible range, and no problems result. The angular accuracy of the MiniFlex II is 0.01° to ensure sufficient precision, even for precision measurements of lattice constants. To take advantage of this precision, it is important to reduce sample surface error (i.e., the deviation attributable to human factors) as much as possible when preparing samples to obtain data with excellent reproducibility.

## 7.11 Reproducibility of intensity of diffracted X-rays

Measuring the intensity of diffracted X-rays using a diffractometer is equivalent to

measuring the diffracted X-rays that form the Debye ring. If the sample is characterized by large crystal grain diameters, the intensity will change each time the sample is refilled. The reason why is obvious if we examine a Debye ring with a two-dimensional detector. Here, we'll consider the relationship between grain diameter and intensity reproducibility by examining a two-dimensional diffracted image.

**Fig. 7.11** shows diffracted images obtained in a measurement of the Debye ring by the reflection method. The measurements were obtained from three different quartz powder samples with significantly different grain diameters prepared as flat plates. Coarse grain causes the Debye ring to appear as spots, while fine grain results in a continuous ring. The ring appears continuous because it is formed of numerous spots.

**Fig. 7.12** shows two-dimensional diffracted images obtained from $Al_2O_3$ powder samples, isolating the section of the Debye ring near the equatorial line. Diffraction equipment like the MiniFlex II examines an even smaller area of the Debye ring near the equatorial line to make a count. When the sample is repacked, the size and the number of spots appearing in a specific area of the Debye ring change. For small grain sizes, the number of particles in the irradiated sample area increases, and the number of particles that contribute to the diffraction increases as well; thus, the change in diffracted spots becomes small even when the sample is repacked.

To improve the reproducibility of diffracted X-ray intensity, we must grind the sample to a fine grain using a mortar or other such method. Ideally, when the powder is rubbed between finger tips, no graininess should be perceivable. Note that organic crystals require caution: Grinding certain organic crystals can break up the crystals.

Using a sample rotation attachment achieves the same effect as finely grinding the sample. In-plane rotation of the sample helps average the number of crystal grains contributing to diffraction. **Fig. 7.13** shows the diffracted image obtained from in-plane rotation of a quartz sample characterized by a large grain diameter indicated at the bottom in Fig. **7.11**. We see that rotating the sample makes the Debye ring continuous,

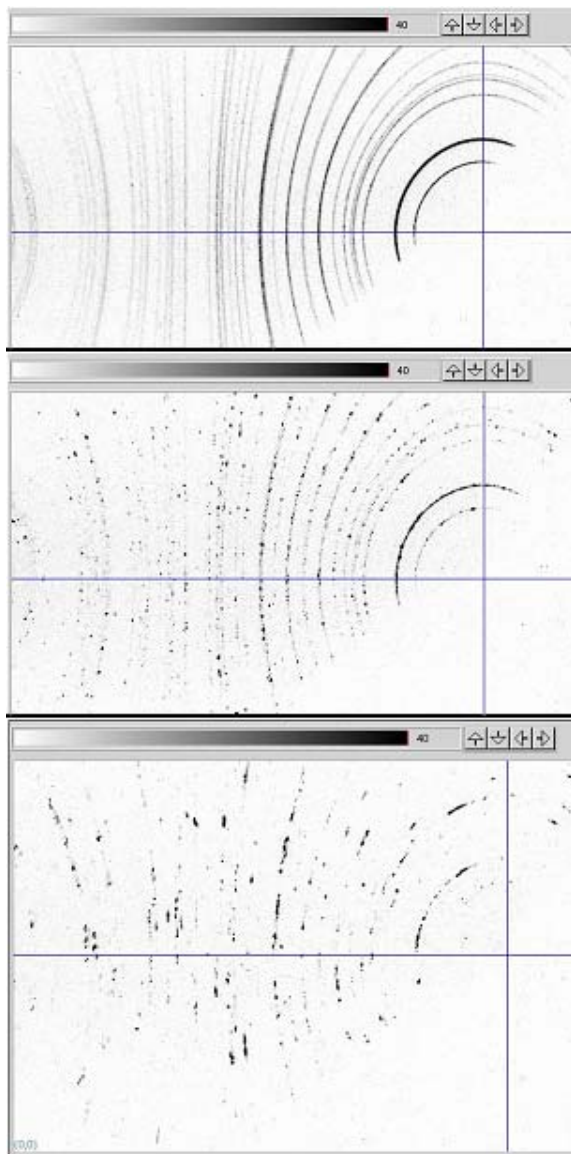just like the one obtained with the sample characterized by a small grain diameter.



**Fig. 7.11** Difference in Debye ring due to quartz grain diameter. Top: Small; Middle: Medium (< 50 μm $\phi$); Bottom: Large
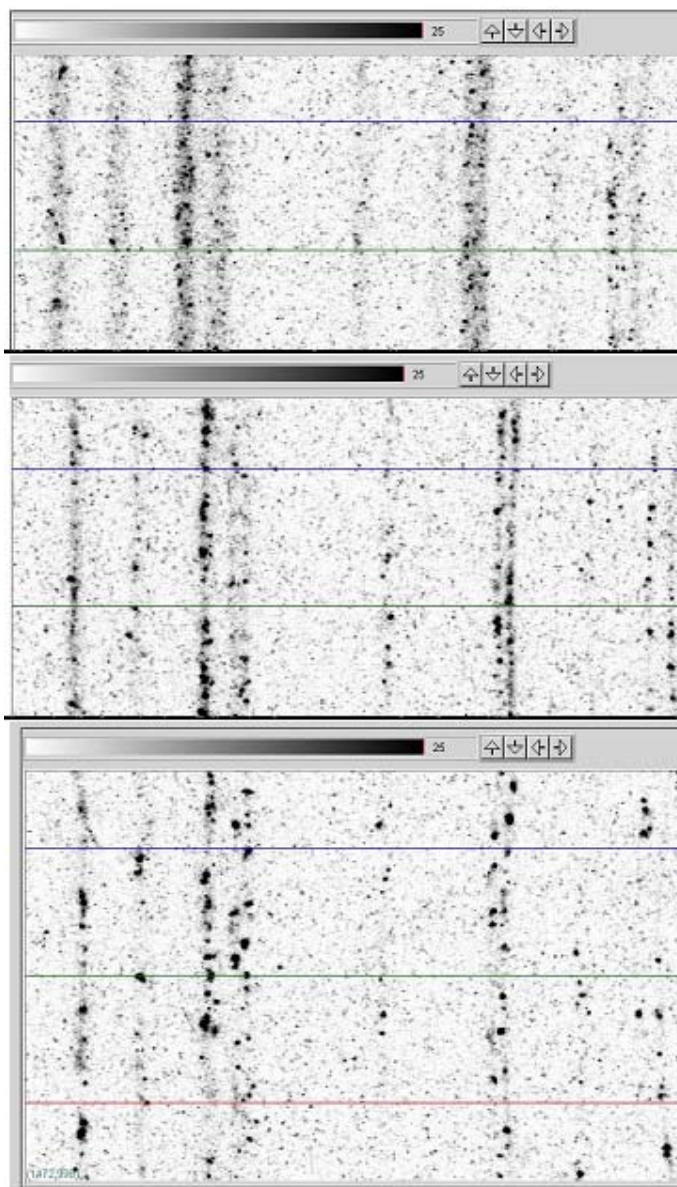
**Fig. 7.12** $Al_2O_3$ with different grain diameters and their Debye rings. Top: 3 μm; Middle: 7 μm; Bottom: 10 μm

Using an ordinary diffractometer, we examined samples with different grain diameters to examine how in-plane sample rotation would change the reproducibility of integrated intensity. Without sample rotation, we cannot achieve adequate reproducibility in the range of grain diameters from 25 to 30 μm. Rotating the sample improves reproducibility to levels that permit use of the resulting data for measurement

purposes, including quantitative analysis. Without sample rotation, quantitative analysis would generally require grinding samples to approximately 10 μm.
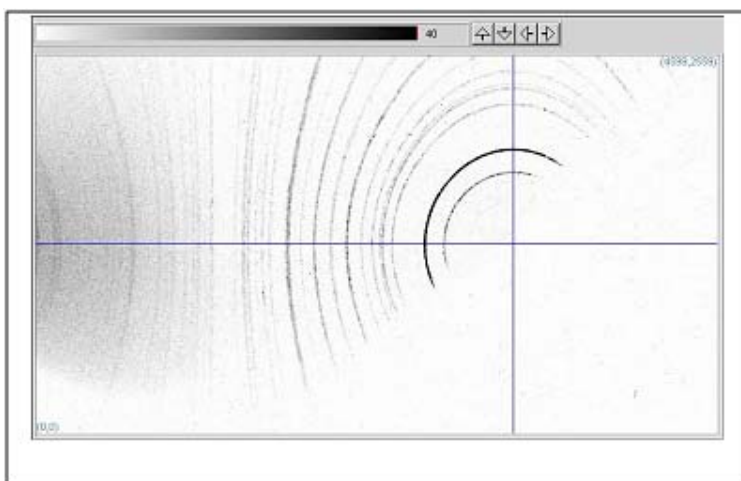


**Fig. 7.13** Effect of sample rotation (using the sample described at the bottom in **Fig. 7.11**)

## 7.12 Statistical fluctuations, reproducibility of integrated intensity, and reproducibility of refilled samples

Measurements of X-ray intensity obtained by a detector contain statistical fluctuations, which can be expressed by $\sqrt{N}$, where N is the measured value of the diffracted beam. **Equation 7.3** gives σ (%), the relative standard deviation:

$$\sigma\ (\%) = \sqrt{N} / N \times 100$$

$$= \ 1/\sqrt{N} \times 100\ (7.3)$$

In cases in which the background cannot be ignored, accounting for the background will reduce the value, but the calculated value may be regarded as approximate. If the integrated intensity reaches 10,000 counts, the relative standard deviation becomes 1%. In general, varying the scanning speed will change the total number of counts. As we can see from **Table 7.3**, which indicates actual data for the integrated reflection intensity of $Al_2O_3$ measured at scanning speeds of 20° and 4° per minute, the standard deviation based on simple reproducibility depends on the total number of counts N. This table

also includes the results of a reproducibility test with refilled samples. The total number of counts is almost the same, but reproducibility is poorer with the repacked samples. The standard deviation is also slightly larger. In general, for measurement errors proportional to simple $\sqrt{N}$, extending the counting time improves reproducibility. However, when the reproducibility for refilled samples is poor, haphazardly increasing the total number of counts will not improve the accuracy of integrated reflection intensity measurements. This is worth keeping in mind.

*Reproducibility of refilled samples > Simple reproducibility*

For the sample shown in the table, refilling the sample did not result in a major change in intensity. Thus, the grain diameter of the sample can be regarded as small and uniform.

| | Simple reproducibility (20°/min) | Simple reproducibility (4°/min) | Reproducibility of refilled samples (4°/min) |
|---|---|---|---|
| 1 | 5468 | 27435 | 27260 |
| 2 | 5642 | 27165 | 28009 |
| 3 | 5587 | 27091 | 28051 |
| 4 | 5479 | 27289 | 27977 |
| 5 | 5464 | 27552 | 28002 |
| 6 | 5508 | 27460 | 27517 |
| 7 | 5625 | 27339 | 28058 |
| 8 | 5710 | 27381 | 27469 |
| 9 | 5792 | 27498 | 27868 |
| 10 | 5635 | 26944 | 28094 |
| Average | 5591 | 27315 | 27831 |
| Standard deviation | 111 | 185 | 284 |
| (%) | 2.0 | 0.7 | 1.0 |

**Table 7.3** Simple reproducibility and reproducibility of refilled samples for integrated intensity of $Al_2O_3$ powder

## 7.13 Sample preparation and orientation

Using samples with small crystals in disordered orientation is the basic condition for

powder X-ray diffraction. In many cases, large sample diameters result in uneven Debye rings and cause spotty images in measurement. It was explained earlier that in rolled polymer film and metal plates, needle-shaped or flat-plate-shaped crystallites are often aligned in a specific direction, resulting in an arc-shaped Debye ring, instead of a circular ring. Let us show an example.
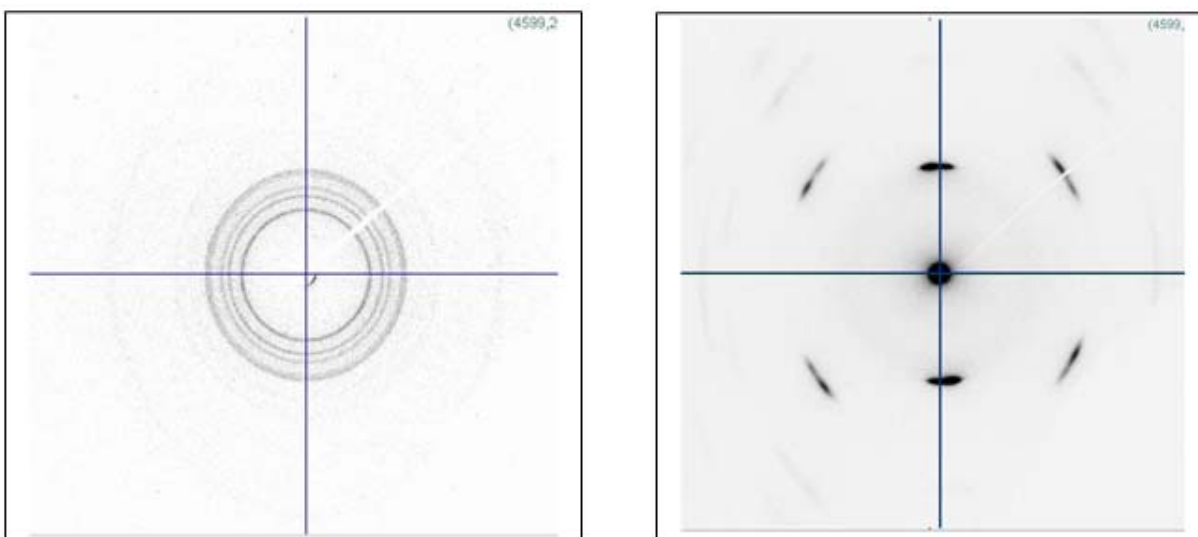


**Fig. 7.14** Examples of observed polymer Debye rings. (a) PP (polypropylene); (b) POM (polyacetal)

The Debye ring of polypropylene (PP) in **Fig. 7.14** is continuous, while that of polyacetal (POM) is discontinuous and appears as arcs. The Debye ring for POM appears as an arc because the lattice planes are aligned in a specific direction due to the POP orientation matrix. In contrast, the Debye ring for PP is a continuous circle, and no orientation is observed.

If we measure a sample with the above-mentioned orientation using a powder X-ray diffractometer, a specific peak will become too strong, preventing use of the data even for simple identification. In certain cases, not even one diffracted beam can be detected. As we see in the two-dimensional diffraction profile of POM in Fig. **7.14b**, if we measure the Debye ring on the equatorial line, for example, no diffracted X-rays will be observed.

Depending on the manner in which a powder sample is prepared and how it is

158

packed on a sample plate, an orientation may appear. **Fig. 7.15** shows how the diffraction pattern can change depending on how the sample (kaolinite) is packed on the sample plate. The greater the amount of the loaded sample, the higher a certain peak intensity becomes, as we can see in the diagram. Even flat-plate-shaped or needle-shaped crystal powder will have orientation, depending on the pressure applied when packing the sample on the sample plate. Thus, preparing samples requires a certain amount of care.
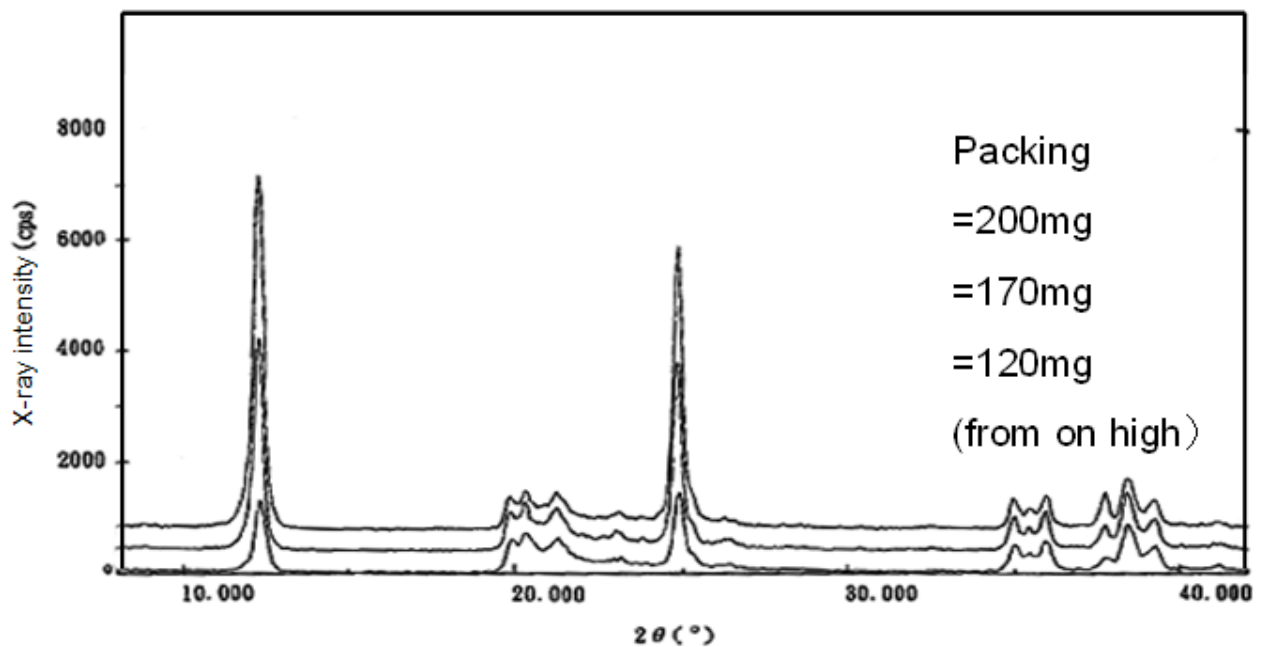


**Fig. 7.15** Amount of loaded powder sample and orientation (sample: kaolinite)

# Appendix: Fundamental Theory of X-Ray Scattering

Thus far, this booklet has discussed the scattering and diffraction of X-rays irradiated onto a substance, showing how we can obtain information on crystal structure, such as the arrangement of atoms, by comparing the intensity of diffracted X-rays to available intensity formulas prepared from theoretical considerations. The subsequent discussion addresses the scattering theory used to create the intensity formula, focusing on three selected fundamental topics related to scattering and diffraction, with the goal of providing the knowledge needed to acquire information on crystal structures by comparing theory to the results of X-ray diffraction experiments on crystals.

# A. X-ray Scattering Caused by Atoms

A molecule is composed of two or more atoms. A substance comprised of atoms and molecules can be regarded as an aggregate of atoms, and the X-ray scattering and diffraction phenomena caused by a substance are described as a collection of waves scattered by the atoms present in the interference region of the incident X-rays. The following focuses on X-ray scattering caused by atoms, the most basic of these phenomena.

## A1 Plane waves and spherical waves

Electromagnetic waves are lateral waves deflected in the direction perpendicular to the direction of propagation of the electromagnetic field. If the electric field vector in the direction of deflection is $E$, and the unit vector in the direction of propagation is $s$, the following equation describes the lateral wave:

$$E \exp\left( -2\pi i \left( \frac{s}{\lambda} \right) r + 2\pi i \left( \frac{c}{\lambda} \right) t \right) \quad \text{(A-1)}$$

In **Equation A-1**, *r* indicates the position vector, *t* represents time, and λ is wavelength. *E* is the electric field vector; its magnitude expresses X-ray amplitude. **Equation A-1** can be expressed as follows by substituting wave number vector *k* for $2\pi s/\lambda$, and angular frequency ω for $2\pi c/\lambda$ ($= 2\pi v$, where *v* indicates frequency).

$$E \exp \{-i\bm{k}\,\bm{r} + i\omega t\} \qquad (A\text{-}2)$$

This equation becomes easier to use as we become accustomed to it. We will use it in the following. Spherical waves are used to express waves that disperse in all directions from a point light source. Since amplitude falls off in direct proportion to the square of distance *r* from the light source, dividing **Equation A-2** by *r* results in an equation for spherical waves.

$$E \exp \{-i\bm{k}r + i\omega t\}/r \quad (A\text{-}3)$$

The equation for expressing electromagnetic waves is needed to account for scattering and diffraction phenomena. Since wave intensity can be obtained by multiplying it by conjugated wave, $E \exp \{i\bm{k}r - i\omega t\}/r$, it is the square of amplitude, $E^2$. The field of spherical waves is $E^2/r^2$. This indicates intensity is inversely proportional to the square of the distance. Note that $E^2$ is proportional to the energy of the electromagnetic waves.

Readers unfamiliar with using an exponent function in an equation for expressing waves can convert the exponent function to the sine function $exp(x) = sin(x) + i\,cos(x)$ and regard it as the first term.

## A2 Thomson scattering

A substance is an aggregate of atoms. An atom consists of a nucleus and electrons. Both the nucleus and electrons carry an electrical charge. Since X-rays are electromagnetic waves, it is reasonable to regard X-ray scattering as the scattering of electromagnetic

waves by charged particles. While the charged nucleus does contribute to scattering, we will see that this contribution is negligible compared to the scattering by electrons and can generally be ignored. We will consider only X-ray scattering caused by electrons.

There are two scattering processes, differing in whether energy is transferred between X-rays and electrons. The process free of energy transfer is called elastic scattering; scattering involving energy transfer is called inelastic scattering. **Thomson scattering** is elastic scattering, while **Compton scattering** is inelastic scattering. Although X-rays are electromagnetic waves, they also behave like photons, with energy $h\nu$. Compton scattering describes the process whereby energy is imparted to electrons, releasing them from atoms, while reducing the energy of the X-rays—that is, to lower-frequency X-rays. The reverse of this scattering process, called **inverse Compton scattering**, involves frontal collisions of visible rays with electrons accelerated by high energy, imparting the low-energy visible rays with energy from the electrons and changing them to high-energy X-rays. Researchers are currently harnessing this process in attempts to create powerful X-ray sources.

Diffraction experiments that examine the structures of substances address elastic scattering only. Although some free electrons do not belong to any atom, most electrons are bound to specific atoms or molecules. Exposing such electrons to the electric field of incident magnetic waves results in forced oscillation, causing the electrons to oscillate at the same frequency and generating electromagnetic waves at this frequency. The amplitude of these scattering waves is given by $-(e^2/mc^2)$, and the process is called **Thomson scattering**.

As shown in **Fig. A-**1, if the incident electromagnetic waves are biased toward the direction perpendicular to the plane (the scattering plane) that includes the incident X-rays and scattering X-rays, the scattering waves will also deflect in that direction. Since the scattering intensity (given by the square of Thomson scattering amplitude, $(e^2/mc^2)^2$) does not change within the scattering plane, **isotropic scattering** results. Here,

the scattering plane refers to the plane that includes the direction of the incident wave and the direction of the scattering wave.
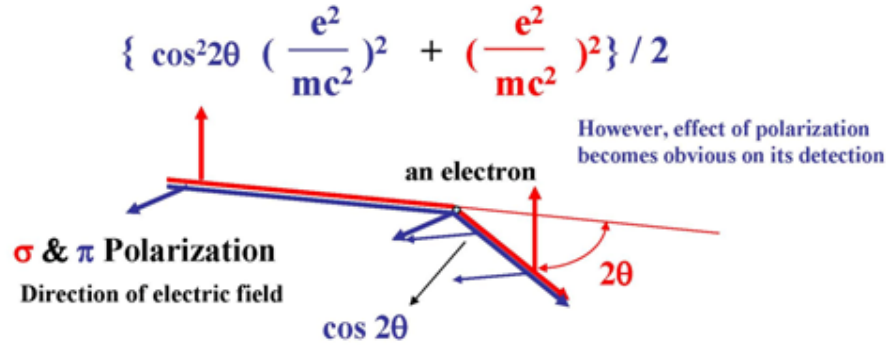
$$\{ \cos^2 2\theta \ (\frac{e^2}{mc^2})^2 \ + \ (\frac{e^2}{mc^2})^2 \} / 2$$

However, effect of polarization becomes obvious on its detection

an electron

σ & π **Polarization**

**Direction of electric field**

$\cos 2\theta$

$2\theta$

**Fig. A-1**Effects of biased electromagnetic waves

If the waves are biased toward the plane, the amplitude viewing angle depends on scattering angle $2\theta$, and the correction $\cos2\theta$ is necessary. Since intensity is the square of the amplitude, $\cos^2 2\theta \ (e^2/mc^2)^2$ is given. Since X-rays polarized in the vertical and horizontal directions do not **interfere** with each other, we can obtain scattering intensity simply by averaging the intensity of the X-rays polarized in those two directions.

$$\{(1 + \cos^2 2\theta)/2\} \ (e^2/mc^2)^2 \quad (A\text{-}4)$$

The coefficient $(1 + \cos^2 2\theta)/2$ in **Equation A-4** is called the **polarization factor**. When the distance from the scatterer to the point of observation is given by $R$, scattering intensity is inversely proportional to the square of $R$. If the accepting solid angle is $d\Omega$, scattering intensity must be as follows:

$$\{(1 + \cos^2 2\theta)/2\} \ (e^2/mc^2)^2 \ d\Omega/R^2 \quad (A\text{-}5)$$

However, $d\Omega/R^2$ can be considered as a commonly appearing coefficient. Thus, we will briefly exclude it from the following discussion.

## A3 X-ray coherence

Now, we'll discuss X-ray **coherence**. The use of the term, "coherence" is not limited to X-rays and can refer to wave phenomena generally. If two waves are **coherent**, they can be added as sine waves. In such cases, coherence occurs when one wave causes elastic scattering at a certain location and coincides with the original wave. If the wave generating source or time differs, the waves become incoherent and must be treated as a different phenomenon entirely. First, the two waves must have the same frequency, but sound waves and electromagnetic waves with a relatively low frequency tend to be coherent. In comparison, light waves and X-rays are low in coherence, since emitted light and X-rays become **wave packets** and their duration time and duration range are finite. Coherence can be observed within that range. Both light and X-rays can be considered partially coherent.

We know of no experiment in which the coherent domain of X-rays from an ordinary X-ray source has been accurately measured, and we will avoid giving a specific value. The author's personal estimate is a value on the order of several tens of microns.

## A4 Phase difference and scattering vector

Assume two scatterers at locations $P$ and $Q$ separated by distance $r$, as shown in **Fig. A-2**. If a plane wave given by wave number vector $k_i$ $(|k_i|=2\pi/\lambda)$ is irradiated and scatters in the direction given by the wave number vector $k_f$ $(|k_f|=2\pi/\lambda)$, the path difference between the wave scattered at P and propagating in the direction of $k_f$ and the wave scattered at Q and propagating in the direction of $k_f$ is P'Q − PQ'. PQ' is a component of PQ $(= r)$ in the direction of $k_f$-, which is equivalent to the scalar product of

*r* and the unit vector of *k_f*. P'Q is a component of *r* in direction *k_i* -, and the scalar product of the unit vector of that direction. Since the size of *k_i* and *k_f* is $2\pi/\lambda$, *k_i r* − *k_f r* indicates the phase difference $\phi$ of the wave, and $\phi$ can be expressed by **Equation A-6**.
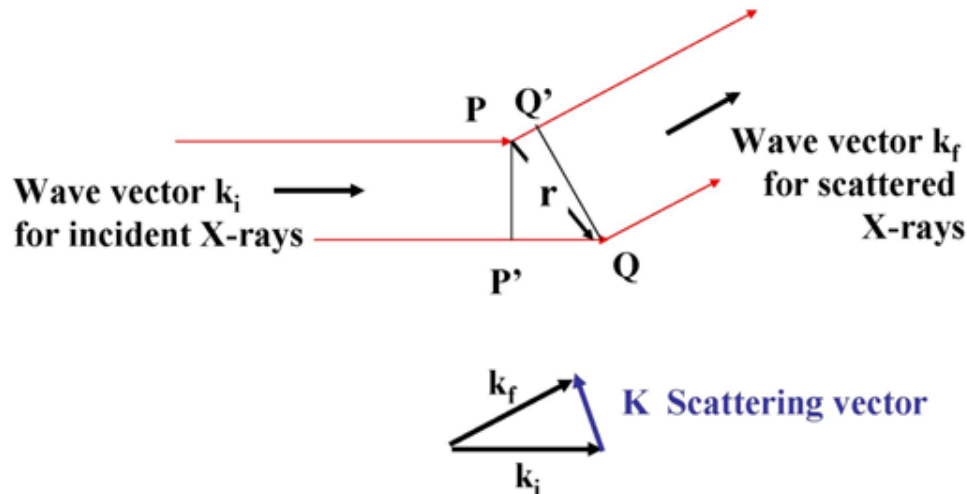


Pass difference = P'Q − PQ'

Phase difference = ( Pass difference )×(2π / λ )

**Fig. A-2** (a) Phase difference and (b) Definition of scattering vector

$$\phi = k_i r - k_f r$$

$$= (k_i - k_f)\, r = Kr \qquad (A\text{-}6)$$

We substituted *K* for *k_f* − *k_i* here. *K* is called the scattering vector. *K* is the vector connecting the end of *k_i* and the end of *k_f*, as shown in **Fig. A-2b**. Since *2θ* is a scattering angle, the size of *K* is given by $4\pi \sin \theta/\lambda$. Using *K*, the angle $\phi$ indicating phase difference can be expressed by the scalar product *Kr* of *K* and *r* (vector expressing the distance between **P** and **Q**).

## A5 Scattering amplitude

Suppose electrons are positioned at locations P and Q and an X-ray beam is irradiated from the direction *k_i* and scattered in the direction *k_f*. Based on the positions of the

waves scattered from P and Q, we can obtain the amplitude of the scattering wave by addition. When electrons are located at P and Q, the scattering amplitude is the same $(e^2/mc^2)$. If location P is the origin point of the coordinates, the wave scattered at location Q has the phase difference $Kr_Q$. We need consider only that phase difference when adding two scattering waves. The amplitude of the scattering wave can be expressed as follows:

$$(e^2/mc^2) + (e^2/mc^2) \exp\{-i\,\boldsymbol{K}r_Q\}$$
$$= (e^2/mc^2)\{1 + \exp(-i\boldsymbol{K}r_Q)\} \quad (A\text{-}7)$$

We will consider the polarization factor when we discuss intensity. Meanwhile, we extract the term for amplitude from **Equation A-7** and indicate it as $A$, as follows:

$$\boldsymbol{A} = (e^2/mc^2)\{1 + \exp(-i\,\boldsymbol{K}r_Q)\} \quad (A\text{-}8)$$

**Equation A-8** means that the contribution of the scattering wave from Q is only $\exp\{-i\boldsymbol{K}r_Q\}$ because it has phase difference $\boldsymbol{K}r_Q$ from the scattering wave from P. Such contribution is called the phase term. Note that $\boldsymbol{A}$ in this case is not a real number but the following imaginary number: $\boldsymbol{A} = A_r + iA_i\,(,\,A^2 = A_r{}^2 + A_i{}^2)$.

If multiple scatterers (a number, N) are located at $r_1$, $r_2$, ..... $r_N$, the aggregate of such electrons causes scattering. To determine the scattering amplitude $A(\boldsymbol{K})$ of the waves propagating in direction $k_f$, we can superimpose the scattering waves by considering the phase of each wave. Then, we can express scattering amplitude, as follows:

$$A(K) = \frac{e^2}{mc^2} \sum_{j=0}^{N} \exp\left(-iKr_j\right) \quad (A\text{-}9)$$

If the scatterers are continually distributed with density $\rho(r)$, only the sum in **Equation A-9** needs to be replaced by integrating, as follows:

$$A(K) = \frac{e^2}{mc^2} \int_{volume} \rho(r)\exp\left(-ikr\right)dr \quad (A\text{-}10)$$

**Equation A-10** has interesting and important implications. The scattering amplitude *A(K)* is the Fourier integral of density distribution $\rho(r)$. Since the scattering intensity *I(K)* is proportional to the square of scattering width, multiplying the square of the Fourier integral of the density distribution $\rho(r)$ of scatters, which is *A\*(K)A(K)*, by the polarization factor gives scattering intensity. Additionally, while density distribution $\rho(r)$ is given as the function of position *r* in real space, the scattering intensity obtained in a scattering experiment is the *K*-space obtained by the Fourier transform of the density distribution. In other words, it is given as the intensity distribution *I(K)* within the space expressed by the scattering angle size $|K|$ *(= sin θ/λ)* and direction *K*.

## A6 Atomic scattering factor of X-rays

Let's consider X-ray scattering caused by atoms with a sizable number of electrons or ions. When its charge density is $\rho_{atom}(r)$, the scattering amplitude *f(K)* is given by the quantity determined by the Fourier integral of $\rho_{atom}(r)$, as you can easily understand from **Equation A-10**.

$$f(K) = \int \rho_{atom}(r) \, exp\{ikr\}dr \quad (A\text{-}11)$$

The *f(K)* above is called the **atomic scattering factor** or **amplitude**. If the wave function $\phi_j(r)$ of the electrons in the atom is known, we can obtain $\rho(r)$ by calculating the density distribution $\rho(r) = \Sigma_j\phi_j(r)^*\phi_j(r)$, and calculating the Fourier integral. Since atoms are bonded in a crystal, the charge density distribution is not necessarily spherically symmetrical. However, since the ratio of nonspherically symmetrical electrons to spherically symmetrical electrons is (except in the case of light elements) very small, it is regarded as spherically symmetric to a first approximation. Specifically, we use the radial distribution function for spherical symmetry obtained by the Hartree-Fock approximation to calculate **Equation A-11**. This numerical calculation was performed

by computer, and the result is posted in the *International Table for X-ray Crystallography, Volume IV.* The calculated value can be used as a reference value.
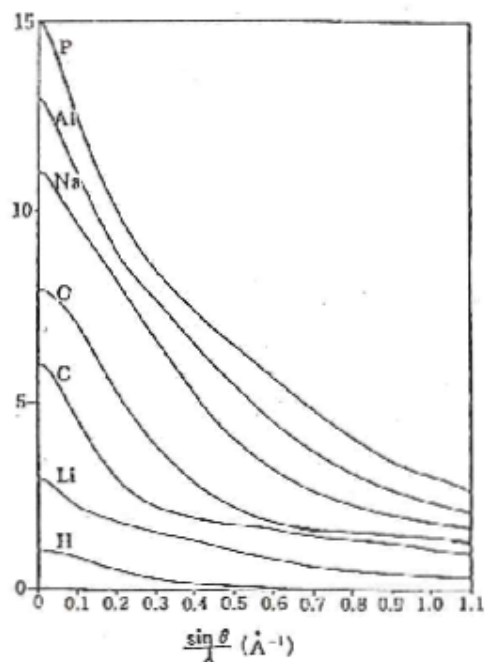


**Fig. A-3** Atomic scattering factor

By referring to the table, we plotted the values of *f(K)* for several types of atoms in relation to the size of the scattering vector, *sin θ/λ*, in **Fig. A-3**. In general, the value of the atomic scattering factor becomes small when the value of *sin θ/λ* increases (when the scattering angle is large). This indicates the scattering is forward scattering. X-ray scattering by one electron is isotropic scattering, setting aside the polarization factor. But if atoms have the electrons surrounding the nuclei with density distributions similar to the spherical Gaussian distribution, forward scattering results. When the scattering angle becomes large, intensity falls dramatically. We know from Fourier transform mathematics that the Fourier transform of a Gaussian function is itself a Gaussian function. Furthermore, as we can see from **Equation A-11**, since the value *f(0)* when *K = 0* is the integration of all charges *ρ(r)*, the atomic number is Z in the case of the neutral atom. As such, the value of the scattering factor is proportional to the atomic

number. When the atomic number becomes large, the difference between adjacent atoms in the periodic table becomes relatively small, making it difficult to distinguish by X-ray diffraction.

## A7 Anomalous dispersion

# B. Diffraction by Crystals

Crystals are composed of atoms and molecules arranged in orderly lattice patterns. X-rays irradiated onto a crystal will scatter. When the Laue condition is met, diffraction occurs. In the following, we will demonstrate that diffraction is nothing more than Bragg reflection. We will also demonstrate how diffraction intensity can be expressed by an equation and what kinds of variables of structure it contains. X-ray scattering from a sample with periodic charge distribution is, mathematically speaking, a Fourier transform of the density distribution with periodic structure. The following section shows that the resulting K-space is also periodic and is called the reciprocal lattice space. The section also describes the geometrical arrangement of the sphere envisioned by Ewald in the reciprocal lattice space. As stressed by Ewald, understanding this helps grasp X-ray diffraction by crystals.

## B1 Scattering and diffraction of X-rays by crystals

For clarity, assume that the unit cell is a three-dimensional orthorhombic crystal lattice with edges $a$, $b$, $c$. Further assume that its charge distribution is $\rho_{cell}$ $(x, y, z)$. We will discuss the arrangement of atoms in the unit cell in a later section. A crystal lattice is formed by this unit cell arranged in the numbers $M$, $N$, and $P$ in directions $a$, $b$, and $c$, respectively. The X-ray scattering amplitude from a unit cell is given by the Fourier transform of the charge distribution of the unit cell, as follows:

$$\int \rho_{cell}(\mathbf{r}) \, exp\{i\mathbf{Kr}\} \, d\mathbf{r} \equiv \mathbf{F(K)} \quad \text{(B-1)}$$

The integration is expressed with $F(\mathbf{K})$, as we see in **Equation B-1** above. This is called the **crystal structure factor** or **structure factor**. Next, consider the scattering amplitude $F_{nmp}(\mathbf{K})$ from the unit cell of a crystal lattice located at a distance of $m\mathbf{a} + n\mathbf{b} + p\mathbf{c}$ (where m, n, and p are integers satisfying the conditions $0 \le m \le M$, $0 \le n \le N$, and $0 \le$

170

p ≤ P). Since this is located *ma + nb + pc* from the unit cell at the origin, it is expressed as having the corresponding phase difference.

$$F(K)exp\{-iK(ma + nb + pc)\} \quad (B\text{-}2)$$

**MISSING FIGURE**

**Fig. B1**

**Fig. B1** illustrates this condition two-dimensionally. If we extend this and consider scattering amplitude *A(K)* from the crystal of size MNP, we see that this is the m, n, p in **Equation B-2** integrated from 0 to M, N, P. Thus the following equation will be obtained.

$$A(K) = F(K) \cdot \{\Sigma_0^M exp(\text{-}i\,mKa)\} \{\Sigma_0^N exp(\text{-}i\,nKb)\} \{\Sigma_0^P exp(\text{-}i\,pKc)\} \quad (B\text{-}3)$$

In **Equation B-3**, *Ka*, *Kb*, and *Kc* indicate the scalar products of the scattering vector *K* and the lattice vectors *a*, *b*, *and c* of the unit cell.

The next step is to calculate the sum *{$\Sigma_0^M$exp(-i mKa)}* of the exponent function, a relatively easy step. It is given by *sin (M Ka /2) / sin (Ka /2)*. Drawing a graph shows that this function has a positive or negative peak at the position at which *Ka*/2 is an integral multiple of π. We introduce here three Laue functions, *La, Lb, and Lc*, obtained by squaring this function.

$$\{sin (M\,Ka /2) / sin (Ka /2)\}^2 \equiv La$$
$$\{sin (M\,Kb /2) / sin (Kb /2)\}^2 \equiv Lb$$
$$\{sin (M\,Kc /2) / sin (Kc /2)\}^2 \equiv Lc \quad (B\text{-}4)$$

Scattering intensity *I(K)* is proportional to the square of the amplitude *A(K)*, and can be expressed as follows:

$$I(K) \sim r_e^2\{(1+cos\,2\theta)/2\}|F(K)|^2La\,Lb\,Lc \quad (B\text{-}5)$$

Here, $r_e$ is the Thomson scattering factor (*F(K)*, crystal structure factor), and $L_a$, $L_b$, $L_c$ are the Laue functions introduced by Laue. **Equation B-5** expresses scattering intensity in direction k that results when X-rays are irradiated onto one crystal from direction $k_0$.

We can account for distance *R* from the sample to the detector by adding the attenuation term $1/R^2$, but since this is a shared proportional constant, we omit it here. More importantly, the intensity shows the profile given by the Laue function and is proportional to the square of the structure factor, $|F(K)|^2$.

## B2 Laue function

The Laue function is defined by **Equation B-4**. With $Ka/2 = x$ as a variable, let's calculate the function $L(x) = \{sin (Mx)/ sin x\}^2$. **Fig. B2** is a graph at $M = 20$. This function results in a sharp peak at the position at which $x$ is an integral multiple of $\pi$ and a low crest at the position that is an integral multiple of $\pi/M$ ($\pi/20$ in the above diagram). We observe an acute peak at $x = h\pi$ ($h$ can be any integer, including 0), and its value is $M^2$. The peak width is $\pi/M$. Since $M$ gives the size of the crystal, the peak value becomes a very large value. The larger the crystal, the greater the large peak becomes, while small peaks become increasingly smaller. We need to focus only on the large peak, which is located at the position at which this function results in a value. This is $x = \pi/M$. However, if the crystallite is small or for thin-film crystals, M is countable, and caution is advisable. We need to note that the peak width is proportional to 1/M and that peak width increases with reduced crystal grain size.

In **Equation B-3**, $Ka/2$ corresponds to $x$. When $h$, $k$, and $\ell$ are integers and $K$ satisfies the following condition, the functions, $L_a$, $L_b$, and $L_c$, have a sharp peak. In other cases, the value approaches 0 when M, N, and P assume large values.

$$Ka = 2\pi h, \quad Kb = 2\pi k, \quad Kc = 2\pi\ell \quad (B\text{-}6)$$

This equation means scattering intensity is high where scattering vector $K$ satisfies the indicated condition but approaches 0 in other locations. The condition given by **Equation B-6** is called the **Laue condition**. The intensity formlua in **Equation B-5**

indicates that scattering intensity becomes high at locations where the scattering vector $K$ satisfies the Laue condition.
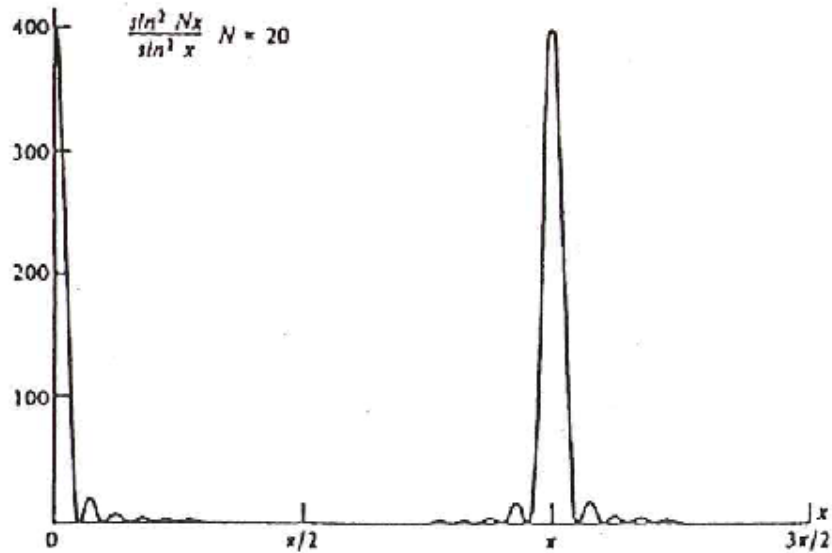


**Fig. B2** Laue function

As mentioned earlier, $K$ is a vector defined within $K$ -space. We select the basic vectors $a'$, $b'$, and $c'$ in that space and express vector $K$ as follows:

$$K = a'\xi + b'\eta + c'\zeta \quad (B\text{-}7)$$

In the **Equation B-7**, $\xi$, $\eta$, and $\zeta$ are the coordinates of the components of the vector $K$ in the directions $a'$, $b'$, and $c'$. If we attempt to seek the condition in which $K$ satisfies the condition in **Equation B-6**, we can verify that $a'$, $b'$, and $c'$ have the following relationships with vectors $a$, $b$, and $c$ defined in real space.

$$
\begin{array}{lll}
a'a = 2\pi & b'a = 0 & c'a = 0 \\
a'b = 0 & b'b = 2\pi & c'b = 0 \\
a'c = 0 & b'c = 0 & c'c = 2\pi \quad (B\text{-}8)
\end{array}
$$

If the values of $\xi$, $\eta$, and $\zeta$ are integers, $h$, $k$, and $\ell$, the condition in **Equation B-6** is satisfied. For confirmation, substitute $K = a'h + b'k + c'\ell$ in the left-hand side of **Equation B-6** and confirm that we can obtain the result on the right-hand side of the equation under the conditions in **Equation B-8**. That is, the Laue function in $K$ space constitutes a

lattice point with $a'$, $b'$, and $c'$ as fundamental vectors; assumes the value $(MNP)^2$ at the lattice point; and has widths proportional to $1/M$, $1/N$, $1/P$ in the directions $a'$, $b'$, and $c'$. Consider the following vector whose fundamental vectors are $a'$, $b'$, and $c'$.

$$G_{hkl} = a' \, h + b' \, k + c' \ell \quad \text{(B-9)}$$

Here, $h$, $k$, and $\ell$ are integers. This equation expresses the lattice in $K$-space with $a'$, $b'$, and $c'$ as a unit cell. This lattice is called the **reciprocal lattice**, while a crystal lattice whose fundamental vectors are $a$, $b$, and $c$ is called a lattice in real space. **Equation B-10**, a modification of the conditions in **Equation B-8**, represents the relationships between $a'$, $b'$, $c'$ and, $a$, $b$, $c$, which are lattices in real space.

$$
\begin{aligned}
a' &= 2\pi \, [b \times c] \,/\, a \cdot [b \times c] \\
b' &= 2\pi \, [c \times a] \,/\, \text{a} \cdot [b \times c] \\
c' &= 2\pi \, [a \times b] \,/\, \text{a} \cdot [b \times c] \quad \text{(B-10)}
\end{aligned}
$$

When the scattering vector $K$ corresponds to the reciprocal lattice vector in **Equation B-9**, the Laue function assumes a value.

$$K = G_{hk\ell} \quad \text{(B-11)}$$

We can regard this equation as satisfying the Laue condition in **Equation B-6**. The fact that strong scattering appears only in a reciprocal lattice in which $K$ is limited by $h$, $k$, and $\ell$ means that scattering waves interfere with each other. The beam scattered in the direction specified by $h$, $k$, and $\ell$ is called the $h\,k\,\ell$ -diffracted beam.

## B3 Lattice in real space and reciprocal lattice

The reciprocal lattice $G_{hk\ell}$ defined by **Equation B-9** and **Equation B-10** has a close relationship to a crystal lattice in real space, as shown below. Consider the lattice plane in real space specified by the Miller indices $h$, $k$, and $\ell$. Let's assign $N$ to the vector in the normal direction to this plane shown in **Fig. B-3** and $d_{hk\ell}$ to the interplanar spacing OP of the plane $h\,k\,\ell$. The relationship to $N$ can be expressed as follows:

$$( aN ) / h = ( bN ) / k = ( cN ) / \ell = d_{hk\ell} |N| \quad (B\text{-}12)$$

Suppose vector $N$ of the normal to the plane $h \, k \, \ell$ is expressed as follows using the reciprocal lattice $a'$, $b'$, $c'$ of this lattice.

$$N = a'\xi + b'\eta + c'\zeta \quad (B\text{-}13)$$
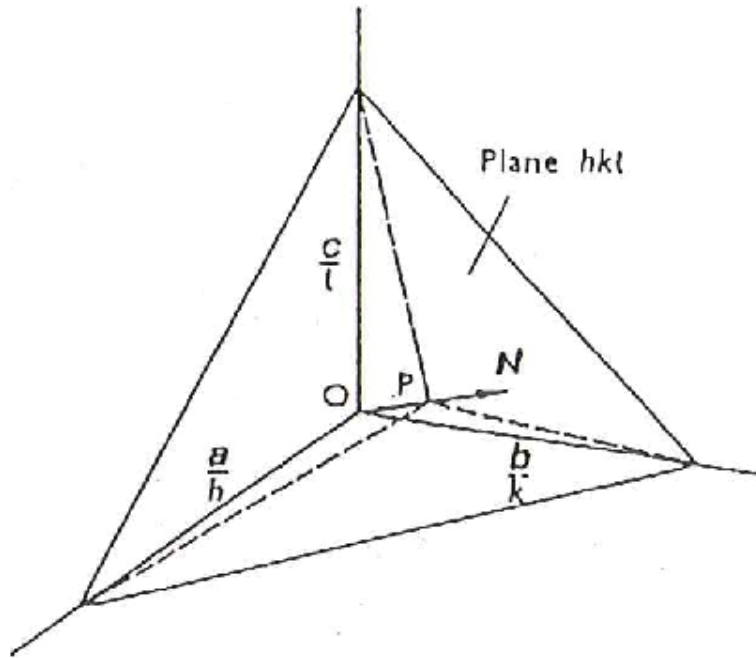


**Fig. B-3** Interplanar spacing expressed by indices hkl

Since $a'$ $b'$ $c'$ satisfies **Equation B-8** if we substitute **Equation B-13** into **Equation B-12**, the following equation is obtained:

$$2\pi\xi / h = 2\pi\eta / k = 2\pi\zeta / l = d_{hk\ell} |N| \quad (B\text{-}14)$$

The left-hand side of **Equation B-14** satisfies the equal condition when $\xi$, $\eta$, and $\zeta$ are integers of $h$, $k$, and $\ell$. This means using the reciprocal lattice vector $G_{hk\ell}$ as the vector $N$ of the normal direction satisfies **Equation B-12**. We can obtain the following relationship:

$$|G_{hkl}| = 2\pi / d_{hkl} \quad (B\text{-}15)$$

This shows that the size up to the reciprocal lattice point, which is $|G_{hk\ell}|$, is in fact

the value obtained by multiplying the inverse of the interplanar spacing $d_{hkl}$ specified by the Miller indices of $h\,k\,\ell$ in real space by $2\pi$. This also means that the vector $G_{hkl}$ is a vector normal to the plane $h\,k\,\ell$. Based on the relationship indicated by **Equation B-15,** we can readily obtain the following equation:

$$(2\pi / d_{hk\ell})^2 \;=\; \mathbf{a'}^2 h^2 + \mathbf{b'}^2 k^2 + \mathbf{c'}^2 l^2$$

$$+\, 2\,\mathbf{a'}\mathbf{b'} \cos\gamma' h\,k + 2\,\mathbf{b'}\mathbf{c'} \cos\alpha'\,k\,l + 2\,\mathbf{c'}\mathbf{a}\cos\beta'\,l\,h \qquad (B\text{-}16)$$

In the **Equation B-16**, $\alpha'$, $\beta'$, and $\gamma'$ are the angles formed by the reciprocal lattice vector pairs $\mathbf{b'}$ and $\mathbf{c'}$, $\mathbf{c'}$ and $\mathbf{a'}$, and $\mathbf{c'}$ and $\mathbf{a'}$. The following equations express the relationships between $\alpha'$, $\beta'$, and $\gamma'$ angles and the angles $\alpha$, $\beta$, and $\gamma$ formed by the unit vectors of the lattice in real space, respectively.

$$\cos\alpha' \;=\; (\cos\beta \cos\gamma - \cos\alpha) / \sin\beta \sin\gamma$$
$$\cos\beta' \;=\; (\cos\gamma \cos\alpha - \cos\beta) / \sin\gamma \sin\alpha$$
$$\cos\gamma' \;=\; (\cos\alpha \cos\beta - \cos\gamma) / \sin\alpha \sin\beta \quad (B\text{-}17)$$

Using the relationships indicated in **Equations B-16** and **B-17**, we can obtain an equation indicating the relationship between lattice constant and interplanar spacing.

## B4 Bragg's law

The value of the scattering vector at the location where the Laue function assumes a value is given by using absolute values on both sides in **Equation B-11**, as follows:

$$|\mathbf{K}| = |\mathbf{G}_{hk\ell}| \quad (B\text{-}18)$$

The absolute value of $\mathbf{K}$ is $4\pi \sin\theta/\lambda$. $|\mathbf{G}_{hk\ell}|$ can be expressed by $2\pi/d_{hk\ell}$, as mentioned in the previous section. Substituting these terms into **Equation B-18** gives the following equation:

$$2d_{hkl}\sin\theta = \lambda \quad (B\text{-}19)$$

**Equation B-19** expresses the Bragg reflection of X-rays by the lattice plane having

interplanar spacing $d_{hk\ell}$. We see that the Laue diffraction condition, **Equation B-6** or **B-11**, is identical to the equation expressing the law of Bragg reflection, **Equation B-19**.

## B5 Ewald's profile

The Laue diffraction condition in **Equation B-6** indicates the occurrence of diffraction when the scattering vector $K$ corresponds to reciprocal vector $G_{hk\ell}$. This diffraction condition in a reciprocal lattice space can be visualized as shown in **Fig. B4**. The reciprocal lattice is three-dimensional; the illustration shows a two-dimensional cross section of a reciprocal lattice. The vector $K$ is expressed as $K = k_f - k_i$ using the wave number vector $k_i$ of the incident wave and wave number vector $k_f$ of the scattering wave. The size of $k_f$, $k_i$ is $2\pi/\lambda$; hence, the correspondence of the vector $K$ to vector $G_{hk\ell}$ means three vectors, $k_f$, $k_i$, and $G_{hk\ell}$, constitute an isosceles triangle in reciprocal lattice space. This means a wave $k_i$ traveling from the apex A to the origin of the reciprocal lattice is Bragg-reflected by the plane h k ℓ in direction $k_f$.
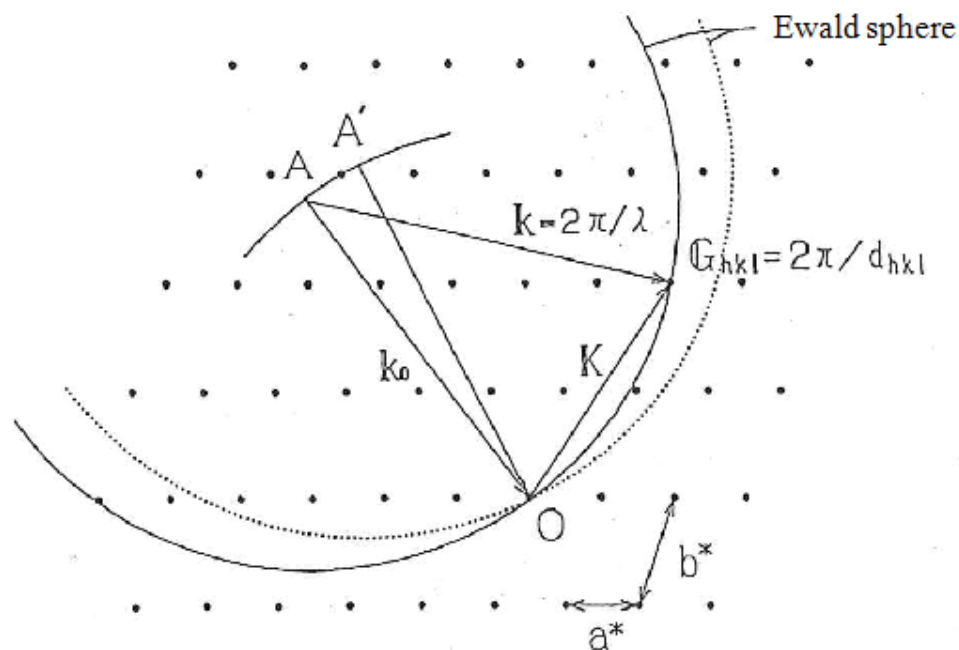


**Fig. B4** Relationship between a reciprocal lattice place and the Ewald sphere

Once the incident direction is set, point A is determined, so that a sphere with a radius of $2\pi/\lambda$ is drawn with A at the center. This sphere contacts the origin of the reciprocal lattice. The reciprocal lattice point $G_{hkl}$ is also located on the spherical surface. This condition satisfies the diffraction condition.

If the X-ray beam enters from the direction slightly displaced from point A, such as point A′ shown in the diagram, the sphere drawn with point A′ at the center deviates from the point $G_{hk\ell}$. This means the X-ray beam entered in a direction that does not satisfy the diffraction condition. The diagram shows that the intensity distribution in the section of the reciprocal lattice space located on the spherical surface spreads in all directions from point A and that if the reciprocal lattice point happens to be on the spherical surface, a Bragg reflection occurs in that direction. This sphere is called the **Ewald sphere**. The center of the Ewald sphere is on the surface of a sphere a radius of $2\pi/\lambda$ away from the origin of the reciprocal lattice.

As shown here, by drawing a reciprocal lattice and recognizing how the Ewald sphere is arranged in the reciprocal lattice, we can predict the direction and type of scattering that will occur. Alternatively, if X-rays are irradiated onto a crystal with a certain orientation from a certain direction and the diffracted image is captured on film, the diffracted image indicates where and how in the reciprocal lattice space intensity is distributed. Drawing the Ewald sphere is highly useful for understanding the diffracted image.

# B6 Crystal structure factor

The crystal structure factor $F(K)$ is defined in Equation **B-20** as the quantity of charge distribution $\rho_{cell}(r)$ in the unit cell after the Fourier transform. The equation is as follows:

$$F(\boldsymbol{K}) = \int \rho_{cell}(\boldsymbol{r}) \, exp\{i\boldsymbol{K}\cdot\boldsymbol{r}\}d\boldsymbol{r} \quad (B\text{-}20)$$

Suppose the charge distribution of an atom $j$ in the unit cell is $\rho_j(r)$. If this atom $j$ is at position $r_j$ in the unit cell, we can write the charge distribution $\rho_{cell}(r)$ in the unit cell as follows:

$$\rho_{cell}\ (r) = \Sigma_j\ \rho_j(\ r - r_j)\quad\text{(B-21)}$$

Thus, **Equation B-20** can be expressed as follows, given that the atomic scattering factor of the atom $j$ is $f_j(K)$.

$$F(K) = \Sigma_j f_i(K)\ exp\{iKr_j\}\ \text{(B-22)}$$

Here, $exp\{iK{\cdot}r_j\}$ is a phase term because the atom $j$ is at position $r_j$. In general, crystal lattices are not stationary, but fluctuate spatially over time due to thermal oscillation. When the temperature rises, the amplitude of thermal oscillation increases. That is, thermal oscillation displaces atoms in the crystal from their equilibrium positions. If the amount of displacement is $u_j$, we can write the atomic position as follows:

$$r_j = <r_j> + u_j\quad\text{(B-23)}$$

Note that $u_j$ changes continuously and is different in each unit cell. Observation takes time. What we observe is the average value of **Equation B-22**. Thus, we obtain the statistical average of the value represented by $<\ >$.

$$\langle F(K)\rangle\ = \Sigma_j f_j(K){<}exp\{iKu_j\}{>}exp\{iK{<}r_j>\ \}\quad\text{(B-24)}$$

$$= \Sigma_j f_j(K)\ T(K,u_j)\ exp\{i\ K{<}r_j>\}\quad\quad\text{(B-25)}$$

In **Equation B-24**, we set the statistical average of $exp\{iKu_j\}$ to $T(K,u_j)$. The result is the same whether we use the temporal or spatial average.

## B7 Temperature factor

**Equation B-25** calculates the average $<exp\{iKu_j\}>$ of the exponent function, including the

displacement $u_j$ of atoms from their equilibrium positions due to thermal oscillation. This is called the **temperature factor or thermal factor**. The following approximation is used for the calculation:

$$<exp\{iX\}> = exp\{ - <X^2> / 2\} \quad (B\text{-}26)$$

If we develop both sides and compare, we find that the above approximation is valid when $X$ is small. The average of the exponent function is expressed as follows within this approximation range.

$$\langle exp\{i\boldsymbol{K}u_j\} = exp\{- 8\pi^2 <u_j^2>(sin\theta/\lambda)^2\}$$

$$= exp\{- B_j (sin\theta/\lambda)^2\} \quad (B\text{-}27)$$

Here we use the relationship, $K^2 = 4\pi^2 sin^2 \theta/\lambda^2$. This coefficient is called the temperature factor or Debye-Waller factor. $<u_j^2>$ expresses the component of displacement $u_j$ in the direction of scattering vector $\boldsymbol{K}$. When $8\pi^2<u_j^2>$ including the root mean square of displacement is replaced by $B_j$, the result is called the temperature or thermal parameter. As we see **Equation B-26**, this is a Gaussian function whose value is 1 when the scattering angle $sin\ \theta/\lambda$ is 0. The value becomes exponentially smaller as the scattering angle increases. The larger the value of $<u_j^2>$ or $B_j$ is, the greater the attenuation. If we regard the temperature as a correction factor to be applied to the atomic scattering factor, we see that it is a coefficient that decreases the atomic scattering factor as the scattering angle increases. If the structure factor is expressed with the temperature factor, **Equation B-25** can be modified as follows:

$$F_{hkl} = \Sigma_j f_j(\boldsymbol{K}) exp\{- B_j ( sin\theta/\lambda)^2\}$$

$$\times exp\{2\pi i(hx_j+ky_j+\ell z_j)\} \quad (B\text{-}28)$$

Since $\boldsymbol{K}$ assumes a value only at the reciprocal lattice point $h\ k\ \ell$, we used $h\ k\ \ell$. We also use $x_j$, $y_j$, $z_j$ to express the coordinates of the atom equilibrium positions. The structure factor expresses a quantity that includes two types of parameters: atomic

coordinates and temperature parameter. Determining the crystal structure means determining these two parameters (atomic coordinates and temperature parameter).

In the case of X-rays, the atomic scattering factor becomes small as the scattering angle increases in forward scattering. This can make the attenuation attributable to thermal oscillation difficult to isolate.

# C. Diffraction Intensity Formula

In the previous chapters, we discussed the X-ray incident conditions that would cause the Laue-Bragg reflection and examined the equation for expressing the diffraction intensity obtained based on the assumption of perfect crystal lattices. We stated that the Laue condition would be satisfied when the scattering vector $K$ corresponds to the reciprocal lattice vector $G_{hkl}$, since it would result in a Bragg reflection, in which the intensity of diffracted X-rays is proportional to the square of the number of lattices MNP in the crystal that contributes to the diffraction. However, it is very difficult to confirm experimentally that a measurement was taken at the peak position. In fact, it is safer to use a measurement method that includes and integrates the peak. This is equivalent to integrating the Laue function. Calculating the integrated intensity shows it is proportional to the number of lattices, MNP. Explained below is the diffraction intensity formula by integrating the Laue-Bragg reflection, as well as a number of required corrections.

## C1 Integrated reflection intensity

We might assume that measuring the Bragg reflection by setting up the measuring equipment so that scattering vector $K$ corresponds to the reciprocal lattice vector $G_{hkl}$ would provide information on crystal structure, allowing structural analysis. In practice, it is all but impossible to achieve the condition required for Bragg reflection in a laboratory. It is not possible to collimate incident X-rays perfectly. Some X-rays are always measured at locations removed from the peak position specified by the Laue function. An experiment cannot measure the intensity of Bragg reflection under conditions in which all incident X-rays satisfy the Bragg condition. How can we resolve this issue?

After observing the profile of the Laue function, examining the location to be measured with high precision in experiments, and studying how to compare measurements with theoretical values, our predecessors concluded that measuring the integrated value of the Bragg reflection would allow accurate comparisons to theoretical values. This technique remains in use. The total number of unit cells in a crystal particle that cause the Bragg reflection—assumed as N here—becomes $N^2$ at the peak position of the Laue function. Its full width at half maximum is $1/N$. If we can integrate the Laue function at a location near the peak position, the value should be $N$, since $N^2 \times (1/N) = N$. This means that the intensity of the obtained integrated value of diffracted X-rays is proportional to the total number of unit cells in the crystal lattice. Obtaining the peak position of the Laue function is difficult in an experiment, but calculating the integrated value is easy and reliable. The next topic is how we can obtain measurements to achieve the effect of integrating the Laue function near the Bragg reflection. This is closely related to the method of measurement.

## C2 Integrated reflection intensity of a single crystal sample

The first idea is to obtain the integrated value by positioning one crystallite and measuring the profile of the resulting Bragg reflection. This requires making incident X-rays with a wavelength of 1 as close as possible to perfectly parallel, placing the detector at the corner where diffracted X-rays are received, making the slits before the detector wide, rotating the crystal at a certain speed, and measuring all reflected X-rays. Intensity should be measured as energy per unit of time and per unit area. The obtained integrated intensity $J(G_{hkl})$ can be expressed as follows:

$$J(G_{hkl}) = \iint I(K - G_{hkl})dtdA \quad (C\text{-}1)$$

Here, $dA$ is the area element on the receiving side, while $dt$ indicates measurement

time. The deviation from the scattering vector $K$ of Bragg reflection is defined as $K - G_{hkl}$ = $q$ $(q_x, q_y, q_z)$. As shown in **Fig. C-1**, when the distance from the sample crystal to the detector is $R$ and the anticipated angles of received rays are $d\beta$ in the horizontal direction and $d\gamma$ in the vertical direction and when the crystal is rotated at an angular speed of $\omega$, rotation angle is given by $d\omega = \omega dt$. The integration variable can be converted to rotation angle $d\omega$ and receiving angle $d\beta d\gamma$.

$$J(G_{hkl}) = \frac{R^2}{\omega} \iiint I(q) d\omega d\beta d\gamma \quad (C\text{-}2)$$

This is not enough to perform integration. Since the variable for intensity is $q$, we need to convert the variables $\omega$, $\beta$, and $\gamma$ to the variables $q_x$, $q_y$, and $q_z$ defined within the reciprocal lattice. If we refer to **Fig. C-1**, we notice the following relationships.

MISSING FIGURE

**Fig. C-1**

$$dq_x = (2\pi/\lambda)\, d\beta \cos\theta$$
$$dq_y = (4\pi/\lambda)\sin\theta\, d\omega$$
$$dq_x = (2\pi/\lambda)\, d\gamma \qquad (C\text{-}3)$$

If we substitute these relationships into **Equation C-2** and perform the conversion, we can obtain the integrated intensity as follows:

$$J(G_{hkl}) = I_0 \left(\frac{e^2}{mc^2}\right)^2 (1 + \cos^2 2\theta) \frac{R^2 \lambda^3 V |F(G_{hkl})|^2}{2\omega v_0 \sin 2\theta} \quad (C\text{-}4)$$

Here, $I_0$ indicates the intensity of the incident X-rays, $V$ the volume of the crystal causing the scattering, and $v_0$ the volume of the unit cell. Note that $R^2 \lambda^3 / v_0 \omega \sin 2\theta$ is a coefficient that appears when converting the integration variable. Mathematically, this is a Jacobian.

This coefficient takes a different form if the method of measuring the integrated intensity changes. For structural analysis focusing on the relative intensity of the Bragg reflection, $R^2 \lambda^3 / \omega v_a$ is a mere constant and can be regarded as proportional. In contrast,

the angle-dependent term *1/sin2θ*, called the Lorentz factor, is important. Additionally, we must consider a polarization factor dependent on the scattering angle included in **Equation C-4**. When this is combined with the Lorentz factor, the coefficient that is dependent on the scattering angle *2θ* can be summarized as follows: *(1+cos²2θ)/2 sin 2θ*. This coefficient is called the Lorentz polarization factor and is abbreviated LP.

$$LP = (1 + cos^2 2\theta)/2\ sin2\theta \quad (C\text{-}5)$$

The LP factor is included in the integrated intensity obtained in the measurement of Bragg reflection in which the window of the counter is opened, the detector is placed at the position *2θ* (twice the Bragg angle), the single crystal is set up in advance in the direction that enables observations of the Bragg reflection, and the Bragg reflection is observed while the sample is in the *ω* rotation.

## C3 Integrated reflection intensity of powder sample

When monochromatic X-rays are irradiated onto a powder sample and the diffracted image is captured on X-ray film, we observe the well-known Debye-Scherrer ring. Let's think of this diffraction condition in reciprocal space. As powder crystals are evenly orientated in all directions, the intensity distribution in reciprocal space shows a collection of concentric spheres obtained by rotating the reciprocal lattice of the single crystal around the origin. The intersection of the concentric spheres and the Ewald sphere with a length of 2π/λ satisfies the diffraction condition. This intersection forms a circle. X-rays scatter in a conical pattern from the center of the Ewald sphere toward the circle formed by the intersection. This can be confirmed in a simple geometrical diagram. We can easily image the Debye-Scherrer ring when this is captured on X-ray film. See **Fig. C-2**.

Now, let's examine the equation that gives the integrated intensity per unit length of

Debye-Scherrer ring. As mentioned earlier, the intensity distribution in reciprocal lattice space forms a concentric sphere with a radius equaling the size, $|G_{hkl}|$ (= $4\pi \sin \theta/\lambda$), of the reciprocal lattice vector $G_{hkl}$ and with the origin of the reciprocal lattice at the center.
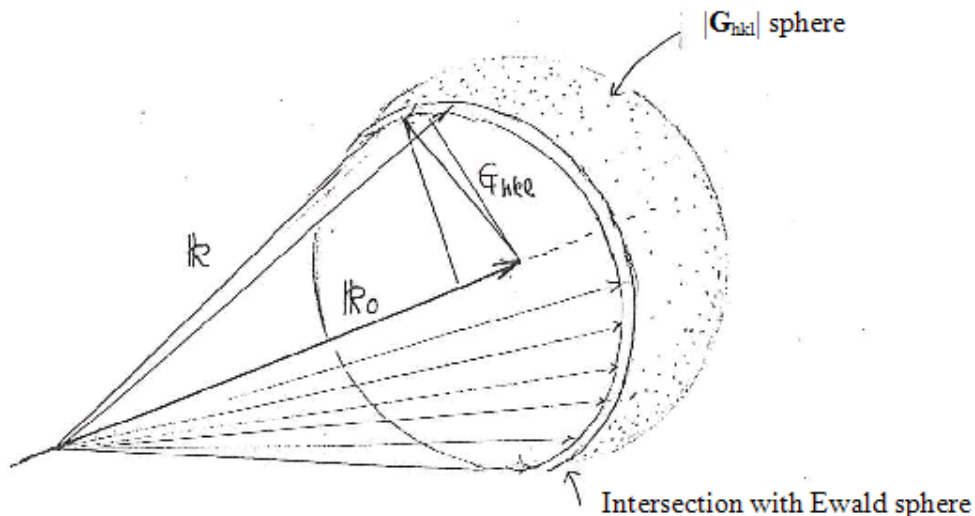


**Fig. C-2** Intersection between reciprocal lattice sphere of powder sample and Ewald sphere

In this case, intensity is distributed uniformly over the spherical surface, but all reflections equivalent to $h,k,l$ are also located on the same spherical surface. The concentric sphere must be multiplied by the number of equivalent reflections, **multiplicity** $m_{hkl}$. Or we can regard the intensity of the sphere to be stronger in the order of the number of equivalent reflections.

When the number of all crystal particles in the sample is $N$, the following equation gives the number of particles distributed in a unit area of the spherical surface:

$$m_{hkl}N /4\pi|G_{hkl}|^2 \quad (C\text{-}6)$$

The number of crystal particles that contribute to diffraction equals the number of particles located at the intersection of the Ewald sphere with radius $2\pi/\lambda$ and the concentric spheres. If the incident X-rays have divergence angle $d\alpha$, the number of crystal particles contributing to diffraction equals the number of crystal particles distributed on the belt with width of $G_{hkl}$ $d\alpha$ on the spherical surface, as shown in

**Figure C-2**. This area is $2\pi G_{hkl}\ cos\theta G_{hkl}\ d\alpha$. The percentage of particles on the belt of the total particles distributed over the entire sphere is given below.

$$N\ 2\pi|G_{hkl}|^2 cos\theta d\alpha/\ 4\pi|G_{hkl}|^2 = N\ cos\theta\ d\alpha\ /\ 2 \quad (C\text{-}7)$$

If the area element on the receiving side is $d\Lambda = R^2 d\beta d\gamma$, when $d\alpha$ corresponds to $d\omega$, and the integrated intensity from one crystal particle to be observed is taken into consideration, the calculation is performed in the same way as for a single crystal. Thus, the constant $1/sin2\theta$ also applies. The intensity equation for the X-rays that scatter in a conical pattern is given below:

$$J(G_{hkl}) = C\ N\ m_{hkl}\ \{\ (1+\ cos^2 2\theta)\ /\ (2sin\theta)\}\ |F_{hkl}|^2 \quad (C\text{-}8)$$

However, the X-rays that are actually measured are part of the X-rays scattered in a conical pattern. This must be taken into consideration. If the distance from the sample is $R$, the intensity is $\frac{1}{2}\pi R\ sin2\theta$. To focus just on the factor dependent on scattering angle $\theta$, we multiply $cos\ \theta$ in **Equation C-7** by $1/sin\ 2\theta$ (for integrated intensity from one crystal particle) and by $1\ /\ 2\pi R\ sin2\theta$.

$$LP=cos\theta/sin^2 2\theta=1/2sin\theta\ sin2\theta$$

This is the Lorentz factor. The integrated intensity obtained from the measurement of part of the Debye-Scherrer ring using a powder sample can be expressed as follows:

$$J(G_{hkl}) = C\ N\ m_{hkl}\ \{\ (1+\ cos^2 2\theta)\ /\ (sin\theta\ sin2\theta)\}\ |F_{hkl}|^2 \quad (C\text{-}9)$$

$(1+cos^2 2\theta)/(sin\theta\ sin2\theta)$ in this equation is the LP factor for the powder sample.

Using white X-rays and analyzing the energy of scattered radiation, we can measure the integrated intensity of diffracted X-rays. This is equivalent to the Laue method or energy dispersion method for X-rays and the TOF method for neutrons. In this case, equation (C-1) is the integration of $d\lambda d\Lambda$. Converting $d\lambda$ to $d\theta$ gives $d\lambda = \lambda\ cot\theta$ $d\theta$. Thus, the Jacobian differs from that in the integration of $dt$. The Lorentz factor also

becomes different. The result is $\lambda^4/\ 2\ sin^2\theta$ for a single crystal and $\lambda^4/\ 2\ sin^3\theta$ for powder. Even if the scattering angle is kept constant during measurement, the integrated intensity varies in proportion to $\lambda^4$. We must also keep in mind that the change due to the scattering angle differs from that in normal cases.

## C4 Absorption factor

Discussions up to this point have disregarded the effects of X-ray absorption by crystals. When scattering is caused by small crystals and the amount of X-ray absorption is negligible, we can use **Equation C-4** to calculate diffraction intensity. Even if the X-ray scattering power of a material is small, however, X-rays can be absorbed to a significant degree, and absorption needs to be taken into account. The intensity of X-rays is reduced by *exp{-μt}* when they pass through a crystal with thickness *t*. As previously noted, $\mu$ is called the **linear absorption coefficient**.
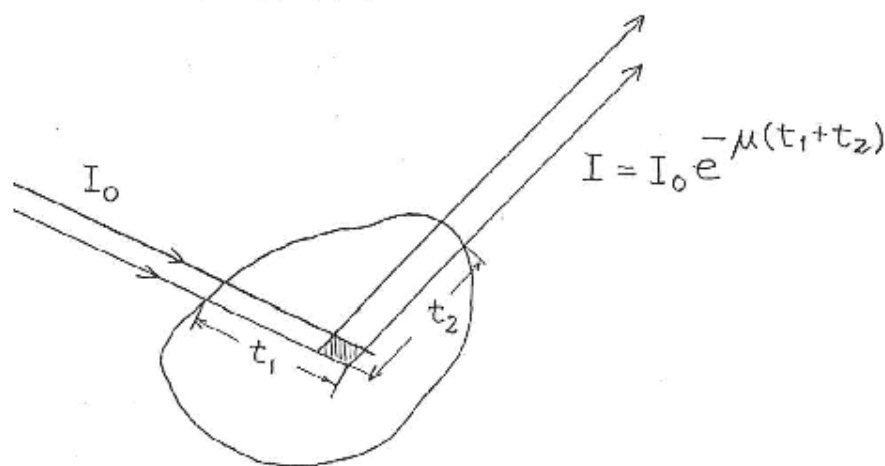


**Fig. C-3** Relationship between X-ray penetrating depth and absorption

When X-rays are irradiated onto a crystal and leave the crystal as diffracted X-rays, they are subject to absorption *exp{-μ(t₁+t₂)}* along each path, as shown in **Fig. C-3**. X-rays travel along various paths. Since they are absorbed in all paths, we calculate the

average.

$$A(\mu) = (1/V)\int_V exp(-\mu x)\,dv \quad (C\text{-}10)$$

$A(\mu)$ is called the **absorption factor**. When X-rays are absorbed, the effective volume $V$ pertaining to scattering is multiplied by $A(\mu)$. Thus, the equation for integrated intensity for single crystals and powder samples can be written as follows:

For single crystals:

$$J(G_{hkl}) = C.V.\,A(\mu)\,Lp(S)\,|\,F(G_{hkl})|^2 \quad (C\text{-}11)$$

For powder samples:

$$J(G_{hkl}) = C\,N\,m_{hkl}\,A(\mu)\,Lp(P)\,|F_{hkl}|^2 \quad (C\text{-}11')$$

Here, $Lp(S)$ and $Lp(P)$ are the Lorentz polarization factors for single crystals and powder samples, respectively. Note that they are not the same.

In the easiest-to-handle case, X-rays are irradiated onto a flat-plate-shaped sample at the angle $\theta_1$ and diffracted at the angle $\theta_2$. As shown in **Fig. C-4**, the following equation is based on P, the power of the reflection in the direction at angle $\theta_2$ from the layer $X_z$ - $X_z'$ with thickness dz, at depth z, and parallel to surface $X_0$ -$X_0'$.
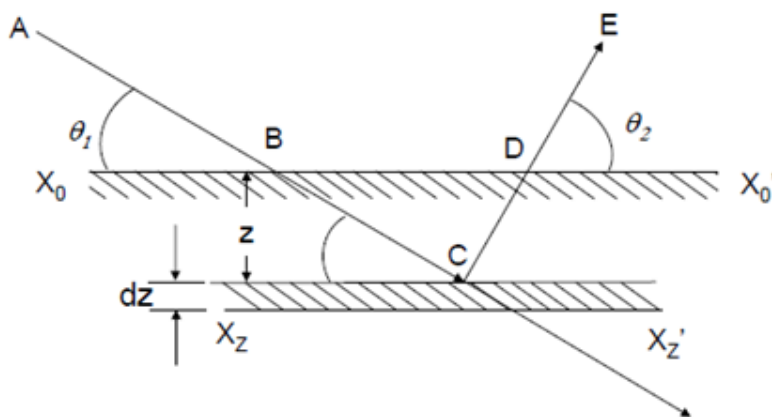


**Fig. C-4** Absorption of X-rays reflected by layer $X_z X_z'$ in sample in asymmetrical direction relative to surface. Absorption correction for flat-plate-shaped sample

The intensity that reaches point E, indicated as $dI_s$, is given as follows:

$$dI_z = I_0 P \exp\{-\mu(BC)\} \, (dz/\sin\theta_l) \, \exp\{-\mu(CD)\} \quad \text{(C-12)}$$

If we substitute for $(BC) = z / \sin\theta_1$, $(CD) = z / \sin\theta_2$ and integrate depth z infinitely from 0, the scattering intensity $I_t$ at point E is given by the following equation:

$$I_t = \int_{z=0}^{\infty} dI_z = \frac{I_0 P}{\sin\theta_1} \int_{z=0}^{\infty} \exp\left[-\{(1/\sin\theta_1)+(1/\sin\theta_2)\}\mu z\right]dz \quad \text{(C-13)}$$

Integration yields the following:

$$I_t = \int_0^{\infty} dI_s = \frac{1}{\mu} I_0 P \frac{1}{1+\sin\theta_1/\sin\theta_2} \quad \text{(C-14)}$$

For semi-infinite samples, scattering intensity can be solved analytically. In this equation, the absorption factor $A(\mu)$ is equivalent to $I_t / I_0 P$. We obtain the following equation:

$$A(\mu) = \sin\theta_2 / (\sin\theta_1 + \sin\theta_2) \cdot \mu \quad \text{(C-15)}$$

In the case of $\theta_1 = \theta_2$ (called the symmetric reflection condition), the absorption factor is quite simple, as shown below:

$$A(\mu) = 1 / 2\mu \quad \text{(C-16)}$$

That is, for the symmetric reflection condition, the absorption factor is consistent without being dependent on the incident angle $\theta$. It is $\tfrac{1}{2}\mu$ of the volume of irradiated X-rays. For crystals of more complex shapes, it is difficult to calculate **Equation C-5** for each Bragg reflection. In recent years, ray tracing has been used for numeric calculations.

In the case of a plate-shaped sample, if the incident angle and emerging angle are the same, $A(\mu)$ is given by $\tfrac{1}{2}\mu$, whether the sample is a single crystal or powder, when absorption is taken into consideration. However, in the case of powder samples, $\mu$ changes, depending on how the sample is packed. We cannot use the absorption

coefficient for single crystals. If $\mu$ is large, it is incorporated into proportional constant C, so this may not pose a problem. If $\mu$ is small, the value changes according to the thickness of the sample, and corrections are needed.

## C5 Extinction effect

Our previous explanations were based on the following assumption: when X-rays are irradiated onto crystallites and the Bragg condition is met, the intensity of diffracted X-rays is proportional to the square of the structure factor $|F_{hkl}|$. But since X-rays are absorbed in the process, intensity decreases only according to the absorption factor. This scattering theory assumes that scattering occurs only once in a sample and is equivalent to the primary Born approximation. In reality, we cannot ignore the possibility that X-rays diffracted within the crystal sample will encounter other planes that satisfy the Bragg condition and will be diffracted a second or third time before reaching the detector, a phenomenon known as **multiple scattering**. When multiple scattering occurs, the diffracted X-rays usually attenuate in intensity. This is called the **extinction effect**.

Two types of extinction can occur with X-ray diffraction in a single crystal: **primary extinction** and **secondary extinction**.

i) Primary extinction effect

Assume an ideal single crystal with no lattice flaws, such as the semi-infinite single crystal shown in **Fig. C-6**. Suppose that a parallel X-ray beam that geometrically satisfies the Bragg condition is irradiated onto a lattice plane parallel to the crystal surface. As we can imagine by looking at the diagram, for X-rays diffracted under this condition, a condition that causes a Bragg reflection exists on the lattice plane on the back side of the crystal. The diffracted X-ray becomes an incident X-ray and returns, but the returned X-ray undergoes a Bragg reflection again. Some X-rays leave the crystal surface after repeating this process. If the crystal has high integrity, incident X-rays and

diffracted X-rays enter a coherent state inside the crystal; therefore, the profile of emerging X-rays differs completely from what we would expect from single scattering. The scattering intensity equals the total reflection condition and is always 1. The range (full width at half maximum) in which this condition is met becomes the width proportional to the absolute value of crystal structure factor. Thus, the integrated intensity becomes *1 x* $|F_{hkl}|$, which differs from the quantity proportional to $|F_{hkl}|^2$ we would expect based on single scattering theory. If X-rays are irradiated onto the crystal plane discussed here and diffracted from that plane, that crystal arrangement is called the **Bragg case**.

<div align="center">MISSING FIGURE C6a/C6b</div>

**Fig. C-6b** shows an arrangement in which the crystal has a finite thickness of **t** and X-rays irradiated onto the surface emerge from the back side as reflected X-rays. This crystal arrangement is called the Laue case. In this case, if the crystal has high integrity, multiple scattering occurs; however, if no absorption occurs, the intensity of emerging X-rays depends on crystal thickness **t**. If **t** is small, an approximation based on the single scattering theory is possible. If **t** is large, the extinction effect becomes prominent. For certain values of **t**, no diffracted X-rays may be observed at all.

This booklet will not attempt a detailed explanation of multiple scattering. Diffraction theory incorporating multiple scattering into perfect crystals is called **dynamic diffraction theory**. In contrast, the single scattering theory we discussed in this booklet is called the **kinematical diffraction theory**.

ii) Secondary extinction effect

In the above discussion, the crystallinity of the sample crystals was assumed to be good. Here, we consider a case in which integrity varies within the crystal. Such a sample is called a mosaic crystal. X-rays diffracted at one location of a crystal are diffracted at a second location and registered as diffracted X-rays once again. This may appear to be identical to the case in i), but the intrinsic difference is that the scattering

that occurs a second time will lose X-ray coherence. The interactions between incident X-rays and diffracted X-rays is not a wave function, but an exchange of energy (intensity). Scattering that undergoes this process is typically limited to large crystal structure factors or scattering of high scattering power. Additionally, the intensity obtained is generally weaker than the integrated intensity we would expect based on kinematical diffraction theory. To distinguish it from the extinction effect in i), this is called the **secondary extinction effect**.

How do these extinction effects in single crystals make themselves apparent in the case of powder X-ray diffraction? This is an important issue. The recommended crystal particle size in powder crystals is several microns or less. If the crystal grain size is small, we can approximate both the Laue case and the Bragg case based on kinematical diffraction theory. Thus, we may conclude that the primary extinction effect need not be considered at all. However, with powder samples, the probability of declining intensity due to X-rays being diffracted twice by a crystal particle is not small if the diffracted X-rays have high intensity. The author believes the secondary extinction effect needs to be considered. If the intensity of high-intensity diffracted X-rays is found to be lower than the value calculated according to kinematical diffraction theory, we should exclude that reflection, rather than attempting to make numeric figures match in our intensity calculations. The experimenter should perform the analysis in a range in which the results can be trusted.

The extinction correction theory for primary and secondary extinction effects was discussed from the early 1970s to 1980s. Listed below are some references.

- T.M. Sabine, R.B. Von Dreele and J.E. Joergensen; Acta Crystallogr., A **4A**, 374 (1988)

# C6 Correction of preferred orientation

Preferred orientation causes significant fluctuations in integrated intensity and results

in adverse effects on analysis results. The effects of preferred orientation are especially marked with X-ray diffraction with flat-plate samples. It is necessary to keep the size of crystallites to 3 μm or less. This and other precautions are mentioned in this booklet. We may also refer to the following documents.

- W.A. Dollase: *J. Appl. Crystallogr.*, **19**, 267 (1986)
- M. Ahtee, M. Nurmela, P. Suortti and M. Jaervinen; *J. Appl. Crystallogr.*, **22**, 261 (1982)